INSIGHTS INTO PROTEIN-BOUND UREMIC TOXINS IN PROXIMAL TUBULE CELL SENESCENCE AND KIDNEY FIBROSIS

YI YANG

杨 逸

Insights into protein-bound uremic toxins in proximal tubule cell senescence and kidney fibrosis

Yi Yang

Insights into protein-bound uremic toxins in proximal tubule cell senescence and kidney fibrosis

Inzicht in eiwitgebonden uremische toxines bij veroudering van de proximale tubuluscel en nierfibrose

(met een samenvatting in het Nederlands)

Proefschrift

ter verkrijging van de graad van doctor aan de
Universiteit Utrecht
op gezag van de
rector magnificus, prof.dr. H.R.B.M. Kummeling,
ingevolge het besluit van het college voor promoties
in het openbaar te verdedigen op

maandag 6 november 2023 des ochtends te 10.15 uur

door

Yi Yang

geboren op 22 april 1993
te Sichuan, China

Promotoren:
Prof. dr. R. Masereeuw
Prof. dr. R. Goldschmeding

Copromotoren:
Dr. M. Mihajlović
Dr. M.J. Janssen

Beoordelingscommissie:
Prof. dr. A. de Bruin
Prof. dr. S. Florquin
Prof. dr. J.J. Molenaar
Dr. F.A.M. Redegeld
Prof. dr. P. Stenvinkel

TABLE OF CONTENTS

Chapter 1

General introduction
and
thesis outline

1. Introduction

Kidney fibrosis leads to kidney failure by an excessive accumulation of extracellular matrix (ECM), which is the common endpoint for a variety of progressive chronic kidney diseases (CKD) [1]. Senescence is a special form of permanent cell cycle arrest, which limits proliferation and is highly related to inflammation and fibrosis. Senescent cells exacerbate these processes by releasing senescence-associated secretory phenotype (SASP) factors, which are of pro-inflammatory and pro-fibrotic nature [2]. Uremic toxins are metabolites that accumulate during kidney disease. Protein-bound uremic toxins (PBUTs) are mostly less than 500 Da, but are poorly removed with kidney dysfunction as they are tightly bound to plasma proteins and can also hardly cross dialyzer membranes [3, 4]. PBUTs, like indoxyl sulfate (IS) and p-cresol sulfate (PCS), accumulate in CKD, maintaining and reinforcing CKD and kidney fibrosis [5, 6]. Recent studies reported that IS and PCS activate the renal RAAS/TGF-β pathway and induce epithelial mesenchymal transition (EMT) [6]. EMT is a common process during fibrosis and concerns the loss of a differentiated epithelial-like state of cells (*e.g.,* cell-to-cell junctions) to acquire a more mesenchymal-like phenotype (*e.g.,* enhanced ECM expression) [7]. Senescence and EMT are both characterised by cells dedifferentiation, loss of epithelial phenotype, cell cycle arrest, and negative effects on surrounding cells [8]. IS triggers senescence [9] and induces EMT with ECM (*i.e.,* α-SMA) deposition [10], which suggests that PBUTs may induce kidney fibrosis by propagating senescence. However, the crosstalk between PBUTs-related fibrosis and senescence-related fibrosis remains unclear. Here, we provide some mechanistic insight into how PBUTs could promote kidney fibrosis by accelerating senescence.

2. The mechanisms of kidney fibrosis

Kidney fibrosis is induced by abnormal accumulation of ECM. It is regarded as a wound healing process, at least, it initiates as the result of a wound healing response. The response is orchestrated by complex activities of different cells, including macrophages and T cells, epithelial cells, myofibroblasts and endothelial cells. Four major phases are involved in this process: 1) primary injury that initiates a fibrotic response, 2) the activation of effector cells triggering the fibrosis signalling (*e.g.,* TGF-β signalling), 3) production of ECM, and 4) deposition of ECM that promotes tissue fibrosis and eventually leads to kidney failure [1].

2.1 Main signalling of fibrosis

Three main signalling pathways are involved in fibrosis, involving transforming growth factor (TGF)-β, wingless/Int (WNT), and yes-associated protein (YAP)/transcriptional coactivator with PDZ-binding motif (TAZ) signalling pathways [11]. TGF-β signals through both canonical (Smad-based) and non-canonical (non-Smad-based) pathways; Smad-based TGF-β signalling plays a central role in the development of renal fibrosis; non-Smad-based profibrotic actions of TGF-β signalling are regulated by interactions with other signalling pathways [12]. The WNT signalling pathway is activated by secreted lipid modified proteins of the WNT family. Activation of WNT signalling stabilizes β-catenin; the nuclear translocation of β-catenin initiates transcription of fibrotic genes such as collagen and fibronectin [13, 14]. YAP and TAZ are major players of the Hippo pathway that is commonly involved in organ development, epithelial homeostasis, tissue regeneration, wound healing and immune modulation; ECM stiffening promotes the nuclear activity of YAP/TAZ, which in turn, promotes development of

a fibrotic cellular phenotype, including an increased expression of connective tissue growth factor (CTGF) and plasminogen activator inhibitor 1 (PAI-1) [15-17]. These three signalling pathways show a cross-talk during fibrosis. Their mechanisms range from modulating the availability of growth factors and the availability of membrane bound receptors to nuclear entry and activation of transcription factors [11]. Recent studies revealed that TGF-β and WNT signalling are also related to senescence [18, 19].

2.2 ECM in kidney fibrosis

The ECM is a non-cellular component of tissue that provides essential structural support for cellular constituents, and acts as an active component in cell signalling. It is composed of water, proteins, and polysaccharides, responsible for cell–cell communication, cell adhesion, and cell proliferation [20, 21]. There are two main types of ECM: interstitial connective tissue matrix (*e.g.,* collagen I and fibronectin) and the basement membrane (*e.g.,* collagen IV and laminins) [22]. Interstitial connective tissue matrix is responsible for tissue structure, while the basement membrane underlies or surrounds most tissues, including epithelial and endothelial tissues, and interact with cells (Figure 1) [22, 23]. Three histologically distinct compartments with a variety of ECMs are affected in kidney fibrosis: the glomeruli, tubulointerstitium, and vasculature (Table 1) [24]. As a result of ECM remodelling, increased deposition of matrix proteins is observed in kidney fibrosis (Table 1).
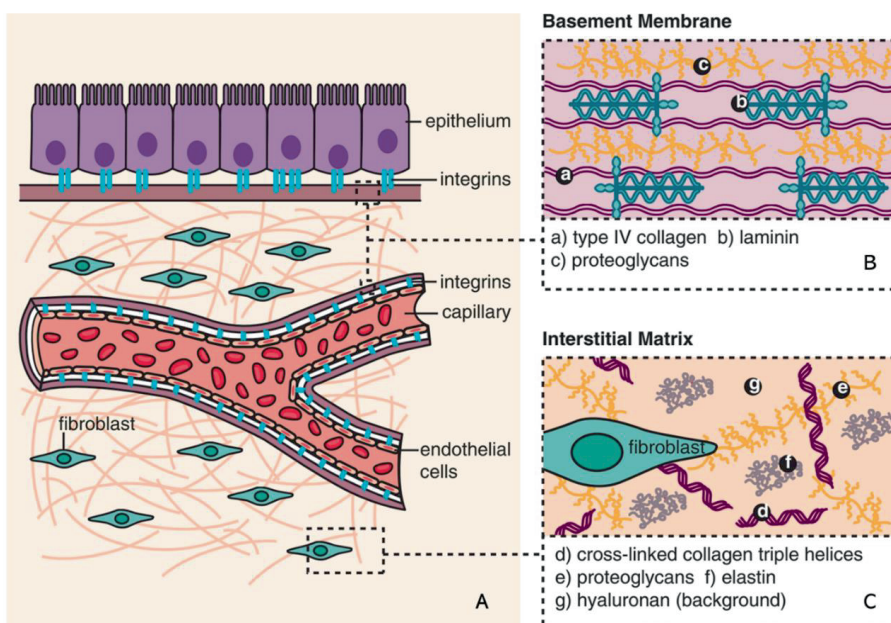

Figure 1. Composition of ECM (adapted from [25]). (A) The basic subdivision of the ECM into (B) basement membrane and (C) interstitial matrix is shown along with major structural components (collagen and elastin), as well as the background matrix made up of proteoglycans and hyaluronan [25].

Table 1. ECM in kidney fibrosis (adapted from [24]).

Compartment	ECM in healthy kidney	Increased ECM in kidney fibrosis
Glomeruli	Mesangial Matrix: collagen IV, V, fibronectin, nidogen, laminin;	Nodular mesangial sclerosis: collagen I, III, IV, V, fibronectin, nidogen, laminin, decorin, biglycan;
	Glomerular basement membrane: collagen I, III, VI, IV, VII, XV, XVII, agrin, perlecan, nidogen, laminin;	Focal segmental glomerulosclerosis: collagen III, IV, heparan sulfate proteoglycans;
	Bowman's capsule: collagen IV, laminins, nidogen, heparan sulfate proteoglycans.	Thickening of glomerular basement membrane: collagen I, III, VI, IV, VII, XV, XVII, perlecan, nidogen, laminin;
		Bowman's capsule: collagen IV and heparan sulfate proteoglycans.
Tubulointerstitium	Tubular basement membrane: collagen IV, agrin, perlecan, laminin;	Thickening of tubular basement membrane: collagen IV, perlecan;
	Interstitium: collagen I, II, III, V, VI, VII, XV, fibronectin, biglycan, decorin, versican;	Interstitial fibrosis: collagen I, II, III, V, VI, VII, XV, fibronectin, biglycan, decorin, ersican;
	Capillary basement membrane: N/A.	Thickening and multilayering of capillary basement membrane: N/A.
Vasculature	Intima with internal elastic lamina: elastin, perlecan, agrin, collagen XVIII, versican, biglycan, decorin;	Neointima: Versican, collagen XVIII, agrin, perlecan;
	Media with external elastic lamina: collagen I, III, XVII, elastin, agrin, perlecan, decorin, verslcan;	Intima with internal elastic lamina: elastin, perlecan, agrin, collagen XVIII, versican;
	Adventitia: collagen I, III, fibronectin, elastin.	Media with external elastic lamina: elastin, collagen XVII, agrin, perlecan, versican;
		Perivascular fibrosis (Thickening of adventitia): N/A.

2.3 ECM remodelling

ECM remodelling is referred to as a balance between degradation and production of ECM. When the balance is disrupted [24], a positive feedback loop resulting in increased ECM production drives the development of fibrosis [26]. The cleavage of ECM by different proteases is the main process during the remodelling, and includes matrix metalloproteinases (MMPs), adamalysins, meprins and metalloproteinase inhibitors (reviewed in REF. [22]).

MMPs are the main enzymes involved in ECM degradation and remodelling. MMPs can cleave ECM components and activate other MMPs and proteins. Various cytokines (interleukin [IL], tumor necrosis factor [TNF]) and growth factors (epidermal growth factor [EGF], transforming growth factor [TGF]) may be involved in the gene expression of MMPs at the transcription level [27]. Adamalysins include a disintegrin and metalloproteinases (ADAMs) and ADAMs

with a thrombospondin motif (ADAMTS); Adamalysins contain twenty-one ADAM, and nineteen ADAMTS proteins, responsible for shedding of various substrates, including adhesion ligands, growth factors and their receptors, and cytokines [28]. Meprins are the only astacin proteinases that can be bound to membranes or secreted as soluble factors; meprin subunits cleave a variety of biologically active peptides, many cytokines and chemokines, leading to an alteration in biological function/activity of those factors/proteins [29]. Tissue inhibitors of metalloproteinases (TIMP) are endogenous inhibitor of MMPs and adamalysins. Each TIMP specifically binds to their target MMPs or adamalysins, regulating the deposition of various ECM components (e.g., collagens, fibronectin and laminins), and the shedding of growth factors and cytokines [30].

3. Senescence

Senescence is a special form of permanent cell cycle arrest, which limits cellular proliferation. It was first reported as a loss of replicative capacity in cultured human fibroblasts in 1961 [31]. Senescent cells are currently regarded as a potentially important contributor to different types of diseases [32], including aging-related diseases [33], kidney [34] and pulmonary disease [35]. Generally, senescent cells can be cleared by immune cells, through chemo-attracting of immune cells, followed by tissue regeneration, which is called acute (short-term) senescence; while chronic (long-term) senescent cells are associated with disease, which accumulate and create a lesion, aggravating the pathology [36, 37]. Major types of senescence are highlighted as replicative senescence (RS) , oncogene-induced senescence (OIS), and stress-induced (premature) senescence (SIS) (Figure 2). RS links to telomere shortening that is associated with cell division. This type of senescence is a consequence of activating a DNA-damage response (DDR), which is induced by short telomeres through the induction of the cell cycle inhibitor p21, arresting proliferation [38-41]. OIS refers to cell cycle arrest by aberrant activation of oncogenic signalling, which promotes the initiation and development of cancer [42]. OIS can be caused by numerous oncogenes including constitutively active variants in the RAS/MAPK pathway (RAS-induced senescence, RIS) as well as in the PI3K/AKT pathway (AKT-induced senescence, AIS), the former undergoes a DDR, while the later is independent of DDR [43]. SIS appears after exposing cells to chemical or physical stresses, including radiation waves, hydrogen peroxide and chemotherapeutic agents [44], leading to cellular stress, increased reactive oxygen species (ROS) generation and subsequent DNA damage, eventually contributing to senescence [37, 44].
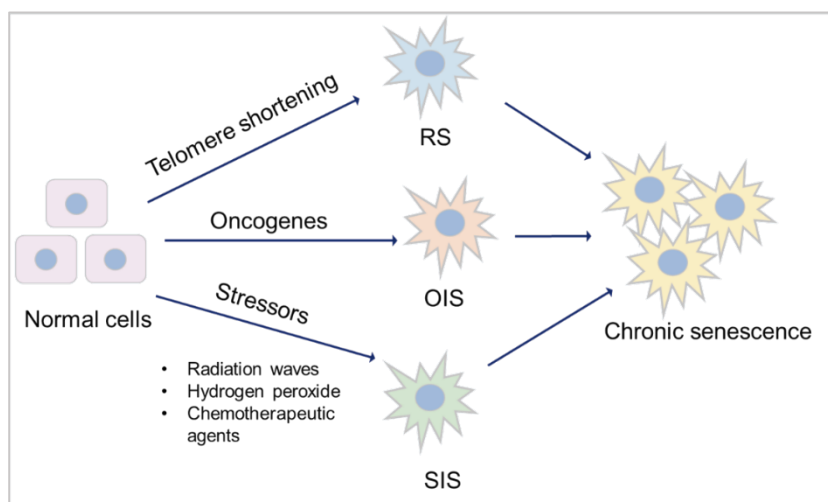
Figure 2. Major types of senescence. Three main types of senescence are identified. Replicative senescence (RS) links to telomere shortening that is associated with cell division. Oncogene-induced senescence (OIS) refers to cell cycle arrest by aberrant activation of oncogenic signalling, which promotes the initiation and development of cancer. Stress-induced (premature) senescence (SIS) appears after exposing cells to chemical or physical stresses. Accumulation of long-term senescent cells leads to chronic senescence.

3.1 Mechanisms of senescence

As discussed, senescence is triggered by various stressors including DNA damage, mitochondrial dysfunction, metabolism and cell stress [2, 45, 46]. Most of them accompany the DDR outcomes, followed by activation of the cell cycle arrest and the release of SASP factors [47, 48].

3.1.1 Cell cycle arrest

Cell cycle arrest in senescence is largely mediated via the p53/p21$^{CIP1/WAF1}$ (p21) and p16^{Ink4a} (p16)/pRb checkpoint pathways controlled by DDR [49, 50], which are independent processes in senescence induction. p53/p21 is activated when DDR occurs, promoting a p21-dependent G0/G1 cell-cycle arrest [51, 52]. p16 suppresses Retinoblastoma 1 (pRb), and prevents the action of the cyclin dependent kinases, which induces a G1 cell cycle arrest [53]. Acute DNA damage drives cell cycle arrest via the p53/p21 pathway, while chronic DNA damage followed by the induction of the p16/pRb pathway maintains cell cycle arrest and senescence [54]. As a key mediator of cell cycle arrest, some studies also demonstrated that p21 can be upregulated via a p53-independent mechanism [55, 56]. Checkpoint signalling pathways are associated to p53-mediated apoptosis [57]. During DDR, the abnormal expression of p53 may further lead to apoptosis resistance.

3.1.2 Apoptosis resistance

Senescent cells are resistant to apoptosis [58], via intrinsic and extrinsic pathways. The intrinsic pathway refers to the mitochondrial pathway of apoptosis, related to mitochondrial outer

membrane permeabilization (MOMP) [59]. In this pathway, MOMP and the release of cytochrome c are required to trigger apoptosis, and involve Bcl-2 and caspase family proteins [60, 61]. The Bcl-2 family is divided into three main groups: anti-apoptotic (Bcl-2, Bcl-xl, and Mcl-1), pro-apoptotic (Bax and Bak), and pro-apoptotic BH3-only (Bim, Bid, Bad and Puma) proteins [62]. The balance between Bcl-2 family members of the pro-apoptotic and anti-apoptotic determines the threshold in MOMP for apoptosis. Caspase proteins are downstream players of MOMP in the intrinsic apoptosis pathway [63]. After the activation of Bax-Bak-dependent MOMP, cytochrome c is released from the mitochondria stimulating the activation of caspase-9 and its downstream executioners, caspases-3 and -7 to initiate apoptosis[61]. The extrinsic pathway is initiated via death receptors that bind death ligands secreted by other cells (*e.g.,* macrophages and natural killer cells), activating caspase-8 and its downstream executioner caspases-3 to initiate apoptosis [59]. Natural ligands, including TNF, Fas-L and TRAIL, are known to bind to their receptors TNFR1, TNFR2, Fas and TRAIL-R to activate caspase-8 [64]. Caspase-8 activation can lead to cleavage of Bid to tBid and initiates the mitochondria-mediated intrinsic apoptosis pathway [59]. Accumulation of dysfunctional mitochondria in senescent cells has been reported [65]. Senescent cells are in a primed apoptotic state, triggered by the abnormal regulation of anti-apoptotic and pro-apoptotic bcl-2 family proteins, keeping cells alive without undergoing proliferation or apoptosis [66]. SASP factors, such as TNF-α [67, 68], released from senescent cells also play a role in the extrinsic apoptosis pathway. This kind of regulation finally inhibits the activation of executioner caspase-3, leading to apoptosis resistance and chronic senescence.

3.1.3 SASP factors

SASP factors are related to a DDR and are generally proinflammatory and/or profibrotic compounds, including numerous cytokines, chemokines, growth factors, and matrix-metalloproteinases (MMPs) [2, 69]. Several reports described that SASP factors are not only responsible for the maintenance and reinforcement of senescence, but also key players during its transmission [70]. Cytokines, such as IL-6 and IL-8, are well proven to play such critical role in stress-induced senescence [71-73]. IL-6 maintains senescence through the p53/p21 pathway [74, 75]. This role of IL-6 in senescence is shared by IL-8, which is expressed as a function of IL-6 [72]. Both cytokines are regulated by IL-1α [76]. Nucleotide-binding oligomerization domain (NOD)-like receptor 3 (NLRP3) inflammasome is upregulated in senescence, which leads to expression of IL-1α and IL-1β, resulting the upregulation of SASP factors and reinforcing paracrine senescence [77]. Chemokine signalling is also reported as being responsible for reinforcing growth arrest by the CXCR2 receptor and CXCR2-binding chemokines [71]. Chemokines including CCLs and CXCLs are involved in stress(radiation)-induced senescence, thus leading to fibrosis [78].Chemokine signalling also plays a role in oncogene-induced senescence; senescent cells increase the survival of cancer cells via CXCL12/CXCR4 signalling, leading the collective invasion in thyroid cancer [79]. Growth factors like CTGF and TGF-β induce senescence and are accompanied with the upregulation of IL-6 and IL-8, thus reinforcing paracrine senescence [80, 81]. TGF-β induces CTGF expression through activation of Smad3 and p53 [82, 83], inducing cell cycle arrest and contributing to senescence [84]. Accumulation of MMPs is also observed in senescence [85]. MMPs shed ectodomains of cell surface receptors and activate other SASP factors, thus promoting paracrine senescence [86].

3.2 Senescence and fibrosis

Senescence contributes to fibrosis in multiple organs [87-89] and is considered to be a result of the release of SASP factors and the pathways triggered by them (Figure 3). TGF-β signalling controls cell proliferation and survival, regulating apoptosis and senescence [84], and initiates fibrosis through the canonical Smad signalling and Smad-independent signalling pathways, with subsequent ECM deposition [90]. CTGF has been shown to contribute to TGF-β signalling through the extracellular signal-regulated kinase (ERK), ADAM17, ribosomal S6 kinases 1 (RSK1) and CCAAT/enhancer-binding protein β (C/EBPβ) signalling pathway in human lung epithelial cells [82, 91]. CTGF is necessary for the TGF-β induced phosphorylation of Smad1 and Erk1/2, but it is not needed for the activation of the Smad3 pathway [92]. Proinflammatory mediators like IL-6 and IL-1β are also involved in fibrosis. IL-6 shifts acute inflammation into a chronic fibrosis state by regulating MMPs and the TGF-β pathway [93, 94]. IL-1β augments TGF-β1-induced EMT through MAPK signalling pathways [95], which may be dependent on IL-17A [96]. MMPs release ectodomains of cell surface receptors and activate other SASP factors [86], thus regulating ECM production and promoting EMT and kidney fibrosis [22]. Other SASP factors like CCL2 and PAI-1 are also important players in fibrosis, exerting their effect through chemokine and TGF-β signalling, respectively [97, 98].
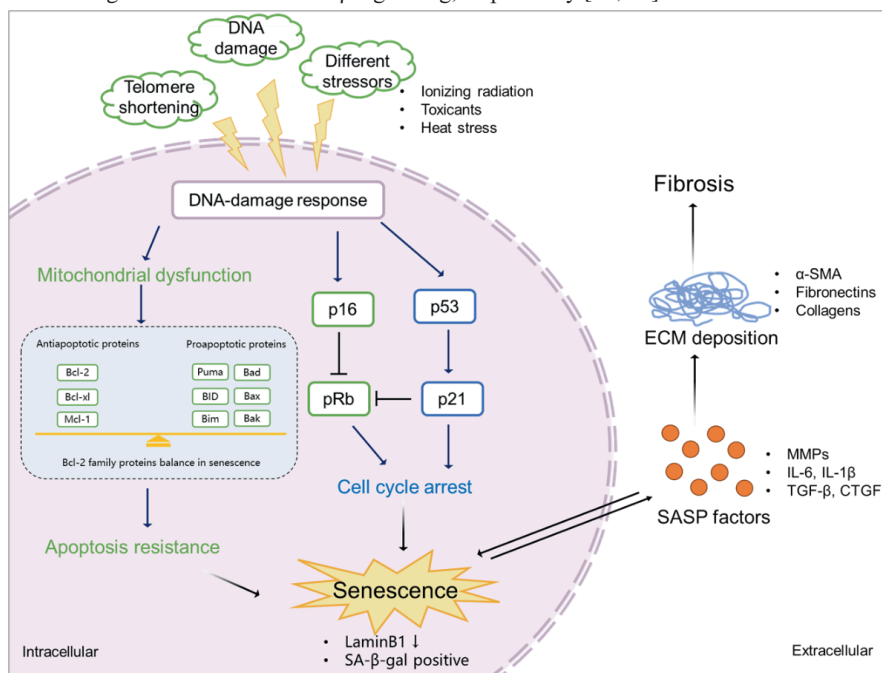
Figure 3. The mechanism of senescence in kidney fibrosis. Senescence is initiated by various stimulations (*e.g.* ionizing radiation, exposure to toxicants, and heat stress), which triggers DDR. This, on the one hand, induces mitochondrial dysfunction, resulting in abnormal expression of Bcl-2 family proteins, eventually leading to apoptosis resistance and promotion of senescence. On the other hand, DDR mediates cell cycle arrest via p53/ p21 and p16/pRb checkpoint pathways, which also results in senescence. Senescent cells show a downregulation of LaminB1 and SA-β-gal. SASP factors, including profibrotic markers (TGF-β and CTGF), proinflammatory markers (IL-6 and IL-1β), and ECM remodelling proteases (MMPs) expressed by senescent cells promote ECM deposition (α-SMA, fibronectins and collagens), finally leading to kidney fibrosis.

4. Protein-bound uremic toxins: drivers of senescence and kidney fibrosis

Uremic toxins are endogenous metabolites that are being excreted into the urine through glomerular filtration and active transport by the proximal epithelial cells [99]. In kidney disease, uremic toxins management is compromised, which leads to systemic accumulation of the toxins and activation of inflammation and oxidative stress. Furthermore, uremic toxins can induce profibrotic effects, promoting progression of kidney damage [100]. Uremic toxins are divided in three distinct groups: 1) small-water soluble compounds (molecular weight <500 Da, *e.g.* creatinine, urea and uric acid); 2) middle molecules (peptides with molecular weight >500 Da, *e.g.* IL-6, IL-8 and TNF-α); and 3) protein bound uremic toxins (PBUTs; molecular weight mostly <500 Da, *e.g.* indoxyl sulfate, p-cresyl sulfate and p-cresol)[99, 101]. Small-water soluble compounds are hydrophilic, which pass through the glomerular barrier and can be removed easily by dialysis [102, 103]. Most of middle molecules are peptides and difficult to remove in the process of dialysis unless the dialyzer pore size is large enough [104]. PBUTs are removed by proximal tubule cells in healthy kidneys through active secretion involving transporter proteins, but poorly removed with kidney dysfunction [105]. the current dialysis therapy is limited, because the high binding to plasma proteins, with albumin being the primary carrier protein, and only a small free fraction is available for transfer across dialyzer membranes [3, 4].

PBUTs accumulate systemically but also in kidney tissue where they can induce oxidative stress and stimulate production of inflammatory factors, which might be a trigger for fibrosis [106]. PBUTs induce ROS production and enhance oxidative stress and IL-1β (SASP) expression in kidney proximal tubule cells [107]. Furthermore, it has been reported that PBUTs induce TGF-β and WNT signalling that promote ECM remodelling [108, 109]. IS and PCS induce EMT by activating the renal TGF-β signalling [6], and contribute to ECM remodelling by upregulating MMP2 and MMP9 in an EGF receptor-dependent manner [110]. As discussed, TGF-β and WNT signalling are also related to senescence [18, 19], which might suggest that PBUTs can be drivers of senescence and kidney fibrosis.

5. Hypothesis: Protein-bound uremic toxins promote fibrosis by accelerating senescence

Kidney failure is accompanied with PBUTs accumulation [103, 111], which leads to ECM remodelling and fibrosis [26]. In turn, PBUTs accumulation promotes kidney disease and fibrosis by oxidative stress and inflammation [106]. The accumulation of PBUTs occurs in a time- and stage-dependent manner during CKD. As the loss of kidney function in CKD is progressive and irreversible, advanced CKD has more severe uremic toxin plasma levels [5] that can potentially induce senescence [9, 112]. Chronic senescence promoted by external factors (*e.g.* ionizing radiation, exposure to toxicants, or heat stress) may develop in a time-dependent manner [113-115]. This suggests that PBUTs may also promote senescence time-dependently during CKD, progressing the disease and reinforcing fibrosis (Figure 4). In CKD animal models, it was shown that the accumulation of PBUTs correlated to fibrosis outcome and/or senescence phenotype (Table 2). We, therefore, hypothesize that PBUTs may promote kidney fibrosis by accelerating senescence, possibly via mitochondrial dysfunction, cell cycle arrest, and the production of SASP factors.

Table 2. Overview of CKD animal models that reported PBUTs accumulation, fibrosis outcome, or senescence phenotype.

CKD model	Species	PBUTs	Fibrosis/EMT markers	Senescence markers/ SASP factors	Invloved pathways/mechanism	Reference
Aristolochic acids-induced	Mouse	PCS, IS	α-SMA, collagen I, α-1 and IV	NR	TGF-β Signalling	[116]
Adenine-induced	Mouse	NR	Collagen (masson staining)	p21, Il-6, and Il-1β	chronic inflammation	[117]
5/6 nephrectomy	Rat	NR	Collagen (masson staining)	TNF-α, IL1β, and IL-6	p38 MAPK/NF-κB signalling pathway	[118]
Ischemia-reperfusion injury	Mouse	NR	Collagen (masson staining), fibronectin and α-SMA	SA–β-gal, p16, p19, p53, p21, MMP-7, PAI-1 and TGF-β1	WNT and TGF-β Signalling	[18]
Adenine-induced	Mouse	PCS, IS, and hippuric acid	Collagen (masson staining) and α-SMA	NR	gut microbiota	[119]
IS-injected mouse and unilateral nephrectomy	Mouse	IS	ZO-1, occludin,claudin-1, and claudin-2	TNF-α, IL-1β and IL-6	mitochondrial dysfunction and mitophagy impairment	[120]
Adenine-induced	Mouse	IS	α-SMA, E-cadherin, and collagen I	TNF-α and IL-6	mTOR activation	[121]
Adenine-induced	Rat	IS	fibronectin, collagen I, α-SMA, vimentin, and E-cadherin	NR	EMT	[122]
Unilateral ureteral obstruction (UUO)	Mouse	IS	Collagen (masson staining), α-SMA, collagen I, fibronectin, vimentin, and E-cadherin	TGF-β1	EMT	[123]
Adenine-induced	Rat	PCS, IS, hippuric acid，p-cresyl glucuronide, and indol-3-acetic acid	NR	TGF-β1	TGF-β Signalling	[124]
Adenine-induced	Mouse	PCS	NR	TNF-α and IL-6	NLRP3 inflammasome pathway	[125]
Adenine-induced	Mouse	PCS, IS and p-cresyl glucuronide	collagen α-1 type 1	TGF-β1, TNF-α, MCP-1 and IL-6	production of uremic toxins, and inflammation	[126]
Unilateral nephrectomy	Mouse	PCS	NR	p38 and IL-1β	Oxidative Stress and inflammation	[127]
5/6 nephrectomy	Rat	Hippuric acid	α-SMA, vimentin, and collagen I	MMP9 and TIMP1	Oxidative Stress and TGF-β Signalling	[108]

NR – Not Reported.

5.1 PBUTs accelerate senescence via mitochondrial dysfunction?

Different types of senescence have been reported to have increased ROS and mitochondrial dysfunction [65], which influences intrinsic apoptosis pathway by abnormal expression of Bcl-2 family and caspase family markers, which in turn, maintain and reinforce senescence [128]. Overproduction of ROS during cell stress leads to mitochondrial dysfunction after kidney injury [129], which is promoted by PBUTs accumulation [130]. A cocktail of PBUTs, consisting of IS, PCS, indoxyl-β-glucuronide, p-cresyl glucuronide, indol-3-acetic acid, hippuric acid, kynurenic acid, and l-kynurenine, have shown to promote ROS production and to upregulate IL-6 in proximal tubule epithelial cells [107, 131]. In addition, ROS-induced senescence was shown to require mammalian target of rapamycin (mTOR) activation [132], and accumulated IS promoted renal fibrosis via mTOR under CKD conditions [121]. Furthermore, the class I phosphoinositide 3-kinase (PI3K) signalling regulates and activates mTOR [133]. PCS activates NADPH oxidase through a mechanism that involves the PI3K signalling, inducing ROS production and TGF-β1 secretion [134]. PBUTs, like IS, PCS and hippuric acid influenced apoptosis by causing an imbalance of caspase-3, caspase-9, Bcl-2, and Bax in hepatocytes, with marked ROS generation and mitochondrial damage [135]. Although there is a lack of evidence showing that PBUTs inhibit apoptosis, IS and PCS increased the expression of the anti-apoptotic genes Bcl-2, Bcl-xl and Bax in proximal tubule cells [136], which is also observed in senescent cells [58, 115].

5.2 PBUTs accelerate senescence via cell cycle arrest?

Cell cycle arrest is necessary for the repair of DNA damage after injury [137], which generally occurs in senescence and is a critical factor for fibrosis development [138]. DDR is a cause of cell cycle arrest mediated by the p53/p21 and p16/pRb pathways [48]. ROS triggers DDR and DDR promotes ROS production by activating its downstream effectors, including p53 and p21 [139]. Recent research have suggested that PBUTs may accelerate senescence via cell cycle arrest and inhibition of cell proliferation [140]. Others have suggested that PCS and IS upregulate p21 and increase senescence-associated beta-galactosidase positive cells [9]. IS also promotes p53 expression, stimulating the expression of TGF-β1 and ECM deposition [141].

5.3 PBUTs accelerate senescence via SASP factors?

During CKD progression, the inflammatory (SASP) factors released activate different pathways and initiate various processes, including senescence and EMT in tubular epithelial cells [142]. As discussed, PBUTs accumulation-induced inflammation might be one reason for senescence development. SASP factors like IL-6, TGF-β1 and CXCL10 were reported to be increased in proximal tubule cells after the treatment with the PBUTs IS and PCS [136]. Furthermore, ROS overproduction can activate the NLRP3 inflammasome, which cleaves pro-caspase-1 and pro-interleukin-1β (IL-1β) into the proinflammatory factors caspase-1 and IL-1β, thus promoting fibrosis [143]. The NLRP3 inflammasome/ IL-1β have also been shown to promote cellular senescence [144]. SASP factors reinforce senescence and induce senescence transmission or paracrine senescence, which is regulated by the inflammasome [77]. Therefore, PBUTs may play an important role during CKD to promote paracrine senescence and senescence transmission.
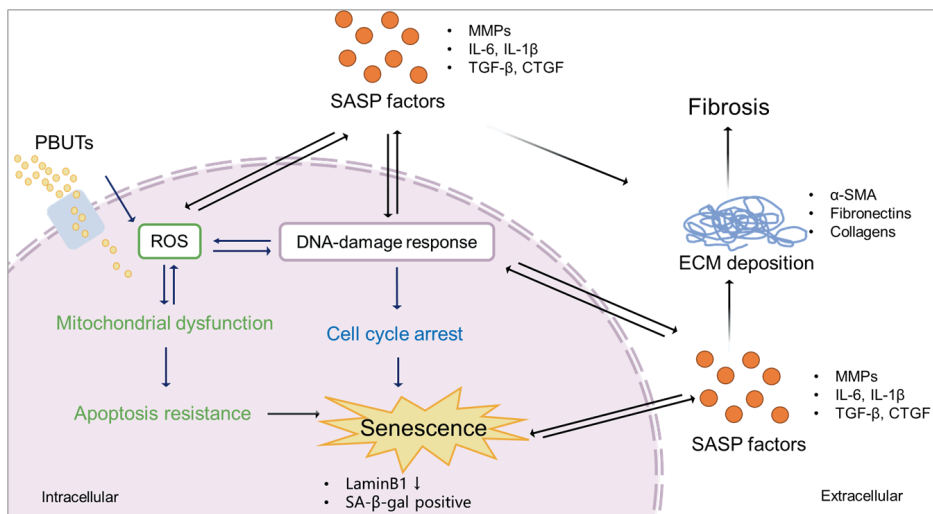
1

Figure 4. Proposed scheme of PBUTs promoting kidney fibrosis by accelerating senescence. After reaching the cells, PBUTs promote ROS production, triggering DDR and mitochondrial dysfunction, inducing apoptosis inhibition, cell cycle arrest and the production of SASP factors, thus promoting senescence. Senescent cells show a downregulation of LaminB1 and SA-β-gal activity. SASP factors expressed by senescent cells promote ECM deposition, leading to kidney fibrosis.

6. Aim and outline of this thesis

PBUTs may play an important role during CKD to promote paracrine senescence and senescence transmission. Recently, our lab set up a cell model, a conditionally immortalized proximal tubule epithelial cell line overexpressing the organic anion transporter 1 (ciPTEC-OAT1), that is a promising platform for highly predictive drug screening during early phases of drug development [145, 146]. Several PBUTs can induce proximal tubular injury via OAT1-mediated uptake [147]. ciPTEC-OAT1 could be a potential model for studying the effects of PBUTs in kidney tubule epithelial cells. The aim of the thesis was to investigate the role that PBUTs play in the development of senescence by using ciPTEC-OAT1 as an experimental model, to acquire novel insights that could aid in the development of novel strategies for CKD.

In **Chapter 2**, we investigated whether ciPTEC-OAT1 could be a valid *in vitro* model for mechanistic research on kidney senescence and the response to senolytics.

In **Chapter 3**, the effect of PBUTs on the NLRP3 inflammasome-mediated IL-1β production in ciPTEC-OAT1 and in CKD rats was evaluated. IL-1β is one of the well-known SASP factors and its production indicates that PBUTs exposure may lead to senescence in CKD. To further examine this, in **Chapter 4**, we investigated whether IS as prototypical PBUT induces senescence in ciPTEC-OAT1. Furthermore, transcriptome analysis was employed to acquire more insights into the underlying mechanisms.

Targeting senescent cells by using senolytics is a potential treatment for CKD. In **Chapter 5**, preliminary experiments were performed to study the uptake of senolytics in ciPTEC-OAT1 and a strategy was designed to synthesize senolytic-lysozyme conjugates as the first step towards a targeted delivery of the drugs.

Finally, in **Chapter 6**, a summary and discussion of the main findings of this thesis are presented, and a future perspective is provided.

1

Reference

1. Rockey, D.C., P.D. Bell, and J.A. Hill, Fibrosis--a common pathway to organ injury and failure. N Engl J Med, 2015. 372(12): p. 1138-49.
2. Hernandez-Segura, A., J. Nehme, and M. Demaria, Hallmarks of Cellular Senescence. Trends Cell Biol, 2018. 28(6): p. 436-453.
3. Masereeuw, R., The Dual Roles of Protein-Bound Solutes as Toxins and Signaling Molecules in Uremia. Toxins (Basel), 2022. 14(6).
4. Maheshwari, V., et al., Removal of Protein-Bound Uremic Toxins Using Binding Competitors in Hemodialysis: A Narrative Review. Toxins (Basel), 2021. 13(9).
5. Nigam, S.K. and K.T. Bush, Uraemic syndrome of chronic kidney disease: altered remote sensing and signalling. Nat Rev Nephrol, 2019. 15(5): p. 301-316.
6. Sun, C.Y., S.C. Chang, and M.S. Wu, Uremic toxins induce kidney fibrosis by activating intrarenal renin-angiotensin-aldosterone system associated epithelial-to-mesenchymal transition. PLoS One, 2012. 7(3): p. e34026.
7. Singh, M., et al., EMT: Mechanisms and therapeutic implications. Pharmacol Ther, 2018. 182: p. 80-94.
8. Faheem, M.M., et al., Convergence of therapy-induced senescence (TIS) and EMT in multistep carcinogenesis: current opinions and emerging perspectives. Cell Death Discov, 2020. 6: p. 51.
9. Kamprom, W., et al., P-cresol and Indoxyl Sulfate Impair Osteogenic Differentiation by Triggering Mesenchymal Stem Cell Senescence. Int J Med Sci, 2021. 18(3): p. 744-755.
10. Kim, S.H., et al., Indoxyl sulfate-induced epithelial-to-mesenchymal transition and apoptosis of renal tubular cells as novel mechanisms of progression of renal disease. Lab Invest, 2012. 92(4): p. 488-98.
11. Piersma, B., R.A. Bank, and M. Boersema, Signaling in Fibrosis: TGF-beta, WNT, and YAP/TAZ Converge. Front Med (Lausanne), 2015. 2: p. 59.
12. Meng, X.M., D.J. Nikolic-Paterson, and H.Y. Lan, TGF-beta: the master regulator of fibrosis. Nat Rev Nephrol, 2016. 12(6): p. 325-38.
13. Rim, E.Y., H. Clevers, and R. Nusse, The Wnt Pathway: From Signaling Mechanisms to Synthetic Modulators. Annu Rev Biochem, 2022. 91: p. 571-598.
14. Tan, R.J., et al., Wnt/β-catenin signaling and kidney fibrosis. Kidney Int Suppl (2011), 2014. 4(1): p. 84-90.
15. Dey, A., X. Varelas, and K.L. Guan, Targeting the Hippo pathway in cancer, fibrosis, wound healing and regenerative medicine. Nat Rev Drug Discov, 2020. 19(7): p. 480-494.
16. Liu, F., et al., Mechanosignaling through YAP and TAZ drives fibroblast activation and fibrosis. Am J Physiol Lung Cell Mol Physiol, 2015. 308(4): p. L344-57.
17. Zhao, B., et al., TEAD mediates YAP-dependent gene induction and growth control. Genes Dev, 2008. 22(14): p. 1962-71.
18. Luo, C., et al., Wnt9a Promotes Renal Fibrosis by Accelerating Cellular Senescence in Tubular Epithelial Cells. J Am Soc Nephrol, 2018. 29(4): p. 1238-1256.
19. Tominaga, K. and H.I. Suzuki, TGF-β Signaling in Cellular Senescence and Aging-Related Pathology. Int J Mol Sci, 2019. 20(20).
20. Genovese, F., et al., The extracellular matrix in the kidney: a source of novel non-invasive biomarkers of kidney fibrosis? Fibrogenesis & tissue repair, 2014. 7(1): p. 4 %@ 1755-1536.
21. Frantz, C., K.M. Stewart, and V.M. Weaver, The extracellular matrix at a glance. J Cell Sci, 2010. 123(Pt 24): p. 4195-200.
22. Bonnans, C., J. Chou, and Z. Werb, Remodelling the extracellular matrix in development and disease. Nat Rev Mol Cell Biol, 2014. 15(12): p. 786-801.
23. Jayadev, R. and D.R. Sherwood, Basement membranes. Curr Biol, 2017. 27(6): p. R207-R211.
24. Bulow, R.D. and P. Boor, Extracellular Matrix in Kidney Fibrosis: More Than Just a Scaffold. J Histochem Cytochem, 2019. 67(9): p. 643-661.
25. Ariza de Schellenberger, A., et al., The Extracellular Matrix as a Target for Biophysical and

Molecular Magnetic Resonance Imaging, in Quantification of Biophysical Parameters in Medical Imaging, I. Sack and T. Schaeffter, Editors. 2018, Springer International Publishing: Cham. p. 123-150.

26. Herrera, J., C.A. Henke, and P.B. Bitterman, Extracellular matrix as a driver of progressive fibrosis. J Clin Invest, 2018. 128(1): p. 45-53.

27. Peng, W.J., et al., Matrix metalloproteinases: a review of their structure and role in systemic sclerosis. J Clin Immunol, 2012. 32(6): p. 1409-14.

28. Przemyslaw, L., et al., ADAM and ADAMTS family proteins and their role in the colorectal cancer etiopathogenesis. BMB Rep, 2013. 46(3): p. 139-50.

29. Aan, G.J., et al., Differences in protein changes between stress-induced premature senescence and replicative senescence states. Electrophoresis, 2013. 34(15): p. 2209-17.

30. Khokha, R., A. Murthy, and A. Weiss, Metalloproteinases and their natural inhibitors in inflammation and immunity. Nat Rev Immunol, 2013. 13(9): p. 649-65.

31. Hayflick, L. and P.S. Moorhead, The serial cultivation of human diploid cell strains. Experimental cell research, 1961. 25(3): p. 585-621

32. He, S. and N.E. Sharpless, Senescence in Health and Disease. Cell, 2017. 169(6): p. 1000-1011.

33. Childs, B.G., et al., Cellular senescence in aging and age-related disease: from mechanisms to therapy. Nat Med, 2015. 21(12): p. 1424-35.

34. Docherty, M.H., et al., Cellular Senescence in the Kidney. J Am Soc Nephrol, 2019. 30(5): p. 726-736.

35. Wang, Z.N., et al., Potential Role of Cellular Senescence in Asthma. Front Cell Dev Biol, 2020. 8: p. 59.

36. Kobbe, C.v., Targeting senescent cells: approaches, opportunities, challenges. Aging 2019. 11: p. 18.

37. Munoz-Espin, D. and M. Serrano, Cellular senescence: from physiology to pathology. Nat Rev Mol Cell Biol, 2014. 15(7): p. 482-96.

38. Marcotte R, W.E., Replicative Senescence Revisited. The Journals of Gerontology Series A: Biological Sciences and Medical Sciences, 2002. 57(7): p. B257-B269.

39. d'Adda di Fagagna, F., et al., A DNA damage checkpoint response in telomere-initiated senescence. Nature, 2003. 426(6963): p. 194-8.

40. Herbig, U., et al., Telomere shortening triggers senescence of human cells through a pathway involving ATM, p53, and p21(CIP1), but not p16(INK4a). Mol Cell, 2004. 14(4): p. 501-13.

41. Rossiello, F., et al., Telomere dysfunction in ageing and age-related diseases. Nat Cell Biol, 2022. 24(2): p. 135-147.

42. Liu, X.L., J. Ding, and L.H. Meng, Oncogene-induced senescence: a double edged sword in cancer. Acta Pharmacol Sin, 2018. 39(10): p. 1553-1558.

43. Zhu, H., et al., Oncogene-induced senescence: From biology to therapy. Mech Ageing Dev, 2020. 187: p. 111229.

44. Suzuki, M. and D.A. Boothman, Stress-induced premature senescence (SIPS)--influence of SIPS on radiotherapy. J Radiat Res, 2008. 49(2): p. 105-12.

45. Chaib, S., T. Tchkonia, and J.L. Kirkland, Cellular senescence and senolytics: the path to the clinic. Nat Med, 2022.

46. Krizhanovsky, R.S.a.V., Cell Senescence, DNA Damage, and Metabolism. Antioxidants & Redox Signaling, 2021. 34(4): p. 324-334.

47. Huang, W., et al., Cellular senescence: the good, the bad and the unknown. Nat Rev Nephrol, 2022.

48. Jackson, S.P. and J. Bartek, The DNA-damage response in human biology and disease. Nature, 2009. 461(7267): p. 1071-8.

49. Kumari, R. and P. Jat, Mechanisms of Cellular Senescence: Cell Cycle Arrest and Senescence Associated Secretory Phenotype. Front Cell Dev Biol, 2021. 9: p. 645593.

50. Mijit, M., et al., Role of p53 in the Regulation of Cellular Senescence. Biomolecules, 2020. 10(3).

51. Ceccaldi, R., et al., Bone marrow failure in Fanconi anemia is triggered by an exacerbated

p53/p21 DNA damage response that impairs hematopoietic stem and progenitor cells. Cell Stem Cell, 2012. 11(1): p. 36-49.

52. Ou, H.L. and B. Schumacher, DNA damage responses and p53 in the aging process. Blood, 2018. 131(5): p. 488-495.

53. Rayess, H., M.B. Wang, and E.S. Srivatsan, Cellular senescence and tumor suppressor gene p16. Int J Cancer, 2012. 130(8): p. 1715-25.

54. Sperka, T., J. Wang, and K.L. Rudolph, DNA damage checkpoints in stem cells, ageing and cancer. Nat Rev Mol Cell Biol, 2012. 13(9): p. 579-90.

55. Ruan, B., et al., NVP-BEZ235 inhibits thyroid cancer growth by p53-dependent/independent p21 upregulation. Int J Biol Sci, 2020. 16(4): p. 682-693.

56. Zhang, Y., et al., DNMT3a plays a role in switches between doxorubicin-induced senescence and apoptosis of colorectal cancer cells. Int J Cancer, 2011. 128(3): p. 551-61.

57. Pietenpol, J. and Z. Stewart, Cell cycle checkpoint signaling: Cell cycle arrest versus apoptosis. toxicology, 2002. 181: p. 475-481.

58. Childs, B.G., et al., Senescence and apoptosis: dueling or complementary cell fates? EMBO Rep, 2014. 15(11): p. 1139-53.

59. D'Arcy, M.S., Cell death: a review of the major forms of apoptosis, necrosis and autophagy. Cell Biol Int, 2019. 43(6): p. 582-592.

60. Ngoi, N.Y.L., et al., Targeting Mitochondrial Apoptosis to Overcome Treatment Resistance in Cancer. Cancers (Basel), 2020. 12(3).

61. Van Opdenbosch, N. and M. Lamkanfi, Caspases in Cell Death, Inflammation, and Disease. Immunity, 2019. 50(6): p. 1352-1364.

62. Anantram, A. and M. Degani, Targeting cancer's Achilles' heel: role of BCL-2 inhibitors in cellular senescence and apoptosis. Future Med Chem, 2019. 11(17): p. 2287-2312.

63. Shalini, S., et al., Old, new and emerging functions of caspases. Cell Death Differ, 2015. 22(4): p. 526-39.

64. Carneiro, B.A. and W.S. El-Deiry, Targeting apoptosis in cancer therapy. Nat Rev Clin Oncol, 2020. 17(7): p. 395-417.

65. Korolchuk, V.I., et al., Mitochondria in Cell Senescence: Is Mitophagy the Weakest Link? EBioMedicine, 2017. 21: p. 7-13.

66. Fan, Y., et al., Senescent Cell Depletion Through Targeting BCL-Family Proteins and Mitochondria. Front Physiol, 2020. 11: p. 593630.

67. Guo, Q., et al., Tumor Necrosis Factor-alpha (TNF-α) Enhances miR-155-Mediated Endothelial Senescence by Targeting Sirtuin1 (SIRT1). Med Sci Monit, 2019. 25: p. 8820-8835.

68. Li, P., et al., The inflammatory cytokine TNF-α promotes the premature senescence of rat nucleus pulposus cells via the PI3K/Akt signaling pathway. Scientific Reports, 2017. 7(1): p. 42938.

69. Birch, J. and J. Gil, Senescence and the SASP: many therapeutic avenues. Genes Dev, 2020. 34(23-24): p. 1565-1576.

70. Kuilman, T. and D.S. Peeper, Senescence-messaging secretome: SMS-ing cellular stress. Nat Rev Cancer, 2009. 9(2): p. 81-94.

71. Acosta, J.C., et al., Chemokine signaling via the CXCR2 receptor reinforces senescence. Cell, 2008. 133(6): p. 1006-18.

72. Kuilman, T., et al., Oncogene-induced senescence relayed by an interleukin-dependent inflammatory network. Cell, 2008. 133(6): p. 1019-31.

73. You, K., et al., Moderate hyperoxia induces senescence in developing human lung fibroblasts. Am J Physiol Lung Cell Mol Physiol, 2019. 317(5): p. L525-l536.

74. Li, Y., et al., Interleukin-6 Knockout Inhibits Senescence of Bone Mesenchymal Stem Cells in High-Fat Diet-Induced Bone Loss. Front Endocrinol (Lausanne), 2020. 11: p. 622950.

75. Effenberger, T., et al., Senescence-associated release of transmembrane proteins involves proteolytic processing by ADAM17 and microvesicle shedding. FASEB J, 2014. 28(11): p. 4847-56.

76. Orjalo, A.V., et al., Cell surface-bound IL-1alpha is an upstream regulator of the senescence-associated IL-6/IL-8 cytokine network. Proc Natl Acad Sci U S A, 2009.

106(40): p. 17031-6.

77. Acosta, J.C., et al., A complex secretory program orchestrated by the inflammasome controls paracrine senescence. Nat Cell Biol, 2013. 15(8): p. 978-90.

78. Su, L., et al., Potential role of senescent macrophages in radiation-induced pulmonary fibrosis. Cell Death Dis, 2021. 12(6): p. 527.

79. Kim, Y.H., et al., Senescent tumor cells lead the collective invasion in thyroid cancer. Nat Commun, 2017. 8: p. 15208.

80. Jun, J.I. and L.F. Lau, CCN2 induces cellular senescence in fibroblasts. J Cell Commun Signal, 2017. 11(1): p. 15-23.

81. Fan, C., et al., TGF-β induces periodontal ligament stem cell senescence through increase of ROS production. Mol Med Rep, 2019. 20(4): p. 3123-3130.

82. Ou, S.C., et al., TGF-β Induced CTGF Expression in Human Lung Epithelial Cells through ERK, ADAM17, RSK1, and C/EBPβ Pathways. Int J Mol Sci, 2020. 21(23).

83. Li, X., et al., DsbA-L mediated renal tubulointerstitial fibrosis in UUO mice. Nat Commun, 2020. 11(1): p. 4467.

84. Zhang, Y., P.B. Alexander, and X.F. Wang, TGF-beta Family Signaling in the Control of Cell Proliferation and Survival. Cold Spring Harb Perspect Biol, 2017. 9(4).

85. Wang, X.-H., et al., GATA4 promotes the senescence of nucleus pulposus cells via NF-κB pathway. Archives of Gerontology and Geriatrics, 2022. 101: p. 104676.

86. Levi, N., et al., The ECM path of senescence in aging: components and modifiers. FEBS J, 2020. 287(13): p. 2636-2646.

87. Hernandez-Gonzalez, F., et al., Cellular Senescence in Lung Fibrosis. Int J Mol Sci, 2021. 22(13).

88. Zhang, M., et al., Hepatic stellate cell senescence in liver fibrosis: Characteristics, mechanisms and perspectives. Mech Ageing Dev, 2021. 199: p. 111572.

89. Chen, M.S., R.T. Lee, and J.C. Garbern, Senescence mechanisms and targets in the heart. Cardiovasc Res, 2022. 118(5): p. 1173-1187.

90. Kim, K.K., D. Sheppard, and H.A. Chapman, TGF-β1 Signaling and Tissue Fibrosis. Cold Spring Harb Perspect Biol, 2018. 10(4).

91. Yanagihara, T., et al., Connective-Tissue Growth Factor Contributes to TGF-β1-induced Lung Fibrosis. Am J Respir Cell Mol Biol, 2022. 66(3): p. 260-270.

92. Nakerakanti, S.S., A.M. Bujor, and M. Trojanowska, CCN2 is required for the TGF-β induced activation of Smad1-Erk1/2 signaling network. PLoS One, 2011. 6(7): p. e21911.

93. Fielding, C.A., et al., Interleukin-6 signaling drives fibrosis in unresolved inflammation. Immunity, 2014. 40(1): p. 40-50.

94. Epstein Shochet, G., et al., TGF-β pathway activation by idiopathic pulmonary fibrosis (IPF) fibroblast derived soluble factors is mediated by IL-6 trans-signaling. Respir Res, 2020. 21(1): p. 56.

95. Zhang, S., et al., IL-1β augments TGF-β inducing epithelial-mesenchymal transition of epithelial cells and associates with poor pulmonary function improvement in neutrophilic asthmatics. Respir Res, 2021. 22(1): p. 216.

96. Wilson, M.S., et al., Bleomycin and IL-1beta-mediated pulmonary fibrosis is IL-17A dependent. J Exp Med, 2010. 207(3): p. 535-52.

97. Xu, L., D. Sharkey, and L.G. Cantley, Tubular GM-CSF Promotes Late MCP-1/CCR2-Mediated Fibrosis and Inflammation after Ischemia/Reperfusion Injury. J Am Soc Nephrol, 2019. 30(10): p. 1825-1840.

98. Gifford, C.C., et al., PAI-1 induction during kidney injury promotes fibrotic epithelial dysfunction via deregulation of klotho, p53, and TGF-β1-receptor signaling. Faseb j, 2021. 35(7): p. e21725.

99. Vanholder, R., et al., Review on uremic toxins: classification, concentration, and interindividual variability. Kidney Int, 2003. 63(5): p. 1934-43.

100. Rocchetti, M.T., et al., Protein-Bound Uremic Toxins and Immunity, in Cytotoxic T-Cells: Methods and Protocols, M. Gigante and E. Ranieri, Editors. 2021, Springer US: New York, NY. p. 215-227.

101. Fujii, H., S. Goto, and M. Fukagawa, Role of Uremic Toxins for Kidney,

Cardiovascular, and Bone Dysfunction. Toxins (Basel), 2018. 10(5).

102.   Vanholder, R., et al., Biochemical and Clinical Impact of Organic Uremic Retention Solutes: A Comprehensive Update. Toxins (Basel), 2018. 10(1).

103.   Chen, J.H. and C.K. Chiang, Uremic Toxins and Protein-Bound Therapeutics in AKI and CKD: Up-to-Date Evidence. Toxins (Basel), 2021. 14(1).

104.   Chmielewski, M., et al., The peptidic middle molecules: is molecular weight doing the trick? Semin Nephrol, 2014. 34(2): p. 118-34.

105.   Smith, H.W., The kidney: structure and function in health and disease. 1951: Oxford University Press, USA.

106.   Chao, C.T. and C.K. Chiang, Uremic toxins, oxidative stress, and renal fibrosis: an interwined complex. J Ren Nutr, 2015. 25(2): p. 155-9.

107.   Mihajlovic, M., et al., Protein-Bound Uremic Toxins Induce Reactive Oxygen Species-Dependent and Inflammasome-Mediated IL-1beta Production in Kidney Proximal Tubule Cells. Biomedicines, 2021. 9(10).

108.   Sun, B., et al., Hippuric Acid Promotes Renal Fibrosis by Disrupting Redox Homeostasis via Facilitation of NRF2-KEAP1-CUL3 Interactions in Chronic Kidney Disease. Antioxidants (Basel), 2020. 9(9).

109.   Zhang, H., et al., Indoxyl sulfate accelerates vascular smooth muscle cell calcification via microRNA-29b dependent regulation of Wnt/β-catenin signaling. Toxicol Lett, 2018. 284: p. 29-36.

110.   Sun, C.Y., et al., Protein-bound uremic toxins induce tissue remodeling by targeting the EGF receptor. J Am Soc Nephrol, 2015. 26(2): p. 281-90.

111.   Schafer, M.J., et al., Targeting Senescent Cells in Fibrosis: Pathology, Paradox, and Practical Considerations. Curr Rheumatol Rep, 2018. 20(1): p. 3.

112.   Niwa, T. and H. Shimizu, Indoxyl sulfate induces nephrovascular senescence. J Ren Nutr, 2012. 22(1): p. 102-6.

113.   Fletcher-Sananikone, E., et al., Elimination of Radiation-Induced Senescence in the Brain Tumor Microenvironment Attenuates Glioblastoma Recurrence. Cancer Res, 2021. 81(23): p. 5935-5947.

114.   Hu, X. and H. Zhang, Doxorubicin-Induced Cancer Cell Senescence Shows a Time Delay Effect and Is Inhibited by Epithelial-Mesenchymal Transition (EMT). Med Sci Monit, 2019. 25: p. 3617-3623.

115.   Yang, Y., et al., A Human Conditionally Immortalized Proximal Tubule Epithelial Cell Line as a Novel Model for Studying Senescence and Response to Senolytics. Front Pharmacol, 2022. 13: p. 791612.

116.   Chang, J.F., et al., Therapeutic Targeting of Aristolochic Acid Induced Uremic Toxin Retention, SMAD 2/3 and JNK/ERK Pathways in Tubulointerstitial Fibrosis: Nephroprotective Role of Propolis in Chronic Kidney Disease. Toxins (Basel), 2020. 12(6).

117.   Tolle, M., et al., Uremic mouse model to study vascular calcification and "inflamm-aging". J Mol Med (Berl), 2022. 100(9): p. 1321-1330.

118.   Li, X., et al., Effects of Uremic Clearance Granules on p38 MAPK/NF-κB Signaling Pathway, Microbial and Metabolic Profiles in End-Stage Renal Disease Rats Receiving Peritoneal Dialysis. Drug Des Devel Ther, 2022. 16: p. 2529-2544.

119.   Wang, X., et al., Aberrant gut microbiota alters host metabolome and impacts renal failure in humans and rodents. Gut, 2020. 69(12): p. 2131-2142.

120.   Huang, Y., et al., Indoxyl sulfate induces intestinal barrier injury through IRF1-DRP1 axis-mediated mitophagy impairment. Theranostics, 2020. 10(16): p. 7384-7400.

121.   Nakano, T., et al., Indoxyl Sulfate Contributes to mTORC1-Induced Renal Fibrosis via The OAT/NADPH Oxidase/ROS Pathway. Toxins (Basel), 2021. 13(12).

122.   Chen, C., et al., Yishen-Qingli-Huoxue formula attenuates renal fibrosis by inhibiting indoxyl sulfate via AhR/snai1 signaling. Phytomedicine, 2023. 108: p. 154546.

123.   Hsieh, Y.H., et al., Rosmarinic acid ameliorates renal interstitial fibrosis by inhibiting the phosphorylated-AKT mediated epithelial-mesenchymal transition in vitro and in vivo. Food Funct, 2022. 13(8): p. 4641-4652.

124.   Cai, H., et al., Lindera aggregata intervents adenine-induced chronic kidney disease by

mediating metabolism and TGF-β/Smad signaling pathway. Biomed Pharmacother, 2021. 134: p. 111098.

125.   Kim, H., et al., Lactobacillus acidophilus KBL409 Reduces Kidney Fibrosis via Immune Modulatory Effects in Mice with Chronic Kidney Disease. Molecular Nutrition & Food Research, 2022. 66(22): p. 2101105.

126.   Barba, C., et al., A low aromatic amino-acid diet improves renal function and prevent kidney fibrosis in mice with chronic kidney disease. Sci Rep, 2021. 11(1): p. 19184.

127.   Sun, C.Y., et al., p-Cresol Sulfate Caused Behavior Disorders and Neurodegeneration in Mice with Unilateral Nephrectomy Involving Oxidative Stress and Neuroinflammation. Int J Mol Sci, 2020. 21(18).

128.   Miwa, S., et al., Mitochondrial dysfunction in cell senescence and aging. J Clin Invest, 2022. 132(13).

129.   Zhao, M., et al., Mitochondrial ROS promote mitochondrial dysfunction and inflammation in ischemic acute kidney injury by disrupting TFAM-mediated mtDNA maintenance. Theranostics, 2021. 11(4): p. 1845-1863.

130.   Rossi, M., et al., Protein-bound uremic toxins, inflammation and oxidative stress: a cross-sectional study in stage 3-4 chronic kidney disease. Arch Med Res, 2014. 45(4): p. 309-17.

131.   Mihajlovic, M., et al., Role of Vitamin D in Maintaining Renal Epithelial Barrier Function in Uremic Conditions. Int J Mol Sci, 2017. 18(12).

132.   Correia-Melo, C., et al., Mitochondria are required for pro-ageing features of the senescent phenotype. Embo j, 2016. 35(7): p. 724-42.

133.   Dibble, C.C. and L.C. Cantley, Regulation of mTORC1 by PI3K signaling. Trends Cell Biol, 2015. 25(9): p. 545-55.

134.   Watanabe, H., et al., p-Cresyl sulfate causes renal tubular cell damage by inducing oxidative stress by activation of NADPH oxidase. Kidney Int, 2013. 83(4): p. 582-92.

135.   Deng, M., et al., Short-Chain Fatty Acids Alleviate Hepatocyte Apoptosis Induced by Gut-Derived Protein-Bound Uremic Toxins. Front Nutr, 2021. 8: p. 756730.

136.   Sun, C.Y., H.H. Hsu, and M.S. Wu, p-Cresol sulfate and indoxyl sulfate induce similar cellular inflammatory gene expressions in cultured proximal renal tubular cells. Nephrol Dial Transplant, 2013. 28(1): p. 70-8.

137.   Branzei, D. and M. Foiani, Regulation of DNA repair throughout the cell cycle. Nat Rev Mol Cell Biol, 2008. 9(4): p. 297-308.

138.   Yang, L., et al., Epithelial cell cycle arrest in G2/M mediates kidney fibrosis after injury. Nat Med, 2010. 16(5): p. 535-43, 1p following 143.

139.   Passos, J.F., et al., Feedback between p21 and reactive oxygen production is necessary for cell senescence. Molecular Systems Biology, 2010. 6(1): p. 347.

140.   Li, L., et al., Protein-bound P-cresol inhibits human umbilical vein endothelial cell proliferation by inducing cell cycle arrest at G(0)/G(1). Am J Transl Res, 2017. 9(4): p. 2013-2023.

141.   Shimizu, H., et al., Indoxyl sulfate enhances p53-TGF-β1-Smad3 pathway in proximal tubular cells. Am J Nephrol, 2013. 37(2): p. 97-103.

142.   Humphreys, B.D., Mechanisms of Renal Fibrosis. Annu Rev Physiol, 2018. 80: p. 309-326.

143.   Liu, Y., et al., The NLRP3 inflammasome in fibrosis and aging: The known unknowns. Ageing Research Reviews, 2022. 79: p. 101638.

144.   Romero, A., et al., Pharmacological Blockade of NLRP3 Inflammasome/IL-1β-Positive Loop Mitigates Endothelial Cell Senescence and Dysfunction. Aging Dis, 2022. 13(1): p. 284-297.

145.   Wilmer, M.J., et al., Novel conditionally immortalized human proximal tubule cell line expressing functional influx and efflux transporters. Cell Tissue Res, 2010. 339(2): p. 449-57.

146.   Nieskens, T.T., et al., A Human Renal Proximal Tubule Cell Line with Stable Organic Anion Transporter 1 and 3 Expression Predictive for Antiviral-Induced Toxicity. Aaps j, 2016. 18(2): p. 465-75.

147.   Motojima, M., et al., Uraemic toxins induce proximal tubular injury via organic anion transporter 1-mediated uptake. British Journal of Pharmacology, 2002. 135(2): p. 555-563.

Chapter 2

A Human Conditionally Immortalized Proximal Tubule Epithelial Cell Line as a Novel Model for Studying Senescence and Response to Senolytics

Yi Yang[1], Milos Mihajlovic[1], Floris Valentijn[2], Tri Q. Nguyen[2], Roel Goldschmeding[2] and Rosalinde Masereeuw[1]

[1]Utrecht Institute for Pharmaceutical Sciences, div. Pharmacology, Utrecht, The Netherlands.

[2]University Medical Center Utrecht, Dept. Pathology, Utrecht, The Netherlands.

Abstract

Accumulating evidence suggests that senescence of kidney tubule epithelial cells leads to fibrosis. These cells secrete senescence-associated secretory phenotype (SASP) factors that are involved in diverse signalling pathways, influencing kidney fibrosis. Here, we investigated whether our previously established conditionally immortalized proximal tubule epithelial cell line overexpressing the organic anion transporter 1 (ciPTEC-OAT1) can be used as a valid in vitro model to study kidney senescence and senolytics response. CiPTEC-OAT1 proliferates rapidly at 33°C and exhibits a "senescence-like" arrest at 37°C, most likely due to suppression of SV40T expression and subsequent reactivation of the p53 and Rb pathways. To understand how permissive (33°C) and non-permissive (37°C) temperatures of the cell culture affect the senescence phenotype, we cultured ciPTEC-OAT1 for up to 12 days and evaluated the apoptosis and SASP markers. Day 0 in both groups is considered as the non-senescence group (control). Further, the potential of navitoclax, dasatinib, quercetin, and the combination of the latter two to clear senescent cells was evaluated. Maturation of ciPTEC-OAT1 at non-permissive temperature affected mRNA and protein levels of senescence markers. A remarkable upregulation in p21 gene expression was found in the non-permissive temperature group, whereas expression of Lamin B1 decreased significantly. SASP factors, including PAI-1A, IL-1β, CTGF, and IL-6 were upregulated, but no significant difference in Bcl-2 and Bcl-xl were found in the non-permissive temperature group. After culturing ciPTEC-OAT1 up to 12 days, cells in the non-permissive temperature group showed an upregulation in the apoptosis-associated proteins Bcl-2, BID, and Bax, and a downregulation in Mcl-1, Bad, Bak, and Bim at various time points. Further, Bcl-xl, Puma, Caspase 3, Caspase 7, and Caspase 9 showed initial upregulations followed by downregulations at later time points. The loss of Lamin B1, upregulation of SA-β-gal expression and increase in its activity, upregulation of p21 levels and downregulation of p53, along with the upregulation of SASP factors, confirmed that maturation at 37°C promotes senescence features. Finally, the senolytics response was evaluated by testing cell viability following exposure to senolytics, to which cells appeared dose-dependently sensitive. Navitoclax was most effective in eliminating senescent cells. In conclusion, culturing ciPTEC-OAT1 at 37°C induces a senescence phenotype characterized by increased expression of cell cycle arrest and anti-apoptosis markers, SASP factors, and responsiveness to senolytics treatment. Therefore, ciPTEC-OAT1 represents a valid model for studying kidney senescence by simply adjusting culture conditions.

Keywords: kidney fibrosis, conditionally immortalized proximal tubule epithelial cell, Bcl-2 family proteins, senescence-associated secretory phenotype (SASP), cell cycle arrest, apoptosis

1 Introduction

Renal fibrosis is the common end point for all progressive kidney diseases, which leads to kidney failure by an excessive accumulation of extracellular matrix [1]. Accumulating evidence suggests that senescence of kidney tubule cells influences kidney fibrosis [2]. Senescence is a special form of permanent cell cycle arrest, which limits cellular proliferative life span. Some senescent cells can be cleared by immune cells, termed acute (short-term) senescent cells, while chronic (long-term) senescent cells keep accumulating and creating early senescence events, finally aggravating the pathology [3, 4]. Different hallmarks of senescence have been recognized which are involved in diverse signalling pathways, including apoptosis markers, senescence-associated secretory phenotype (SASP) factors, and cyclin-dependent kinase inhibitors [5].

Senescent cells show resistance to apoptosis [6] and accumulate dysfunctional mitochondria [7]. Mitochondrial outer membrane permeabilization (MOMP) is responsible for apoptosis in numerous cell death pathways [8]. In the intrinsic apoptosis pathway, Bcl-2 and the caspase family proteins play important roles [9, 10]. The Bcl-2 family is divided into three main groups: anti-apoptotic (Bcl-2, Bcl-xl, and Mcl-1), pro-apoptotic (Bax and Bak), and pro-apoptotic BH3-only (Bim, Bid, Bad, and Puma) [11]. Senescent cells are known to be in a primed apoptotic state, triggered by the abnormal upregulation of anti-apoptotic and pro-apoptotic proteins [12]. Caspase family proteins are downstream players of MOMP in the intrinsic apoptosis pathway [13], and after the activation of the Bax-Bak-dependent MOMP, cytochrome C is released from the mitochondria stimulating caspase-9 activation and its downstream executioners, caspases-3 and -7, to initiate apoptosis [9].

Cell cycle arrest is another typical characteristic of senescent cells, which is largely mediated through activation of either one or both p53/p21$^{CIP1/WAF1}$ (p21) and p16^{Ink4a} (p16)/pRb pathways [14]. p53/p21 is activated during DNA damage response, resulting in a p21-dependent G0/G1 cell-cycle arrest [15, 16]. On the other hand, p16 inactivates Retinoblastoma 1 (pRb) thereby inhibiting the action of the cyclin dependent kinases, leading to G1 cell cycle arrest [17]. Both p53/p21 and p16/pRb pathways are independent in senescence induction. Acute DNA damage causes a cell cycle arrest via the p53/p21 pathway, while chronic DNA damage followed by the induction of the p16/pRB pathway maintains cell cycle arrest and senescence [18]. As a key mediator of cell-cycle arrest, p21 also shows a p53-independent upregulation according to some research [19, 20]. Furthermore, p53 is also involved in the apoptosis process, as described previously [16, 21].

SASP factors are related to a DNA damage response and are generally proinflammatory and/or profibrotic compounds including numerous cytokines (e.g., IL-6 and IL-8), growth factors (e.g., TGF-β and CTGF), chemokines (e.g., CCL2), and matrix-metalloproteinases (e.g., MMP-1 and MMP-3) [5, 22]. Those proteins induce or maintain senescence through different pathways, contributing to kidney fibrosis [23]. Current efforts are focused on clearing senescent cells as a treatment option for prevention of kidney fibrosis development and progression. Senolytics represent a good option as they can selectively eliminate senescent cells participating in senescence associated pathways by interfering with anti- and pro-survival signaling [24]. However, suitable cell models are required to evaluate senescence development in kidney

tubule epithelial cells and their response to senolytics.

We previously developed a conditionally immortalized proximal tubule epithelial cell line overexpressing the organic anion transporter 1 (ciPTEC-OAT1) and applied it successfully for pharmacological and toxicological investigations, including drug disposition and interaction studies [25, 26]. OAT1 is a first step in the elimination of organic anions in humans and is responsible for the uptake of many anionic (waste) products in kidney proximal tubules [27]. Since the expression of OAT1 is rapidly lost when culturing (primary) PTEC in vitro, OAT1 was stably expressed in ciPTEC by lentiviral transduction. This cell line now allows prediction of drug-induced nephrotoxicity and drug-drug interactions of organic anions in vitro [26]. OAT1 is also involved in the uptake of uremic toxins, known to participate in the uremic syndrome typical of chronic kidney disease [28]. Since senescence is a key factor contributing to chronic kidney disease, uremic toxins might play a role in this process as well.

CiPTEC was created by means of a temperature sensitive mutant U19tsA58 of SV40 large T antigen (SV40T) and the essential catalytic subunit of human telomerase (hTERT), to keep the characteristics of primary cells [25]. Temperature-sensitive SV40T allows cells to proliferate at the permissive low temperature of 33°C but induces a proliferation block that resembles senescence at a non-permissive temperature of 37°C [25, 29]. The hTERT maintains telomere length, preventing replicative senescence induced by telomere shortening [30]. Some studies already showed a relation between senescence and SV40T conditional models, because both pRb and p53 are activated by SV40T at the non-permissive temperature leading to a senescence-like arrest in the cells [29, 31]. Therefore, we hypothesized that ciPTEC-OAT1 exhibits a senescence phenotype when cultured at non-permissive temperatures that can be used to study senescence development in kidney tubule epithelial cells and their response to senolytics. In the present study, we evaluated apoptosis markers and other common senescence markers in ciPTEC-OAT1 cultured at permissive and non-permissive temperatures at different time points, to investigate whether these cells can be implemented as a valid in vitro model to study kidney senescence. Day 0 in both groups is considered as the non-senescence group (control). Finally, the senolytics response was detected by means of cell viability assessment and senescence-associated β-galactosidase (SA-β-gal) activity.

2 Materials and Methods

2.1 Quantitative Real-Time PCR

CiPTEC-OAT1 cells were seeded into 6-well format plates and grown at 33°C; then half of the plates were transferred to 37°C and cultured for up to 7 d. Afterward, cells were lysed in Trizol (Thermo-Fisher, Massachusetts, United States) followed by 5 min centrifugation at 4°C. After RNA isolation, RNA quantity was determined using Nanodrop 2000 (Thermo-Fisher, Massachusetts, United States). For RNA analysis, a cDNA library was synthesized using 3 μg RNA per sample with SuperScript III reverse transcriptase (Thermo-Fisher, Massachusetts, United States). Samples were mixed with TaqMan Gene Expression Assays (Table 1) and run on a ViiA 7 real-time PCR system (Applied Biosystems, California, United States). TATA-box binding protein (TBP) was used as an internal reference gene. Samples were run in duplicate and H2O samples were used to control for potential contamination of reaction. The ΔΔCT method was used to calculate relative expression levels.

Table 1. Primers used for real-time polymerase chain reaction.

Gene	Taqman Gene Expression Assay
TBP	Hs00427620_m1
Lamin B1	Hs01059210_m1
p21 (CDKN1A)	Hs00355782_m1
CTGF	Hs00170014_m1
PAI-1(SERPINE1)	Hs00167155_m1
IL-1β	Hs01555410_m1
IL-6	Hs00174131_m1
BCL-2	Hs00608023_m1
Bcl-xl (BCL2L1)	Hs00236329_m1

2.2 ciPTEC-OAT1 Maturation Process

CiPTEC-OAT1 were grown and expanded at 33°C. Following the seeding, cells were either kept at a permissive temperature of 33°C or incubated for a desired time up to 12 d at a non-permissive temperature of 37°C. The culture medium and cell lysate were collected on Day 0, 3, 6, 9, and 12, and used for the assessment of senescence markers and phenotype.

The ciPTEC-OAT1 cell line was cultured as reported previously [32]. Briefly, cells were cultured in phenol-red free DMEM-HAM's F12 medium (Gibco, Life Technologies, Paisley, United Kingdom) supplemented with 10% (v/v) fetal calf serum (FCS) (Greiner Bio-One, Alphenaan den Rijn, the Netherlands), 5 μg/ml insulin, 5 μg/ml transferrin, 5 μg/ml selenium, 35 ng/ml hydrocortisone, 10 ng/ml epidermal growth factor (EGF), and 40 pg/ml tri-iodothyronine to form complete culture medium, up to a maximum of 60 passages. Cells were cultured at 33°C and 5% (v/v) CO_2 to allow proliferation. Cells were grown up to 90% confluence at 33°C, then transferred for 7 d or 9 d at 37°C, 5% (v/v) CO_2 for maturation, refreshing the medium every other day.

2.3 Senescence and Senolytics Response

2.3.1 Cell viability Assay

Cell viability was measured using PrestoBlue® cell viability reagent (Thermo Scientific, Vienna, Austria). CiPTEC-OAT1 cells were seeded into 96-well format plates at a density of 63,000 per well, cultured for 24 h at 33°C and matured for 9 d at 37°C. Matured cells (37°C) were exposed to 100-μl medium with different concentrations of navitoclax, dasatinib, quercetin, or dasatnib and quercetin combinations. Senolytics were obtained from MedchemExpress, the Netherlands. All experiments were performed in a 96-well plate setup in triplicate with a minimum of three independent experiments.

2.3.2 SA-β-Gal Staining Assay

CiPTEC-OAT1 cells were seeded into 12-well format plates, grown at 33°C, then transferred to 37°C for maturation and culturing for 9 d. The cells matured at 37°C for 0 d and 9 d were exposed to 1-ml medium with different concentrations of navitoclax, dasatinib, or dasatinib and quercetin combinations. The SA-β-gal-positive cells were detected using Senescence Detection

Kit (ab65351, Abcam, United Kingdom), and evaluated for blue colorization using an optical microscope (200x magnification).

2.4 Western Blot

CiPTEC-OAT1 cells were lysed in ice-cold RIPA Lysis Buffer (Thermo Scientific, Vienna, Austria) for 30 min followed by 20 min centrifugation at 4°C and obtained protein samples were quantified by BCA Protein Assay Kit (Thermo Scientific, Vantaa, Finland). Proteins were loaded and separated on 14–20% acrylamide gradient SDS gels (Bio-Rad Laboratories, Hercules, CA), transferred to PVDF membranes (Bio-Rad Laboratories, Hercules, CA) in appropriate transferring conditions (25V, 7 min). The membranes were blocked in 5% skim milk-TBST for 2 h and incubated with the primary antibody overnight at 4°C and anti-rabbit (1:3000, Dako, P0448, United States) or anti-mouse (1:3,000, Dako, P0260, United States) secondary antibodies for 1 h at room temperature. The membrane was exposed to Clarity Western ECL Blotting Substrate following manufacturer's instructions (Bio-Rad Laboratories, Hercules, CA) then imaged using the ChemiDoc™ MP Imaging System (Bio-Rad Laboratories, Hercules, CA) to detect the protein bands, which were quantified using ImageJ software (version 1.53c, National Institutes of Health, United States).

The following proteins were detected by Western blotting: Bcl-2, Bcl-xl, Mcl-1, Bad, Bak, Bim, BID, Bax, Puma, Caspase-3, Caspase-7, Caspase-9, p53, p21, and β-gal, for which primary antibodies were purchased from Cell Signaling Technology (United Kingdom). LaminB1 primary antibody was purchased from Abcam (United Kingdom). The dilution of all primary antibodies was 1:1000.

2.5 ELISA

Cell culture supernatants were centrifuged for 10 min, 240 x g, 4°C, and stored at −20°C. To determine the concentration of SASP factors in the culture supernatants, the ELISA Kits of IL-6 (88-7066-88, Invitrogen, Carlsbad, CA), IL-8 (88-8086-88, Invitrogen, Carlsbad, CA), CTGF (DY9190-05, R&D System, United Kingdom), TNF-α (88-7346-88, Invitrogen, Carlsbad, CA), and TGF-β1(88-8350-88, Invitrogen, Carlsbad, CA) were used according to the manufacturer's instructions.

2.6 Statistics

All data analysis and statistics were performed using the GraphPad Prism (version 8.3.0; GraphPad software, La Jolla, CA), and expressed as mean ± SEM. For comparison of two groups at different temperature and different time points, two-way ANOVA was used followed by Sidak's multiple comparison test. To compare multiple groups in the same condition, one-way ANOVA was used followed by Dunnett's multiple comparison test. $p < 0.05$ was considered significant. Cell viability was expressed as inhibitory constants at 50% of control viability levels (IC50 values), which were calculated by plotting log senolytics concentration vs. viability following background subtraction. Nonlinear regression with a variable slope constraining the bottom to 0 was used to fit the normalized data. For cell viability at Day 9 compared to Day 0 evaluations at different concentrations, two-way ANOVA was used followed by Sidak's multiple comparison test. For cell viability of increasing concentrations of dasatinib

combined with quercetin compared to dasatinib alone, a two-way ANOVA was used followed by Dunnett's multiple comparisons test.

3 Results

3.1 Growing ciPTEC-OAT1 at Non-Permissive Temperature (37°C) Induces Expression of Senescence-Associated Genes

To understand if non-permissive temperature leads to cellular senescence, we compared expression of several senescence markers on mRNA level after culturing ciPTEC-OAT1 for 7 d at permissive (33°C) and non-permissive temperature (37°C). Compared to the permissive temperature group, no significant difference in the mRNA levels of Bcl-2 and Bcl-xl was observed (Figures 1A,B). On the other hand, a significant upregulation of p21 mRNA levels was found in the non-permissive temperature group compared to the permissive temperature group ($p < 0.0001$; Figure 1C). Furthermore, Lamin B1 mRNA levels decreased when cells were cultured at non-permissive temperature ($p < 0.01$; Figure 1D). SASP factors including PAI-1, IL-1β, CTGF, and IL-6 were all upregulated in the non-permissive temperature group ($p < 0.05$, $p < 0.05$, $p < 0.001$, and $p < 0.05$, respectively; Figure 1E-H).
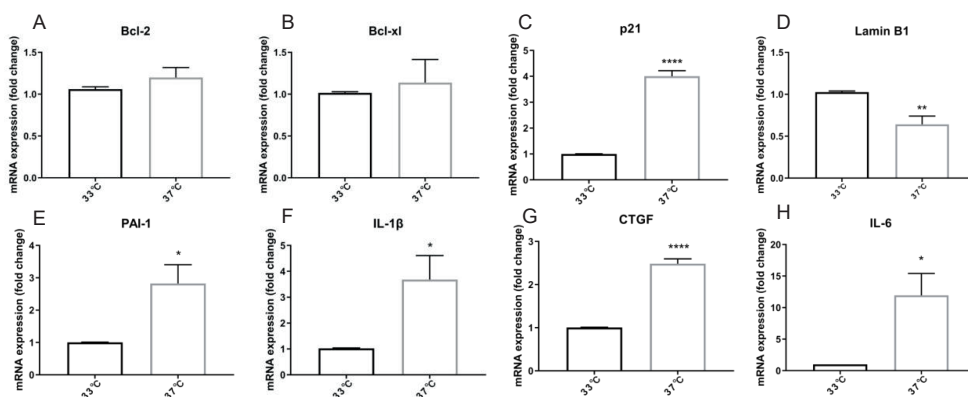

Figure 1. Growing ciPTEC at non-permissive temperature (37°C) induces expression of senescence-associated genes. (A) Bcl-2. (B) Bcl-xl. (C) p21. (D) LaminB1. (E) PAI-1. (F) IL-1β. (G) CTGF. (H) IL-6. Four independent experiments in triplicates were performed. *P<0.05, **P<0.01, and ****P<0.0001 (unpaired t test). For clarity, only one-sided error bars are shown.

3.2 Maturation at Non-Permissive Temperature of 37°C Affects Protein Levels of Apoptosis-Associated Markers in ciPTEC-OAT1

Senescent cells are characterized by an anti-apoptotic profile (Munoz-Espin and Serrano, 2014). To test whether maturation at the non-permissive temperature of 37°C would affect protein levels of apoptosis-associated markers in ciPTEC-OAT1, both anti- (Figures 2A–D) and pro-apoptotic (Figures 2E–P) protein markers were evaluated.

Representative Western blots and quantitative relative expression data indicate that there is an increased expression of Bcl-2 (Figure 2B) over time regardless of the temperature. However, there is a trend of different expression levels between the two temperature conditions at each day. The protein levels of Mcl-1 on the other hand (Figure 2C) decreased with time at all

conditions tested, compared to Day 0, the non-senescence group. Bcl-xl (Figure 2D) levels showed an upregulation at both 33 and 37°C at almost all time points.

With respect to the pro-apoptotic proteins, we observed that all Bcl-2 family members tested, including Puma (Figure 2F), Bax (Figure 2H), BID (Figure 2I), and Bad (Figure 2L) showed an increase at both permissive (33°C) and non-permissive (37°C) groups at different time points. Significant differences in expression levels between 37 and 33°C groups were observed for Bax on Day 3 through Day 12, as well as for Bad on Day 3. Unlike other pro-apoptotic proteins among the Bcl-2 family members, Bim (Figure 2G) showed an upregulation at the permissive temperature at various time points, while an initial upregulation on Day 3 through Day 6 followed by a downregulation on Day 9 and Day 12 at the non-permissive temperature. In addition, the protein levels of Bim at 37°C were lower than at 33°C on Day 9 and Day 12. On the other hand, Bak (Figure 2K) showed an increased expression at 33°C on Day 3 through Day 12, while a decrease in protein levels was observed at 37°C starting from Day 3. For the pro-apoptotic caspases, procaspase-3 (Figure 2N), procaspase-7 (Figure 2O), and procaspase-9 (Figure 2P), we found a non-significant trend for overtime upregulation at a permissive temperature, while at a non-permissive temperature, after an initial upregulation, there was a non-significant trend of downregulation at later time points, starting at Day 3 for procaspases-3 and -9, and at Day 6 for procaspase-7.
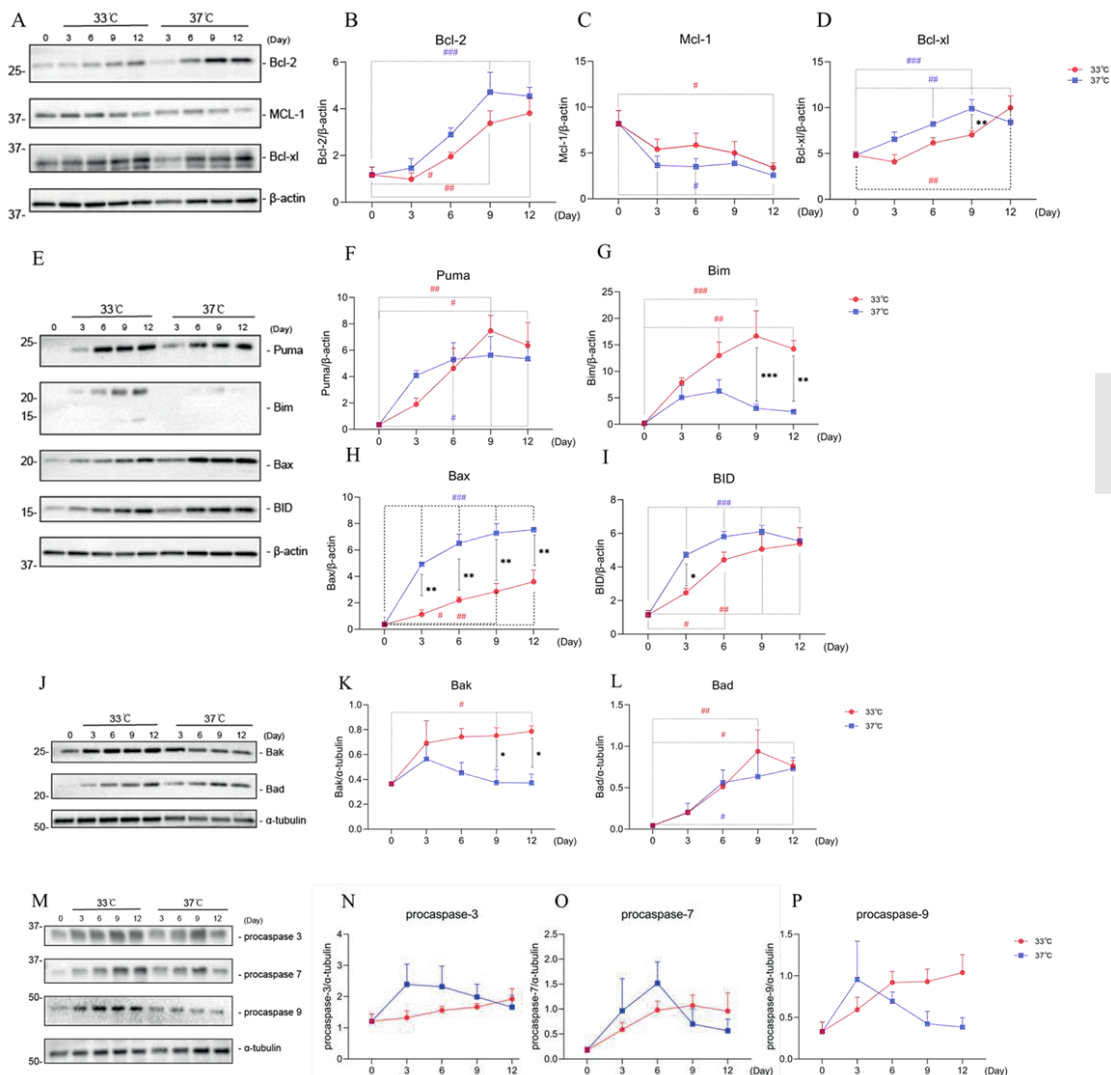
Figure 2. Maturation at non-permissive temperature of 37°C affects protein levels of apoptosis-associated markers in ciPTEC-OAT1. (A) Representative Western blots showing expression of anti-apoptotic proteins Bcl-2, Bcl-xl and Mcl-1 belonging to the Bcl-2 family. (B) (C) and (D) Relative expression of Bcl-2, Bcl-xl and Mcl-1 over time (day 0 to day 12) at both permissive and non-permissive temperatures of 33 °C and 37 °C, respectively. (E) and (J) Representative Western blots of the pro-apoptotic proteins' expression (Puma, Bim, Bax and BID show in E, Bak and Bad shown in J) of Bcl-2 families. (F)-(L) Relative expression levels of Puma, Bim, Bax, BID, Bak and Bad over time at 33 °C and 37 °C. (M) Representative Western blots showing expression of procaspase-3, procaspase-7 and procaspase-9. (N) (O) and (P) Relative expression of procaspase-3, procaspase-7 and procaspase-9 at different time points, at 33 °C and 37 °C. Protein expression levels were normalized against α-tubulin or β-actin and expressed as mean ± SEM. Three independent experiments in triplicates were performed. *P<0.05, **P<0.01, ***P<0.001 (expression levels at 37 °C compared to 33 °C at the same time point; Multiple t-test, Holm-Sidak multiple comparison test). # P<0.05, ## P<0.01, ### P<0.001 (expression levels at day 3, 6, 9 or 12 compared to day 0, at 33 °C or 37 °C; One-way ANOVA, Dunnett's multiple comparison test). For clarity, only one-sided error bars are shown.

3.3 Maturation of ciPTEC-OAT1 at Non-Permissive Temperature Affects Expression Levels of Common Senescence Makers

To further characterize the development of the senescence phenotype in our ciPTEC-OAT1 model, the expression levels of known senescence hallmarks (p53, LaminB1, p21, and β-gal) were evaluated over time at permissive and non-permissive temperatures of 33 and 37°C, respectively [5]. The obtained results suggest that the expression of these markers in ciPTEC-OAT1 is influenced by maturation in non-permissive conditions of 37°C (Figure 3). The total-p53 levels (Figures 3A,C) were markedly upregulated in a time-dependent manner in the proliferation group at 33°C but presented a decreasing trend of expression in the maturation group at 37°C. The expression levels of total-p53 were different on all days tested between the two groups, with higher levels at 33°C. The expression of LaminB1 (Figures 3B,D) showed a non-significant trend of decreased expression especially after longer culture (Days 9 and 12) at both temperatures, with the most evident trend of different expression between the two groups being at Day 9. Furthermore, the results show that p21 levels (Figures 3E,F) were increased at both 33 and 37°C, and that compared to Day 0, p21 was significantly upregulated on Day 12 at 33°C and on Days 3 through 12 at 37°C. In addition, in non-permissive conditions, there was a significant increase of p21 expression compared to permissive temperature at Days 3 and 6. Regarding β-gal (Figures 3E,G), the protein expression levels show an increasing trend at both 33 and 37°C temperatures, there were significant increases of β-gal expression compared to non-senescent cells (Day 0) at Days 3 and 6 at 37°C, with levels being markedly higher at non-permissive compared to permissive conditions at Day 6.
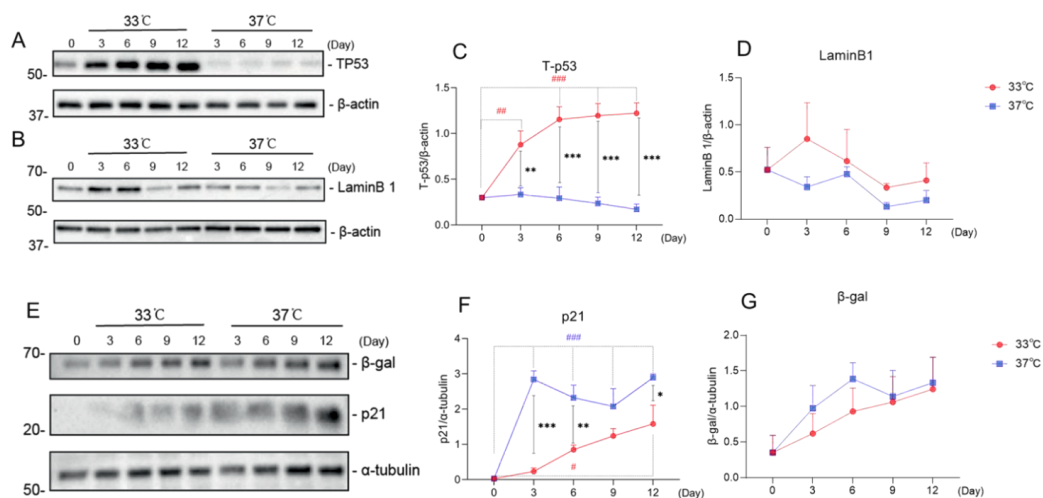
Figure 3. Maturation at non permissive temperature of 37°C affects common senescence markers expression in ciPTEC-OAT1. Representative western blots showing expression of (A) Total-p53 (Tp53), (B) LaminB1, (E) p21 and β-gal. (C), (D), (F) and (G) Relative expression levels of (C) total-p53, (D) LaminB1, (F) p21 and (G) β-gal over time (day 0 to day 12), at both permissive (33 °C) and non-permissive temperatures (37 °C). Protein expression levels were normalized against α-tubulin or β-actin and expressed as mean ± SEM. Three independent experiments in triplicates were performed. *P<0.05, **P<0.01, ***P<0.001 (expression levels at 37 °C compared to 33 °C at the same time point; Multiple t-test, Holm-Sidak multiple comparison test). # P<0.05, ## P<0.01, ### P<0.001 (expression levels at day 3, 6, 9 or 12 compared to day 0, at 33°C or 37°C; One-way ANOVA, Dunnett's multiple comparison test). For clarity, only one-sided error bars are shown.

3.4 Maturation of ciPTEC-OAT1 at Non-Permissive Temperature Induces Common SASP Factors Secretion

As shown in Figure 4, the secretion profile of some typical SASP factors (IL-6, TGF-β1, TNF-α, IL-8, and CTGF) clearly correlate with prolonged culture at 37°C, which is indicative of a senescence phenotype. IL-6 is increasingly secreted (Figure 4A) over time, both at 33 and 37°C culture conditions. The secretion of IL-6 was significantly higher at the non-permissive temperature compared to the permissive temperature at Days 3, 6, and 12. The secreted levels of TGF-β1 did not seem to differ between two culture conditions especially at later time points (Figure 4B). The levels of TNF-α (Figure 4C) were not different over time and between the culture conditions. The secretion profile of IL-8 (Figure 4D) showed a time-dependent increase at both temperature conditions, with a higher trend of expression levels at 37°C compared to 33°C. Finally, the CTGF results (Figure 4E) showed an initial increasing trend in secretion, followed by a trend for reduction and return to basal levels starting from Day 3, at both culture conditions. Compared to the permissive culture conditions, the concentration of CTGF at a non-permissive temperature was slightly higher at all time points.
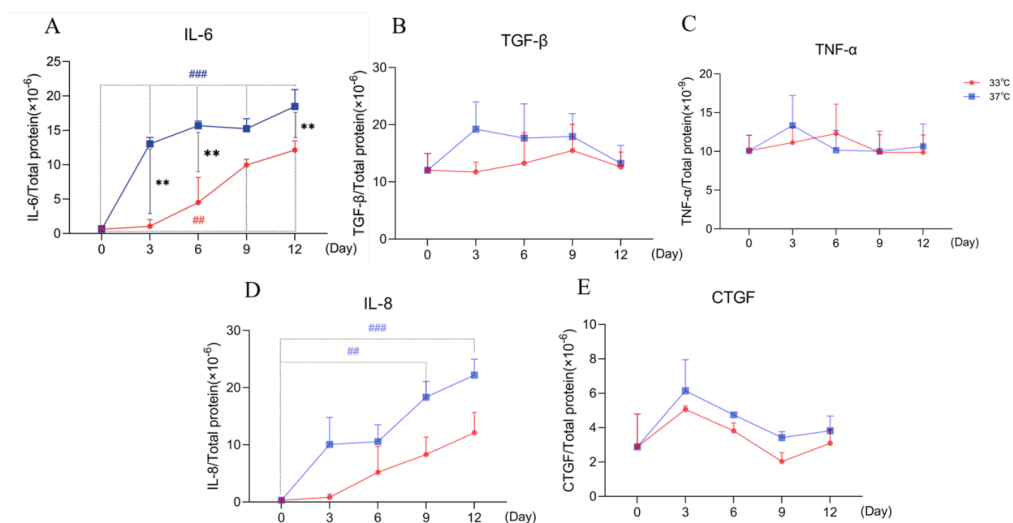
Figure 4. Maturation at non-permissive temperature of 37°C affects common SASP factors secretion by ciPTEC-OAT1. Release of (A) IL-6, (B) TGF-β1, (C) TNF-α, (D) IL-8 and (E) CTGF by ciPTEC-OAT1 over time at 33 °C and 37 °C. Concentration is expressed as pg/ml and normalized for total protein (ug/ml). Three independent experiments were performed in triplicates. *P<0.05, **P<0.01, ***P<0.001 (secreted levels at 37 °C compared to 33 °C at the same time point; Multiple t-test, Holm-Sidak multiple comparison test). # P<0.05, ## P<0.01, ### P<0.001 (secreted levels at day 3, 6, 9 or 12 compared to day 0, at 33 °C or 37 °C; One-way ANOVA, Dunnett's multiple comparison test). For clarity, only one-sided error bars are shown.

3.5 CiPTEC-OAT1 Exhibiting a Senescence-like Phenotype Are Susceptible to Common Senolytics

Our data suggest that ciPTEC-OAT1 cultured progressively in non-permissive conditions obtains a senescence-like phenotype as indicated by some of the most important markers and SASP factors, especially evident after 9 d of culturing. For that reason, this time point was selected to test the effects of senolytics, a class of small molecules that can selectively eliminate senescent cells participating in associated pathways by interfering with anti- and pro-survival signalling pathways [24]. For this, navitoclax, dasatinib, and quercetin were employed to first assess the cell viability after exposures at Day 0 or after 9 d of culture.

As shown in Figure 5; Table 2, quercetin (Figure 5A) did not significantly affect the viability of senescent cells (Day 9 of culture) compared to non-senescent cells (Day 0), while dasatinib (Figure 5B) and navitoclax (Figure 5C) were more effective in selectively reducing the viability of senescent cells at Day 9 compared to Day 0 and therefore can selectively target ciPTEC-OAT1 at a non-permissive temperature. The combination of dasatinib and quercetin (Figure 5D) induced cell death in both culture conditions. The concentrations of quercetin used in this combination treatment are non-toxic to the cells regardless of culture conditions. However, after combining quercetin with increasing concentrations of dasatinib, the viability of the cells reduced compared to each single treatment. Notably, dasatinib combined with the highest quercetin dose appeared the most effective in reducing cell viability. This suggests that the co-treatment of dasatinib and quercetin can selectively target ciPTEC-OAT1 presenting senescence-like phenotype (Figure 5D). IC50 values of different senolytics are lower at Day 9

of cell maturation at a non-permissive temperature compared to 0 d (Table 2). Finally, the cells cultured for 0 or 7 d at 33°C were shown not to be sensitive to navitoclax in contrast to cells cultured at 37°C for 7 d (Supplementary Figure S2), which suggests that the cells are senescent when cultured at 37°C for prolonged time (7 d or more).
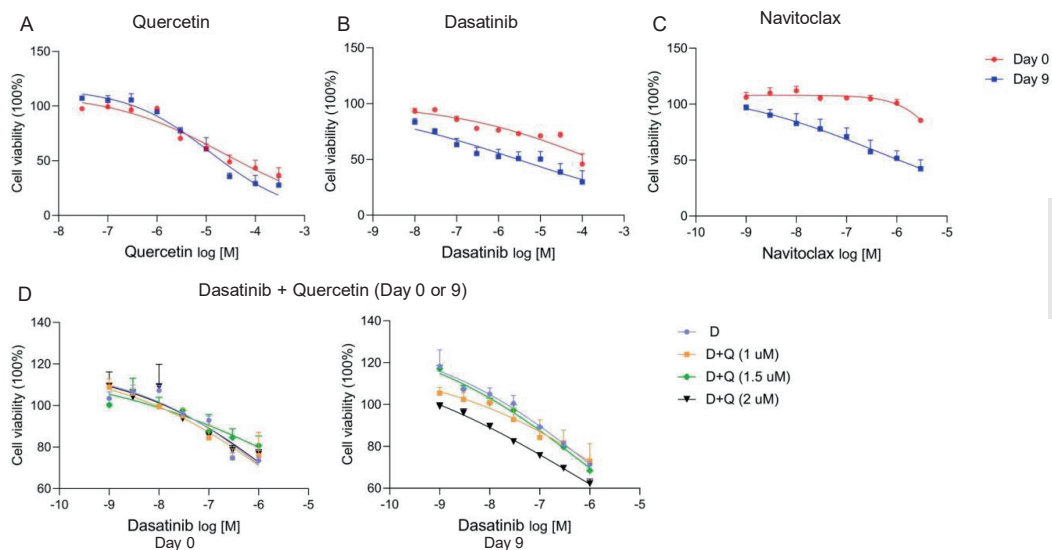

Figure 5. CiPTEC-OAT1 cultured at non-permissive temperature and exhibiting a senescence-like phenotype are susceptible to common senolytics. Cell viability of ciPTEC-OAT1 cultured for 0 or 9 days at non-permissive temperature of 37 °C and exposed to 100 μL medium with increasing concentrations of (A) quercetin (Q), (B) dasatinib (D), and (C) navitoclax (N) for 24 h. Cell viability of ciPTEC-OAT1 cultured for 0 and 9 days (D) at non-permissive temperature end exposed to 100 μL medium with increasing concentrations of dasatinib combined with quercetin (1 μM, 1.5 μM or 2 μM) for 24h. Four independent experiments were performed in triple. Data are presented as mean ± SEM, for which results were normalized to unexposed cells. For clarity, only one-sided error bars are shown.

Table 2. IC50 of (A)-(D) from Figure 5.

IC50	Q	D	N	D(Q=0μM)	D(Q=1μM)	D (Q=1.5μM)	D(Q=2μM)
Day 0	>10 μM	>3μM	>3μM	>3μM	>4μM	>3μM	>4μM
Day 9	>3 μM	>1μM	>0.4μM	>1μM	>6μM	>1μM	>0.7μM

3.6 Senolytics Clear Senescent ciPTEC-OAT1 as Evaluated by Functional SA-β-Gal Expression

The activity of the lysosomal senescence-associated beta-galactosidase (SA-β-gal) is commonly used as a marker for senescent cells, reflecting increased metabolic activity and enhanced lysosomal content typical of these cells [5]. We tested the senolytics for their effect on β-gal activity and expression levels. Representative images of SA-β-gal staining upon culturing are shown in Supplementary Figure S3, which gives an overview of senescence process during the maturation of ciPTEC-OAT1 cells. The results obtained (Figures 6A,B) show that ciPTEC-OAT1 cultured for 9 d at 37°C is positive for SA-β-gal staining and that total

β-gal protein was increased. Moreover, following exposure to navitoclax, the number of SA-β-gal positive cells was reduced in a dose-dependent fashion (Figure 6A). The expression levels of total β-gal showed a downregulation trend in the presence of navitoclax, with a concentration of 100 nM being the most effective (Figures 6C,D). Furthermore, the number of SA-β-gal positive cells was also reduced dose-dependently after the treatment with both dasatinib alone and dasatinib-quercetin combination, which seemed to be slightly more effective than dasatinib alone (Figure 6B), accompanied by a downregulation of total β-gal (Figures 6E,F). Interestingly, although a lower number of SA-β-gal positive cells was observed after the exposure to higher doses of dasatinib-quercetin combination, there were no differences in protein levels in cells cultured for 9 d at the non-permissive temperature.
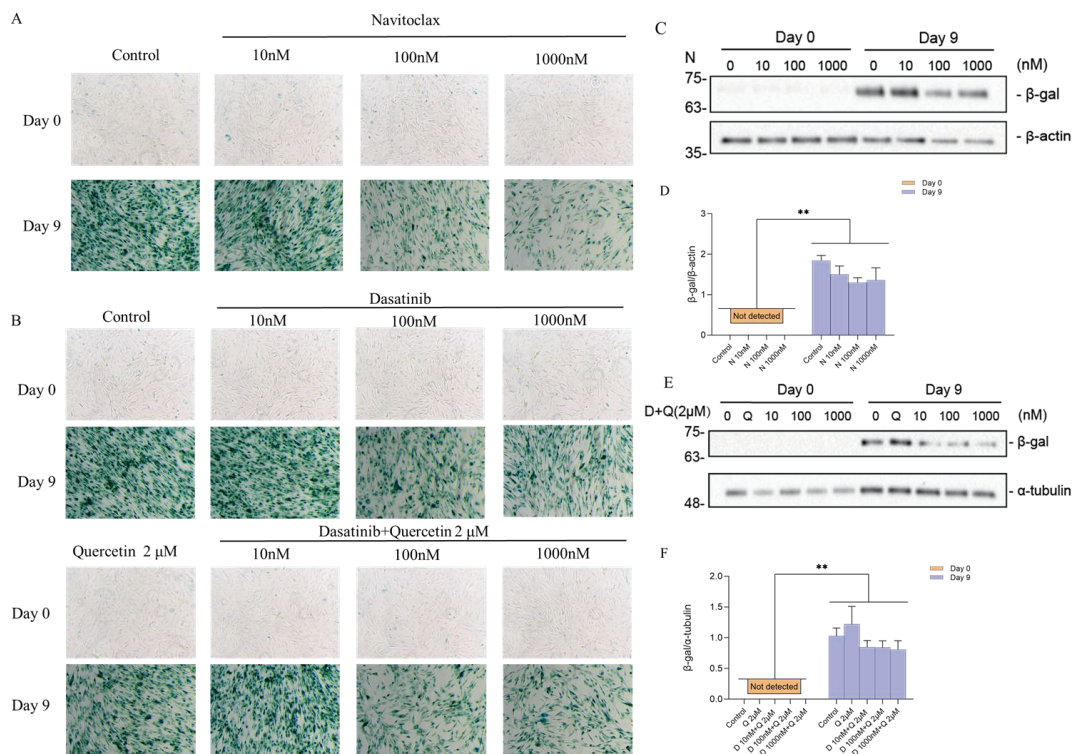

Figure 6. Effects of senolytics on SA-β-gal activity and protein levels in ciPTEC-OAT1 cultured for 9 days at non-permissive temperature. Representative images of SA-β-gal staining in ciPTEC-OAT1 cultured for 0 and 9 days at 37 °C and after 24 h exposure to 1 mL medium with different concentrations of (A) navitoclax (N) (10 nM, 100 nM, or 1000 nM) and (B) dasatinib (D) alone (10 nM, 100 nM, or 1000 nM) or combined with quercetin (Q) 2 μM. (C) Representative western blots showing expression of total β-gal after 24 h exposure to different concentrations of navitoclax in ciPTEC-OAT1 cultured for 0 or 9 days at non-permissive temperature. (D) Relative expression of total β-gal after 24 h exposure to different concentrations of navitoclax. (E) Representative western blots showing expression of total β-gal after 24 h exposure to different concentrations of dasatinib combined with quercetin 2 μM in ciPTEC-OAT1 cultured for either 0 or 9 days at non-permissive temperature. (F) Relative expression of total β-gal after 24 h exposure to different concentrations of dasatinib and quercetin 2 μM. Protein expression levels were normalized to α-tubulin or β-actin, and expressed as mean ± SEM. Three independent experiments were performed in triple. *$P<0.05$, **$P<0.01$, (expression levels at 37 °C compared to 33 °C at the same time point; Multiple t-test, Holm-Sidak multiple comparison test). For clarity, only one-sided error bars are shown.

4 Discussion

Cellular senescence is an irreversible condition with cell cycle arrest, SASP, and apoptosis resistance, which contribute to chronic kidney disease, leading to fibrosis [5, 33]. We previously developed ciPTEC-OAT1 to be used in drug screening and nephrotoxicity studies [26]. In the present study, we demonstrate that the cell model is also suitable for studying tubular senescence in the kidney. We detected differential expression of apoptosis-associated markers, common senescence markers, and some typical SASP factors suggesting that ciPTEC-OAT1 obtains a senescence-like phenotype when cultured at a non-permissive temperature for 9 d. Furthermore, senescent cells appeared sensitive to senolytic drugs.

In the present study, we demonstrated that the ciPTEC-OAT1 cultured at a non-permissive temperature expressed common senescence markers. In particular, the decrease in Lamin B1 [34] and upregulation in p21[35] have been described as characteristic features that are involved in maintaining senescence phenotype by regulating JNK and caspase signalling [36]. Further, increased SASP factors have been reported as proinflammatory and matrix-degrading molecules [37], including PAI-1 [38], IL-1β [39], CTGF [40], and IL-6 [41]. Another feature entails apoptosis, responsible for cell turnover and maintaining extracellular environment. For instance, the Bcl-2 family members modulate the delicate balance between pro- and anti-apoptosis [10]. The upregulations of Bcl-2 and Bcl-xl suggest that ciPTEC-OAT1 became anti-apoptotic upon maturation in both conditions, whereas culturing at 37°C speeds up the process and induces a more prominent senescence phenotype. Senescent cells show downregulation of Mcl-1 on protein levels [42], which is consistent with our findings. Furthermore, the effectors Bax and Bak shuttle between cytosol and mitochondrial outer membrane with different rates [43], which might explain why we observed a differential expression in the proteins. BH3-only proteins bind to the BH3 domain of the anti-apoptotic Bcl-2 proteins via hydrophobic interactions, thereby promoting cellular apoptosis [11]. Of BH3-only proteins, Bid showed higher protein levels at different time points in the maturation group. The increasing trend in all other proteins points toward a priming of cells to undergo apoptosis, but the execution of the death program is restrained. These findings are in line with previous reports showing that following senescence induction by ionizing radiation, senescent cells upregulate pro-apoptosis markers [44, 45]. Therefore, cellular senescence in our model with an upregulation of pro-apoptotic markers despite having an anti-apoptotic phenotype argues for cells searching for a new balance to maintain homeostasis.

Caspases are another group of proteins involved in cell death mediated by apoptosis and important senescent markers [13]. After MOMP, caspase activation takes place often within minutes, leading to cell death [43]. Inhibition of caspases therefore blocks apoptosis. Here we detected that the activator (procaspase-9) and executioner (procaspase-3 and procaspase-7) were upregulated in a permissive temperature group but show a differential pattern when cells are cultured at the non-permissive temperature. When mitochondrial-mediated apoptosis is induced and caspase-9 and caspase-3 are activated, the expression of Bax a nd Bcl-2 has been reported to show different levels to maintain their balance [46]. Irradiation-induced senescence is accompanied by an upregulation of procaspase-3, -7, and -9 [44, 45] but a downregulation of activated caspase-3 [44], in line with our results. The final downregulation of procaspases observed in our study might be explained by the cleavage of procaspase-9 finally to active

caspase-3 and caspase-7. But because of senescence induction and an adapted balance in Bcl-2 family proteins, procaspase-9 is inhibited, finally leading to apoptosis-resistance (Figure 7).
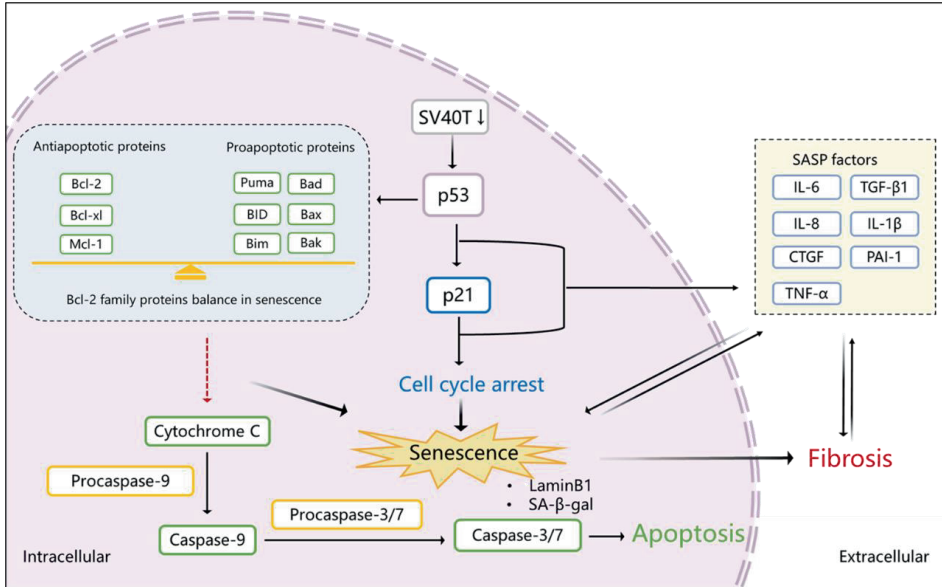

Figure 7. Proposed scheme of senescence induction in ciPTEC-OAT1 after maturation at non-permissive temperature. After transfer of cells to 37 °C and subsequent downregulation of SV40T, p53 is activated which transcriptionally upregulates p21, inducing cell cycle arrest and eventually leading to senescence. SASP factors are released during this process as well. Activated p53 also influences the expression of Bcl-2 family proteins that become abnormally upregulated. Procaspase 9 and its downstream proteins procaspases 3/7 are activated at the beginning of this process, and with time going by, the Bcl-2 family reach a balance between anti-apoptotic and pro-apoptotic proteins expression, halting the activation of procaspases and inhibiting apoptosis. In addition, senescent cells show a downregulation of LaminB1 and an upregulation of SA-β-gal and SASP factors, which may further contribute to kidney fibrosis.

The observed loss of LaminB1 and upregulation of β-gal, well-known indicators of senescence [5], in ciPTEC-OAT1 cultured at a non-permissive temperature further confirms the phenotypical changes. Silencing LaminB1 immediately leads to inhibition of proliferation and the induction of senescence [34]. Our previous research regarding cell cycle analysis of ciPTEC-OAT1 at permissive and non-permissive temperatures [47] has shown that ciPTEC-OAT1 when cultured at 37°C for 1 or 7 d exhibits significantly reduced proliferation (less cells in the S phase) and an increased number of cells in the G0/G1 phase of the cell cycle, indicating halted proliferation at a non-permissive temperature. This is in line with our current results. The activity of the lysosomal β-gal reflects increased metabolic activity and enhanced lysosomal content typical of senescent cells [5]. Transfection with the temperature sensitive SV40T gene allows the cells to become conditionally immortalized [25]. Although downregulation of SV40T at 37°C allows activation of p53 and pRb, factors involved in both p53/p21 and p16/pRb pathways, there was no significant difference in their mRNA expression (Supplementary Figure S1) and p16 protein expression appeared undetectable. This suggests that senescence of ciPTEC-OAT1 may not be induced by the p16/pRb pathway. On the other hand, p53 is pivotal in determining the fate of the cells, implying that the p53/p21 pathway is key in the initiation of senescence [48]. Previously published works described a decline of total-p53 levels in stress-

induced senescence in mice [49] and p21's role in maintaining senescence in mice [36], which is also in accordance with our in vitro data showing a decline in p53 levels and an increase in p21 levels at 37°C. Therefore, our results suggest that ciPTEC-OAT1 cultured at 37°C promotes senescence through the p53/p21 pathway.

In addition to previously tested markers, SASP factors are also important players in senescence. IL-6 maintains senescence through the p53/p21 pathway [50, 51], shared by IL-8, which is expressed as a function of IL-6 [52]. TGF-β1 and CTGF are other SASP factors reported to mediate senescence [40, 53]. CTGF is a downstream mediator of TGF-β1 and is regulated by TGF-β1 [54]. TGF-β1 induces kidney fibrosis by accumulation of extracellular matrix and CTGF expression by activation of Smad3 and p53 [55]. Meanwhile, both CTGF and TGF-β1 induce senescence and are accompanied with the upregulation of IL-6 and IL-8 [40, 56]. Although not significant, our results show an increasing trend of both TGF-β1 and CTGF in 37°C group compared to 33°C group. PAI-1 is a major TGF-β1/p53 target gene in kidney fibrosis and is known to be elevated in senescent cells, correlating with increased tissue TGF-β1 levels [57, 58]. In our study, PAI-1 and CTGF increased remarkably on the mRNA level, suggesting cellular senescence. TNF-α is another SASP factor and inducer of senescence [59], but our results showed no important differences over time and between the culture conditions, indicating the senescence of ciPTEC-OAT1 is not induced or maintained by TNF-α. There are some discrepancies between mRNA and protein levels of the obtained results. Despite being difficult to explain, these discrepancies might be due to differences in the regulation of transcription and protein translation processes, as well as protein turnover rate. Taken together, the results of the mRNA and protein levels, we believe that the cells exhibit a senescence phenotype at a non-permissive temperature.

Finally, the senolytics navitoclax, dasatinib, and quercetin were evaluated. Our results suggest that ciPTEC-OAT1 cultured at a non-permissive temperature was sensitive to senolytics, and the Bcl-2 family inhibitor, navitoclax [44, 60], appeared most effective in selectively reducing viability of cells presenting senescent phenotype. A clinical trial of the dasatinib and quercetin cocktail demonstrated a decrease in p21 and p16 positive human adipose tissue cells and plasma SASP factors of diabetic kidney disease participants [61]. Senolytics treatment of ciPTEC-OAT1 led to a dose-dependent reduction of SA-β-gal positive cells, in line with previous results [24]. It has been suggested that SA-β-gal activity may be an outcome rather than a cause of senescence [62, 63], and our findings argue for a clearance of senescent cells leading to a reduction in total cell number. Our follow-up research will focus on investigating the underlying mechanisms of senolytics used in this study.

In conclusion, our results suggest ciPTEC-OAT1 can be used as a valid proximal tubule cell model both for mechanistic studies inherent to kidney senescence and fibrosis and for senolytic effects of newly developed drugs and their combinations.

Data Availability Statement

The raw data supporting the conclusions of this article will be made available by the authors, without undue reservation.

Author Contributions

Conceptualization, YY, MM, TN, RG and RM; methodology, YY, MM, FV, TN, RG and RM; investigation, YY and FV; writing original draft preparation, YY; writing review and editing, YY, MM, and RM; supervision, MM, TN, RG and RM; funding acquisition, YY, RG, and RM. All authors have read and agreed to the published version of the manuscript.

Conflict of Interest

The authors declare that the research was conducted in the absence of any commercial or financial relationships that could be construed as a potential conflict of interest.

Reference

1. Boor, P., T. Ostendorf, and J. Floege, Renal fibrosis: novel insights into mechanisms and therapeutic targets. Nat Rev Nephrol, 2010. 6(11): p. 643-56.
2. Schafer, M.J., et al., Targeting Senescent Cells in Fibrosis: Pathology, Paradox, and Practical Considerations. Curr Rheumatol Rep, 2018. 20(1): p. 3.
3. Munoz-Espin, D. and M. Serrano, Cellular senescence: from physiology to pathology. Nat Rev Mol Cell Biol, 2014. 15(7): p. 482-96.
4. Kobbe, C.v., Targeting senescent cells: approaches, opportunities, challenges. Aging 2019. 11: p. 18.
5. Hernandez-Segura, A., J. Nehme, and M. Demaria, Hallmarks of Cellular Senescence. Trends Cell Biol, 2018. 28(6): p. 436-453.
6. Childs, B.G., et al., Senescence and apoptosis: dueling or complementary cell fates? EMBO Rep, 2014. 15(11): p. 1139-53.
7. Korolchuk, V.I., et al., Mitochondria in Cell Senescence: Is Mitophagy the Weakest Link? EBioMedicine, 2017. 21: p. 7-13.
8. Chipuk, J.E., L. Bouchier-Hayes, and D.R. Green, Mitochondrial outer membrane permeabilization during apoptosis: the innocent bystander scenario. Cell Death Differ, 2006. 13(8): p. 1396-402.
9. Van Opdenbosch, N. and M. Lamkanfi, Caspases in Cell Death, Inflammation, and Disease. Immunity, 2019. 50(6): p. 1352-1364.
10. Ngoi, N.Y.L., et al., Targeting Mitochondrial Apoptosis to Overcome Treatment Resistance in Cancer. Cancers (Basel), 2020. 12(3).
11. Anantram, A. and M. Degani, Targeting cancer's Achilles' heel: role of BCL-2 inhibitors in cellular senescence and apoptosis. Future Med Chem, 2019. 11(17): p. 2287-2312.
12. Fan, Y., et al., Senescent Cell Depletion Through Targeting BCL-Family Proteins and Mitochondria. Front Physiol, 2020. 11: p. 593630.
13. Shalini, S., et al., Old, new and emerging functions of caspases. Cell Death Differ, 2015. 22(4): p. 526-39.
14. Kumari, R. and P. Jat, Mechanisms of Cellular Senescence: Cell Cycle Arrest and Senescence Associated Secretory Phenotype. Front Cell Dev Biol, 2021. 9: p. 645593.
15. Ceccaldi, R., et al., Bone marrow failure in Fanconi anemia is triggered by an exacerbated p53/p21 DNA damage response that impairs hematopoietic stem and progenitor cells. Cell Stem Cell, 2012. 11(1): p. 36-49.
16. Ou, H.L. and B. Schumacher, DNA damage responses and p53 in the aging process. Blood, 2018. 131(5): p. 488-495.
17. Rayess, H., M.B. Wang, and E.S. Srivatsan, Cellular senescence and tumor suppressor gene p16. Int J Cancer, 2012. 130(8): p. 1715-25.
18. Sperka, T., J. Wang, and K.L. Rudolph, DNA damage checkpoints in stem cells, ageing and cancer. Nat Rev Mol Cell Biol, 2012. 13(9): p. 579-90.
19. Zhang, Y., et al., DNMT3a plays a role in switches between doxorubicin-induced senescence and apoptosis of colorectal cancer cells. Int J Cancer, 2011. 128(3): p. 551-61.
20. Ruan, B., et al., NVP-BEZ235 inhibits thyroid cancer growth by p53-dependent/independent p21 upregulation. Int J Biol Sci, 2020. 16(4): p. 682-693.
21. Rufini, A., et al., Senescence and aging: the critical roles of p53. Oncogene, 2013. 32(43): p. 5129-43.
22. Birch, J. and J. Gil, Senescence and the SASP: many therapeutic avenues. Genes Dev, 2020. 34(23-24): p. 1565-1576.
23. Docherty, M.H., et al., Cellular Senescence in the Kidney. J Am Soc Nephrol, 2019. 30(5): p. 726-736.
24. Zhu, Y., et al., The Achilles' heel of senescent cells: from transcriptome to senolytic drugs. Aging Cell, 2015. 14(4): p. 644-58.
25. Wilmer, M.J., et al., Novel conditionally immortalized human proximal tubule cell line expressing functional influx and efflux transporters. Cell Tissue Res, 2010. 339(2): p. 449-57.

26. Nieskens, T.T., et al., A Human Renal Proximal Tubule Cell Line with Stable Organic Anion Transporter 1 and 3 Expression Predictive for Antiviral-Induced Toxicity. Aaps j, 2016. 18(2): p. 465-75.

27. Pou Casellas, C., et al., Regulation of Solute Carriers OCT2 and OAT1/3 in the Kidney: A Phylogenetic, Ontogenetic and Cell Dynamic Perspective. Physiol Rev, 2021.

28. Nigam, S.K. and K.T. Bush, Uraemic syndrome of chronic kidney disease: altered remote sensing and signalling. Nat Rev Nephrol, 2019. 15(5): p. 301-316.

29. Larsson, O., et al., Kinetics of senescence-associated changes of gene expression in an epithelial, temperature-sensitive SV40 large T antigen model. Cancer Res, 2004. 64(2): p. 482-9.

30. Bodnar, A.G., et al., Extension of life-span by introduction of telomerase into normal human cells. Science, 1998. 279(5349): p. 349-52.

31. Brookes, S., et al., Evidence for a CDK4-dependent checkpoint in a conditional model of cellular senescence. Cell Cycle, 2015. 14(8): p. 1164-73.

32. Mihajlovic, M., et al., Role of Vitamin D in Maintaining Renal Epithelial Barrier Function in Uremic Conditions. Int J Mol Sci, 2017. 18(12).

33. Stenvinkel, P. and T.E. Larsson, Chronic kidney disease: a clinical model of premature aging. Am J Kidney Dis, 2013. 62(2): p. 339-51.

34. Shimi, T., et al., The role of nuclear lamin B1 in cell proliferation and senescence. Genes Dev, 2011. 25(24): p. 2579-93.

35. Calcinotto, A., et al., Cellular Senescence: Aging, Cancer, and Injury. Physiol Rev, 2019. 99(2): p. 1047-1078.

36. Yosef, R., et al., p21 maintains senescent cell viability under persistent DNA damage response by restraining JNK and caspase signaling. EMBO J, 2017. 36(15): p. 2280-2295.

37. Childs, B.G., et al., Cellular senescence in aging and age-related disease: from mechanisms to therapy. Nat Med, 2015. 21(12): p. 1424-35.

38. Sun, T., et al., PAI-1 contributes to homocysteine-induced cellular senescence. Cell Signal, 2019. 64: p. 109394.

39. Shi, L., et al., Cellular senescence induced by S100A9 in mesenchymal stromal cells through NLRP3 inflammasome activation. Aging (Albany NY), 2019. 11(21): p. 9626-9642.

40. Jun, J.I. and L.F. Lau, CCN2 induces cellular senescence in fibroblasts. J Cell Commun Signal, 2017. 11(1): p. 15-23.

41. Mosteiro, L., et al., Senescence promotes in vivo reprogramming through p16(INK)(4a) and IL-6. Aging Cell, 2018. 17(2).

42. Lee, Y.C., et al., ABT-263-induced MCL1 upregulation depends on autophagy-mediated 4EBP1 downregulation in human leukemia cells. Cancer Lett, 2018. 432: p. 191-204.

43. Pena-Blanco, A. and A.J. Garcia-Saez, Bax, Bak and beyond - mitochondrial performance in apoptosis. FEBS J, 2018. 285(3): p. 416-431.

44. Chang, J., et al., Clearance of senescent cells by ABT263 rejuvenates aged hematopoietic stem cells in mice. Nat Med, 2016. 22(1): p. 78-83.

45. Baar, M.P., et al., Targeted Apoptosis of Senescent Cells Restores Tissue Homeostasis in Response to Chemotoxicity and Aging. Cell, 2017. 169(1): p. 132-147 e16.

46. Zhang, Y., et al., Curcumin in combination with homoharringtonine suppresses lymphoma cell growth by inhibiting the TGF-β/Smad3 signaling pathway. Aging (Albany NY), 2021. 13(14): p. 18757-18768.

47. Mihajlovic, M., et al., Safety evaluation of conditionally immortalized cells for renal replacement therapy. Oncotarget, 2019. 10(51).

48. Mijit, M., et al., Role of p53 in the Regulation of Cellular Senescence. Biomolecules, 2020. 10(3).

49. Feng, Z., et al., Declining p53 function in the aging process: a possible mechanism for the increased tumor incidence in older populations. Proc Natl Acad Sci U S A, 2007. 104(42): p. 16633-8.

50. Effenberger, T., et al., Senescence-associated release of transmembrane proteins involves proteolytic processing by ADAM17 and microvesicle shedding. FASEB J, 2014. 28(11): p. 4847-56.

51. Li, Y., et al., Interleukin-6 Knockout Inhibits Senescence of Bone Mesenchymal Stem Cells in High-Fat Diet-Induced Bone Loss. Front Endocrinol (Lausanne), 2020. 11: p. 622950.

52. Kuilman, T., et al., Oncogene-induced senescence relayed by an interleukin-dependent inflammatory network. Cell, 2008. 133(6): p. 1019-31.

53. You, W., et al., TGF-β mediates aortic smooth muscle cell senescence in Marfan syndrome. Aging (Albany NY), 2019. 11(11): p. 3574-3584.

54. Ou, S.C., et al., TGF-β Induced CTGF Expression in Human Lung Epithelial Cells through ERK, ADAM17, RSK1, and C/EBPβ Pathways. Int J Mol Sci, 2020. 21(23).

55. Li, X., et al., DsbA-L mediated renal tubulointerstitial fibrosis in UUO mice. Nat Commun, 2020. 11(1): p. 4467.

56. Fan, C., et al., TGF-β induces periodontal ligament stem cell senescence through increase of ROS production. Mol Med Rep, 2019. 20(4): p. 3123-3130.

57. Samarakoon, R., et al., The TGF-beta1/p53/PAI-1 Signaling Axis in Vascular Senescence: Role of Caveolin-1. Biomolecules, 2019. 9(8).

58. Rana, T., et al., PAI-1 Regulation of TGF-β1-induced Alveolar Type II Cell Senescence, SASP Secretion, and SASP-mediated Activation of Alveolar Macrophages. Am J Respir Cell Mol Biol, 2020. 62(3): p. 319-330.

59. Guo, Q., et al., Tumor Necrosis Factor-alpha (TNF-α) Enhances miR-155-Mediated Endothelial Senescence by Targeting Sirtuin1 (SIRT1). Med Sci Monit, 2019. 25: p. 8820-8835.

60. Tse, C., et al., ABT-263: a potent and orally bioavailable Bcl-2 family inhibitor. Cancer Res, 2008. 68(9): p. 3421-8.

61. Hickson, L.J., et al., Senolytics decrease senescent cells in humans: Preliminary report from a clinical trial of Dasatinib plus Quercetin in individuals with diabetic kidney disease. EBioMedicine, 2019. 47: p. 446-456.

62. Lee, B.Y., et al., Senescence-associated beta-galactosidase is lysosomal beta-galactosidase. Aging Cell, 2006. 5(2): p. 187-95.

63. Piechota, M., et al., Is senescence-associated β-galactosidase a marker of neuronal senescence? Oncotarget, 2016. 7(49): p. 81099-81109.
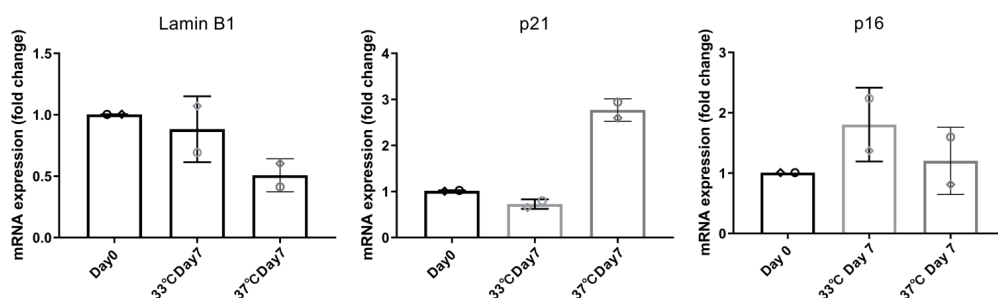
2

Supplementary Material

Figure S1. Gene expression levels of Lamin B1, p21 and p16 at permissive and non-permissive temperatures. mRNA levels of LaminB1, p21 and p16 detected after culturing ciPTEC-OAT1 for 0 or 7 days at permissive (33 °C) and non-permissive temperature (37 °C). Two independent experiments in triplicates were performed.
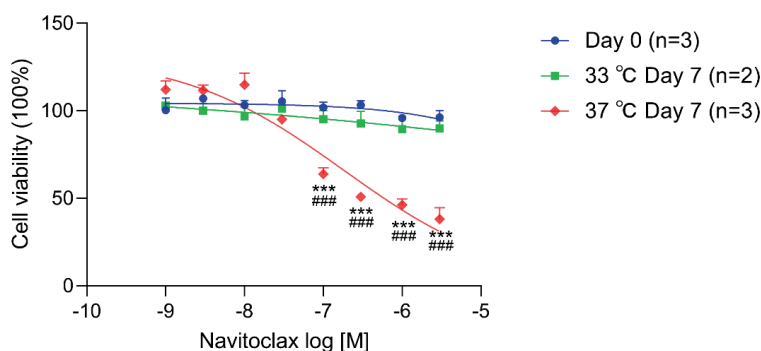

Figure S2. CiPTEC-OAT1 cultured at non-permissive temperature and exhibiting a senescence-like phenotype are susceptible to navitoclax. Cell viability of ciPTEC-OAT1 cultured for 0 or 7 days at permissive (33 °C) and non-permissive temperature (37 °C) and exposed increasing concentrations of navitoclax. At least two independent experiments in triplicates were performed. Data are presented as mean ± SEM, for which results were normalized to unexposed cells. *P<0.05, **P<0.01, ***P<0.001 (cell viability at 37°C Day 7 compared to Day 0 at the same concentration; Multiple t-test, Holm-Sidak multiple comparison test). #P<0.05, ##P<0.01, ###P<0.001 (cell viability at 37°C Day 7 compared to 33°C Day 7 at the same concentration; Multiple t-test, Holm-Sidak multiple comparison test).
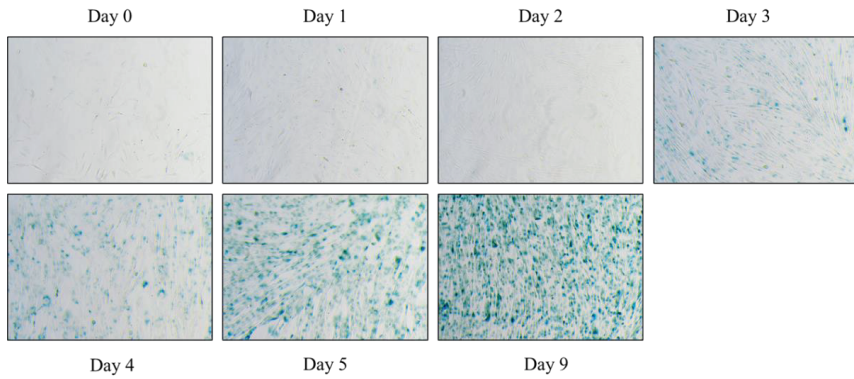
Figure S3. SA-β-gal activity in CiPTEC-OAT1 during culture at non-permissive temperature. Representative images of SA-β-gal staining in ciPTEC-OAT1 cultured for 0 through 9 days at 37 ℃. Three independent experiments were performed.

*The Supplementary Material for this article can be found online at: https://www.frontiersin.org/articles/10.3389/fphar.2022.791612/full#supplementary-material

2

Chapter 3

Protein-Bound Uremic Toxins Induce Reactive Oxygen Species-Dependent and Inflammasome-Mediated IL-1β Production in Kidney Proximal Tubule Cells

Milos Mihajlovic,[1] Merle M. Krebber,[2] Yi Yang,[1] Sabbir Ahmed,[1] Valeria Lozovanu,[1] Daria Andreeva,[1] Marianne C. Verhaar,[2] and Rosalinde Masereeuw[1]

[1]Utrecht Institute for Pharmaceutical Sciences, div. Pharmacology, Utrecht, The Netherlands.

[2]Department Nephrology and Hypertension, University Medical Center Utrecht, 3508 GA Utrecht, The Netherlands.

Abstract

Protein bound-uremic toxins (PBUTs) are not efficiently removed by haemodialysis in chronic kidney disease (CKD) patients and their accumulation leads to various co-morbidities via cellular dysfunction, inflammation and oxidative stress. Moreover, it has been shown that increased intrarenal expression of the NLRP3 receptor and IL-1β are associated with reduced kidney function, suggesting a critical role for the NLRP3 inflammasome in CKD progression. Here, we evaluated the effect of PBUTs on inflammasome-mediated IL-1β production in vitro and in vivo. Exposure of human conditionally immortalized proximal tubule epithelial cells to indoxyl sulfate (IS) and a mixture of anionic PBUTs (UT mix) increased expression levels of NLRP3, caspase-1 and IL-1β, accompanied by a significant increase in IL-1β secretion and caspase-1 activity. Furthermore, IS and UT mix induced the production of intracellular reactive oxygen species, and caspase-1 activity and IL-1β secretion were reduced in the presence of antioxidant N-acetylcysteine. IS and UT mix also induced NF-κB activation as evidenced by p65 nuclear translocation and IL-1β production, which was counteracted by an IKK inhibitor. In vivo, using subtotal nephrectomy CKD rats, a significant increase in total plasma levels of IS and the PBUTs, kynurenic acid and hippuric acid, was found, as well as enhanced urinary malondialdehyde levels. CKD kidney tissue showed an increasing trend in expression of NLRP3 inflammasome components, and a decreasing trend in superoxide dismutase-1 levels. In conclusion, we showed that PBUTs induce inflammasome-mediated IL-1β production in proximal tubule cells via oxidative stress and NF-κB signalling, suggesting their involvement in disease-associated inflammatory processes.

Keywords: chronic kidney disease, protein-bound uremic toxins, indoxyl sulfate, NLRP3 inflammasome, IL-1β, kidney inflammation, oxidative stress, NF-κB, subtotal nephrectomy, con

1. Introduction

Chronic kidney disease (CKD) is a pathological condition characterized by a progressive loss of kidney function, leading to end stage kidney disease (ESKD) and the need for kidney replacement therapies. It has a global estimated prevalence of 11–15%, which further confirms its huge impact on both socio-economic aspects and the health system [1,2].

It has been recognized that CKD is accompanied by persistent local and systemic inflammation, characterized by increased production of multiple inflammatory mediators, oxidative stress, acidosis and intestinal dysbiosis [3,4]. The inflammatory processes present in CKD have been shown to contribute to many complications, especially cardiovascular events such as coronary artery calcification, atherosclerosis and heart failure, but also to insulin resistance, endothelial dysfunction, bone disorders, cognitive dysfunction, susceptibility to infections and overall increased CKD mortality [5,6,7,8,9,10,11,12].

Among the main players involved in the development and progression of CKD-associated inflammation are uremic retention solutes [13]. These toxins can be classified into three groups based on their molecular weight and protein binding capacity: (1) small water-soluble molecules, (2) middle molecules and (3) protein-bound molecules, frequently denominated protein-bound uremic toxins (PBUTs) [14,15]. The latter category is particularly troublesome for ESKD patients as these toxins are not easily removed by dialysis treatment due to their high binding capacity to albumin [16]. Many PBUTs, including indoxyl sulfate (IS) and p-cresyl sulfate, find their origin in the gut as products of microbial metabolism and have been shown to be involved in the development of CKD-related co-morbidities, mostly by mediating pro-inflammatory and oxidative processes [17,18].

The inflammasome is one of the inflammation-related mechanisms that recently has gained a lot of attention for its pathogenic role in kidney diseases [19]. These large multiprotein intracellular complexes are in most cases comprised of a sensor protein, typically a member of the nucleotide-binding oligomerization domain (NOD)-like receptor (NLRs), the absent in melanoma 2 (AIM2)-like receptor (ALRs) or the retinoic acid-inducible gene-I (RIG-I)-like receptor (RLRs) families, the adaptor protein apoptosis-associated speck-like protein containing a caspase recruitment domain (ASC) and caspase-1. These are assembled and activated in the presence of danger and stress-associated stimuli leading to caspase-1 activation and subsequent pro-inflammatory interleukin-1β (IL-1β) and interleukin-18 (IL-18) release and pyroptosis [20].

One of the most studied inflammasomes is NLRP3 that usually requires two signals for its activation: the first one to induce transcription of pro-IL-1β and responsiveness of NLRP3 to the second signal that triggers its activation [21]. These signals include various pathogen-associated molecular patterns (PAMPs) and damage-associated molecular patterns (DAMPs), such as ATP, uric acid and calcium pyrophosphate dehydrate (CPPD) crystals and amyloid-β fibrils [22,23,24,25,26,27]. Although not fully elucidated as of yet, the main proposed mechanisms of NLRP3 inflammasome activation include the ion channel model, the lysosome rupture model, and the reactive species (ROS) model. The latter one proposes that ROS cause dissociation of thioredoxin/thioredoxin-interacting protein (TXNIP) complex, and TXNIP subsequently binding to and activation of NLRP3 [28,29].

Based on the findings that the inflammasome plays a role in CKD pathogenesis and progression and the fact that PBUTs have a prominent pro-inflammatory capacity, we hypothesized that this group of uremic toxins are drivers of inflammasome-related inflammation within the kidney proximal tubule. This is an important segment of the nephron because of its role in PBUTs uptake and active tubular secretion and its susceptibility to PBUTs' toxic effects [30,31]. The present work was designed to study the effects of IS, a representative PBUT, and a mixture of several anionic PBUTs [32] (UT mix; Table 1) on NLRP3 inflammasome activation. Given that the organic anion transporter 1 (OAT1) is an important transporter responsible for the uptake of anionic uremic toxins into proximal tubule cells thus contributing to their removal, previously established and characterized human conditionally immortalized proximal tubule epithelial cells overexpressing OAT1 (ciPTEC-OAT1) were employed for in vitro studies [32,33,34,35].

Table 1. Concentrations of selected protein-bound uremic toxins (PBUTs) in healthy individuals, kidney disease patients and as applied within UT mixture in the present study [1].

Protein-bound uremic toxin (PBUT)	Normal concentrations (μM) (Mean ± SD)	Uremic concentrations (μM) (Mean ± SD)	1x UT mix (μM)	2.5x UT mix (μM)
Indoxyl sulfate (IS)	2.3 ± 18.8	174 ± 122	100	250
L-kynurenine (Kyn)	1.9	3.3 ± 0.9	5	12.5
Indol-3-acetic acid (3-IAA)	2.9 ± 1.7	11.4 ± 2.3	3	7.5
Kynurenic acid (KA)	0.03 ± 0.01	0.8 ± 0.4	3	7.5
Hippuric acid (HA)	16.7 ± 11.2	608 ± 363	300	750
Indoxyl-β-glucuronide (IG)	3.1 ± 1.3	9.4 ± 9.4	10	25
p-cresyl glucuronide (pCG)	0.3 ± 0.2	30.1 ± 6.7	40	100
p-cresyl sulfate (pCS)	10.1 ± 12.2	122 ± 90	125	312.5

[1] Concentrations reported and used are adapted from EUTox Uremic Solutes Database (https://www.uremic-toxins.org accessed on 19 August 2021) and Mihajlovic et al. [32].

In addition, the link between PBUTs and kidney tissue-specific expression of inflammasome-related components in a rat subtotal nephrectomy (SNX) model was evaluated in vivo. We examined the effect of IS and UT mix in vitro on the expression of all inflammasome components (NLRP3, ASC, caspase-1 and IL-1β) in ciPTEC-OAT1, on caspase-1 activity and IL-1β secretion, as well as their ability to induce oxidative stress. In addition, we evaluated the role of NF-κB signalling pathway as the priming signal in PBUTs-mediated inflammasome activation. Finally, the expression of NLRP3, caspase-1 and IL-1β in kidney tissue, plasma levels of various PBUTs and oxidative status in the CKD animal model were assessed. Determining the role of PBUTs in inflammasome activation in the proximal tubule and unravelling the mechanisms by which this occurs could lead to new intervention modalities aimed at reducing inflammation-mediated kidney injury.

2. Materials and Methods

2.1. Reagents

All reagents were purchased from Sigma-Aldrich (Zwijndrecht, The Netherlands) unless stated otherwise. In the present study, lipopolysaccharide (LPS) from Escherichia coli 0127:B8 was used. The toxins, p-cresyl glucuronide (pCG) and p-cresyl sulfate (pCS), were synthesized by

the Institute for Molecules and Materials, Radboud University, Nijmegen, The Netherlands, as previously described [36]. IκB kinase (IKK) inhibitor BMS-345541 was obtained from Axon Medchem (Groningen, The Netherlands). Water (LC-MS grade), acetonitrile (ACN; HPLC-S grade) and methanol (HPLC grade) were obtained from Biosolve (Valkenswaard, The Netherlands). Formic acid (analytical grade) was purchased at Merck (Darmstadt, Germany). Ultrapure water was produced by a Milli-Q® Advantage A10 Water Purification Systems (Merck, Schiphol-Rijk, The Netherlands). Cell culture plates were obtained from Greiner Bio-One (Monroe, NC, USA).

2.2. CiPTEC-OAT1 Cell Culture

The ciPTEC-OAT1 cell line was cultured in Dulbecco's Modified Eagle Medium/Nutrient Mixture F-12 (1:1 DMEM/F-12) (Gibco, Life Technologies, Paisley, UK) supplemented with 10% fetal calf serum (FCS) (Greiner Bio-One, Alphen aan den Rijn, The Netherlands), 5 μg/mL insulin, 5 μg/mL transferrin, 5 μg/mL selenium, 35 ng/mL hydrocortisone, 10 ng/mL epidermal growth factor and 40 pg/mL tri-iodothyronine, without addition of antibiotics and up to a maximum of 60 passages, as reported previously [35]. Cells were kept in culture at 33 °C and 5% (v/v) CO2. Prior to the experiments, cells were seeded at a density of 55,000 cell/cm2, grown for one day at 33 °C, 5% (v/v) CO2, and cultured for 7 days at 37 °C, 5% (v/v) CO2 to allow maturation, refreshing the medium every other day.

2.3. CiPTEC-OAT1 Exposure to PBUTs

IS concentrations used for treatment of ciPTEC-OAT1 were: 200 μM, 1 mM and 2 mM. PBUTs mixture (UT mix) was prepared as described previously [32] with slightly adjusted concentrations (Table 1) to replicate PBUTs plasma levels observed in CKD patients. The mixture was prepared as a 100× solution and subsequently diluted to 1× or 2.5× for treatment of ciPTEC-OAT1.

2.4. Caspase-1 Activity

To measure caspase-1 activity, ciPTEC-OAT1 cells were exposed to desired treatment conditions for 2 h (in case of LPS/ATP co-treatment, ATP was added during the final 30 min of exposure) and incubated at 37 °C, 5% (v/v) CO2, in the absence or presence of specific inhibitors ac-YVAD-cmk or N-acetyl cysteine (NAC; both added 30 min prior to the start of the treatments). Following incubation, caspase-1 activity was determined using Caspase-Glo® 1 inflammasome assay kit (Promega, Leiden, The Netherlands) according to manufacturer's instructions. Luminescence was measured using the Fluoroskan Ascent FL microplate reader (Thermo Fisher Scientific, Vantaa, Finland). Measured luminescence values were corrected for background and used to calculate relative caspase-1 activity, using untreated cells as the reference.

2.5. Enzyme-Linked Immunosorbent Assay (ELISA)

The production of IL-1β was measured using an Enzyme-Linked Immunosorbent Assay (ELISA). Cell culture supernatants were collected after 24 h of the treatments, in the absence or presence of specific inhibitors. Afterwards, cell culture supernatants were centrifuged for 10

min, 240× g, 4 °C and stored at −20 °C until analysed. DuoSet® ELISA Development Systems kit (Human IL-1 beta/IL-1F2 #DY201; R&D Systems, Abingdon, UK) was used to quantify IL-1β levels in cell culture supernatants following manufacturer's instructions. The optical density was determined using the iMark Microplate Absorbance Reader (Bio-Rad Laboratories, Hercules, CA, USA) set to 450 nm. Each sample was measured in duplicates and quantification was done using Microplate Manager software (version 6.0, Bio-Rad Laboratories, Hercules, CA, USA), generating a four-parameter logistic (4-PL) curve-fit.

2.6. RNA Extraction, cDNA Synthesis and Real-Time PCR

Total RNA from ciPTEC-OAT1 exposed to uremic toxins or LPS/ATP co-treatment, in the absence or presence of BMS-345541 (added 1 h prior to the treatments), for either 4 h or 24 h, was isolated using the RNeasy Mini kit (Qiagen, Venlo, The Netherlands) following the manufacturer's instructions and quantified using the NanoDrop® ND-1000 spectrophotometer (Thermo Fisher Scientific, Wilmington, DE, USA). The synthesis of cDNA was performed using 800 ng of total mRNA per sample and by means of the iScriptTM Reverse Transcription Supermix (Bio-Rad Laboratories, Hercules, CA, USA) and T100™ Thermal Cycler (Bio-Rad Laboratories, Hercules, CA, USA). Subsequently, Real-Time PCR was performed using the iQ SYBR® Green Supermix (Bio-Rad Laboratories, Hercules, CA, USA) as indicated in manufacturer's protocol and by means of CFX96TM Real-Time PCR Detection System (Bio-Rad Laboratories, Hercules, CA, USA). The data were analyzed using Bio-Rad CFX ManagerTM Software version 3.1 (Bio-Rad Laboratories, Hercules, CA, USA) and expressed as relative gene expression, using untreated cells as the reference sample. HPRT1 and RPS13 were used as housekeeping genes for normalization. Specific sense and anti-sense primers for HPRT1 (forward: ACATCTGGAGTCCTATTGACATCG; reverse: CCGCCCAAAGGGAACTGATAG), RPS13 (forward: GCTCTCCTTTCGTTGCCTGA; reverse: ACTTCAACCAAGTGGGGACG), NLRP3 (forward: GATCTTCGCTGCGATCAACA; reverse: GGGATTCGAAACACGTGCATTA), PYCARD (ASC; forward: CAGCAACACTCCGGTCAG; reverse: AGCTGGCTTTTCGTATATTGTG), CASP1 (caspase-1; forward: GCCTGTTCCTGTGATGTGGAG; reverse: TGCCCACAGACATTCATACAGTTTC), IL1B (IL-1β; forward: TCGCCAGTGAAATGATGGCT; reverse: TGGAAGGAGCACTTCATCTGTT), HMOX1 (heme oxygenase 1; forward: GACCCATGACACCAAGGACC; reverse: TCCACGGGGGGCAGAATCTTG), NFKBIA (NFκB inhibitor alpha; forward: AATGCTCAGGAGCCCTGTAA; reverse: CTGTTGACATCAGCCCCACA) and TNF (TNF-α; forward: TGTTGTAGCAAACCCTCAAGC; reverse: TATCTCTCAGCTCCACGCCA) were synthesized by Biolegio (Nijmegen, The Netherlands).

2.7. Intracellular Reactive Oxygen Species (ROS) Detection

Intracellular ROS generation was measured using chloromethyl-2′,7′-dichlorofluorescein diacetate (CM-H2DCFDA; #C6827; Invitrogen, Carlsbad, CA, USA) and following the manufacturer's instructions. Briefly, cells were washed once with Hank's Balanced Salt Solution (HBSS; Gibco, Life Technologies, Paisley, UK), immediately loaded with CM-H2DCFDA (10 µM in HBSS) and incubated at 37 °C, 5% (v/v) CO2, in the dark for 25 min. Afterwards, cells were washed with a complete culture medium and left to recover for 15 min.

Next, cells were exposed to various concentrations of uremic toxins, in the absence or presence of antioxidant agents, NAC (1.8 mM) or 6-hydroxy-2,5,7,8-tetramethylchroman-2-carboxylic acid (Trolox; 100 µM), for 2 h at 37 °C, 5% (v/v) CO_2, in the dark. Hydrogen peroxide (H_2O_2; 200 µM) was used as a positive control. Following the incubation, fluorescence was measured at an excitation wavelength of 492 nm and emission wavelength of 518 nm, using a fluorescent microplate reader (Fluoroskan Ascent FL, Thermo Fisher Scientific, Vantaa, Finland). Fluorescence intensities measured were corrected for the blank sample (non-stained cells) and used to calculate relative intracellular ROS production, using untreated cells as the reference.

2.8. Protein Extraction and Quantification

After exposing cells for 24 h to different concentrations of uremic toxins or LPS/ATP combinatory treatment, cell lysates were obtained by washing the cells twice with cold HBSS and incubating them on ice for 5 min with 350 µL cold RIPA lysis buffer (Thermo Scientific, Rockford, IL, USA) containing 1% (v/v) protease inhibitor (Halt Protease Inhibitor Cocktail; Thermo Scientific, Rockford, IL, USA). The lysates were then gathered using a cell scraper and centrifuged at 14,000× g, at 4 °C for 15 min. The supernatants were collected for further analyses.

Snap-frozen kidney tissues were dissected on ice into small pieces weighing between 10 and 20 mg, washed once in ice-cold PBS, incubated in ice-cold RIPA buffer (approx. 500 µL per 10 mg of tissue) for 20 min and beads-homogenized thoroughly. The lysed homogenates were then centrifuged at 14,000× g, at 4 °C for 15 min and the supernatants were collected for further analyses. The total protein content was determined by using Pierce™ BCA Protein Assay Kit (Thermo Scientific, Waltham, MA, USA) as indicated in manufacturer's protocol and the samples were stored at −80 °C until further usage.

2.9. SDS-PAGE and Western Blot Analysis

The protein samples were denatured and reduced in Laemmli Sample Buffer 4× (Bio-Rad Laboratories, Hercules, CA, USA) containing 2% β-mercaptoethanol for 5 min at 95 °C using the Eppendorf ThermoMixer® C instrument (Eppendorf, Hamburg, Germany). A total 15 µg of proteins per sample were separated using the Mini-PROTEAN® TGX™ 4–20% precast gels by the means of sodium dodecyl sulfate polyacrylamide gel electrophoresis (SDS-PAGE; Bio-Rad Laboratories, Hercules, CA, USA) for 90 min at 100 V and subsequently transferred to a 0.2 µm nitrocellulose membrane (Bio-Rad Laboratories, Hercules, CA, USA) using Trans-Blot® Turbo™ Transfer Pack (Bio-Rad Laboratories, Hercules, CA, USA) and Trans-Blot® Turbo™ Transfer System (Bio-Rad Laboratories, Hercules, CA, USA) for 30 min at 25 V.

Afterwards, the membranes were blocked for 20 min with 5% fat-free dry milk (Nutricia Protifar, Fulda, Germany) in PBS/0.1% Tween-20 (PBS-T) and probed overnight at 4 °C with following primary antibodies, depending on the protein being detected: rabbit anti-NLRP3 (1:250; D4D8T, Cell Signalling Technology, Leiden, The Netherlands), rabbit anti-NLRP3 (1:500; EPR23094-1, Abcam, Amsterdam, The Netherlands), rabbit anti-caspase-1 (1:250; Enzo Life Sciences, Raamsdonksveer, The Netherlands), rabbit anti-IL-1β (1:250; Abcam, Amsterdam, The Netherlands), rabbit anti-SOD-1 (1:50,000; EP1727Y, Abcam, Amsterdam, The Netherlands), mouse anti-ASC (1:500; Santa Cruz Biotechnology, Dallas, TX, USA),

mouse anti-β-actin (1:5000; Novus Biologicals, Abingdon, UK), mouse anti-β-actin (1:1000; mAbcam 8226, Abcam, Amsterdam, The Netherlands) and mouse anti-α-tubulin (1:1000; Abcam, Amsterdam, The Netherlands). The membranes were then probed with one of the following HRP-conjugated secondary antibodies: goat anti-rabbit (1:5000; Dako, Carpinteria, CA, USA), or rabbit anti-mouse (1:5000; Dako, Carpinteria, CA, USA). Finally, chemiluminescence was developed with Clarity™ Western ECL Substrate (Bio-Rad Laboratories, Hercules, CA, USA) and the images acquired using the ChemiDoc™ MP Imaging System (Bio-Rad Laboratories, Hercules, CA, USA). The data were analyzed using the Image Lab software (version 5.2, Bio-Rad Laboratories, Hercules, CA, USA), and the imaged bands were quantified by densitometric analysis using ImageJ software version 1.49 (National Institutes of Health, Bethesda, MD, USA). The results are presented as relative protein expression normalized against β-actin or α-tubulin.

2.10. Immunocytochemistry

To assess the nuclear expression levels of p65, ciPTEC-OAT1 monolayers pre-incubated with BMS-345541 for 1 h were treated with uremic toxins, LPS or TNF-α for 1 h, then washed with warm HBSS twice and fixated with 4% (v/v) paraformaldehyde (PFA) in PBS for 10 min. After additional three washing steps with PBS-T, cells were permeabilized with 0.3% (v/v) Triton-X for 10 min. Following three more washing steps in PBS-T, cells were incubated for 30 min in a blocking solution (2% (v/v) FCS, 2% (w/v) bovine serum albumin (BSA), 0.1% (v/v) Tween-20 in HBSS) and exposed to primary antibody rabbit anti-NF-κB p65 (Invitrogen, Carlsbad, CA, USA), diluted in blocking buffer (1:100) and incubated for 1 h at room temperature. Following three washing steps with PBS-T, the secondary antibody donkey anti-rabbit IgG AlexaFluor 488 (Life Technologies, Eugene, OR, USA) was added in a concentration of 1:250 and incubated for 1 h at room temperature. Finally, cells were washed three more times with PBS-T and imaged using a Cell Voyager 7000 (CV7000) confocal microscope (Yokogawa Electric Corporation, Tokyo, Japan) with 20× magnification. At least 3 fields per condition were analysed using ImageJ software version 1.49 (National Institutes of Health, Bethesda, MD, USA). In total, at least 300 nuclei per condition were used for quantification and statistical analysis. Data were normalized to untreated control and presented as relative expression.

2.11. Experimental Animals

Female outbred Sprague Dawley rats (SD, Envigo, Horst, The Netherlands), aged 8 weeks and weighing approximately 200 g were used and housed socially (up to n = 4 per cage) under standard climate-controlled conditions with ad libitum access to water and food. Animals were acclimated for 7 days prior to start of the study. The study protocol was approved by the Animal Ethics Committee of the University of Utrecht (CCD; AVD115002015310) and in agreement with the current Dutch law on animal experiments. Animals were matched between healthy Sham and CKD groups based on baseline measurements of proteinuria, creatinine, urea and systolic blood pressure (SBP).

2.12. CKD Model in Rats

Animals were used as part of a pilot to monitor progression to CKD, using an altered protocol of our previously published surgical 5/6th nephrectomy (SNX) [37]. A week before the SNX,

baseline measurements to determine systolic blood pressure (SBP), proteinuria, plasma urea, urine and plasma creatinine were taken. Animals were stratified and randomly assigned to either Sham or CKD group.

In short, CKD was induced by removing the whole left kidney and polectomy (2/3rd) of the right kidney using retroperitoneal incisions in animal weighing over 200 g in a single procedure. In Sham animals, both kidneys were externalized, the renal capsule was removed and the intact kidneys were placed back. Surgery was performed under isoflurane gas anesthesia (4% induction, 2.5% maintenance and O2). The incisions were closed by suturing the muscle layers with continuous stitches (5.0 Vicryl—Ethicon V303H, Lidingö, Sweden) and the skin with continuous intracutaneous stitches (4.0 Vicryl—Ethicon V392H, Lidingö, Sweden). Postoperative buprenorphine (Temgesic, 0.03 mg/kg) was given subcutaneously for a period of 48 h and rats were kept individually overnight on heat pads to recover.

Rats were subsequently weighed each week and longitudinal measurements were taken every other week to follow CKD progression. SBP was measured by tail cuff sphygmomanometer (LE 5002 LETICA®, Panlab, Barcelona, Spain). To determine proteinuria, 24 h urine samples were collected during which rats were placed in metabolic cages without food but with free access to water with 2% glucose. Urine was collected in antibiotic/antimycotic solution (A5955; Sigma, St Louis, MO, USA) and stored at −80 °C. Blood samples were collected from the tail vein into EDTA Microtainers (#365974; BD, Vianen, The Netherlands). Urinary protein levels were measured by Bradford Assay (Bio-Rad Laboratories, Hercules, CA, USA). Sodium and potassium levels were determined by flame photometry. Plasma and urinary urea were determined by DiaSys Urea CT FS (DiaSys Diagnostic Systems, Holzheim, Germany). Plasma and urinary creatinine levels were determined by DiaSys Creatinine PAP FS kit (DiaSys Diagnostic Systems, Holzheim, Germany).

Animals were sacrificed when humane endpoints (HEPs), as determined beforehand, were reached. HEPs included progressive proteinuria (>400 mg/24 h for any given measurement), progressive uremia (>20 mmol/L for any given measurement), progressive weight loss (>15% within 7 days) or a cumulative decreased welfare score based on the rat grimace scale (Intensity >4 as visually determined by two independent observers) [38]. CKD and age-matched Sham animals were sacrificed by exsanguination through cardiac punction under isoflurane anesthesia. Terminal blood was collected, and kidneys were dissected and subsequently snap-frozen (−80 °C) for later analysis or fixed in 4% PFA and embedded in paraffin for sectioning.

2.13. Immunohistochemistry

Tubulo-interstitial (TI) damage was scored on periodic-acid Schiff (PAS) 3 μm thick stained slides [39]. After incubation with 1% periodic acid, slides were stained in Schiffs reagent in the dark and counterstained with haematoxylin.

In short, TI was scored on a scale from 0–5 and independently defined as inflammatory cell infiltrate, tubular atrophy, dilatation or interstitial fibrosis. At least 10 non-overlapping field were analyzed by an experienced researcher blinded to group allocation.

Pan-macrophages were stained using ED1+ (monocyte/macrophage marker; mouse anti-rat CD68, ab31630, 1:250; Abcam, Cambridge, UK). 3 μm deparaffinized sections were first blocked with 5% hydrogen peroxide in PBS and subsequently subjected to indirect heat-induced antigen retrieval (TRIS/EDTA, pH 9.0). After blocking with SuperblockTM (Thermo Fischer Scientific, San Jose, CA, USA), the primary antibody was incubated for 1 h at room temperature. Sections were covered with entellan after incubation with secondary horseradish peroxidase (HRP)-conjugated goat-anti-mouse IgG (Brightvision Immunologic, Duiven, The Netherlands) visualization with Nova Red and haematoxylin counterstain. To analyze ED1+ cells, least 50 glomeruli and 20 non-overlapping tubular fields were manually counted. Pictures were taken on a BX-51 microscope (Olympus, Leiderdorp, The Netherlands).

2.14. Thiobarbituric Acid Reactive Substances (TBARS) Assay for Lipid Peroxidation Detection

Lipid peroxidation end-product, malondialdehyde (MDA), was quantified in urine samples using Lipid peroxidation (MDA) assay kit (Sigma-Aldrich, Zwijndrecht, The Netherlands) and following instructions as described in manufacturer's protocol. Values measured were corrected for background and used to calculate MDA levels, expressed as nmol/mL.

2.15. PBUTs Plasma Levels Quantification by LC-MS

An Accela LC system (quaternary pump and autosampler) coupled to a TSQ Quantum Ultra triple quadrupole mass spectrometer with heated electrospray ionization (ESI) was used for this study. Equipment and software for controlling, data recording and processing (Xcalibur version 2.07) were supplied by Thermo Fischer Scientific (San Jose, CA, USA). A Waters ACQUITY UPLC HSS T3 column (100 mm × 2.1 mm, 1.8 μm particles) combined with an ACQUITY UPLC HSS T3 VanGuard pre-column (5 mm × 2.1 mm, 1.8 μm particles) was used and kept at a temperature of 40 °C. Mixed isocratic and gradient elution at a flow rate of 0.45 mL/min was applied for analyte separation. In the mobile phase, solvent A consisted of 0.2% (v/v) acetic acid, and solvent B was ACN. The final method was an initial isocratic composition of 5% B held for 1 min, followed by a linear increase to 15% B for the next 1 min, and to 20% B in another 1 min. Then, B was increased linearly to 80% over the next min to flush the column. To re-equilibrate, B was reduced back to the initial isocratic composition of 5% and was held for 2 min.

Plasma samples were processed prior to LC-MS analysis. A volume of 20 μL plasma or surrogate matrix was pipetted into a 1.5 mL Eppendorf tube (Eppendorf, Hamburg, Germany). Ultra-pure water was used as a surrogate matrix for calibration curve and quality control samples. For the calibration curve and quality control samples, the 20 μL water sample contained the standards. Next, 30 μL of cold (4 °C) ACN with internal standards d4-kynurenine, d5-kynurenic acid, 13C6-indoxyl sulfate, d5- indole-3-acetic acid, d7-p-cresyl sulfate, d7-p-cresyl glucuronide and d5-hippuric acid were added. Samples were vortexed for 5 min on a plate shaker and centrifuged for 5 min at 4000 rpm. A 35 μL sample of the supernatant was then collected in 1 mL round-bottom well of a polypropylene 96-deep well plate and diluted with 200 μL of ultra-pure water. Finally, the plate was gently shaken before placing in the autosampler for analysis. Analyzed data are expressed as ng/mL or μg/mL.

2.16. Data Analysis

All data are presented as mean ± standard error of the mean (SEM). Statistical analysis was performed using one-way or two-way ANOVA followed by Dunnett's and Sidak's multiple comparison tests respectively, or where appropriate, an unpaired t-test. A p-value < 0.05 was considered significant and indicated using one asterisk. Software used for statistical analysis was GraphPad Prism (version 8.43; GraphPad software, La Jolla, CA, USA). Most experiments were repeated independently at least three times and in duplicates, unless otherwise stated. The exact sample size for each experiment is indicated in the corresponding figure legend.

3. Results

3.1. CiPTEC-OAT1 Respond to NLRP3 Inflammasome-Activating Stimuli
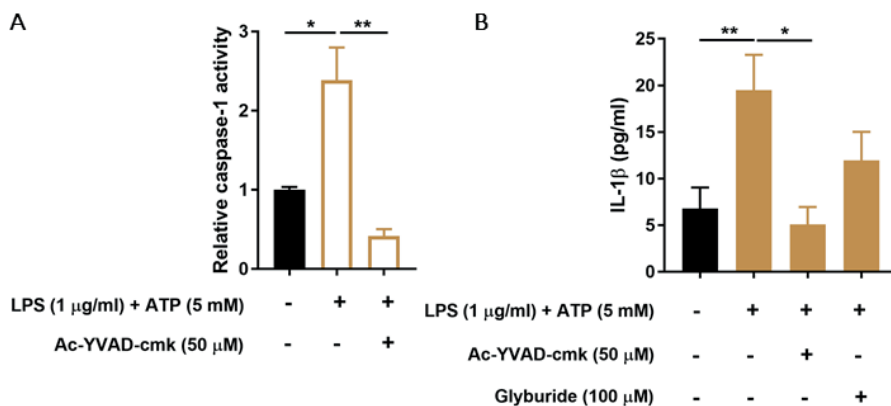

Figure 1. Effect of LPS and ATP on caspase-1 activity and IL-1β production in ciPEC-OAT1. (A) Relative caspase-1 activity in ciPTEC-OAT1 upon exposure to LPS (1 μg/mL; 2 h) and ATP (5 mM; 30 min) in the absence or presence of specific caspase-1 inhibitor, ac-YVAD-cmk (50 μM). (B) IL-1β secreted levels (pg/mL) by ciPEC-OAT1 following 24 h treatment with LPS (1 μg/mL; 24 h) and ATP (5 mM; 30 min), in the absence or presence of inhibitors ac-YVAD-cmk (50 μM) or glyburide (100 μM). Data are derived from three independent experiments performed in duplicate and expressed as mean ± SEM. * p < 0.05, ** p < 0.01 (One-way ANOVA followed by Dunnett's multiple comparison test, using as LPS/ATP treated cells as a control).

Known activating stimuli of the NLRP3 inflammasome, LPS and ATP, were used to determine whether ciPTEC-OAT1 cells respond with inflammasome activation, as evaluated by caspase-1 activity and IL-1β secretion. As shown in Figure 1A, 24 h exposure to LPS and exposure to ATP in the last 30 min of stimulation significantly increased caspase-1 activity, which was drastically reduced in the presence of a known inhibitor of caspase-1 function, ac-YVAD-cmk. Similarly, IL-1β secretion was increased upon LPS and ATP stimulation (Figure 1B). Specific inhibitors of caspase-1 activity (ac-YVAD-cmk) and of an ATP-sensitive potassium channel and NLRP3 (glyburide), reduced IL-1β secreted levels by approximately 75% and 39%, respectively.

3.2. PBUTs Induce Expression of NLRP3 Inflammasome-Related Genes in Proximal Tubule Cells

Next, we determined the expression levels of the NLRP3 inflammasome and its related components, ASC, caspase-1 and IL-1β, in ciPTEC-OAT1 upon exposure to PBUTs. The data show that IS was responsible for a dose-dependent increase of NLRP3 expression, with more than 2-fold increase at the highest concentration tested (Figure 2A). ASC expression levels, on the other hand, were reduced by IS while UT mix did not affect ASC mRNA levels (Figure 2B). Further, caspase-1 was upregulated after IS and UT mix stimulation (Figure 2C) as well as IL-1β expression levels in a dose-dependent manner (Figure 2D). Control treatment with LPS and ATP showed similar profiles of ASC, caspase-1 and IL-1β expression levels, while NLRP3 expression was reduced by more than 50% (Figure S1A–D).
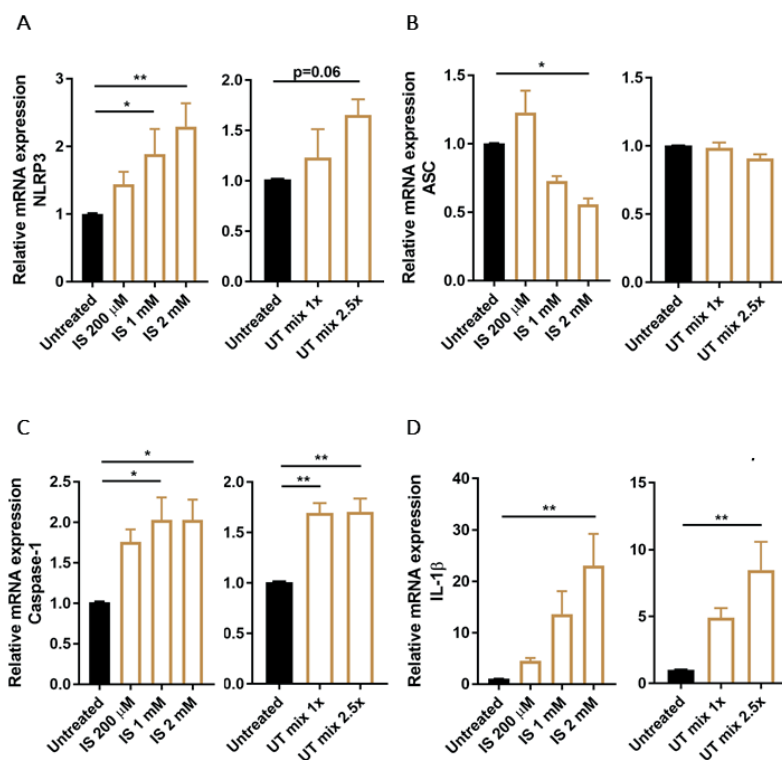

Figure 2. Expression of NLRP3 inflammasome related genes in ciPTEC-OAT1 after exposure to PBUTs. Relative mRNA expression of (A) NLRP3, (B) ASC, (C) caspase-1 and (D) IL-1β upon exposure to either IS (200 μM, 1 mM, 2 mM) or UT mix (1×, 2.5×), compared to control (untreated ciPTEC-OAT1). Data are derived from three independent experiments performed in duplicate and expressed as mean ± SEM. * p < 0.05, ** p < 0.01 (One-way ANOVA followed by Dunnett's multiple comparison test, using untreated cells as a control).

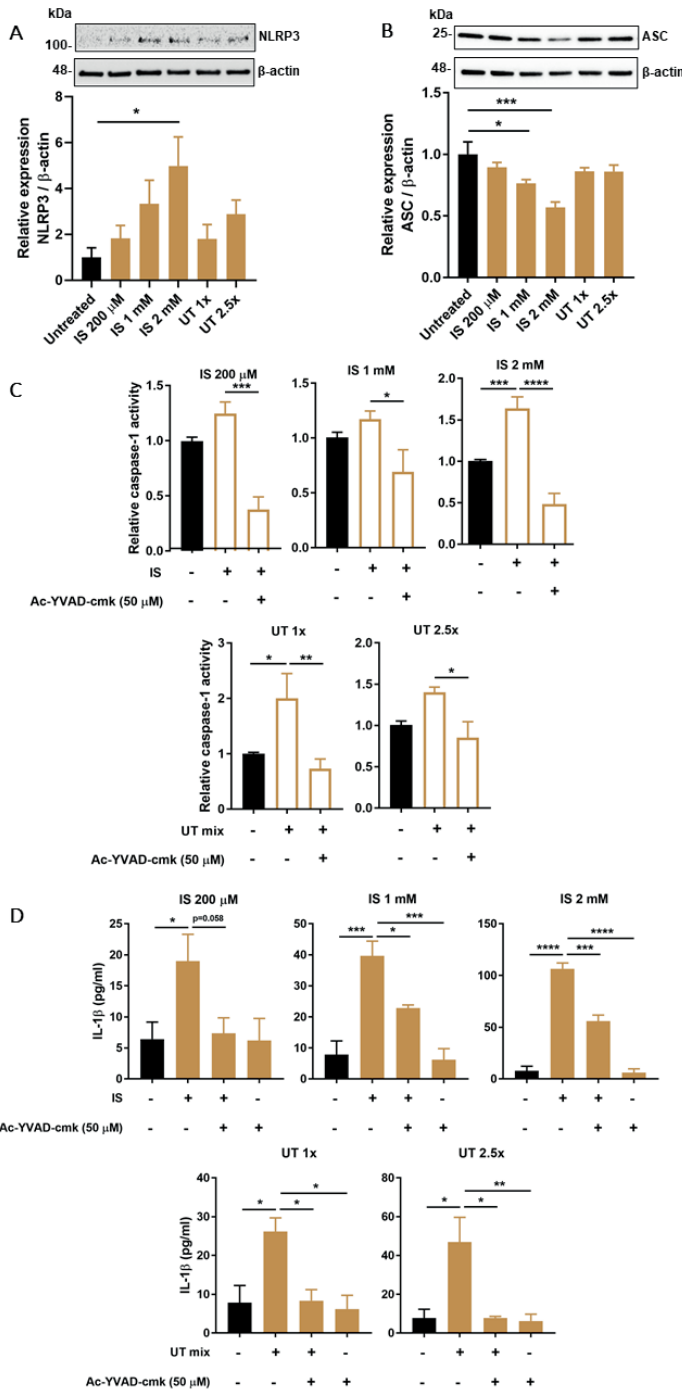### 3.3.PBUTs Induce Expression of NLRP3 Inflammasome-Related Proteins

Figure 3. Effect of PBUTs on protein levels or functional activity of NLRP3 inflammasome-related components in ciPTEC-OAT1. Representative Western blot and quantification of relative expression of (A) NLRP3 and (B) ASC in ciPTEC-OAT1 following 24 h exposure to IS (200 μM, 1 mM, 2 mM) and UT mix (1×, 2.5×); normalized to β-actin. (C) Relative caspase-1 activity in ciPTEC-OAT1 upon 2 h exposure to IS (200 μM, 1 mM, 2 mM) and UT mix (1×, 2.5×), in the absence or presence of specific caspase-1 inhibitor, ac-YVAD-cmk (50 μM). (D) IL-1β secreted levels (pg/mL) by ciPEC-OAT1 upon 24 h treatment with IS (200 μM, 1 mM, 2 mM) and UT mix (1×, 2.5×), in the absence or presence of ac-YVAD-cmk (50 μM). Data are derived from at least three independent experiments performed in triplicate and expressed as mean ± SEM. * $p < 0.05$, ** $p < 0.01$, *** $p < 0.001$, **** $p < 0.0001$ (One-way ANOVA followed by Dunnett's multiple comparison test, using either untreated or PBUTs treated cells as a control).

3

Following 24 h exposure to increasing concentrations of IS or UT mix, NLRP3 levels showed a dose-dependent increase at all tested concentrations (Figure 3A). Similar to what was observed for mRNA levels, ASC protein expression was downregulated in a dose-dependent manner after exposure to IS, while UT mix did not have a significant impact (Figure 3B). Treatment with LPS and ATP also did not significantly affect NLRP3 or ASC levels (Figure S1E,F). Caspase-1 activity was slightly increased after both IS and UT mix treatments at all concentrations evaluated, which was counteracted by ac-YVAD-cmk treatment (Figure 3C). One of the main indicators of inflammasome activation, IL-1β secretion, was also increased at all concentrations of IS and UT mix tested, which was reduced in the presence of ac-YVAD-cmk (Figure 3D).

3.4. PBUTs Induce Oxidative Stress and ROS-Dependent Caspase-1 Activity and IL-1β Production.

To evaluate the effects of PBUTs on oxidative stress, which is a known trigger of NLRP3 inflammasome activation, the intracellular production of ROS was measured following 2 h exposure to either increasing concentrations of IS or UT mix. Results indicate a clear increase of ROS production in ciPTEC-OAT1 after exposures, with H_2O_2 serving as positive control (Figure 4A). In all conditions tested, ROS were reduced to almost baseline levels in the presence of NAC (Figure 4A) or Trolox (Figure S2A) as antioxidant agents.

To determine the role of oxidative stress on the inflammasome activation, caspase-1 activity and IL-1β secretion were evaluated after treatment with PBUTs in the absence or presence of antioxidant NAC. As shown in Figure 4B, lower concentrations of IS caused an increasing trend in caspase-1 activity, while high IS concentrations induced a significant increase in caspase-1 activity that was abolished to baseline levels in the presence of NAC. UT mix significantly increased caspase-1 activity that was counteracted by NAC. The secreted levels of IL-1β were also affected by PBUTs-mediated oxidative stress (Figure 4C). IS treatments increased IL-1β levels, which were significantly reduced when NAC was present as a co-treatment. NAC was also able to counteract the UT mix-mediated IL-1β increased levels. A similar, although less pronounced, pattern of IL-1β secretion was observed when Trolox was used as antioxidant for the co-treatment with PBUTs (Figure S2B).

Figure 4. Effect of PBUTs-induced oxidative stress on caspase-1 activity and IL-1β production in ciPTEC-OAT1. (A) Relative intracellular ROS production in ciPTEC-OAT1 after 2 h exposure to IS (200 μM, 1 mM, 2 mM), UT mix (1×, 2.5×) and H_2O_2 (200 μM, positive control), in the absence or presence of ROS inhibitor NAC (1.8 mM). (B) Relative caspase-1 activity in ciPTEC-OAT1 following 2 h exposure to IS (200 μM, 1 mM, 2 mM) and UT mix (1×, 2.5×), in the absence or presence of NAC (1.8 mM). (C) IL-1β secreted levels (pg/mL) by ciPEC-OAT1 upon 24 h treatment with IS (200 μM, 1 mM, 2 mM) and UT mix (1×, 2.5×), in the absence or presence of NAC (1.8 mM). Data are derived from at least three independent experiments performed in triplicate and expressed as mean ± SEM. * $p < 0.05$, ** $p < 0.01$, *** $p < 0.001$, **** $p < 0.0001$ (One-way ANOVA followed by Dunnett's multiple comparison test, using PBUTs treated cells as a control).
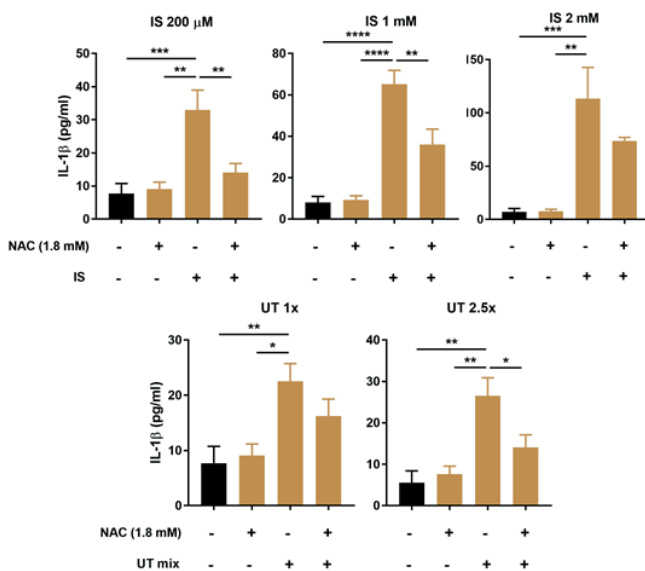
3
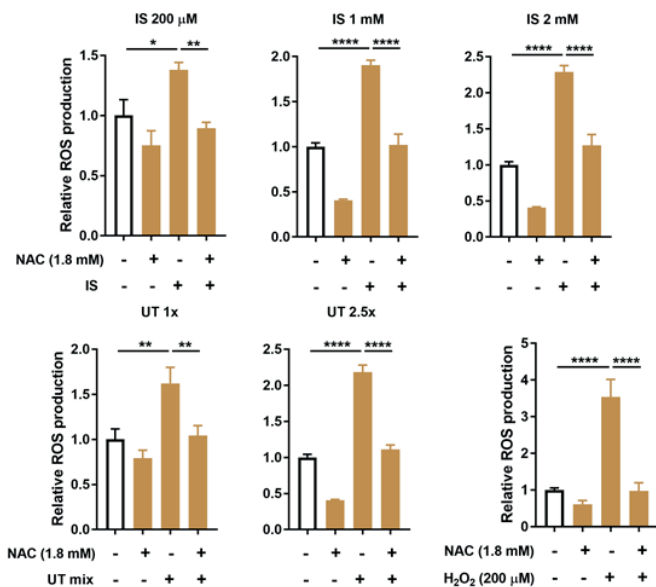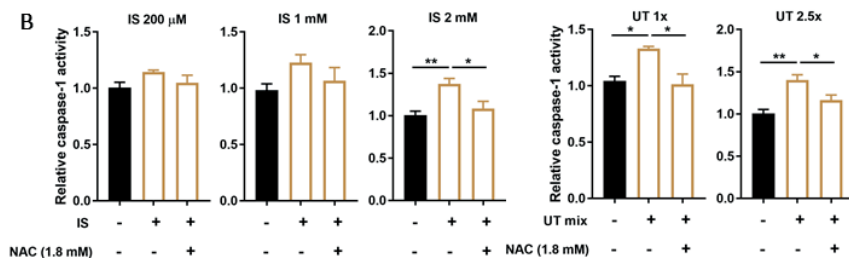
3.5. PBUTs Activate NF-κB Leading to IL-1β Production.

NF-κB activation is usually required as a priming step in inflammasome-mediated IL-1β production. As an indication of NF-κB activation, nuclear translocation of p65 was assessed after exposing ciPTEC-OAT1 to PBUTs. Increased nuclear intensity of p65 was observed after all treatment conditions, including positive control treatments with either LPS or TNF-α (Figure 5A,B). As further evidence of NF-κB activation, mRNA levels of some of the most relevant target genes were determined. Among those, IL-1β mRNA levels were significantly upregulated following 4 h exposure to IS and UT mix in the presence of the selective IKK inhibitor, BMS-345541 (Figure 5C). Comparable expression patterns were observed for other NF-κB target genes, HMOX1, NFKBIA and TNF (Figure S3A–C). Finally, IL-1β secretion was measured after co-treatment with PBUTs and BMS-345541. As shown in Figure 5D, all treatment conditions significantly increased IL-1β levels, while in the presence of the IKK inhibitor there was a significant reduction of IL-1β secretion.

Figure 5. Effect of PBUTs on NF-κB signaling and the role of NF-κB on PBUTs-mediated caspase-1 activity and IL-1β production in ciPTEC-OAT1. (A) Representative images (20×) and (B) quantification of p65 nuclear expression in ciPTEC-OAT1 after 1 h incubation with IS (200 μM, 1 mM, 2 mM), UT mix (1×, 2.5×), LPS (200 μg/mL) or TNF-α (100 ng/mL). (C) Relative mRNA expression of IL-1β upon 4 h exposure to either IS (200 μM, 1 mM, 2 mM) or UT mix (1×, 2.5×), in the absence or presence of specific IKK inhibitor BMS-345541 (4 μM) and compared to control (untreated ciPTEC-OAT1). (D) IL-1β secreted levels (pg/mL) by ciPEC-OAT1 following 24 h treatment with IS (200 μM, 1 mM, 2 mM) and UT mix (1×, 2.5×), in the absence or presence of BMS-345541 (4 μM). Data are derived from at least two independent experiments performed at least in duplicate and expressed as mean ± SEM. * $p < 0.05$, ** $p < 0.01$, *** $p < 0.001$, **** $p < 0.0001$ (One-way ANOVA followed by Dunnett's multiple comparison test, using either untreated or PBUTs treated cells as a control).
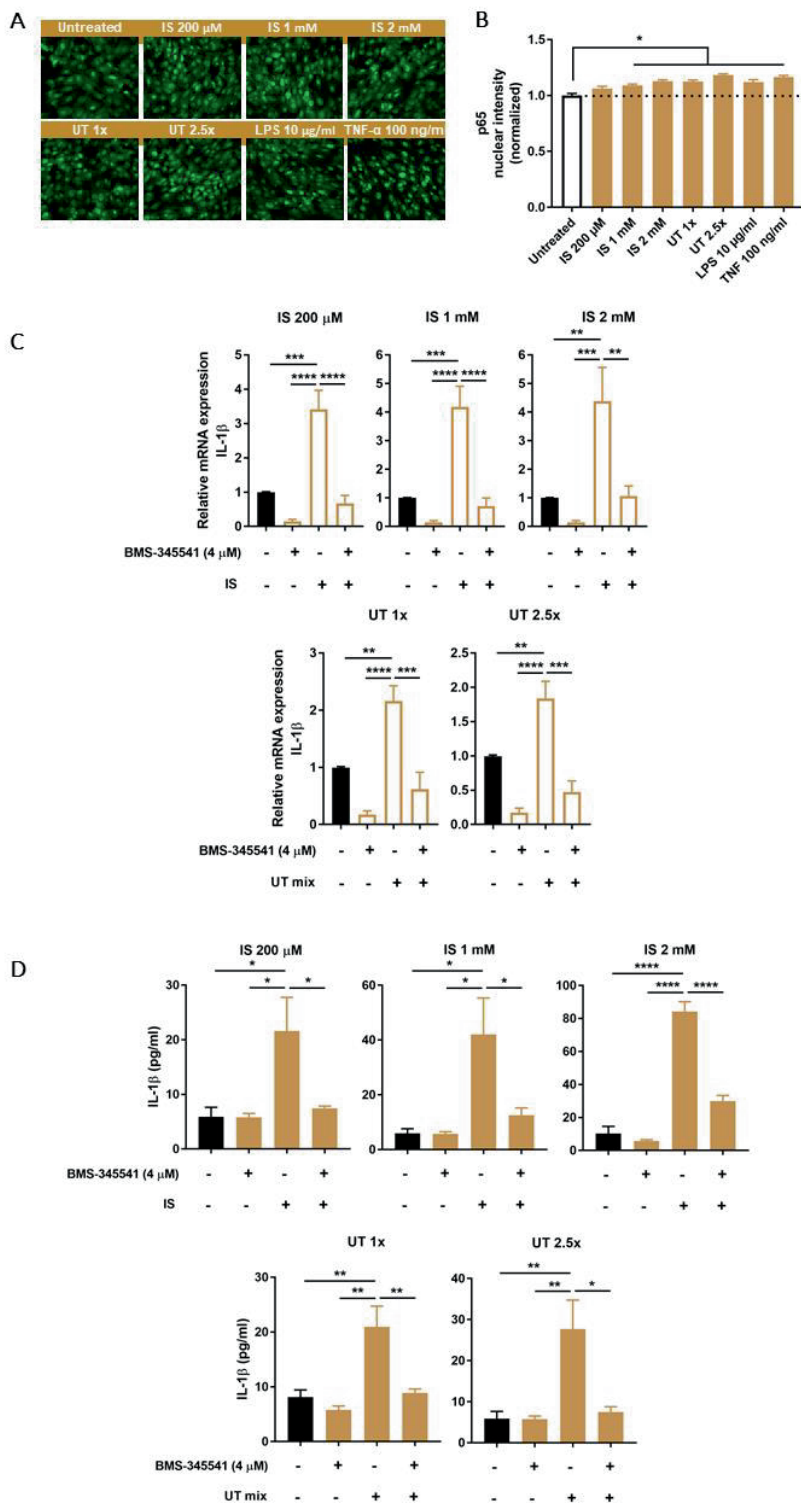
3.6. Increased PBUTs Plasma Levels, Oxidative Stress and NLRP3 Inflammasome-Related Protein Expression in a CKD Rat Model

Our CKD rat model was created via single-procedure SNX in female Sprague Dawley rats. Prior to CKD induction, 9-weeks old rats in Sham and CKD groups showed similar baseline values for body weight and several CKD-related experimental parameters (Table 2). At approximately 5 months after SNX, the successful induction of CKD was confirmed by increased values of SBP, plasma creatinine and urea, and proteinuria in CKD compared with Sham. Progression to CKD was confirmed by histological analyses of the kidney remnants, both by high TI injury score (Figure 6A–E) and abundant presence of immune cells (macrophages, ED1+), especially in the TI area of CKD animals (Figure 6F–J).

Next, plasma levels of seven PBUTs were measured in both Sham and CKD animals (Figure 7A–G) and the results obtained showed a significant increase of IS, kynurenic acid, hippuric acid, and an increasing trend of L-kynurenine, indole-3-acetic acid, p-cresyl glucuronide and p-cresyl sulfate in the CKD group. Moreover, urine MDA levels, used as an indicator of CKD-associated oxidative damage, showed a 3.3-fold increase in the CKD group compared with Sham animals (Figure 7H).

To determine the effects of CKD on the inflammasome regulation in kidney tissue, protein levels of NLRP3, and inflammasome-related proteins pro-caspase-1 (p45), caspase-1 (p20), and pro-IL-1β were measured together with superoxide dismutase-1 (SOD-1) as an additional marker of oxidative stress. The results obtained show that there was an increasing trend of expression in kidney tissue of two different isoforms of NLRP3 in CKD animals (Figure 7I–K). An increasing trend for caspase-1 (p20) in the CKD animals and no difference in expression levels of pro-caspase-1 (p45) were found in the two groups (Figure 7L–N), while pro-IL-1β was detectable only in the Sham group (Figure 7O–P). Finally, the kidney levels of SOD-1 showed a strong decreasing trend in the CKD group compared to Sham (Figure 7O,Q).

Table 2. Main parameters (baseline and endpoint) evaluated in healthy (Sham; n = 3) and CKD (SNX; n = 4) animals 1.

Parameter	Baseline		Endpoint	
	Healthy (Sham)	CKD (SNX)	Healthy (Sham)	CKD (SNX)
Age (weeks)	9	9	29	31
Body weight (g)	174.3 ± 10.7	182.5 ± 7.0	276.0 ± 16.0 **	293.0 ± 18.6 ***
Systolic blood pressure (SBP) (mmHg)	120.7 ± 5.8	142.7 ± 16.0	128.0 ± 5.4	202.9 ± 18.8 *#
Hematocrit (%)	41.3 ± 0.9	40.5 ± 0.7	42.7 ± 0.9	41.3 ± 1.0
Plasma creatinine (µmol/L)	33.9 ± 8.6	29.1 ± 3.8	34.3 ± 5.6	77.1 ± 9.9 **#
Urine creatinine (µmol/24 h)	42.4 ± 1.2	39.2 ± 2.4	78.2 ± 10.7	89.1 ± 14.8 *
Plasma urea (mmol/L)	5.1 ± 0.3	4.9 ± 0.4	6.7 ± 0.6	16.3 ± 2.8 **#
Urine Na^+ (µmol/24 h)	451.1 ± 88.2	386.4 ± 45.7	509.1 ± 48.3	540.9 ± 110.4
Urine K^+ (µmol/24 h)	914.3 ± 81.6	773.9 ± 59.3	975.6 ± 133.0	1840.1 ± 353.7 *
Proteinuria (mg/24 h)	2.3 ± 0.5	2.3 ± 0.3	2.1 ± 0.1	329.4 ± 55.9 ***###

[1] Age is presented as median, all the other parameters are presented as mean $\pm$ SEM. * $p < 0.05$, ** $p < 0.01$, *** $p < 0.001$ (Two-way ANOVA followed by Sidak's multiple comparison test, using corresponding baseline values as controls); # $p < 0.05$, ### $p < 0.001$ (Two-way ANOVA followed by Sidak's multiple comparison test, using corresponding Sham values as controls).
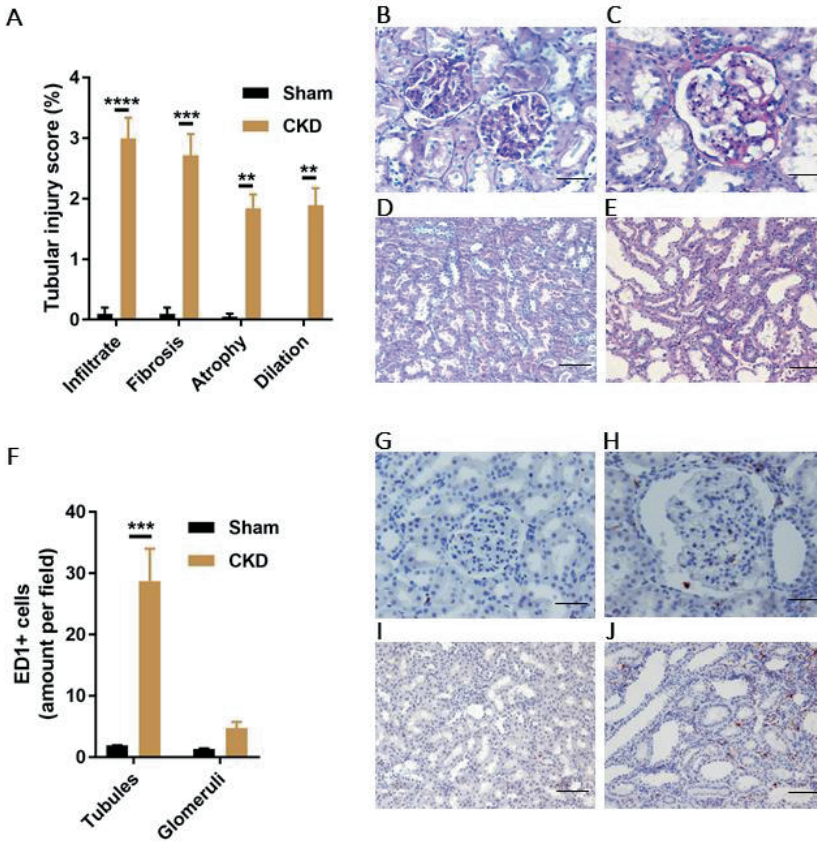
3

Figure 6.Characteristics of the CKD model in female Sprague Dawley rats created using single-procedure SNX. (A) Tubular injury score (%) in CKD and Sham rats, characterized by infiltrate, tubular fibrosis, atrophy and dilation. Representative PAS-staining images of glomeruli (20×) in (B) Sham and (C) CKD rats. Scale bars 50 μm. Representative PAS-staining images of tubules (10×) in (D) Sham and (E) CKD rats. Scale bars 100 μm. (F) Quantification of ED1 positive cells in tubules and glomeruli of Sham and CKD rats. Representative images of ED1 staining in glomeruli (20×) of (G) Sham and (H) CKD animals. Scale bars 50 μm. Representative images of ED1 staining in tubules (10×) of (I) Sham and (J) CKD animals. Scale bars 100 μm. Data are derived from n = 3 Sham and n = 4 CKD animals and presented as mean ± SEM. *** $p < 0.001$, **** $p < 0.0001$ (Two-way ANOVA followed by Sidaks's multiple comparison test).

Figure 7. PBUTs plasma levels, oxidative damage and NLRP3 inflammasome components protein expression in CKD model. Quantification of total plasma levels (μg/mL or ng/mL) of (A) indoxyl sulfate (IS), (B) L-kynurenine (Kyn), (C) Indole-3-acetic acid (3-IAA), (D) kynurenic acid (KA), (E) hippuric acid (HA), (F) p-cresyl glucuronide (pCG) and G) p-cresyl sulfate (pCS) in Sham and CKD rats. (H) Urine MDA levels (nmol/mL) in Sham and CKD animals. (I–K) Representative Western blot and quantification of relative expression of NLRP3 in Sham and CKD rats; normalized to β-actin. (L–N) Representative Western blot and quantification of relative expression of pro-caspase-1 (p45) and caspase-1 (p20) in Sham and CKD rats; normalized to α-tubulin. (O) Representative Western blot of pro-IL-1β and SOD-1 in Sham and CKD rats. Quantification of relative expression of (P) pro-IL-1β and (Q) SOD-1; normalized to α-tubulin. Data are derived from n = 3 Sham and n = 4 CKD animals and presented as mean ± SEM. * $p < 0.05$, **** $p < 0.0001$ (Unpaired t-test).
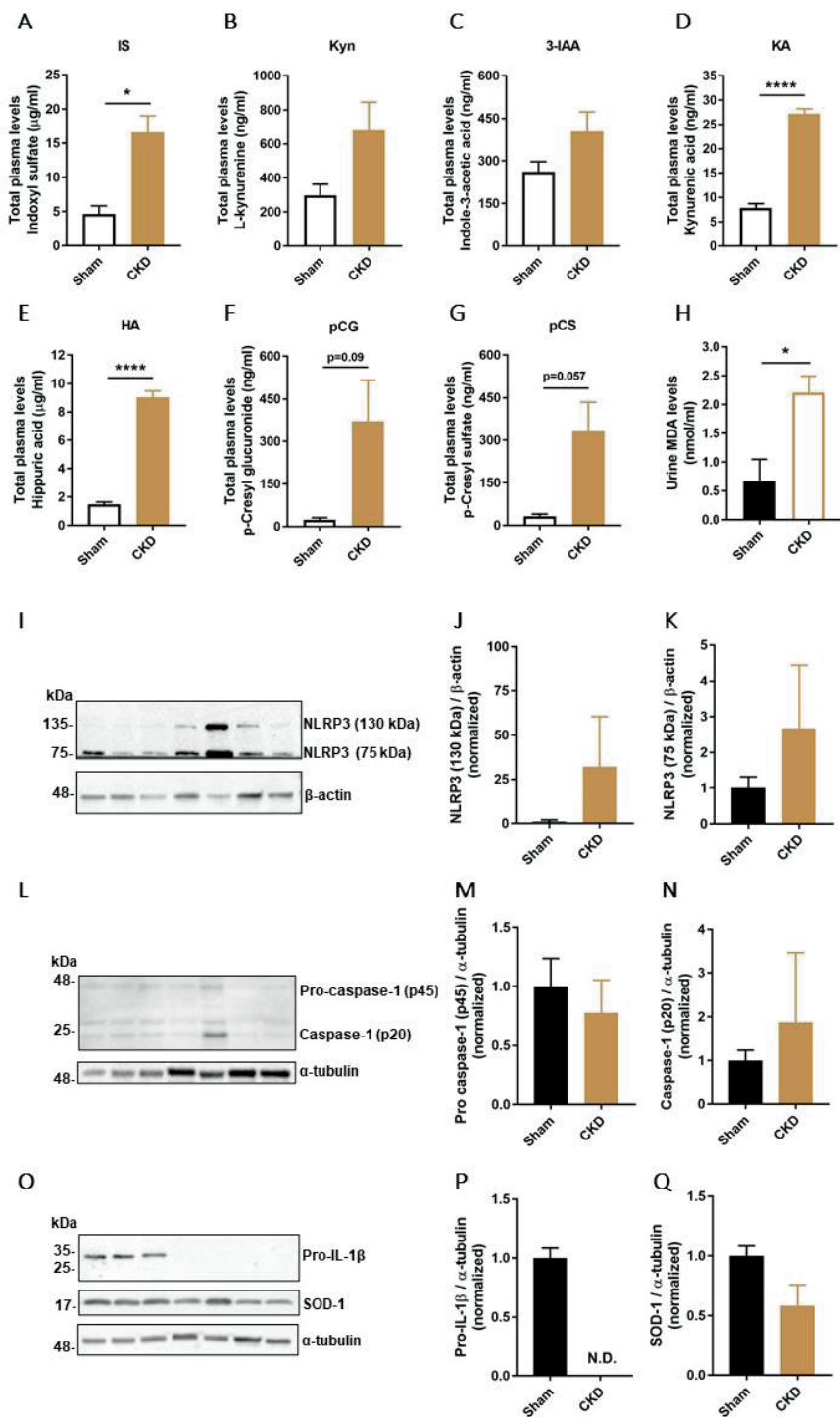
4. Discussion

PBUTs are known pro-inflammatory and pro-oxidative metabolites whose negative consequences in the context of CKD are well-described [18,40]. IL-1β, a pro-inflammatory mediator known to have systemic consequences, is a marker of NLRP3 inflammasome activation and can promote kidney inflammation [41]. The NLRP3 inflammasome has also been shown to be involved in various CKD-related conditions, as demonstrated in different experimental models of kidney disease. For instance, reduced expression and maturation of IL-1β, IL-18 and caspase-1 activation and reduced tubular damage and fibrosis in an NLRP3 knockout unilateral ureteral obstruction (UUO) model was observed [42]. The NLRP3 inflammasome inhibition has been also shown to ameliorate TI damage in a remnant kidney model [43]. Furthermore, various factors related to CKD such as proteinuria, aldosterone, calcinosis and mitochondrial dysfunction have been shown to directly interfere with inflammasome and subsequent kidney injury [44,45,46]. In addition, the NLRP3 inflammasome involvement has been described in other forms of kidney disease, including crystalline nephropathies, diabetic nephropathy, IgA nephropathy as well as lupus nephritis [26,47]. Finally, it has been demonstrated that NLRP3 inflammasome is activated in CKD patients undergoing dialysis treatment [48,49]. On the other hand, IS has been shown to influence IL-1β secretion during kidney injury in various cell types, including endothelial cells, macrophages and monocytes, via ROS, NF-κB and/or mitogen-activated protein kinase pathways [50,51,52,53]. However, the effects of PBUTs on IL-1β production by kidney epithelial cells, in particular proximal tubule cells, and the molecular mechanisms involved, are still unclear.

In the present study, we demonstrated that PBUTs are capable of inducing inflammasome-mediated IL-1β production and secretion in human proximal tubule epithelial cells (ciPTEC-OAT1). Our results point towards a PBUT-mediated inflammasome activation, which is dependent on oxidative stress and activation of the NF-κB signaling pathway (summarized in Figure 8). Upon entering the cells via organic anion transporter 1 (OAT-1), or interacting with surface receptors, such as epidermal growth factor receptor (EGFR) [54,55], IS, and presumably other anionic PBUTs, stimulate NF-κB with subsequent p50/p65 translocation to the nucleus and transcription initiation, as well as ROS generation and oxidative stress. Following enhanced transcription of IL-1β, ROS-mediated NLRP3 inflammasome assembly leads to caspase-1 activation and subsequent proteolytic cleavage of pro-IL-1β into IL-1β that is secreted by the cells.
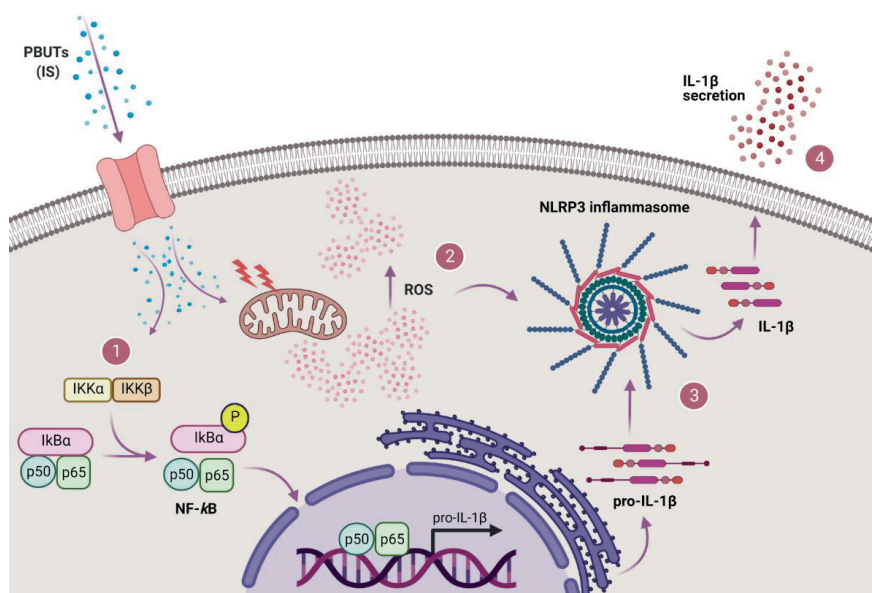
Figure 8. Proposed mechanism of PBUTs-ROS-driven NLRP3 inflammasome-mediated IL-1β production in proximal tubule epithelial cells. After reaching the cells, IS and other PBUTs lead to both (1) NF-κB signaling activation (p50/p65 translocation to the nucleus and transcription initiation) and (2) ROS production and oxidative stress. Following enhanced transcription of IL-1β and production of pro-IL-1β, ROS-mediated NLRP3 inflammasome is assembled thus leading to caspase-1 activation, and subsequent (3) proteolytic cleavage of pro-IL-1β into IL-1β that is (4) secreted by the cells. Created with BioRender.com.

To our knowledge, we showed for the first time that IS (and the PBUTs mixture) induced NLRP3 expression both at mRNA and protein levels in proximal tubule cells, accompanied by increased caspase-1 activity and IL-1β expression and secretion. These findings are in accordance with a previously published study focusing on IS effects on rat myoblast cells in the context of cardiac contractile dysfunction associated with CKD, in which an upregulation of NLRP3, IL-1β and activation of NF-κB were observed [56]. However, conflicting effects of IS on NLRP3 inflammasome regulation have been reported as well. Wakamatsu et al. observed that NLRP3 expression was reduced in macrophages exposed to IS, whereas caspase-1 and IL-1β expression were increased [51]. Similarly, another study with macrophages showed that IS decreased NLRP3 protein expression, while increasing IL-1β secretion, in addition to showing that IS exposure prior to inflammasome induction suppressed caspase-1 maturation and NLRP3 expression [57]. Both these studies focused on THP-1-derived macrophages, in contrast to myoblasts and to our study which addressed tubular epithelial cells. Immune cells, including macrophages, different from other cell types, are specialized in orchestrating efficient activation of the inflammasome in response to danger signals [58]. This suggests that different cell types could present distinct responses to certain stimuli. Proximal tubular cells are specialized in the uptake and excretion of IS thanks to the abundant expression of transporters of the organic anion pathway, and therefore can be more susceptible to their biological effects compared to other cell types [30,59,60]. In fact, IS is directly cytotoxic to renal tubules and is

considered as one of the most important toxins contributing to CKD progression [61]. The oxidative stress induced by IS, associated with a production of a plethora of pro-inflammatory and pro-fibrotic factors, is one of the key players of IS-mediated cytotoxicity of tubular cells [31,61]. Therefore, the contrasting observations on how IS influences NLRP3 inflammasome activation and the lack of relevant studies suggest that further research implementing different cell types and animal models is required to better understand the role of PBUTs in inflammasome regulation in specific tissues and organs.

As mentioned earlier, inflammasome activation and subsequent IL-1β production requires two signals: the first enhances pro-inflammatory cytokines (IL-1β, IL-18) synthesis and the second triggers inflammasome formation [21,62]. We have shown that PBUTs are able to provide both signals. In line with literature describing the effects of IS on NF-κB pathway activation, we observed that IS induced p65 nuclear translocation and subsequent increase in target genes expression levels (IL1B, HMOX1, NFKBIA and TNF), confirming the ability of IS to provide the first signal in inflammasome activation [51,63]. Moreover, we showed that IS-mediated increase of intracellular ROS levels is also important in the regulation of IL-1β production, since the use of ROS inhibitor NAC abolished both caspase-1 activity and IL-1β secretion, suggesting its crucial role in inflammasome activation. This finding is in accordance with previous studies focusing on IS effects on redox imbalance and ROS production in various cell types [64,65,66].

Treatment with LPS and ATP augmented caspase-1 activity and IL-1β secretion in ciPTEC-OAT1, which proves that the cell model used in this study responds effectively to NLRP3 inflammasome-stimulating agents. Previous studies have shown that this particular PAMPs/DAMPs treatment combination is a very potent stimulus, as the pro-inflammatory LPS provides a priming step causing IL-1β upregulation via TLR4/NF-κB signalling and extracellular ATP provides a necessary triggering signal for NLRP3 inflammasome assembly and activation by inducing K+ efflux through interaction with purinergic P2X7 receptor [67,68]. In line with literature, LPS/ATP-treated ciPTEC-OAT1 responded to both the specific caspase-1 inhibitor ac-YVAD-cmk and the indirect inflammasome inhibitor glyburide with a decreased IL-1β production [69,70,71]. Consistently, ASC expression did not change on mRNA nor protein levels after 24 h exposure, while IL-1β and caspase-1 were both upregulated [62]. NLRP3, however, did show a slight increasing trend in protein levels, and downregulation on mRNA levels, potentially indicating the presence of a tissue (kidney) specific negative regulatory mechanism [72].

Finally, our SNX model presented typical characteristics of progressing CKD, including hypertension, proteinuria, uremia, as well as histological features reflecting tubular atrophy, fibrosis and abundant TI inflammation [37]. We showed a significant difference of several PBUTs plasma levels in CKD compared to Sham rats, as well as urine levels of MDA, clearly suggesting ongoing pro-inflammatory and oxidative status in these diseased animals. Moreover, the increased PBUTs plasma levels, urine MDA and low kidney SOD-1 correlate with the expression of some of the NLRP3 inflammasome-related markers as well. We observed strong tendencies for increased NLRP3 expression in CKD kidney tissue for two different molecular bands of NLRP3 with respect to healthy tissue, similar to what was observed for other CKD models [42]. While the expected size of NLRP3 is 118 kDa, most likely the high molecular

band of approximately 130 kDa that we detected in kidney tissue is the result of a co-migration of the 118 kDa isoform and an isoform lacking two leucine-rich repeats (LRRs), whereas the low molecular band (75 kDa) is a short isoform lacking all the LRRs, and is prevalently derived from immune cells [73]. Moreover, it has been shown that the LRR domain of the NLRP3 is subject to alternative splicing that can be regulated on single cell level, and that can lead to NLRP3 increased functional diversity especially in the innate immune cells [74]. Comparable but less pronounced expression pattern was observed for activated caspase-1 (p20), while no expression of IL-1β could be detected. This is most likely due to the rapid secretion and depletion of the produced IL-1β given that the kidney is the main site of IL-1β metabolic degradation, in association also with a low half-life of the cytokine and possibly late time point used here for detection [75,76]. On the other hand, pro-IL-1β was only detected in healthy kidneys, suggesting that less IL-1β was produced in healthy rats compared to CKD rats in which a more enhanced IL-1β processing could have taken place. The expression levels of SOD-1 detected were lower in CKD compared to Sham rats which is in accordance with previous findings showing markedly reduced SOD-1 expression and superoxide scavenging activity (SOD activity equivalent) in CKD rats, further aggravated by IS [77]. For more conclusive findings, a larger number of animals and multiple time points for markers detection should be taken along in future studies. Studies involving knock out models for NLRP3 inflammasome and its components and/or PBUTs-relevant enzymes and transporters could greatly help understand better how PBUTs regulate NLRP3 inflammasome in proximal tubule cells and improve the comprehension of incongruous observations.

In conclusion, in the present study we showed for the first time that IS and PBUTs are involved in inflammasome-mediated IL-1β secretion by proximal tubule cells and that the most likely mechanism of NLRP3 inflammasome activation is the ROS model [29]. This suggests that the observed PBUTs-mediated interplay between pro-inflammatory and oxidative signalling pathways in the proximal tubule leads to IL-1β release, which could potentially be exploited for specific treatments aimed at contrasting CKD-associated inflammation.

Acknowledgments

Author Contributions

Conceptualization, M.M. and R.M.; methodology, M.M., M.M.K., M.C.V. and R.M.; validation, M.M., M.M.K. and S.A.; formal analysis, M.M. and M.M.K.; investigation, M.M., M.M.K., Y.Y., S.A., V.L. and D.A.; writing—original draft preparation, M.M.; writing—review and editing, M.M., M.M.K., Y.Y., S.A., M.C.V. and R.M.; visualization, M.M., M.M.K. and Y.Y.; supervision, M.C.V. and R.M.; funding acquisition, M.C.V. and R.M. All authors have read and agreed to the published version of the manuscript.

Funding

Institutional Review Board Statement

All animal experiments were performed in agreement with the current Dutch law on animal experiments and were approved by the Animal Ethics Committee of the University of Utrecht (CCD; AVD115002015310).

Data Availability Statement

All data generated or analysed during this study are included in the published article.

Conflicts of Interest

The authors declare no conflict of interest. The funders had no role in the design of the study; in the collection, analyses, or interpretation of data; in the writing of the manuscript, or in the decision to publish the results.

References

1. Coresh J. Update on the burden of ckd. J. Am. Soc. Nephrol. 2017;28:1020–1022.
2. Hill N.R., Fatoba S.T., Oke J.L., Hirst J.A., O'Callaghan C.A., Lasserson D.S., Hobbs F.D. Global prevalence of chronic kidney disease—A systematic review and meta-analysis. PLoS ONE. 2016;11:e0158765.
3. Mihai S., Codrici E., Popescu I.D., Enciu A.M., Albulescu L., Necula L.G., Mambet C., Anton G., Tanase C. Inflammation-related mechanisms in chronic kidney disease prediction, progression, and outcome. J. Immunol. Res. 2018;2018:2180373.
4. Akchurin O.M., Kaskel F. Update on inflammation in chronic kidney disease. Blood Purif. 2015;39:84–92.
5. Go A.S., Chertow G.M., Fan D., McCulloch C.E., Hsu C.Y. Chronic kidney disease and the risks of death, cardiovascular events, and hospitalization. N. Engl. J. Med. 2004;351:1296–1305.
6. Goligorsky M.S. Pathogenesis of endothelial cell dysfunction in chronic kidney disease: A retrospective and what the future may hold. Kidney Res. Clin. Pract. 2015;34:76–82.
7. Gupta J., Mitra N., Kanetsky P.A., Devaney J., Wing M.R., Reilly M., Shah V.O., Balakrishnan V.S., Guzman N.J., Girndt M., et al. Association between albuminuria, kidney function, and inflammatory biomarker profile in ckd in cric. Clin. J. Am. Soc. Nephrol. 2012;7:1938–1946.
8. Stenvinkel P., Heimburger O., Paultre F., Diczfalusy U., Wang T., Berglund L., Jogestrand T. Strong association between malnutrition, inflammation, and atherosclerosis in chronic renal failure. Kidney Int. 1999;55:1899–1911.
9. Floege J., Drueke T.B. Mineral and bone disorder in chronic kidney disease: Pioneering studies. Kidney Int. 2020;98:807–811.
10. Bugnicourt J.M., Godefroy O., Chillon J.M., Choukroun G., Massy Z.A. Cognitive disorders and dementia in ckd: The neglected kidney-brain axis. J. Am. Soc. Nephrol. 2013;24:353–363.
11. Dalrymple L.S., Go A.S. Epidemiology of acute infections among patients with chronic kidney disease. Clin. J. Am. Soc. Nephrol. 2008;3:1487–1493.
12. Tonelli M., Wiebe N., Culleton B., House A., Rabbat C., Fok M., McAlister F., Garg A.X. Chronic kidney disease and mortality risk: A systematic review. J. Am. Soc. Nephrol. 2006;17:2034–2047.
13. Borges Bonan N., Schepers E., Pecoits-Filho R., Dhondt A., Pletinck A., De Somer F., Vanholder R., Van Biesen W., Moreno-Amaral A., Glorieux G. Contribution of the uremic milieu to an increased pro-inflammatory monocytic phenotype in chronic kidney disease. Sci. Rep. 2019;9:10236.
14. Vanholder R., Baurmeister U., Brunet P., Cohen G., Glorieux G., Jankowski J., European Uremic Toxin Work Group A bench to bedside view of uremic toxins. J. Am. Soc. Nephrol. 2008;19:863–870.
15. Vanholder R., De Smet R., Glorieux G., Argiles A., Baurmeister U., Brunet P., Clark W., Cohen G., De Deyn P.P., Deppisch R., et al. Review on uremic toxins: Classification, concentration, and interindividual variability. Kidney Int. 2003;63:1934–1943.
16. Dhondt A., Vanholder R., Van Biesen W., Lameire N. The removal of uremic toxins. Kidney Int. 2000;58((Suppl. 76)):S47–S59.
17. Mair R.D., Sirich T.L., Plummer N.S., Meyer T.W. Characteristics of colon-derived uremic solutes. Clin. J. Am. Soc. Nephrol. 2018;13:1398–1404.
18. Rossi M., Campbell K.L., Johnson D.W., Stanton T., Vesey D.A., Coombes J.S., Weston K.S., Hawley C.M., McWhinney B.C., Ungerer J.P., et al. Protein-bound uremic toxins, inflammation and oxidative stress: A cross-sectional study in stage 3–4 chronic kidney disease. Arch. Med. Res. 2014;45:309–317.
19. Xiang H., Zhu F., Xu Z., Xiong J. Role of inflammasomes in kidney diseases via both canonical and non-canonical pathways. Front. Cell Dev. Biol. 2020;8:106.
20. De Zoete M.R., Palm N.W., Zhu S., Flavell R.A. Inflammasomes. Cold Spring Harb. Perspect. Biol. 2014;6:a016287.

3

21. Swanson K.V., Deng M., Ting J.P. The nlrp3 inflammasome: Molecular activation and regulation to therapeutics. Nat. Rev. Immunol. 2019;19:477–489.
22. Mariathasan S., Weiss D.S., Newton K., McBride J., O'Rourke K., Roose-Girma M., Lee W.P., Weinrauch Y., Monack D.M., Dixit V.M. Cryopyrin activates the inflammasome in response to toxins and atp. Nature. 2006;440:228–232.
23. He X., Mekasha S., Mavrogiorgos N., Fitzgerald K.A., Lien E., Ingalls R.R. Inflammation and fibrosis during chlamydia pneumoniae infection is regulated by il-1 and the nlrp3/asc inflammasome. J. Immunol. 2010;184:5743–5754.
24. Thomas P.G., Dash P., Aldridge J.R., Jr., Ellebedy A.H., Reynolds C., Funk A.J., Martin W.J., Lamkanfi M., Webby R.J., Boyd K.L., et al. The intracellular sensor nlrp3 mediates key innate and healing responses to influenza a virus via the regulation of caspase-1. Immunity. 2009;30:566–575.
25. Joly S., Ma N., Sadler J.J., Soll D.R., Cassel S.L., Sutterwala F.S. Cutting edge: Candida albicans hyphae formation triggers activation of the nlrp3 inflammasome. J. Immunol. 2009;183:3578–3581.
26. Braga T.T., Forni M.F., Correa-Costa M., Ramos R.N., Barbuto J.A., Branco P., Castoldi A., Hiyane M.I., Davanso M.R., Latz E., et al. Soluble uric acid activates the nlrp3 inflammasome. Sci. Rep. 2017;7:39884.
27. Halle A., Hornung V., Petzold G.C., Stewart C.R., Monks B.G., Reinheckel T., Fitzgerald K.A., Latz E., Moore K.J., Golenbock D.T. The nalp3 inflammasome is involved in the innate immune response to amyloid-beta. Nat. Immunol. 2008;9:857–865.
28. Jin C., Flavell R.A. Molecular mechanism of nlrp3 inflammasome activation. J. Clin. Immunol. 2010;30:628–631.
29. Tschopp J., Schroder K. Nlrp3 inflammasome activation: The convergence of multiple signalling pathways on ros production? Nat. Rev. Immunol. 2010;10:210–215.
30. Masereeuw R., Russel F.G. Therapeutic implications of renal anionic drug transporters. Pharmacol. Ther. 2010;126:200–216.
31. Motojima M., Hosokawa A., Yamato H., Muraki T., Yoshioka T. Uremic toxins of organic anions up-regulate pai-1 expression by induction of nf-kappab and free radical in proximal tubular cells. Kidney Int. 2003;63:1671–1680.
32. Mihajlovic M., Fedecostante M., Oost M.J., Steenhuis S.K.P., Lentjes E., Maitimu-Smeele I., Janssen M.J., Hilbrands L.B., Masereeuw R. Role of vitamin d in maintaining renal epithelial barrier function in uremic conditions. Int. J. Mol. Sci. 2017;18:2531.
33. Wilmer M.J., Saleem M.A., Masereeuw R., Ni L., van der Velden T.J., Russel F.G., Mathieson P.W., Monnens L.A., van den Heuvel L.P., Levtchenko E.N. Novel conditionally immortalized human proximal tubule cell line expressing functional influx and efflux transporters. Cell Tissue Res. 2010;339:449–457.
34. Jansen J., Schophuizen C.M., Wilmer M.J., Lahham S.H., Mutsaers H.A., Wetzels J.F., Bank R.A., van den Heuvel L.P., Hoenderop J.G., Masereeuw R. A morphological and functional comparison of proximal tubule cell lines established from human urine and kidney tissue. Exp. Cell Res. 2014;323:87–99.
35. Nieskens T.T., Peters J.G., Schreurs M.J., Smits N., Woestenenk R., Jansen K., van der Made T.K., Roring M., Hilgendorf C., Wilmer M.J., et al. A human renal proximal tubule cell line with stable organic anion transporter 1 and 3 expression predictive for antiviral-induced toxicity. AAPS J. 2016;18:465–475.
36. Jansen J., Fedecostante M., Wilmer M.J., Peters J.G., Kreuser U.M., van den Broek P.H., Mensink R.A., Boltje T.J., Stamatialis D., Wetzels J.F., et al. Bioengineered kidney tubules efficiently excrete uremic toxins. Sci. Rep. 2016;6:26715.
37. Van Koppen A., Verhaar M.C., Bongartz L.G., Joles J.A. 5/6th nephrectomy in combination with high salt diet and nitric oxide synthase inhibition to induce chronic kidney disease in the lewis rat. J. Vis. Exp. 2013;77:e50398.
38. Sotocinal S.G., Sorge R.E., Zaloum A., Tuttle A.H., Martin L.J., Wieskopf J.S., Mapplebeck J.C., Wei P., Zhan S., Zhang S., et al. The rat grimace scale: A partially automated method for quantifying pain in the laboratory rat via facial expressions. Mol. Pain. 2011;7:55.

39. Joles J.A., Kunter U., Janssen U., Kriz W., Rabelink T.J., Koomans H.A., Floege J. Early mechanisms of renal injury in hypercholesterolemic or hypertriglyceridemic rats. J. Am. Soc. Nephrol. 2000;11:669–683.

40. Ito S., Yoshida M. Protein-bound uremic toxins: New culprits of cardiovascular events in chronic kidney disease patients. Toxins. 2014;6:665–678.

41. Anders H.J. Of inflammasomes and alarmins: Il-1beta and il-1alpha in kidney disease. J. Am. Soc. Nephrol. 2016;27:2564–2575.

42. Vilaysane A., Chun J., Seamone M.E., Wang W., Chin R., Hirota S., Li Y., Clark S.A., Tschopp J., Trpkov K., et al. The nlrp3 inflammasome promotes renal inflammation and contributes to ckd. J. Am. Soc. Nephrol. 2010;21:1732–1744.

43. Foresto-Neto O., Avila V.F., Arias S.C.A., Zambom F.F.F., Rempel L.C.T., Faustino V.D., Machado F.G., Malheiros D., Abensur H., Camara N.O.S., et al. Nlrp3 inflammasome inhibition ameliorates tubulointerstitial injury in the remnant kidney model. Lab. Investig. 2018;98:773–782.

44. Nishi Y., Satoh M., Nagasu H., Kadoya H., Ihoriya C., Kidokoro K., Sasaki T., Kashihara N. Selective estrogen receptor modulation attenuates proteinuria-induced renal tubular damage by modulating mitochondrial oxidative status. Kidney Int. 2013;83:662–673.

45. Ding W., Guo H., Xu C., Wang B., Zhang M., Ding F. Mitochondrial reactive oxygen species-mediated nlrp3 inflammasome activation contributes to aldosterone-induced renal tubular cells injury. Oncotarget. 2016;7:17479–17491.

46. Gong W., Mao S., Yu J., Song J., Jia Z., Huang S., Zhang A. Nlrp3 deletion protects against renal fibrosis and attenuates mitochondrial abnormality in mouse with 5/6 nephrectomy. Am. J. Physiol.-Renal Physiol. 2016;310:F1081–F1088.

47. Mulay S.R. Multifactorial functions of the inflammasome component nlrp3 in pathogenesis of chronic kidney diseases. Kidney Int. 2019;96:58–66.

48. Granata S., Masola V., Zoratti E., Scupoli M.T., Baruzzi A., Messa M., Sallustio F., Gesualdo L., Lupo A., Zaza G. Nlrp3 inflammasome activation in dialyzed chronic kidney disease patients. PLoS ONE. 2015;10:e0122272.

49. Ulrich C., Wildgrube S., Fiedler R., Seibert E., Kneser L., Fick S., Schafer C., Markau S., Trojanowicz B., Girndt M. Nlrp3 inflammasome activation in hemodialysis and hypertensive patients with intact kidney function. Toxins. 2020;12:675.

50. Shen W.C., Liang C.J., Huang T.M., Liu C.W., Wang S.H., Young G.H., Tsai J.S., Tseng Y.C., Peng Y.S., Wu V.C., et al. Indoxyl sulfate enhances il-1beta-induced e-selectin expression in endothelial cells in acute kidney injury by the ros/mapks/nfkappab/ap-1 pathway. Arch. Toxicol. 2016;90:2779–2792.

51. Wakamatsu T., Yamamoto S., Ito T., Sato Y., Matsuo K., Takahashi Y., Kaneko Y., Goto S., Kazama J.J., Gejyo F., et al. Indoxyl sulfate promotes macrophage il-1beta production by activating aryl hydrocarbon receptor/nf-kappa/mapk cascades, but the nlrp3 inflammasome was not activated. Toxins. 2018;10:124.

52. Nakano T., Katsuki S., Chen M., Decano J.L., Halu A., Lee L.H., Pestana D.V.S., Kum A.S.T., Kuromoto R.K., Golden W.S., et al. Uremic toxin indoxyl sulfate promotes proinflammatory macrophage activation via the interplay of oatp2b1 and dll4-notch signaling. Circulation. 2019;139:78–96.

53. Lekawanvijit S., Adrahtas A., Kelly D.J., Kompa A.R., Wang B.H., Krum H. Does indoxyl sulfate, a uraemic toxin, have direct effects on cardiac fibroblasts and myocytes? Eur. Heart J. 2010;31:1771–1779.

54. Sun C.Y., Young G.H., Hsieh Y.T., Chen Y.H., Wu M.S., Wu V.C., Lee J.H., Lee C.C. Protein-bound uremic toxins induce tissue remodeling by targeting the egf receptor. J. Am. Soc. Nephrol. 2015;26:281–290.

55. Jansen J., Jansen K., Neven E., Poesen R., Othman A., van Mil A., Sluijter J., Sastre Torano J., Zaal E.A., Berkers C.R., et al. Remote sensing and signaling in kidney proximal tubules stimulates gut microbiome-derived organic anion secretion. Proc. Natl. Acad. Sci. USA. 2019;116:16105–16110.

56. Chin L.H., Hsu Y.J., Hsu S.C., Chen Y.H., Chang Y.L., Huang S.M., Tsai C.S., Lin C.Y. The regulation of nlrp3 inflammasome expression during the development of cardiac

3

contractile dysfunction in chronic kidney disease. Oncotarget. 2017;8:113303–113317.

57. Ho L.C., Wu T.Y., Lin T.M., Liou H.H., Hung S.Y. Indoxyl sulfate mediates the low inducibility of the nlrp3 inflammasome in hemodialysis patients. Toxins. 2021;13:38.

58. Martinon F., Mayor A., Tschopp J. The inflammasomes: Guardians of the body. Annu. Rev. Immunol. 2009;27:229–265.

59. Wang L., Sweet D.H. Renal organic anion transporters (slc22 family): Expression, regulation, roles in toxicity, and impact on injury and disease. AAPS J. 2013;15:53–69.

60. Burckhardt G., Burckhardt B.C. Handbook of Experimental Pharmacology Book Series. Volume 201. Springer; Berlin/Heidelberg, Germany: 2011. In vitro and in vivo evidence of the importance of organic anion transporters (oats) in drug therapy; pp. 29–104.

61. Cheng T.H., Ma M.C., Liao M.T., Zheng C.M., Lu K.C., Liao C.H., Hou Y.C., Liu W.C., Lu C.L. Indoxyl sulfate, a tubular toxin, contributes to the development of chronic kidney disease. Toxins. 2020;12:684.

62. Gritsenko A., Yu S., Martin-Sanchez F., Diaz-Del-Olmo I., Nichols E.M., Davis D.M., Brough D., Lopez-Castejon G. Priming is dispensable for nlrp3 inflammasome activation in human monocytes in vitro. Front. Immunol. 2020;11:565924.

63. Shimizu H., Bolati D., Adijiang A., Muteliefu G., Enomoto A., Nishijima F., Dateki M., Niwa T. Nf-kappab plays an important role in indoxyl sulfate-induced cellular senescence, fibrotic gene expression, and inhibition of proliferation in proximal tubular cells. Am. J. Physiol. Cell Physiol. 2011;301:C1201–C1212.

64. Gelasco A.K., Raymond J.R. Indoxyl sulfate induces complex redox alterations in mesangial cells. Am. J. Physiol.-Renal Physiol. 2006;290:F1551–F1558.

65. Ishima Y., Narisoko T., Kragh-Hansen U., Kotani S., Nakajima M., Otagiri M., Maruyama T. Nitration of indoxyl sulfate facilitates its cytotoxicity in human renal proximal tubular cells via expression of heme oxygenase-1. Biochem. Biophys. Res. Commun. 2015;465:481–487.

66. Yu M., Kim Y.J., Kang D.H. Indoxyl sulfate-induced endothelial dysfunction in patients with chronic kidney disease via an induction of oxidative stress. Clin. J. Am. Soc. Nephrol. 2011;6:30–39. doi: 10.2215/CJN.05340610. [

67. Bauernfeind F.G., Horvath G., Stutz A., Alnemri E.S., MacDonald K., Speert D., Fernandes-Alnemri T., Wu J., Monks B.G., Fitzgerald K.A., et al. Cutting edge: Nf-kappab activating pattern recognition and cytokine receptors license nlrp3 inflammasome activation by regulating nlrp3 expression. J. Immunol. 2009;183:787–791.

68. Petrilli V., Papin S., Dostert C., Mayor A., Martinon F., Tschopp J. Activation of the nalp3 inflammasome is triggered by low intracellular potassium concentration. Cell Death Differ. 2007;14:1583–1589.

69. Meng N., Xia M., Lu Y.Q., Wang M., Boini K.M., Li P.L., Tang W.X. Activation of nlrp3 inflammasomes in mouse hepatic stellate cells during schistosoma j. Infection. Oncotarget. 2016;7:39316–39331.

70. Lamkanfi M., Mueller J.L., Vitari A.C., Misaghi S., Fedorova A., Deshayes K., Lee W.P., Hoffman H.M., Dixit V.M. Glyburide inhibits the cryopyrin/nalp3 inflammasome. J. Cell Biol. 2009;187:61–70.

71. Juliana C., Fernandes-Alnemri T., Wu J., Datta P., Solorzano L., Yu J.W., Meng R., Quong A.A., Latz E., Scott C.P., et al. Anti-inflammatory compounds parthenolide and bay 11-7082 are direct inhibitors of the inflammasome. J. Biol. Chem. 2010;285:9792–9802.

72. Paik S., Kim J.K., Silwal P., Sasakawa C., Jo E.K. An update on the regulatory mechanisms of nlrp3 inflammasome activation. Cell Mol. Immunol. 2021;18:1141–1160.

73. Kummer J.A., Broekhuizen R., Everett H., Agostini L., Kuijk L., Martinon F., van Bruggen R., Tschopp J. Inflammasome components nalp 1 and 3 show distinct but separate expression profiles in human tissues suggesting a site-specific role in the inflammatory response. J. Histochem. Cytochem. 2007;55:443–452.

74. Hoss F., Mueller J.L., Rojas Ringeling F., Rodriguez-Alcazar J.F., Brinkschulte R., Seifert G., Stahl R., Broderick L., Putnam C.D., Kolodner R.D., et al. Alternative splicing regulates stochastic nlrp3 activity. Nat. Commun. 2019;10:3238.

75. Kudo S., Mizuno K., Hirai Y., Shimizu T. Clearance and tissue distribution of recombinant

human interleukin 1 beta in rats. Cancer Res. 1990;50:5751–5755.

76. Lopez-Castejon G., Brough D. Understanding the mechanism of il-1beta secretion. Cytokine Growth Factor Rev. 2011;22:189–195.

77. Owada S., Goto S., Bannai K., Hayashi H., Nishijima F., Niwa T. Indoxyl sulfate reduces superoxide scavenging activity in the kidneys of normal and uremic rats. Am. J. Nephrol. 2008;28:446–454.

3

Supplementary Materials
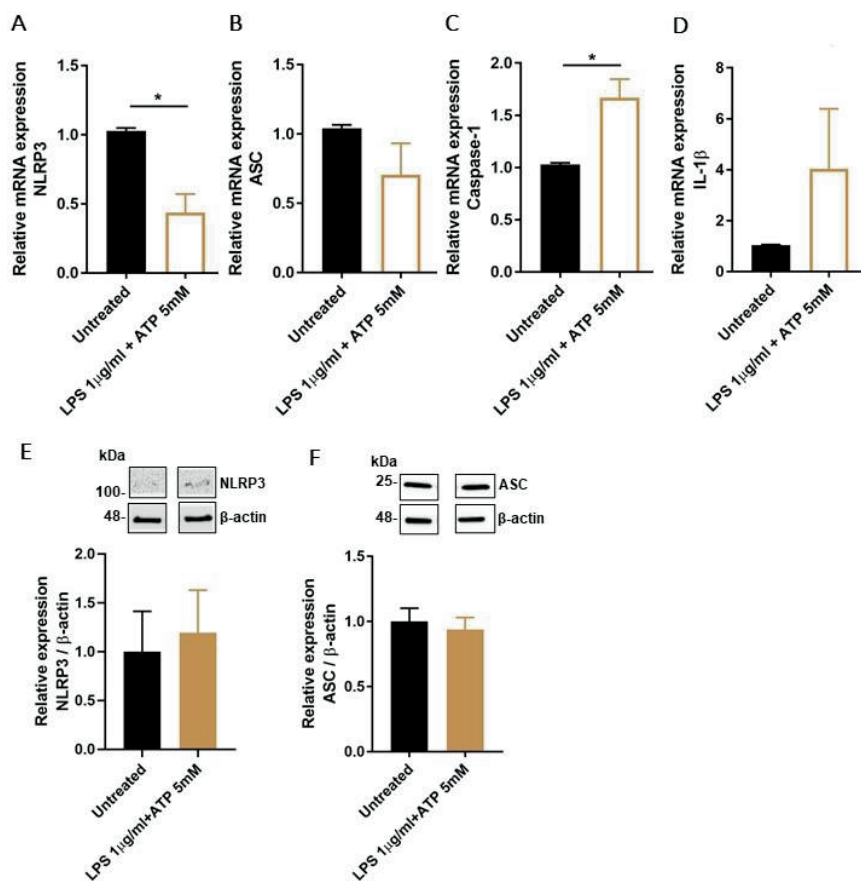
Figure S1. Effect of LPS/ATP treatment on expression of NLRP3 inflammasome-related components in ciPTEC-OAT1. Relative mRNA expression of **A**) NLRP3, **B**) ASC, **C**) caspase-1 and **D**) IL-1β upon exposure to LPS (1 μg/ml; 24 h) and ATP (5 mM; 30 min), compared to control (untreated ciPTEC-OAT1). Representative Western blot and quantification of relative expression of **E**) NLRP3 and **F**) ASC in ciPTEC-OAT1 following exposure to LPS (1 μg/ml; 24 h) and ATP (5 mM; 30 min); normalized to β-actin. Data are derived from three independent experiments performed in triplicate and expressed as mean ± SEM. * p<0.05 (Unpaired t test).

3
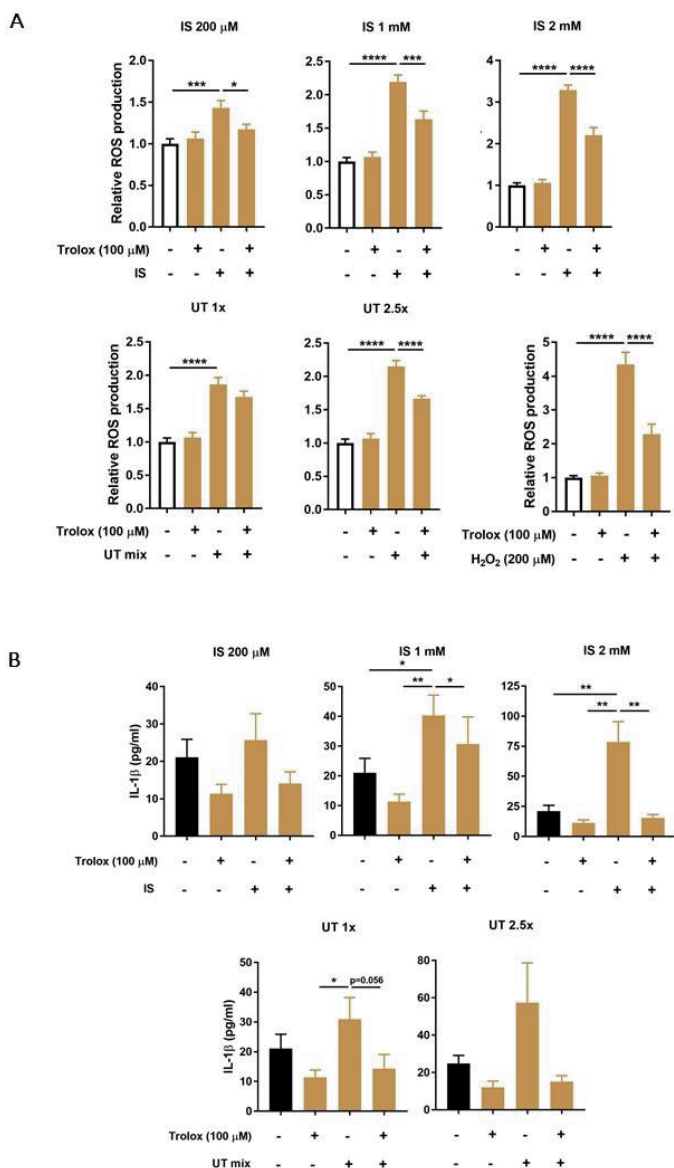
Figure S2. Effect of PBUTs-induced oxidative stress and antioxidant Trolox on IL-1β production in ciPTEC-OAT1. A) Relative intracellular ROS production in ciPTEC-OAT1 after 2 h exposure to IS (200 μM, 1 mM, 2 mM), UT mix (1x, 2.5x) and H2O2 (200 μM, positive control), in the absence or presence of ROS inhibitor Trolox (100 μM). **B**) IL- 1β secreted levels (pg/ml) by ciPEC-OAT1 upon 24 h treatment with IS (200 μM, 1 mM, 2 mM) and UT mix (1x, 2.5x), in the absence or presence of Trolox (100 μM). Data are derived from three independent experiments performed in triplicate and expressed as mean ± SEM. * p<0.05, ** p<0.01, *** p<0.001, **** p<0.0001 (One-way ANOVA followed by Dunnett's multiple comparison test, using PBUTs treated cells as a control).
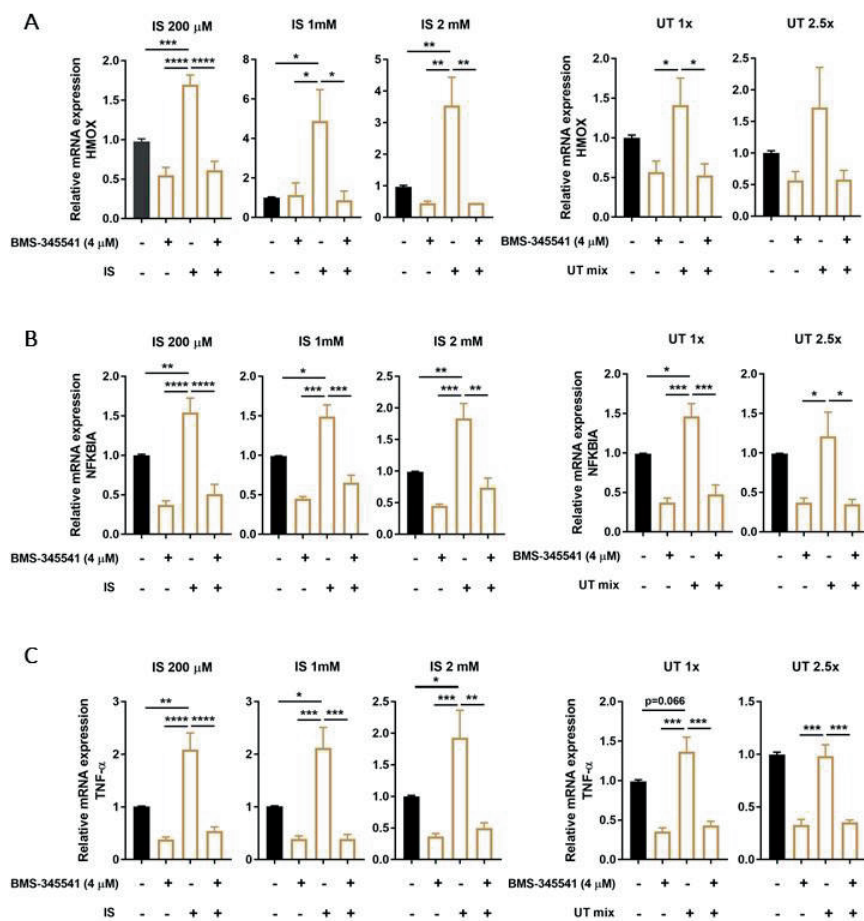
Figure S3. Effect of PBUTs on NF-κB target genes expression levels in ciPTEC-OAT1. Relative mRNA expression of A) heme oxygenase 1 (*HMOX1*), B) NFκB inhibitor alpha (*NFKBIA*) and C) TNF-α (*TNF*) upon 4 h exposure to either IS (200 μM, 1 mM, 2 mM) or UT mix (1x, 2.5x), in the absence or presence of specific IKK inhibitor BMS- 345541 (4 μM) and compared to control (untreated ciPTEC-OAT1). Data are derived from three independent experiments performed in duplicate and expressed as mean ± SEM. * p<0.05, ** p<0.01, *** p<0.001, **** p<0.0001 (One-way ANOVA followed by Dunnett's multiple comparison test, using PBUTs treated cells as a control).

*The Supplementary Material for this article can be found online at:
https://www.mdpi.com/article/10.3390/biomedicines9101326/s1

Chapter 4

The Uremic Toxin Indoxyl Sulfate Accelerates Senescence in Kidney Proximal Tubule Cells

Yi Yang[1], Milos Mihajlovic[1], Manoe J. Janssen[1] and Rosalinde Masereeuw[1]

[1]Division of Pharmacology, Utrecht Institute for Pharmaceutical Sciences, Utrecht University, 3584 CG Utrecht, The Netherlands.

Abstract

Kidney fibrosis is the common final pathway of nearly all chronic and progressive nephropathies. One cause may be the accumulation of senescent cells that secrete factors (senescence associated secretory phenotype, SASP) promoting fibrosis and inflammation. It has been suggested that uremic toxins, such as indoxyl sulfate (IS), play a role in this. Here, we investigated whether IS accelerates senescence in conditionally immortalized proximal tubule epithelial cells overexpressing the organic anion transporter 1 (ciPTEC-OAT1), thereby promoting kidney fibrosis. Cell viability results suggested that the tolerance of ciPTEC-OAT1 against IS increased in a time-dependent manner at the same dose of IS. This was accompanied by SA-β-gal staining, confirming the accumulation of senescent cells, as well as an upregulation of p21 and downregulation of laminB1 at different time points, accompanied by an upregulation in the SASP factors IL-1β, IL-6 and IL-8. RNA-sequencing and transcriptome analysis revealed that IS accelerates senescence, and that cell cycle appears to be the most relevant factor during the process. IS accelerates senescence via TNF-α and NF-κB signalling early on, and the epithelial-mesenchymal transition process at later time points. In conclusion, our results suggest that IS accelerates cellular senescence in proximal tubule epithelial cells.

Keywords: kidney fibrosis, conditionally immortalized proximal tubule epithelial cells, senescence-associated secretory phenotype (SASP), transcriptome

1. Introduction

The accumulation of senescent cells is a feature of chronic kidney disease (CKD) and contributes to the progression of the endpoint kidney fibrosis [1]. Acute (short-term) senescent cells can be cleared by the immune system, through chemo-attracting of immune cells, followed by tissue regeneration, while chronic (long-term) senescent cells establish a pro-inflammatory environment and aggravate the disease [2,3]. Senescent cells can be identified by their permanent cell cycle arrest, proliferation limitation and secretion of senescence-associated secretory phenotype (SASP) factors [4].

Cell cycle arrest in senescence is mainly executed by two pathways: the p53/p21$^{CIP1/WAF1}$ (p21) and p16^{Ink4a} (p16)/pRb checkpoint pathways [5], which are activated independently during the senescence process. First, p53 is activated following DNA damage, promoting a p21-dependent cell-cycle arrest [6,7]. Second, p16 prevents the action of the cyclin dependent kinases by suppressing Retinoblastoma 1 (pRb), thus leading to cell cycle arrest [8].

Chronic (long-term) senescent cells are alive, metabolically active and show resistance to apoptosis, which is a common feature of proliferation limitation. Two main pathways contribute to apoptosis-resistance. One is the intrinsic pathway resulting from mitochondrial dysfunction and involving Bcl-2 family members [9]. The abnormal regulation of anti-apoptotic and pro-apoptotic Bcl-2 family proteins triggers the senescent cells to be in a primed apoptotic state, thus making cells stay alive without undergoing proliferation or apoptosis [10]. The other is the extrinsic pathway, regulated by death receptors [11]. Death receptors interact with death ligands, activating caspase proteins and inducing apoptosis [9]. Death receptors, such as tumour necrosis factor receptors (TNFR) (e.g., TNFR1 and TNFR2) and their ligands (e.g., TNF-α), are also found to be important SASP factors [12,13]. Senescent cells primed by TNF-α amplify the senescence process via a paracrine effect [14]. The alteration of intrinsic and extrinsic pathways finally results in apoptosis resistance and senescence [15,16].

SASP factors include proinflammatory and/or profibrotic compounds, such as numerous cytokines (e.g., IL-1β and IL-6), chemokines (e.g., CXCL8 and CCL2), growth factors (e.g., CTGF and TGF-β) and matrix-metalloproteinases (MMPs) [17,18]. The factors are involved in various pathways to maintain and reinforce senescence, but are also key players in its transmission and can undergo paracrine signalling [19,20].

Uremic toxins are endogenous metabolites that accumulate systemically during kidney function decline. In healthy conditions, the waste solutes are renally cleared through glomerular filtration or active secretion by the proximal tubular epithelial cells [21]. Protein-bound uremic toxins, such as indoxyl sulfate (IS), are highly retained during kidney failure, poorly removed by dialysis therapy, and associated with comorbidities in CKD [22]. IS is taken up by proximal tubular cells via organic anion transporter 1 and 3 (OAT1 and OAT3) [23,24]. It was reported that uremic toxins (including IS) can induce proximal tubular injury via OAT1-mediated uptake [24], and can regulate the secretion of organic anions through AhR and EGFR mediated signalling [25]. Furthermore, IS displays proinflammatory and prooxidative effects during CKD, stimulating the expression of SASP factors [26,27]. This uremic toxin may contribute to senescence through the generation of reactive oxygen species (ROS), and p53 and NF-κB signalling [28,29,30]. It has been demonstrated that IS also upregulates the SASP factors MCP-

1 and ICAM-1 in kidney epithelial cells via p53 and NF-κB signalling [31,32]. We previously showed that IS activates the inflammasome NLRP3, thereby inducing the expression of IL-1β with an increase in ROS [33]. Here, we hypothesize that IS maintains and accelerates senescence by regulating SASP factors.

We recently demonstrated that a human conditionally immortalized proximal tubule epithelial cell line overexpressing the organic anion transporter 1 (ciPTEC-OAT1) acquires a conditional senescent phenotype when cells are cultured at a non-permissive temperature [34]. Considering the facts that the main focus of the present work is the effect of IS in kidney senescence and that (primary) PTEC rapidly lose the expression of OAT1 when cultured in vitro, the ciPTEC-OAT1 cell model, showing stable OAT1 expression and function, was used in this study [35]. In this experimental in vitro model, p53 and p21 are active at a permissive temperature (33 °C) through the expression of the temperature-sensitive mutant U19tsA58 of the SV40 large T antigen (SV40T). Furthermore, the cells show a senescence-like arrest when switched to a non-permissive temperature (37 °C) [36].

In this study, we employed ciPTEC-OAT1 as a model to investigate whether IS accelerates the senescence phenotype. Further, transcriptome analysis was conducted to understand the underlying mechanisms.

2. Results

2.1. Proximal Tubule Cells Show Increased Cellular Tolerance against Indoxyl Sulfate over Time

To understand the appropriate time point for senescence acceleration of IS, we used clinically relevant IS concentrations for up to 9 days and confirmed cellular senescence via SA-β-gal staining. We previously demonstrated that IS exerts an IC50 value for cell viability of 2.0 mM after 24 h exposure, which is beyond clinically relevant IS concentrations (on average in severe uremia approx. 200 µM [37]). Dox was employed as a control due to its known senescence inducing effect and regulation of cell death pathways [38,39,40]. The tolerance of ciPTEC-OAT1 to IS increased over time when maintaining the IS concentrations (Figure 1A).

In fact, cell viability at Day 6 (for 200 µM IS) and Day 9 (for 200 and 400 µM IS) was significantly different when compared to Day 3, while Dox (Figure 1B) did not show differences amongst the three time points. The half maximal inhibitory concentrations (IC50, described in the legend), as a measure of the potency of IS and Dox, showed a dose- and time-dependent cell viability reduction. SA-β-gal staining confirmed the accumulation of senescent cells (Figure 1C,D). The results suggest that doxorubicin not only induces senescence but also eliminates senescent cells, while IS-induced senescence is more stable.
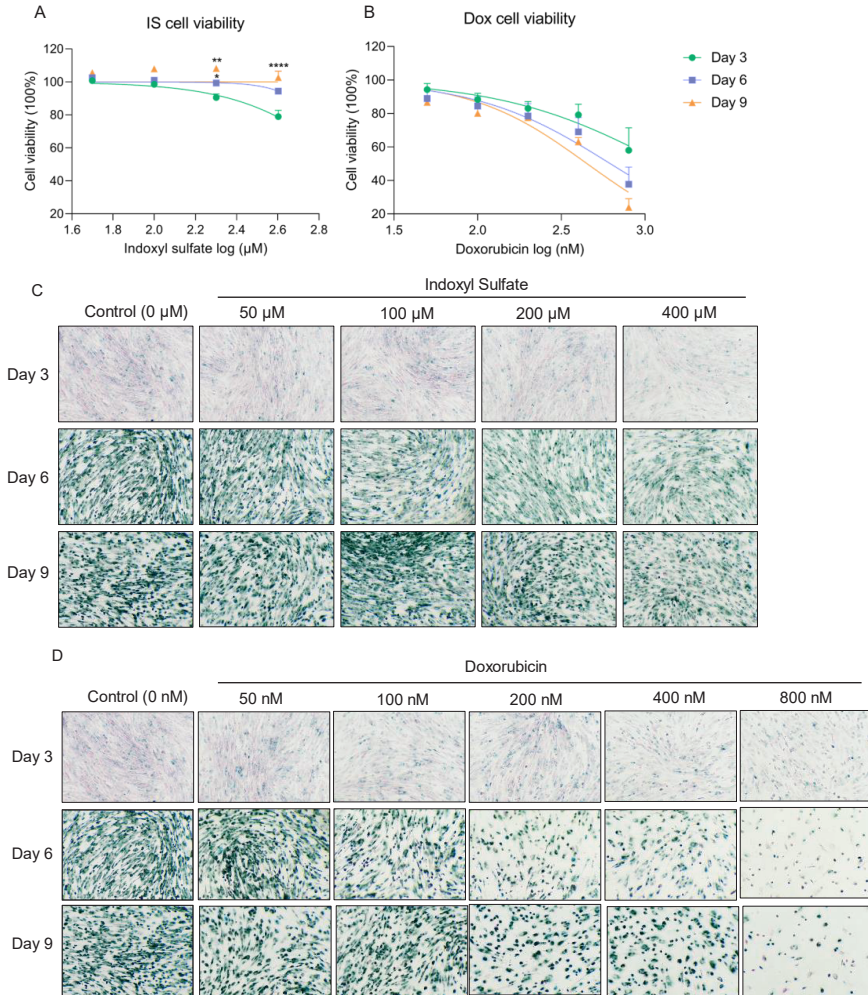
Figure 1.Cellular tolerance against indoxyl sulfate (IS) increased over time, while doxorubicin (Dox) reduced cell viability dose- and time-dependently. Cell viability of ciPTEC-OAT1 exposure to 100 µL medium increased at 0, 3, 6 or 9 days under a non-permissive temperature of 37 °C: (A) indoxyl sulfate (IS) and (B) doxorubicin (Dox). IC50 values for IS are over 400 µM at all time points; IC50 values for Dox at Day 3, Day 6 and Day 9 are over 800 nM, 600 nM and 400 nM, respectively. SA-gal staining in ciPTEC-OAT1 cultures grown for 3, 6 and 9 days at 37 °C with various doses: (C) IS (50 µM, 100 µM, 200 µM or 400 µM) and (D) Dox (50 nM, 100 nM, 200 nM, 400 nM and 800 nM). * $p < 0.05$, ** $p < 0.01$, **** $p < 0.001$ (cell viability at Day 6 and Day 9 compared to Day 3, Two-way ANOVA, Sidak's multiple comparison).

2.2. Indoxyl Sulfate Exposure Results in Sustained Expression of Common Senescence Markers

To investigate further the senescence phenotype development after IS treatment, we determined the gene and protein expression levels of p21 and LaminB1 as known senescence hallmarks (Figure 2). Compared to the non-senescent group (Day 0), LaminB1 was downregulated at

37 °C at Day 9 for protein level (Figure 2A,B) and on Day 6 and Day 9 for mRNA level (Figure 2F), whereas p21 was upregulated at 37 °C for both protein level (Figure 2C,D) and mRNA level (Figure 2E) at different time points. These findings suggest that the cells obtained a senescence phenotype over time, consistent with our previous results [34]. This effect was sustained when cells were treated with IS, as shown by clear differences and upregulation and downregulation trends (Figure 2A–F).
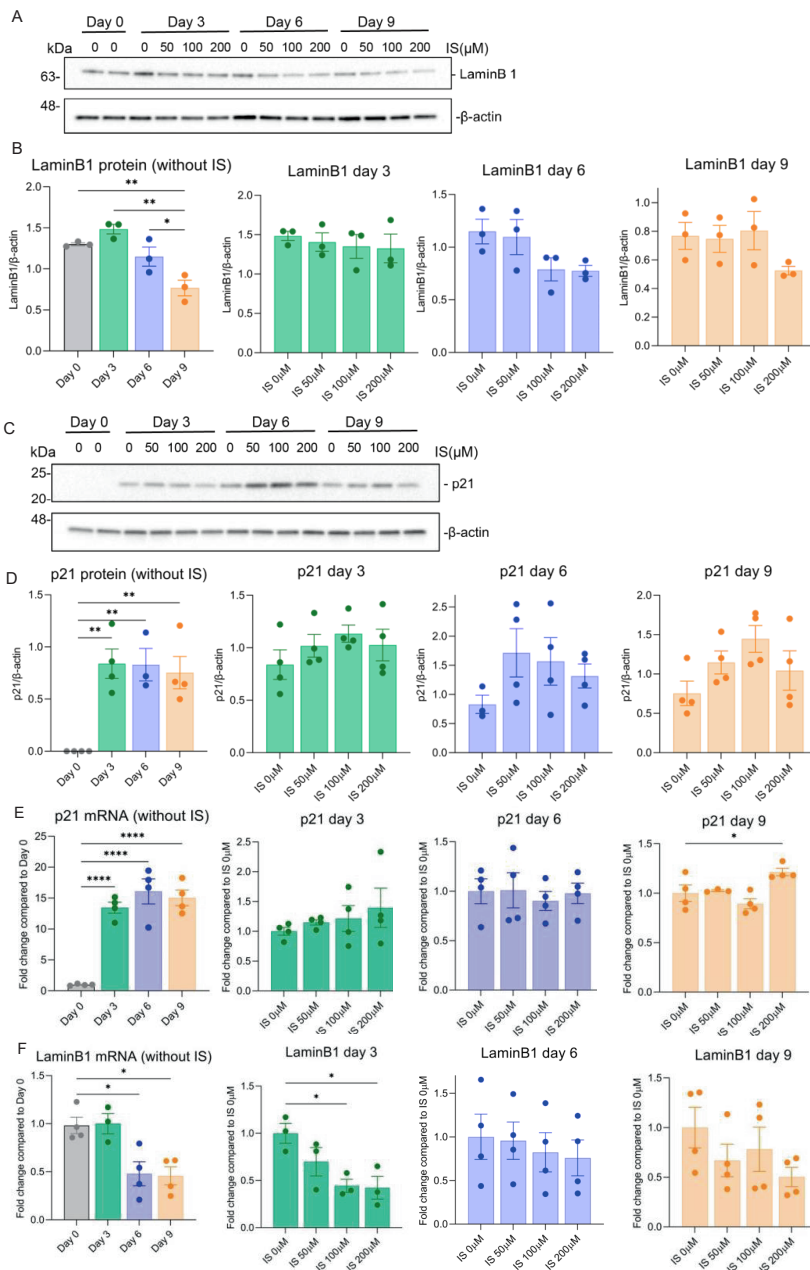
Figure 2. Exposure to IS leads to sustained common senescence markers expression in ciPTEC-OAT1 at a non-permissive temperature of 37 °C. The ciPTEC were exposed to IS (50 µM, 100 µM or 200 µM) for 0, 3, 6 and 9 days. Representative Western blots showing expression of (A) LaminB1 and (C) p21. Relative protein expression levels of (B) LaminB1 and (D) p21 over time (Day 0 to Day 9). (E) Gene expression levels of p21 and (F) LaminB1 over time (Day 0 to Day 9). At least three independent experiments were performed in triplicates. * p < 0.05, ** p < 0.01, **** p < 0.0001 (secreted levels at Days 3, 6, or 9 compared to Day 0 or the non-treatment group at 37 °C; one-way ANOVA, Dunnett's multiple comparison).

2.3. Indoxyl Sulfate Accelerates Common SASP Factors Secretion

SASP factors maintain and reinforce senescence. Here, we evaluated the secretion of typical SASP factors (IL-6, IL-8 and IL-1β) to further investigate the effect of IS on senescence development. All SASP factors were upregulated over time at 37 °C in ciPTEC-OAT1 cells during maturation (Figure 3). Following exposure to IS, IL-6 was upregulated on Day 3 at all concentrations (Figure 3A).
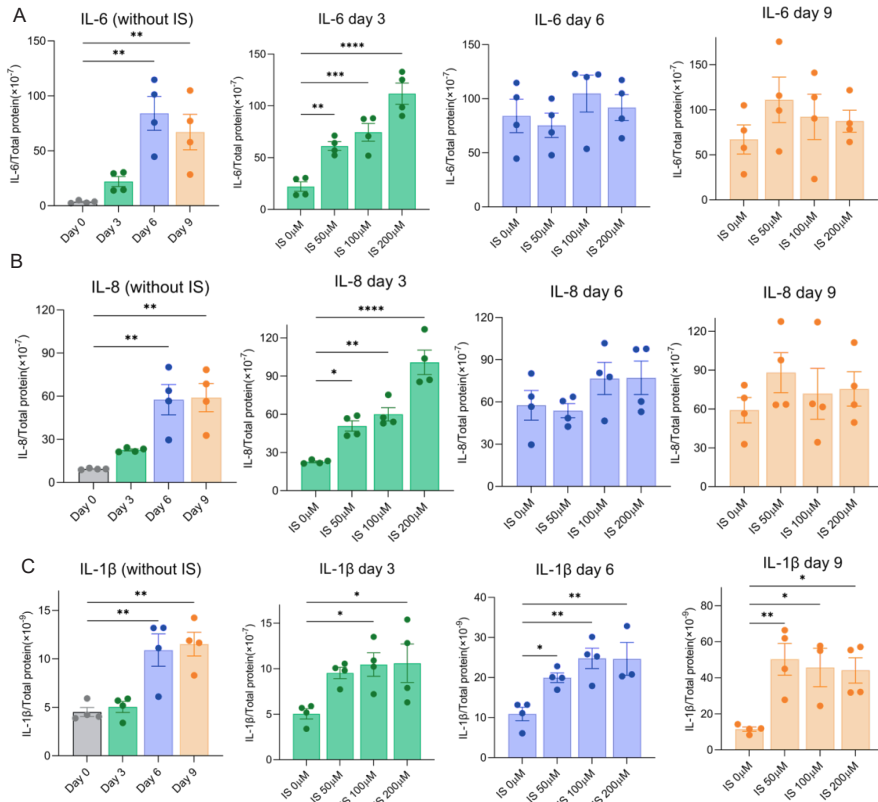
Figure 3. IS accelerated SASP factors secretion by ciPTEC-OAT1 under a non-permissive temperature of 37 °C. Release of (A) IL-6, (B) IL-8 and (C) IL-1β by ciPTEC-OAT1 over time. The concentration is presented as pg/mL and is normalized for total protein (µg/mL). Triplicates of four independent experiments were performed. * p < 0.05, ** p < 0.01, *** p < 0.001, **** p < 0.0001 (secreted levels at Days 3, 6 or 9 compared to Day 0 or the non-treatment group at 37 °C; one-way ANOVA, Dunnett's multiple comparison).

Similarly, as shown in Figure 3B, the levels of IL-8 were elevated by IS on Day 3 and further

increased to equally high levels of IL-6 and IL-8 at Day 6 and Day 9, a process that was also observed for IL-1β (Figure 3C). Our results suggest that IS accelerates high secreted levels of common SASP factors during senescence development.

2.4. Transcriptomic Analysis Reveals Large Scale Changes in Gene Expression during Maturation
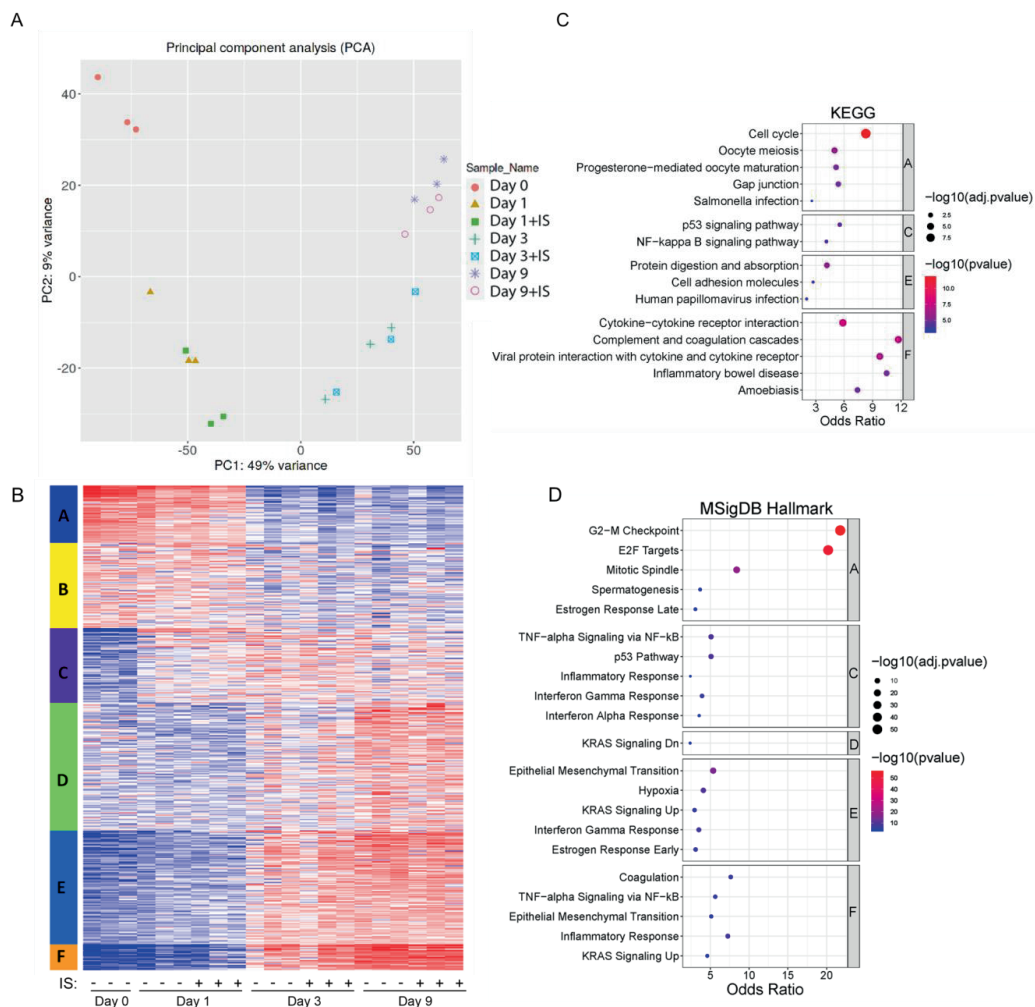
Figure 4. Transcriptomics shows activation of senescence-related pathways over time. (A) Principal Component Analysis (PCA) plots from the transcriptome of ciPTEC-OAT1. Different colours and different shapes correspond to different time points and treatments (day 0, and day 1, 3, and 9 in the presence or absence of IS (200 µM). (B) K-means clustering of RNA-seq among different samples from 5000 most variable genes. (C) Gene networks identified through Kyoto Encyclopedia of Genes and Genomes (KEGG) of top 5 pathways in different clusters, adjusted p (adj.p) < 0.05. (D) Enrichment analysis of top 5 pathways in different clusters through MSigDB Hallmark, adj.p < 0.05.

Figure 4 shows the transcriptome analysis and an overview of the responses of ciPTEC-OAT1 upon culturing in the absence or presence of IS. PCA plots demonstrate that the main source of variation across the transcriptome is linked to the maturation time (Figure 4A), and PC1 is mostly composed of the genes involved in cell cycle-related processes (Figure S1). Further, there are significant correlations between protein levels and the mRNA abundance of IL-6, IL-8 and IL-1β, validating the transcriptome analysis (Figure S2). Based on the expression patterns, several gene clusters can be identified, and the genes for whose expression goes down over time (Cluster A) and can be linked to pathways associated with cell growth and cell division. On the other hand, genes that go up over time (Clusters E and F) contain genes linked to inflammation and epithelial to mesenchymal transition (Figure 4B–D). This is in line with what we expect for cells undergoing senescence and cell cycle arrest, with a clear change between Day 1 and Day 3. A list of enriched pathways (from KEGG and MSigDB Hallmark analyses) and associated differentially expressed genes can be found in Tables S1 and S2.

2.5. IS Accelerates Senescence by Regulating Senescence Markers

During maturation for 9 days, many senescence related genes are changed (Figure 5A). The upregulation of SASP factors and p21 observed is consistent with our previous findings [34]. The expression levels of common senescence markers are shown in Figure 5B. Compared with the non-senescence group (Day 0), p21 (CDKN1A) was upregulated from Day 1 onwards; β-gal (GLB1) was upregulated on Day 3 and Day 9, whereas a downregulation of LaminB1 (LMNB1) was observed at day 1 in the IS-treatment group and in all groups at later time points.

The upregulation of common SASP factors is shown in Figure 5C, with upregulations observed for IL-8 (CXCL8) at Day 3 in the IS treatment group, IL-6 (IL6) in both the IS-treated and non-treated group at Day 3, IL-1β (IL1B) and MMP-1 (MMP1) in IS-exposed groups at Day 3 and Day 9, IL-1α (IL-1A) in IS treatment groups at Day 1 and Day 9, and MMP-3 (MMP3) at Day 9 after IS exposure. SASP factors such as IL-8, IL-1β, IL-1α and MMP1 showed significant upregulations on Day 3 and Day 9, IL-6 showed remarkable upregulation on Day 3, and MMP3 had significant upregulation on Day 9.The observed trend in IS-mediated upregulation of p21, decrease of LaminB1 and increase of IL8, IL-1α, IL-1β, MMP-1 and MMP-3 at Day 9 would suggest that IS accelerates senescence by regulating common senescence markers, SASP factors and epithelial-mesenchymal transition (EMT) markers.

4

A

B

C
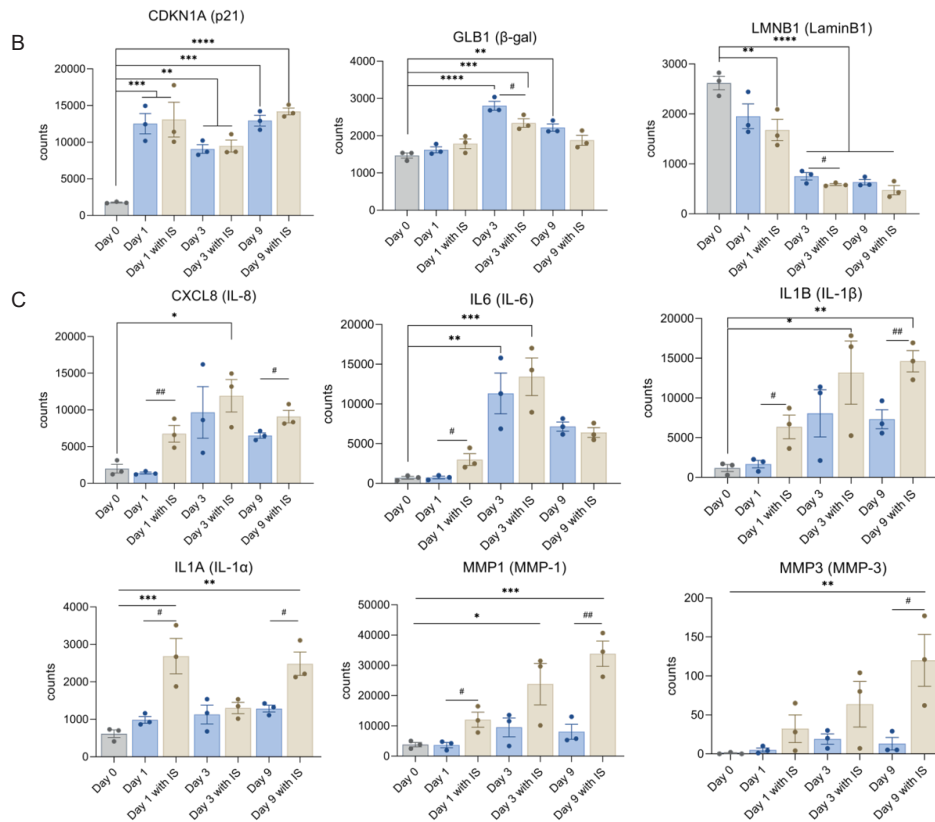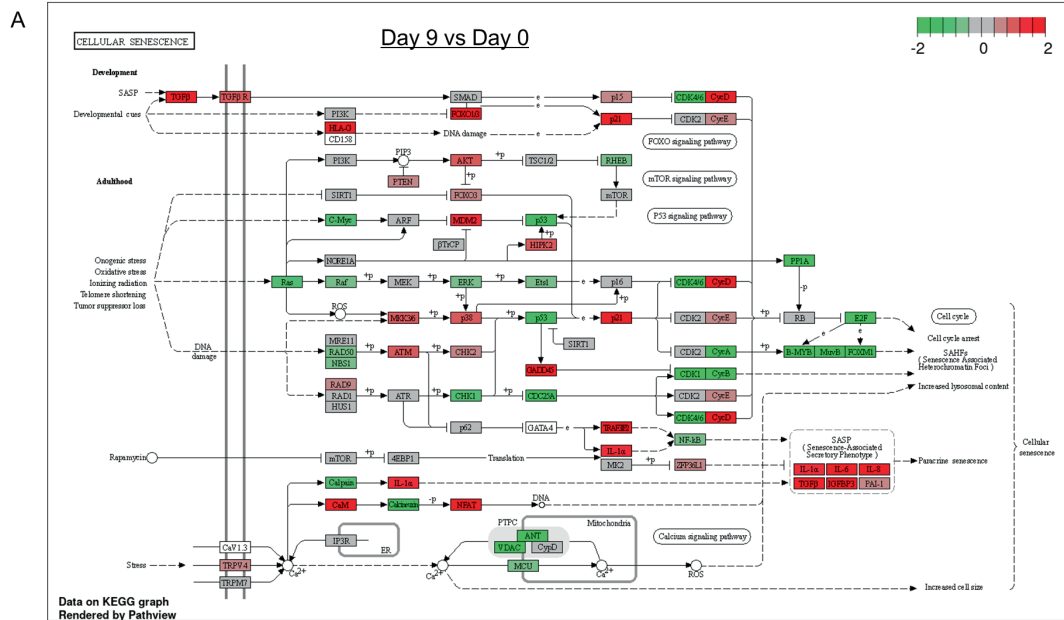
Figure 5. IS accelerates senescence by regulating senescence markers. (A) Schematic representation of the cellular senescence pathway at Day 9 compared to Day 0, with indicated upregulation (red) and downregulation (green) of different genes involved in the process. Gene expression levels of (B) common senescence markers and (C) common SASP factors. * $p < 0.05$, ** $p < 0.01$, *** $p < 0.001$, **** $p < 0.0001$ (secreted levels at Days 3, 6 or 9 compared to Day 0 at 37 °C; one-way ANOVA, Dunnett's multiple comparison). # $p < 0.05$, ## $p < 0.01$ (secreted levels of the IS-treated group compared to the non-treated group at the same day; Unpaired t test).

2.6. IS Induces Expression of SASP Factors and EMT Markers

The enrichment pathways from the MSigDB Hallmark of DEGs indicate that IS accelerates senescence by regulating the genes involved in TNF-alpha Signalling via the NF-κB (TNF-α/NF-κB) pathway at early time points (Days 1 and 3), and genes involved in the EMT process between Day 3 and Day 9 (Figure 6). A list of differentially expressed genes in these pathways in the presence of IS can be found in Table S3.

4
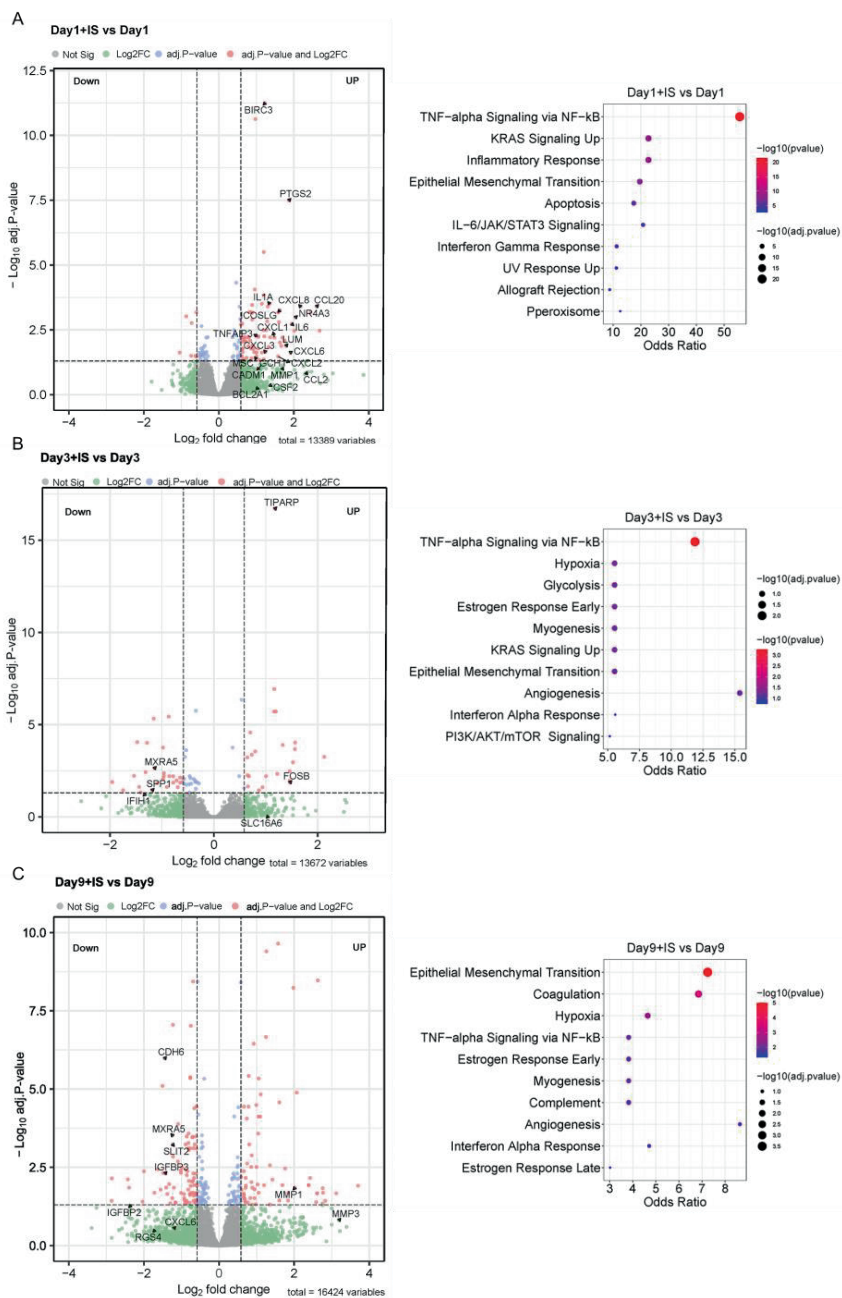
Figure 6. IS induces expression of SASP factors and EMT markers. (A–C) Volcano plots of differentially expressed genes (DEGs) at different time points, and the top 10 enrichment pathways from MSigDB Hallmark of DEGs in IS-treatment groups compared to non-treatment groups. Volcano plots are representative of DEGs of ciPTEC-OAT1 cultured at 37 °C for 1 to 9 days with or without IS (200 µM) exposure (adj.p < 0.05, |log2 fold change| > 1.5). The most significant DEGs are involved in TNF-alpha Signaling via NF-κB and Epithelial Mesenchymal Transition pathway from MSigDB Hallmark.

3. Discussion

Cellular senescence is identified as cell cycle arrest and the limitation of cell proliferation, which is related to kidney disease and fibrosis [41]. Chronic (long-term) senescent cells accumulate and finally aggravate the disease [2,3]. Senescent cells excrete SASP factors, which are key players in the paracrine induction of secondary senescence or senescence transmission [19]. IS, as a protein-bound uremic toxin, is a well-known proinflammatory and prooxidative metabolite with negative effects in CKD [26,27]. IS is poorly removed by dialysis therapy, and associated with many comorbidities in chronic kidney dysfunction [22]. We previously proved that ciPTEC-OAT1 maturation can be employed as a senescence model and described how IS induces inflammasome-mediated IL-1β production [33,34]. In the present study, we demonstrated that IS accelerates senescence in ciPTEC-OAT1 as seen by senescence phenotypes.

Our cell viability results demonstrated that cells become tolerant to IS exposure over time in a concentration-dependent manner, accompanied by increased SA-β-gal expression and activity. This suggest that this uremic toxin accelerates senescent cell accumulation at relevant uremic concentrations, as the average IS plasma concentration in CKD patients is around 200 μM [33]. In contrast, Dox reduced cell viability dose- and time-dependently. Dox is a chemotherapeutic agent that regulates cell death pathways [40], and is often used to induce senescence in experimental research [38,39]. Our findings are in agreement with Dox-eliminating senescent cells, as reflected by the decreased number of senescent cells with increasing dose and exposure time.

Furthermore, the upregulation trend of p21 [42] and downregulation trend of LaminB1 [43] is consistent with the induction of senescence. p21 is a cyclin-dependent kinase inhibitor, and its upregulation is indicative of cell cycle arrest at either G1/S or G2/M checkpoints [44]. The p53/p21 pathway plays a key role in the initiation of senescence [45]. We previously demonstrated that senescence is mainly induced via the p53/p21 pathway in ciPTEC-OAT1 [34]. Here, our findings suggest that IS accelerates or maintains the expression of p21 at a high level [46], which results in a permanent cell cycle arrest and leads to chronic senescence. LaminB1 regulates cell proliferation and senescence via the mitochondrial ROS signalling pathway [43]. Loss of LaminB1 induces and accelerates senescence [43,47], and its decreased expression was observed earlier in ciPTEC-OAT1 upon culturing [34]. Current results suggest that there is a decreasing trend of LaminB1 levels after IS treatment. There are some discrepancies between mRNA and protein levels of the results. This is because the changes in mRNA levels do not always reflect protein levels directly, due to translation, but may influence other protein modification processes and/or various levels of regulation between the transcript and the protein product.

IL-6, IL-8 and IL-1β are typical proinflammatory mediators released in senescence, and are referred to as SASP factors [17,18,48]. IL-6 and IL-8 induce senescence and inflammation, which promote paracrine senescence [49]. IL-1β produced by senescent cells follows IS-induced and ROS-mediated activation of NLRP3 [33,50], thus promoting inflammatory stress and reinforcing senescence [51]. IS is known to stimulate the expression of IL-6 and IL-1β both in vitro and in vivo [52,53] and upregulation of IL-8 in vitro [54]. Current results suggest that IS induces IL-1β expression time-dependently and promotes IL-6 and IL-8 expression early on

during the process. SASP factors are involved in various pathways to maintain and reinforce senescence, and are key players in senescence transmission through paracrine signalling [19,20]. The expression level of SASP factors is higher or kept at a high level in an IS treatment group compared to a no-treatment group; therefore, we believe that IS maintains and reinforces senescence.

To obtain an overview of the most important molecular changes underlying the role of IS in acceleration of senescence, bulk-transcriptomic analysis in ciPTEC-OAT1 cells exposed to IS for up to 9 days was performed. The results suggest that the main source of variation across the transcriptome is the maturation time. Gene expression linked to cell cycle (KEGG pathways) and G2/M checkpoints (MSigDB Hallmark) go down, confirming cell cycle arrest. Senescence has a permanent cell cycle arrest in the G1 or possibly the G2 phase of the cell cycle [4,55]. High expression of p21 is known to be responsible for G2/M arrest in human renal proximal tubular cells, accompanied by the loss of laminB1 [56,57], which is in line with results of this study.

We demonstrated previously that ciPTEC-OAT1 becomes senescent after 9 days maturation at a non-permissive temperature (37 °C) [34], and the transcriptomic results aid in exploring the underlying mechanisms further. Different pathways are involved in senescence process, including FOXO, mTOR, p53 and calcium signalling pathways, which results in cell cycle arrest and accumulation of SASP factors. The expression of senescence markers (p21, β-gal and LaminB1) and SASP factors (IL-6, IL-8 and IL-β) evaluated by transcriptomic analysis is consistent with our findings described earlier. IL-1α, MMP-1and MMP-3 are also important SASP factors [18]. IL-1α regulates other SASP factors, such as IL-6 and IL-8, promoting senescence [58]. MMP-1and MMP-3 belong to the MMP family. MMPs shed ectodomains of cell surface receptors and activate other SASP factors [59], thus regulating the extracellular matrix and promoting EMT and kidney fibrosis [60].

Transcriptome analysis shows that IS exposure increases expression of SASP factors and EMT markers in the senescence process. Those genes are mainly involved in TNF-α/NF-κB pathway at early time points (Day 1), and in the process of EMT at Day 9. The TNF-α/NF-κB pathway is a crucial mediator of inflammatory and immune responses [61], while EMT is an important cellular programme that regulates embryogenesis and wound healing processes, and it is commonly active after kidney injury [62,63]. Both pathways are known to promote senescence and are involved in modulation, production and/or release of proinflammatory and profibrotic SASP factors [4,64,65,66]. IS has been described to contribute to both inflammation and fibrotic processes in CKD via SASP factors [18,67,68,69], which is in line with the current results.

In conclusion, the present results indicate that IS may contribute to kidney disease by accelerating senescence, through the regulation of senescence markers and by modulating inflammatory and profibrotic processes, as evidenced by changes in the TNF-α/NF-κB pathway and the EMT process (Figure 7).
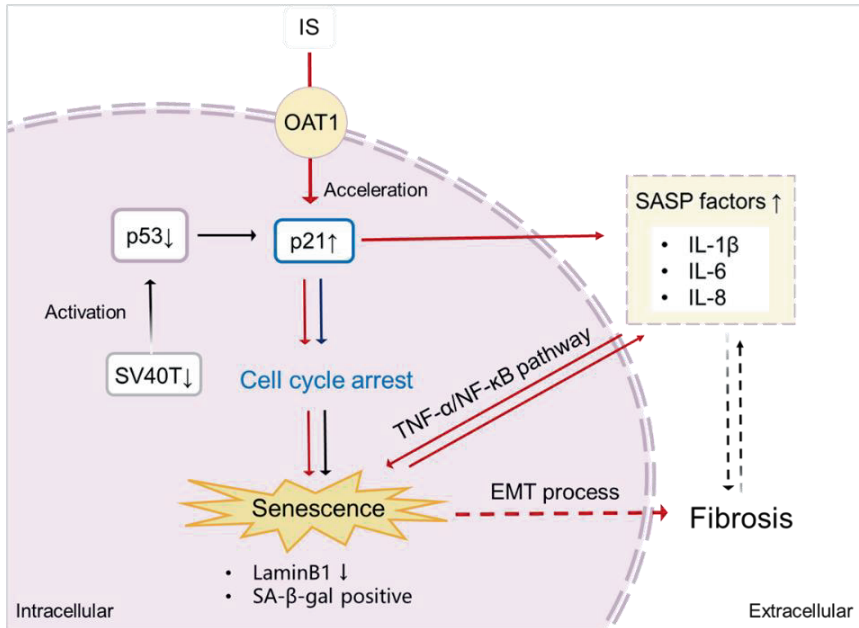
Figure 7. Proposed scheme of senescence acceleration by IS in ciPTEC-OAT1. Downregulation of SV40T and p53 (at 37 °C) leads to transcriptional upregulation of p21, thus inducing cell cycle arrest and eventually causing senescence [34]. After being taken up by the proximal tubule cells via the OAT1 transporter, IS promotes the expression of p21, which results in cell cycle arrest. Moreover, IS specifically upregulates various SASP factors, further accelerating senescence through the TNF-α/NF-κB pathway. The senescence process is potentiated by SASP subsequent promotion of fibrosis through the EMT process. Senescent cells show typical SA-β-gal activity and downregulation of LaminB1, characterizing senescence. Red arrows indicate the senescence process accelerated by IS; ↑ upregulation; ↓ downregulation.

Our study has its limitations as we only used one model of senescence in vitro. However, there is currently no other cell model available that has features that come close to adult human PTEC. An animal study would not yield more insight into the uremic toxin-induced effects either, as the kidney pathology in animals does not fully reflect human kidney etiology and is limited by ethical considerations. Thus, a perfect model does not exist, and one has to compromise on the inclusion of some details of kidney senescence. Our current study focused on the contribution of IS in senescence to investigate the possible pathways that IS may be involved in, and paving the way for future experiments using 3D and in vivo models of chronic kidney disease to test therapeutic interventions such as senolytics.

4. Materials and Methods

4.1. Culture ciPTEC-OAT1

The ciPTEC-OAT1 [35] were cultured in a complete culture medium, consisting of phenol-red free DMEM-HAM's F12 medium supplied by Gibco (Paisly, UK), supplemented with 5 μg/mL insulin, transferrin and selenium separately, 35 ng/mL hydrocortisone, 10 ng/mL epidermal growth factor, 40 pg/mL triiodothyronine and 10% (v/v) fetal calf serum (FCS) purchased from

Greiner Bio-One (Alphenaan den Rijn, The Netherlands). Cells were cultured until 90% confluence at 33 °C, and then transferred to 37 °C with 5% (v/v) CO_2 to mature for up to 9 days coculturing with or without IS and the medium was replaced every three days. Cells were seeded in 96-well format plates for cell viability assay, and in 6-well plates for Western blot, Elisa, Real-time PCR and RNA-Seq.

4.2. Cell Viability Assay

PrestoBlue® cell viability reagent was used to test cell metabolic activity, which was purchased from Thermo Scientific (Vienna, Austria). The ciPTEC-OAT1 were cultured at 33 °C, and then matured at 37 °C for up to 9 days. Expose cells to increasing concentrations of indoxyl sulfate (IS) and doxorubicin (Dox) during maturation. Cell viability was evaluated at 0, 3, 6 or 9 days. IS was purchased from Sigma-Aldrich (Zwijndrecht, The Netherlands), Dox was obtained from MedchemExpress (Huissen, The Netherlands). GraphPad Prism (version 9.3.0, La Jolla, CA, USA) was used to obtain the cell viability curve.

IC50 values (inhibitory constants at 50% of control viability levels) were used to express cell viability. The results of cell viability were plotted via log IS and Dox concentration versus-viability with background subtraction. The normalized data were fitted using nonlinear regression with a variable slope restricting the bottom to 0. Six replicates of a minimum of three different experiments were performed.

4.3. SA-β-Gal Staining Assay

After the exposure, cells were washed twice with Hanks' Balanced Salt Solution (HBSS; Gibco, Life Technologies, Paisly, UK). An SA-β-gal staining assay was performed according to the manufacturer's instructions. A Senescence Detection Kit was used to identify the SA-gal-positive cells (ab65351, Abcam, Bristol, UK). The staining was evaluated for the appearance of a blue colour through an optical microscope (200× total magnification).

4.4. Western Blot

The ciPTEC-OAT1 were exposed to increasing concentrations of IS at 37 °C for up to 9 days. Afterwards, ice-cold RIPA Lysis Buffer was used to lyse the cells at 0, 3, 6 or 9 days for 30 min. The mixture was centrifuged at 14,000× g, at 4 °C for 20 min and then quantified the supernatant by BCA Protein Assay Kit. RIPA Lysis Buffer and BCA Protein Assay Kit were purchased from Thermo Scientific (Vienna, Austria).

SDS gels (14–20% acrylamide gradient) were used to separate the proteins. Proteins were separated for 65 min at 120 V (Bio-Rad Laboratories, Hercules, CA, USA), and then transferred to PVDF membranes (Bio-Rad Laboratories, Hercules, CA, USA) using Trans-Blot® Turbo™ Transfer Pack (Bio-Rad Laboratories) and Trans-Blot® Turbo™ Transfer System (Bio-Rad Laboratories) for 7 min at 25 V. A total of 5% skim milk-TBST was used to block the membranes for 2 h, and then the membranes were incubated at 4 °C with the primary antibody overnight and anti-mouse (1:3000, Dako, P0260, Carpinteria, CA, USA) or anti-rabbit (1:3000, Dako, P0448, Carpinteria, CA, USA) secondary antibodies at room temperature for at least 1 h. After that, Clarity Western ECL Blotting Substrate was used to treat the membrane as

directed by the manufacturer (Bio-Rad Laboratories, Hercules, CA, USA). Then, the bands were imaged using the ChemiDocTM MP Imaging System. To calculate the density of the bands, Image Lab software (version 6.0.1, Bio-Rad Laboratories, Hercules, CA, USA) was employed. The dilution of primary antibodies was 1:1000. The antibody to detect p21 was purchased from Cell Signaling Technology (Leiden, The Netherlands), and the antibody for LaminB1 was purchased at Abcam (Cambridge, UK).

4.5. Real-Time PCR

Total RNA from ciPTEC-OAT1 exposed to IS at different time points was isolated using the RNeasy Mini kit (Qiagen, Venlo, The Netherlands) according to the manufacturer's instructions. RNA quantity was determined using Nanodrop 2000 (Thermo-Fisher, Waltham, MA, USA). A total of 800 ng mRNA per sample was used to synthesize cDNA by employing the iScriptTM Reverse Transcription Supermix (Bio-Rad Laboratories, Hercules, CA, USA) and the T100™ Thermal Cycler (Bio-Rad Laboratories, Hercules, CA, USA). Real-time PCR was performed using the CFX96TM Real-Time PCR Detection System and the iQ SYBR® Green Supermix (Bio-Rad Laboratories, Hercules, CA, USA) following the manufacturer's instructions (Bio-Rad Laboratories, Hercules, CA, USA). β-actin was used as a housekeeping gene for normalization. Relative expression levels were calculated using the ΔΔCT method. The primers of different genes are listed as follows (Table 1).

Table 1. Primers used for real-time polymerase chain reaction.

Gene	Forward Primer	Reverse Primer
p21 (CDKN1A)	TGTCCGTCAGAACCCATGC	AAAGTCGAAGTTCCATCGCTC
laminB1 (LMNB1)	AAGCATGAAACGCGCTTGG	AGTTTGGCATGGTAAGTCTGC
β-actin (ACTB)	CATGTACGTTGCTATCCAGGC	CTCCTTAATGTCACGCACGAT

4.6. ELISA

Following exposure, cell culture supernatants were collected, centrifuged at 240× g, at 4 °C for 10 min and stored at −20 °C until further analysis. The following ELISA Kits from Invitrogen were used according to the manufacturer's instructions to measure the concentration of SASP factors in the culture supernatants: IL-6 (88-7066-88, Invitrogen, Carlsbad, CA, USA), IL-8 (88-8086-88, Invitrogen, Carlsbad, CA, USA) and IL-1β (88-7261-88, Invitrogen, Carlsbad, CA, USA).

4.7. RNA-Seq Differential Gene Expression Analysis

Cells were cultured in the presence or absence of 200 µM IS for 0, 1, 3 and 9 days, and each experiment was performed in triplicate. Cells were directly lysed in 400 µL RLT buffer (Cat. No. 79216, QIAGEN) and stored at −80 °C before RNA extraction on a QIAsymphony isolation robot using the QIAsymphony RNA Kit (931636, QIAGEN) and miRNA CT 400 protocol. RNA quality was checked with the Agilent Fragment Analyzer 5300 system using the RNA Kit (15 nt) (Cat. DNF-471-1000, Agilent, Santa Clara, CA, USA) and RNA quantity was measured with the Invitrogen™ Qubit Flex™ Fluorometer using the Qubit RNA HS Assay Kit (Cat. Q32855). For each sample, 100 ng of total RNA was used to prepare TruSeq Stranded mRNA libraries (Cat. 20020594, Illumina, San Diego, CA, USA) following the manufacturers protocol and with custom 384 xGen UDI-UMI adapters from IDT. Libraries were checked with the

Fragment Analyzer system dsDNA 910 Reagent Kit (35–1500 bp) (Cat. DNF-910-K1000, Agilent) and with Qubit dsDNA HS Assay Kit (Cat. Q32854, Invitrogen). Sample libraries were pooled equimolarly before sequencing on a Nextseq2000 (Illumina) using a P2 flowcell with 50 bp paired-end reads, resulting in an average of 20 million reads/sample.

RNA-Seq analysis Quality control on the sequence reads from the raw FASTQ files was done with FastQC (v0.11.8). TrimGalore (v0.6.5) as used to trim reads based on quality and adapter presence, after which FastQC was again used to check the resulting quality. rRNA reads were filtered out using SortMeRNA (v4.3.3), after which the resulting reads were aligned to the reference genome fasta (GCA_000001405.15_GRCh38_no_alt_analysis_set.fna) using the STAR (v2.7.3a) aligner. Follow up QC on the mapped (bam) files was done using Sambamba (v0.7.0), RSeQC (v3.0.1) and PreSeq (v2.0.3). Readcounts were then generated using the Subread FeatureCounts module (v2.0.0) with the Homo_sapiens.GRCh38.106.ncbi.gtf file as an annotation, after which normalization was done using the R-package edgeR (v3.28). Data were analysed using integrated Differential Expression and Pathway analysis (iDEP) [70]. The Kyoto Encyclopedia of Genes and Genomes (KEGG) [71] and MSigDB Hallmark [72] were used to perform the enrichment analysis of the differentially expressed genes (DEGs). The RNAseq raw read counts can be found in Table S4. Data visualization was prepared by https://www.bioinformatics.com.cn/srplot (last accessed on 22 October 2022), a free online platform for data analysis and visualization.

4.8. Statistics

All data analysis and statistics were performed using GraphPad Prism (version 9.3.0; GraphPad software, La Jolla, CA, USA), and expressed as mean ± SEM. Dunnett's multiple comparison test was employed after the one-way ANOVA to compare different groups. It was considered significant at $p < 0.05$.

Acknowledgments

Funding Statement

Key Contribution

Kidney proximal tubule cells show increased cellular tolerance against indoxyl sulfate over time; this observation is accompanied by SA-β-gal staining and an upregulation in the SASP factors IL-1β, IL-6 and IL-8, confirming the accumulation of senescent cells; RNA-sequencing and transcriptome analysis revealed that indoxyl sulfate accelerates senescence through cell cycle arrest; in this process, TNF-α and NF-κB signalling play a dominant role early on, and the epithelial-mesenchymal transition process at later time points.

Author Contributions

Conceptualization, Y.Y., M.M. and R.M.; methodology, Y.Y., M.M., M.J.J. and R.M.; investigation, Y.Y., M.M. and M.J.J.; writing original draft preparation, Y.Y.; writing review and editing, Y.Y., M.M., M.J.J. and R.M.; supervision, M.M., M.J.J. and R.M.; funding acquisition, Y.Y. and R.M. All authors have read and agreed to the published version of the manuscript.

Institutional Review Board Statement

The study was conducted in accordance with the Declaration of Helsinki, and the protocol was approved by and the collection of these samples was approved by the committee on research involving human subjects (Commissie Mensgebonden Onderzoek) of the Radboudumc. Additional consent was obtained from the original donor of the ciPTEC cells to perform RNA and DNA sequencing.

Informed Consent Statement

All subjects gave their informed consent for inclusion before they participated in the study.

Data Availability Statement

RNAseq read counts used for Differential Expression and Pathway analysis have been provided as supplementary data to this manuscript. The RNAseq raw FASTQ files have not been made publicly available for privacy reasons and risk of re-identification of the donor.

4

Conflicts of Interest

Rosalinde Masereeuw is co-inventor of the cell line ciPTEC-OAT1, for which the patent is held by Radboud University Nijmegen, the Netherlands.

References

1. Schafer, M.J.; Haak, A.J.; Tschumperlin, D.J.; LeBrasseur, N.K. Targeting Senescent Cells in Fibrosis: Pathology, Paradox, and Practical Considerations. Curr Rheumatol Rep 2018, 20, 3, doi:10.1007/s11926-018-0712-x.
2. Kobbe, C.v. Targeting senescent cells: approaches, opportunities, challenges. Aging 2019, 11, 18.
3. Munoz-Espin, D.; Serrano, M. Cellular senescence: from physiology to pathology. Nat Rev Mol Cell Biol 2014, 15, 482-496, doi:10.1038/nrm3823.
4. Huang, W.; Hickson, L.J.; Eirin, A.; Kirkland, J.L.; Lerman, L.O. Cellular senescence: the good, the bad and the unknown. Nature reviews. Nephrology 2022, doi:10.1038/s41581-022-00601-z.
5. Kumari, R.; Jat, P. Mechanisms of Cellular Senescence: Cell Cycle Arrest and Senescence Associated Secretory Phenotype. Front Cell Dev Biol 2021, 9, 645593, doi:10.3389/fcell.2021.645593.
6. Ceccaldi, R.; Parmar, K.; Mouly, E.; Delord, M.; Kim, J.M.; Regairaz, M.; Pla, M.; Vasquez, N.; Zhang, Q.S.; Pondarre, C.; et al. Bone marrow failure in Fanconi anemia is triggered by an exacerbated p53/p21 DNA damage response that impairs hematopoietic stem and progenitor cells. Cell stem cell 2012, 11, 36-49, doi:10.1016/j.stem.2012.05.013.
7. Ou, H.L.; Schumacher, B. DNA damage responses and p53 in the aging process. Blood 2018, 131, 488-495, doi:10.1182/blood-2017-07-746396.
8. Rayess, H.; Wang, M.B.; Srivatsan, E.S. Cellular senescence and tumor suppressor gene p16. Int J Cancer 2012, 130, 1715-1725, doi:10.1002/ijc.27316.
9. D'Arcy, M.S. Cell death: a review of the major forms of apoptosis, necrosis and autophagy. Cell Biol Int 2019, 43, 582-592, doi:10.1002/cbin.11137.
10. Fan, Y.; Cheng, J.; Zeng, H.; Shao, L. Senescent Cell Depletion Through Targeting BCL-Family Proteins and Mitochondria. Front Physiol 2020, 11, 593630, doi:10.3389/fphys.2020.593630.
11. Carneiro, B.A.; El-Deiry, W.S. Targeting apoptosis in cancer therapy. Nat Rev Clin Oncol 2020, 17, 395-417, doi:10.1038/s41571-020-0341-y.
12. Mabrouk, N.; Ghione, S.; Laurens, V.; Plenchette, S.; Bettaieb, A.; Paul, C. Senescence and Cancer: Role of Nitric Oxide (NO) in SASP. Cancers (Basel) 2020, 12, doi:10.3390/cancers12051145.
13. Coppé, J.P.; Desprez, P.Y.; Krtolica, A.; Campisi, J. The senescence-associated secretory phenotype: the dark side of tumor suppression. Annual review of pathology 2010, 5, 99-118, doi:10.1146/annurev-pathol-121808-102144.
14. Ashraf, S.; Santerre, P.; Kandel, R. Induced senescence of healthy nucleus pulposus cells is mediated by paracrine signaling from TNF-α-activated cells. Faseb j 2021, 35, e21795, doi:10.1096/fj.202002201R.
15. Guo, Q.; Zhang, H.; Zhang, B.; Zhang, E.; Wu, Y. Tumor Necrosis Factor-alpha (TNF-α) Enhances miR-155-Mediated Endothelial Senescence by Targeting Sirtuin1 (SIRT1). Medical science monitor : international medical journal of experimental and clinical research 2019, 25, 8820-8835, doi:10.12659/msm.919721.
16. Li, P.; Gan, Y.; Xu, Y.; Song, L.; Wang, L.; Ouyang, B.; Zhang, C.; Zhou, Q. The inflammatory cytokine TNF-α promotes the premature senescence of rat nucleus pulposus cells via the PI3K/Akt signaling pathway. Scientific reports 2017, 7, 42938, doi:10.1038/srep42938.
17. Birch, J.; Gil, J. Senescence and the SASP: many therapeutic avenues. Genes Dev 2020, 34, 1565-1576, doi:10.1101/gad.343129.120.
18. Hernandez-Segura, A.; Nehme, J.; Demaria, M. Hallmarks of Cellular Senescence. Trends Cell Biol 2018, 28, 436-453, doi:10.1016/j.tcb.2018.02.001.
19. Kuilman, T.; Peeper, D.S. Senescence-messaging secretome: SMS-ing cellular stress. Nat Rev Cancer 2009, 9, 81-94, doi:10.1038/nrc2560.
20. Gonzalez-Meljem, J.M.; Apps, J.R.; Fraser, H.C.; Martinez-Barbera, J.P. Paracrine roles of cellular senescence in promoting tumourigenesis. Br J Cancer 2018, 118, 1283-1288,

doi:10.1038/s41416-018-0066-1.

21. Vanholder, R.; De Smet, R.; Glorieux, G.; Argilés, A.; Baurmeister, U.; Brunet, P.; Clark, W.; Cohen, G.; De Deyn, P.P.; Deppisch, R.; et al. Review on uremic toxins: classification, concentration, and interindividual variability. Kidney Int 2003, 63, 1934-1943, doi:10.1046/j.1523-1755.2003.00924.x.

22. Lim, Y.J.; Sidor, N.A.; Tonial, N.C.; Che, A.; Urquhart, B.L. Uremic Toxins in the Progression of Chronic Kidney Disease and Cardiovascular Disease: Mechanisms and Therapeutic Targets. Toxins (Basel) 2021, 13, doi:10.3390/toxins13020142.

23. Enomoto, A.; Takeda, M.; Taki, K.; Takayama, F.; Noshiro, R.; Niwa, T.; Endou, H. Interactions of human organic anion as well as cation transporters with indoxyl sulfate. European Journal of Pharmacology 2003, 466, 13-20, doi:https://doi.org/10.1016/S0014-2999(03)01530-9.

24. Motojima, M.; Hosokawa, A.; Yamato, H.; Muraki, T.; Yoshioka, T. Uraemic toxins induce proximal tubular injury via organic anion transporter 1-mediated uptake. British Journal of Pharmacology 2002, 135, 555-563, doi:https://doi.org/10.1038/sj.bjp.0704482.

25. Jansen, J.; Jansen, K.; Neven, E.; Poesen, R.; Othman, A.; van Mil, A.; Sluijter, J.; Sastre Torano, J.; Zaal, E.A.; Berkers, C.R.; et al. Remote sensing and signaling in kidney proximal tubules stimulates gut microbiome-derived organic anion secretion. Proceedings of the National Academy of Sciences 2019, 116, 16105-16110, doi:doi:10.1073/pnas.1821809116.

26. Liu, W.C.; Tomino, Y.; Lu, K.C. Impacts of Indoxyl Sulfate and p-Cresol Sulfate on Chronic Kidney Disease and Mitigating Effects of AST-120. Toxins (Basel) 2018, 10, doi:10.3390/toxins10090367.

27. Rossi, M.; Campbell, K.L.; Johnson, D.W.; Stanton, T.; Vesey, D.A.; Coombes, J.S.; Weston, K.S.; Hawley, C.M.; McWhinney, B.C.; Ungerer, J.P.; et al. Protein-bound uremic toxins, inflammation and oxidative stress: a cross-sectional study in stage 3-4 chronic kidney disease. Archives of medical research 2014, 45, 309-317, doi:10.1016/j.arcmed.2014.04.002.

28. Niwa, T.; Shimizu, H. Indoxyl sulfate induces nephrovascular senescence. Journal of renal nutrition : the official journal of the Council on Renal Nutrition of the National Kidney Foundation 2012, 22, 102-106, doi:10.1053/j.jrn.2011.10.032.

29. Shimizu, H.; Bolati, D.; Adijiang, A.; Muteliefu, G.; Enomoto, A.; Nishijima, F.; Dateki, M.; Niwa, T. NF-κB plays an important role in indoxyl sulfate-induced cellular senescence, fibrotic gene expression, and inhibition of proliferation in proximal tubular cells. American Journal of Physiology-Cell Physiology 2011, 301, C1201-C1212.

30. Adelibieke, Y.; Shimizu, H.; Muteliefu, G.; Bolati, D.; Niwa, T. Indoxyl sulfate induces endothelial cell senescence by increasing reactive oxygen species production and p53 activity. Journal of Renal Nutrition 2012, 22, 86-89.

31. Bolesta, E.; Pfannenstiel, L.W.; Demelash, A.; Lesniewski, M.L.; Tobin, M.; Schlanger, S.E.; Nallar, S.C.; Papadimitriou, J.C.; Kalvakolanu, D.V.; Gastman, B.R. Inhibition of Mcl-1 promotes senescence in cancer cells: implications for preventing tumor growth and chemotherapy resistance. Mol Cell Biol 2012, 32, 1879-1892, doi:10.1128/MCB.06214-11.

32. Shimizu, H.; Yisireyili, M.; Higashiyama, Y.; Nishijima, F.; Niwa, T. Indoxyl sulfate upregulates renal expression of ICAM-1 via production of ROS and activation of NF-κB and p53 in proximal tubular cells. Life Sci 2013, 92, 143-148, doi:10.1016/j.lfs.2012.11.012.

33. Mihajlovic, M.; Krebber, M.M.; Yang, Y.; Ahmed, S.; Lozovanu, V.; Andreeva, D.; Verhaar, M.C.; Masereeuw, R. Protein-Bound Uremic Toxins Induce Reactive Oxygen Species-Dependent and Inflammasome-Mediated IL-1beta Production in Kidney Proximal Tubule Cells. Biomedicines 2021, 9, doi:10.3390/biomedicines9101326.

34. Yang, Y.; Mihajlovic, M.; Valentijn, F.; Nguyen, T.Q.; Goldschmeding, R.; Masereeuw, R. A Human Conditionally Immortalized Proximal Tubule Epithelial Cell Line as a Novel Model for Studying Senescence and Response to Senolytics. Front Pharmacol 2022, 13, 791612, doi:10.3389/fphar.2022.791612.

35. Nieskens, T.T.; Peters, J.G.; Schreurs, M.J.; Smits, N.; Woestenenk, R.; Jansen, K.; van der

Made, T.K.; Röring, M.; Hilgendorf, C.; Wilmer, M.J.; et al. A Human Renal Proximal Tubule Cell Line with Stable Organic Anion Transporter 1 and 3 Expression Predictive for Antiviral-Induced Toxicity. The AAPS journal 2016, 18, 465-475, doi:10.1208/s12248-016-9871-8.

36. Larsson, O.; Scheele, C.; Liang, Z.; Moll, J.; Karlsson, C.; Wahlestedt, C. Kinetics of senescence-associated changes of gene expression in an epithelial, temperature-sensitive SV40 large T antigen model. Cancer research 2004, 64, 482-489, doi:10.1158/0008-5472.can-03-1872.

37. Duranton, F.; Cohen, G.; De Smet, R.; Rodriguez, M.; Jankowski, J.; Vanholder, R.; Argiles, A. Normal and pathologic concentrations of uremic toxins. J Am Soc Nephrol 2012, 23, 1258-1270, doi:10.1681/asn.2011121175.

38. Bojko, A.; Staniak, K.; Czarnecka-Herok, J.; Sunderland, P.; Dudkowska, M.; Śliwińska, M.A.; Salmina, K.; Sikora, E. Improved Autophagic Flux in Escapers from Doxorubicin-Induced Senescence/Polyploidy of Breast Cancer Cells. Int J Mol Sci 2020, 21, doi:10.3390/ijms21176084.

39. Huang, P.; Bai, L.; Liu, L.; Fu, J.; Wu, K.; Liu, H.; Liu, Y.; Qi, B.; Qi, B. Redd1 knockdown prevents doxorubicin-induced cardiac senescence. Aging (Albany NY) 2021, 13, 13788-13806, doi:10.18632/aging.202972.

40. Christidi, E.; Brunham, L.R. Regulated cell death pathways in doxorubicin-induced cardiotoxicity. Cell Death Dis 2021, 12, 339, doi:10.1038/s41419-021-03614-x.

41. Docherty, M.H.; O'Sullivan, E.D.; Bonventre, J.V.; Ferenbach, D.A. Cellular Senescence in the Kidney. J Am Soc Nephrol 2019, 30, 726-736, doi:10.1681/ASN.2018121251.

42. Calcinotto, A.; Kohli, J.; Zagato, E.; Pellegrini, L.; Demaria, M.; Alimonti, A. Cellular Senescence: Aging, Cancer, and Injury. Physiol Rev 2019, 99, 1047-1078, doi:10.1152/physrev.00020.2018.

43. Shimi, T.; Butin-Israeli, V.; Adam, S.A.; Hamanaka, R.B.; Goldman, A.E.; Lucas, C.A.; Shumaker, D.K.; Kosak, S.T.; Chandel, N.S.; Goldman, R.D. The role of nuclear lamin B1 in cell proliferation and senescence. Genes Dev 2011, 25, 2579-2593, doi:10.1101/gad.179515.111.

44. Engeland, K. Cell cycle regulation: p53-p21-RB signaling. Cell Death & Differentiation 2022, 29, 946-960, doi:10.1038/s41418-022-00988-z.

45. Mijit, M.; Caracciolo, V.; Melillo, A.; Amicarelli, F.; Giordano, A. Role of p53 in the Regulation of Cellular Senescence. Biomolecules 2020, 10, doi:10.3390/biom10030420.

46. Yosef, R.; Pilpel, N.; Papismadov, N.; Gal, H.; Ovadya, Y.; Vadai, E.; Miller, S.; Porat, Z.; Ben-Dor, S.; Krizhanovsky, V. p21 maintains senescent cell viability under persistent DNA damage response by restraining JNK and caspase signaling. EMBO J 2017, 36, 2280-2295, doi:10.15252/embj.201695553.

47. Saito, N.; Araya, J.; Ito, S.; Tsubouchi, K.; Minagawa, S.; Hara, H.; Ito, A.; Nakano, T.; Hosaka, Y.; Ichikawa, A.; et al. Involvement of Lamin B1 Reduction in Accelerated Cellular Senescence during Chronic Obstructive Pulmonary Disease Pathogenesis. J Immunol 2019, 202, 1428-1440, doi:10.4049/jimmunol.1801293.

48. He, S.; Sharpless, N.E. Senescence in Health and Disease. Cell 2017, 169, 1000-1011, doi:10.1016/j.cell.2017.05.015.

49. Ortiz-Montero, P.; Londoño-Vallejo, A.; Vernot, J.P. Senescence-associated IL-6 and IL-8 cytokines induce a self- and cross-reinforced senescence/inflammatory milieu strengthening tumorigenic capabilities in the MCF-7 breast cancer cell line. Cell communication and signaling : CCS 2017, 15, 17, doi:10.1186/s12964-017-0172-3.

50. Shi, L.; Zhao, Y.; Fei, C.; Guo, J.; Jia, Y.; Wu, D.; Wu, L.; Chang, C. Cellular senescence induced by S100A9 in mesenchymal stromal cells through NLRP3 inflammasome activation. Aging (Albany NY) 2019, 11, 9626-9642, doi:10.18632/aging.102409.

51. Romero, A.; Dongil, P.; Valencia, I.; Vallejo, S.; Hipólito-Luengo Á, S.; Díaz-Araya, G.; Bartha, J.L.; González-Arlanzón, M.M.; Rivilla, F.; de la Cuesta, F.; et al. Pharmacological Blockade of NLRP3 Inflammasome/IL-1β-Positive Loop Mitigates Endothelial Cell Senescence and Dysfunction. Aging and disease 2022, 13, 284-297, doi:10.14336/ad.2021.0617.

52. Lekawanvijit, S.; Adrahtas, A.; Kelly, D.J.; Kompa, A.R.; Wang, B.H.; Krum, H. Does indoxyl sulfate, a uraemic toxin, have direct effects on cardiac fibroblasts and myocytes? European heart journal 2010, 31, 1771-1779, doi:10.1093/eurheartj/ehp574.

53. Rapa, S.F.; Prisco, F.; Popolo, A.; Iovane, V.; Autore, G.; Di Iorio, B.R.; Dal Piaz, F.; Paciello, O.; Nishijima, F.; Marzocco, S. Pro-Inflammatory Effects of Indoxyl Sulfate in Mice: Impairment of Intestinal Homeostasis and Immune Response. International Journal of Molecular Sciences 2021, 22, 1135.

54. Savira, F.; Kompa, A.R.; Magaye, R.; Xiong, X.; Huang, L.; Jucker, B.M.; Willette, R.N.; Kelly, D.J.; Wang, B.H. Apoptosis signal-regulating kinase 1 inhibition reverses deleterious indoxyl sulfate-mediated endothelial effects. Life Sciences 2021, 272, 119267, doi:https://doi.org/10.1016/j.lfs.2021.119267.

55. Gire, V.; Dulic, V. Senescence from G2 arrest, revisited. Cell Cycle 2015, 14, 297-304, doi:10.1080/15384101.2014.1000134.

56. Lu, W.; Ren, S.; Dong, W.; Li, X.; Zheng, Z.; Jia, Y.; Xue, Y. Albumin-induced premature senescence in human renal proximal tubular cells and its relationship with intercellular fibrosis. Acta Biochimica et Biophysica Sinica 2022, 54, 893, doi:https://doi.org/10.3724/abbs.2022055.

57. Fischer, M.; Quaas, M.; Steiner, L.; Engeland, K. The p53-p21-DREAM-CDE/CHR pathway regulates G2/M cell cycle genes. Nucleic Acids Res 2016, 44, 164-174, doi:10.1093/nar/gkv927.

58. Orjalo, A.V.; Bhaumik, D.; Gengler, B.K.; Scott, G.K.; Campisi, J. Cell surface-bound IL-1alpha is an upstream regulator of the senescence-associated IL-6/IL-8 cytokine network. Proceedings of the National Academy of Sciences of the United States of America 2009, 106, 17031-17036, doi:10.1073/pnas.0905299106.

59. Levi, N.; Papismadov, N.; Solomonov, I.; Sagi, I.; Krizhanovsky, V. The ECM path of senescence in aging: components and modifiers. FEBS J 2020, 287, 2636-2646, doi:10.1111/febs.15282.

60. Bonnans, C.; Chou, J.; Werb, Z. Remodelling the extracellular matrix in development and disease. Nat Rev Mol Cell Biol 2014, 15, 786-801, doi:10.1038/nrm3904.

61. Liu, T.; Zhang, L.; Joo, D.; Sun, S.-C. NF-κB signaling in inflammation. Signal Transduction and Targeted Therapy 2017, 2, 17023, doi:10.1038/sigtrans.2017.23.

62. Dongre, A.; Weinberg, R.A. New insights into the mechanisms of epithelial–mesenchymal transition and implications for cancer. Nature Reviews Molecular Cell Biology 2019, 20, 69-84, doi:10.1038/s41580-018-0080-4.

63. Kriz, W.; Kaissling, B.; Le Hir, M. Epithelial-mesenchymal transition (EMT) in kidney fibrosis: fact or fantasy? J Clin Invest 2011, 121, 468-474, doi:10.1172/jci44595.

64. Wang, X.-H.; Gao, J.-W.; Bao, J.-P.; Zhu, L.; Xie, Z.-Y.; Chen, L.; Peng, X.; Zhang, C.; Wu, X.-T. GATA4 promotes the senescence of nucleus pulposus cells via NF-κB pathway. Archives of Gerontology and Geriatrics 2022, 101, 104676, doi:https://doi.org/10.1016/j.archger.2022.104676.

65. Faheem, M.M.; Seligson, N.D.; Ahmad, S.M.; Rasool, R.U.; Gandhi, S.G.; Bhagat, M.; Goswami, A. Convergence of therapy-induced senescence (TIS) and EMT in multistep carcinogenesis: current opinions and emerging perspectives. Cell death discovery 2020, 6, 51, doi:10.1038/s41420-020-0286-z.

66. Chio, II; Sasaki, M.; Ghazarian, D.; Moreno, J.; Done, S.; Ueda, T.; Inoue, S.; Chang, Y.L.; Chen, N.J.; Mak, T.W. TRADD contributes to tumour suppression by regulating ULF-dependent p19Arf ubiquitylation. Nat Cell Biol 2012, 14, 625-633, doi:10.1038/ncb2496.

67. Nakano, T.; Katsuki, S.; Chen, M.; Decano, J.L.; Halu, A.; Lee, L.H.; Pestana, D.V.S.; Kum, A.S.T.; Kuromoto, R.K.; Golden, W.S.; et al. Uremic Toxin Indoxyl Sulfate Promotes Proinflammatory Macrophage Activation Via the Interplay of OATP2B1 and Dll4-Notch Signaling. Circulation 2019, 139, 78-96, doi:10.1161/CIRCULATIONAHA.118.034588.

68. Tanaka, S.; Watanabe, H.; Nakano, T.; Imafuku, T.; Kato, H.; Tokumaru, K.; Arimura, N.; Enoki, Y.; Maeda, H.; Tanaka, M.; et al. Indoxyl Sulfate Contributes to Adipose Tissue Inflammation through the Activation of NADPH Oxidase. Toxins (Basel) 2020, 12, doi:10.3390/toxins12080502.

69. Nakano, T.; Watanabe, H.; Imafuku, T.; Tokumaru, K.; Fujita, I.; Arimura, N.; Maeda, H.; Tanaka, M.; Matsushita, K.; Fukagawa, M.; et al. Indoxyl Sulfate Contributes to mTORC1-Induced Renal Fibrosis via The OAT/NADPH Oxidase/ROS Pathway. Toxins (Basel) 2021, 13, doi:10.3390/toxins13120909.

70. Ge, S.X.; Son, E.W.; Yao, R. iDEP: an integrated web application for differential expression and pathway analysis of RNA-Seq data. BMC Bioinformatics 2018, 19, 534, doi:10.1186/s12859-018-2486-6.

71. Kanehisa, M.; Goto, S. KEGG: kyoto encyclopedia of genes and genomes. Nucleic Acids Res 2000, 28, 27-30, doi:10.1093/nar/28.1.27.

72. Liberzon, A.; Birger, C.; Thorvaldsdóttir, H.; Ghandi, M.; Mesirov, J.P.; Tamayo, P. The Molecular Signatures Database (MSigDB) hallmark gene set collection. Cell systems 2015, 1, 417-425, doi:10.1016/j.cels.2015.12.004.

Supplementary Material

Table S1. top 5 significant p-values and adj.p-values for KEGG 2021 Human in each cluster.

Cluster	Term	p-value	adj.p-value	Overlap_genes
A	Cell cycle	1.30E-12	3.02E-10	[CDKN2C, PLK1, BUB1B, TTK, CDC6, CDC25C, PKMYT1, CDC25A, CDC20, CCNA2, CCNB2, CCNB1, ORC6, DBF4, PTTG1, ORC1, ESPL1, CDK1, E2F2, SFN, BUB1, MAD2L1]
	Oocyte meiosis	1.56E-06	1.81E-04	[PLK1, CDC25C, FBXO43, PKMYT1, AURKA, CDC20, SGO1, CCNB2, CCNB1, PTTG1, ESPL1, CDK1, FBXO5, BUB1, MAD2L1]
	Progesterone-mediated oocyte maturation	1.24E-05	9.64E-04	[CCNA2, CCNB2, CCNB1, PLK1, CDK1, KIF22, CDC25C, PKMYT1, BUB1, CDC25A, AURKA, MAD2L1]
	Gap junction	1.93E-05	1.12E-03	[TUBA1C, TUBA1B, TUBB6, TUBB2B, GUCY1B1, TUBA1A, TUBB2A, TUBB, CDK1, TUBB4B, TUBB4A]
	Salmonella infection	9.63E-04	4.49E-02	[ANXA2, TUBB, TUBB4B, TUBB4A, TNF, PIK3CG, TUBA1C, TUBA1B, TUBB2B, TUBB6, TUBA1A, TUBB2A, IRAK1, PODXL, RHOJ, S100A10]
C	p53 signaling pathway	3.80E-05	9.71E-03	[PIDD1, CDKN1A, RRM2B, ZMAT3, SESN1, SESN2, ADGRB1, MDM2, BBC3, DDB2]
	NF-kappa B signaling pathway	1.75E-04	2.23E-02	[PIDD1, VCAM1, TNFSF14, BCL2A1, TNFAIP3, CXCL3, PTGS2, CXCL2, CARD11, EDA2R, BIRC3]
E	Protein digestion and absorption	2.00E-06	6.45E-04	[COL15A1, COL16A1, MME, COL25A1, COL11A1, COL12A1, SLC1A1, SLC16A10, ATP1B2, ATP1B1, COL1A2, COL6A2, COL7A1, COL4A6, COL8A2, COL4A5, COL8A1, COL6A5]
	Cell adhesion molecules	3.34E-04	3.91E-02	[CD274, NTNG2, CADM1, NEGR1, SDC2, HLA-B, HLA-A, F11R, HLA-F, L1CAM, HLA-G, CLDN5, PECAM1, ITGB8, NRCAM, CLDN16, TIGIT, JAM2]
	Human papillomavirus infection	4.26E-04	3.91E-02	[NOTCH3, TNXB, WNT2B, NOTCH4, FOXO1, OASL, PARD6B, CCND2, WNT11, ITGB8, WNT2, FZD3, WNT5B, STAT1, MX2, WNT5A, ITGA1, HLA-B, HLA-A, AXIN2, HLA-F, HLA-G, VEGFA, COL1A2, DLG3, COL6A2, COL4A6, COL4A5, ITGA7, MAML3, COL6A5]
F	Cytokine-cytokine receptor interaction	1.31E-08	3.00E-06	[IL33, CXCL6, CSF3, CCL20, GDF15, EBI3, IL24, CXCR4, TNFRSF11B, TNFRSF1B, CX3CL1, IL6, IL36B, IL1B, CCL4, CCL3, ACKR3, IL36RN]
	Complement and coagulation cascades	5.76E-08	6.00E-06	[C3, THBD, C1R, C5AR1, BDKRB2, ITGAX, BDKRB1, C8B, C8A, CLU]
	Viral protein interaction with cytokine and cytokine receptor	2.74E-07	1.80E-05	[CXCL6, IL6, CCL20, IL24, CCL4, CCL3, CXCR4, ACKR3, TNFRSF1B, CX3CL1]
	Inflammatory bowel disease	1.07E-05	5.34E-04	[IL6, IL1B, RORC, STAT4, RORA, NOD2, TLR2]
	Amoebiasis	2.65E-05	9.10E-04	[IL6, GNA15, MUC2, IL1B, CD1D, C8B, C8A, TLR2]

4

Table S2. Top 5 significant p-values and adj.p-values for MSigDB Hallmark 2020 in each cluster.

Cluster	Term	p-value	adj.p-value	Overlap_genes
A	G2-M Checkpoint	5.93E-57	2.79E-55	[TOP2A, H2AX, JPT1, SUV39H1, CCNF, KIF11, MKI67, BRCA2, SMC4, KIF15, LMNB1, CKS1B, CDC20, PTTG1, EXO1, STMN1, PBK, NUSAP1, NEK2, MYBL2, FBXO5, KPNA2, HMGN2, KIF23, KNL1, KIF22, CDC25A, TRAIP, CCNA2, DDX39A, DBF4, ESPL1, INCENP, CKS2, BIRC5, KIF2C, KIF20B, TROAP, TTK, HMMR, CENPA, AURKB, AURKA, CCNB2, ORC6, RACGAP1, E2F2, BUB1, PLK4, H2AZ1, GINS2, POLQ, STIL, CDKN2C, UBE2C, PLK1, CDC6, NDC80, TPX2, CENPE, CENPF, UBE2S, PRC1, KIF4A, TACC3, CDK1, MAD2L1, CDKN3]
	E2F Targets	5.53E-53	1.30E-51	[TOP2A, H2AX, JPT1, SUV39H1, DSCC1, HMGB2, BUB1B, MKI67, BRCA2, SMC4, CKS1B, LMNB1, CDC20, PTTG1, STMN1, MYBL2, TK1, KPNA2, DLGAP5, RFC3, TUBB, KIF22, CDC25A, NME1, DDX39A, MELK, ESPL1, CKS2, DEPDC1, TIMELESS, BIRC5, KIF2C, DCTPP1, ASF1B, CDCA3, CDCA8, HMMR, AURKB, AURKA, RAD51AP1, CCNB2, ORC6, RACGAP1, LYAR, PLK4, GINS1, H2AZ1, CDKN2C, RRM2, SPAG5, GINS3, PLK1, GINS4, CENPE, KIF18B, DIAPH3, UBE2S, KIF4A, TACC3, CDK1, TRIP13, SPC24, MAD2L1, CDKN3, SPC25]
	Mitotic Spindle	3.51E-19	5.50E-18	[TOP2A, PIF1, TTK, KIF11, BRCA2, SMC4, KIF15, LMNB1, AURKA, CCNB2, RACGAP1, NUSAP1, NEK2, FBXO5, SYNPO, BUB1, DLGAP5, PLK1, KIF23, KIF22, NDC80, ANLN, TPX2, CENPE, CENPF, ESPL1, INCENP, PRC1, KIF4A, CDK1, BIRC5, KIF2C, KIF20B, EZR, DOCK2]
	Spermatogenesis	2.38E-04	2.60E-03	[CCNB2, ARL4A, DBF4, CAMK4, CDK1, NEK2, KIF2C, TTK, BUB1, NCAPH, AURKA, CDKN3]
	Estrogen Response Late	2.77E-04	2.60E-03	[PLK4, TOP2A, GINS2, SLC26A2, STIL, CAV1, CDC6, CDC20, FABP5, ACOX2, PRKAR2B, GJA1, ID2, SFN, KIF20A]
C	TNF-alpha Signaling via NF-kB	5.21E-10	1.04E-08	[BTG2, CDKN1A, CEBPB, CSF2, BCL2A1, CEBPD, TNFAIP3, PTGS2, CXCL3, CXCL2, IFIH1, MAP3K8, ICOSLG, IL15RA, GCH1, GFPT2, SOD2, PNRC1, IL1A, NINJ1, FOSB, PTX3, CD69, PLPP3, BIRC3]
	p53 Pathway	5.21E-10	1.04E-08	[CYFIP2, CDKN1A, BTG2, GLS2, DGKA, HSPA4L, NDRG1, PIDD1, SOCS1, ZMAT3, SESN1, FDXR, CLCA2, CASP1, PHLDA3, ST14, RHBDF2, IRAG2, DDB2, IL1A, KRT17, NINJ1, MDM2, NUPR1, ADA]
	Interferon Gamma Response	1.10E-06	1.47E-05	[IL15RA, CDKN1A, CIITA, VCAM1, GCH1, MX1, TNFAIP3, ISG15, PTGS2, DDX60, SOD2, USP18, IFIH1, SOCS1, IFI27, TNFSF10, CASP1, IRF7, CD69, HERC6]
	Interferon Alpha Response	1.71E-03	1.71E-02	[IFIH1, IFI27, MX1, CASP1, IRF7, ISG15, DDX60, USP18, HERC6]
	Inflammatory Response	4.69E-03	3.75E-02	[NPFFR2, IL15RA, CDKN1A, BTG2, GCH1, LPAR1, RASGRP1, IL1A, RNF144B, TNFSF10, IRF7, CD69, ICOSLG]
D	KRAS Signaling Dn	7.42E-04	2.97E-02	[PRKN, EDN1, TGFB2, EDN2, KRT4, RSAD2, ARPP21, SLC30A3, IGFBP2, ALOX12B, YBX2, MACROH2A2, P2RX6, P2RY4, NTF3, EFHD1, CDH16, GPR19, RIBC2, TAS2R4]
E	Epithelial Mesenchymal Transition	6.92E-16	3.18E-14	[COL16A1, CXCL8, LRP1, COL11A1, COL12A1, PLOD2, FBLN1, CXCL1, PLOD1, ENO2, FSTL1, SAT1, FBLN5, GJA1, QSOX1, SLIT2, TGM2, CTHRC1, CADM1, PRRX1, IGFBP4, MMP1, LUM, FUCA1, MMP2, WNT5A, APLP1, MMP3, BGN, INHBA, VEGFA, GREM1, COL1A2, FAP, LOX, COL6A2, COL7A1, COL8A2, FMOD, MXRA5, SNTB1, FBN1]
	Hypoxia	1.90E-10	4.37E-09	[SCARB1, PFKFB3, SDC2, ADM, VLDLR, ENO2, HK2, CSRP2, FAM162A, STC2, MXI1, PDK3, GPC4, B4GALNT2, PPARGC1A, ANKZF1, PDK1, TGM2, WSB1, DTNA, GAA, BGN, FOS, AMPD3, HS3ST1, VEGFA, EFNA3, PPP1R3C, LOX, P4HA1, DDIT4, RRAGD, ALDOC, TMEM45A]
	Interferon Gamma Response	4.34E-08	6.65E-07	[LGALS3BP, CD274, CFH, C1S, FPR1, SECTM1, IFI44L, OASL, CCL7, NAMPT, DHX58, EPSTI1, ST8SIA4, PDE4B, CCL2, AUTS2, STAT1, MX2, HLA-B, IFI44, ARID5B, HLA-A, HLA-G, BST2, PLSCR1, OAS3, SSPN, CMPK2, XAF1, CFB]
	Estrogen Response Early	1.70E-06	1.96E-05	[SCARB1, FOXC1, FCMR, WWC1, HSPB8, SLC1A1, ABAT, ADD3, SLC7A2, GJA1, PDLIM3, ABLIM1, DEPTOR, RPS6KA2, STC2, TGM2, BCL11B, IGFBP4, GFRA1, FOS, GAB2, IL17RB, DHRS3, AR, ELF3, SYT12, RAB17]
	KRAS Signaling Up	5.33E-06	4.91E-05	[ADAMDEC1, ABCB1, CFH, SATB1, HOXD11, TFPI, HSD11B1, CCND2, ADGRA2, PRKG2, ST6GAL1, JUP, PRRX1, FUCA1, IGF2, LAPTM5, INHBA, TRAF1, RBP4, GPRC5B, MAFB, HKDC1, SCG5, PECAM1, TRIB1, CFB]
F	Inflammatory Response	1.45E-08	5.65E-07	[CXCL6, CSF3, TNFAIP6, CCL20, AQP9, EBI3, C5AR1, NOD2, TNFRSF1B, CX3CL1, IL6, GNA15, IL1B, BDKRB1, TLR2]
	Coagulation	6.94E-07	1.35E-05	[C3, DPP4, THBD, MMP7, GDA, C1R, TFPI2, HTRA1, C8B, CLU, C8A]
	TNF-alpha Signaling via NF-kB	4.38E-06	5.69E-05	[DUSP4, NR4A2, CXCL6, IL6, TNFAIP6, CCL20, IL1B, KYNU, CCL4, SLC16A6, ACKR3, TLR2]
	Epithelial Mesenchymal Transition	2.48E-05	2.42E-04	[LRRC15, CXCL6, IL6, IGFBP3, TFPI2, HTRA1, TNFRSF11B, THBS2, SCG2, NID2, DCN]
	KRAS Signaling Up	1.28E-04	1.00E-03	[IL33, SNAP25, SLPI, FGF9, CCL20, IL1B, IGFBP3, CXCR4, PRDM1, TNFRSF1B]

Table S3. top 10 enrichment pathways from MSigDB Hallmark of DEGs in IS-treatment groups compared to non-treatment groups at different time points.

Group	Term	P-value	Adjusted P-value	Genes
Day1+IS vs Day1	TNF-alpha Signaling via NF-kB	3.69E-22	8.50E-21	CXCL6; CSF2;BCL2A1;GCH1;CCL20;TNFAIP3;CXCL1;CXCL3;PTGS2;CXCL2;IL1A;IL6;NR4A3;CCL2;MSC;ICOSLG;BIRC3
	KRAS Signaling Up	1.47E-09	1.13E-08	GPRC5B;CSF2;ABCB1;CCL20;TNFAIP3;SOX9;PTGS2;EREG;BIR
	Inflammatory Response	1.47E-09	1.13E-08	CXCL6;
	Epithelial Mesenchymal Transition	3.26E-08	1.87E-07	CXCL6;
	Apoptosis	2.94E-06	1.35E-05	IL1A;
	IL-6/JAK/STAT3 Signaling	6.60E-05	2.53E-04	IL6; CSF2;CXCL1;CXCL3
	Interferon Gamma Response	1.40E-04	4.59E-04	IL6;GCH1;TNFAIP3;CCL2;PTGS2
	UV Response Up	6.51E-04	1.87E-03	IL6;ABCB1;GCH1;CXCL2
	Allograft Rejection	1.56E-03	3.99E-03	IL6;CCL2;ICOSLG;EREG
	Pperoxisome	2.24E-03	5.16E-03	ABCB1;CADM1;SERPINA6
Day3+IS vs Day3	TNF-alpha Signaling via NF-kB	5.49E-04	9.33E-03	IFIH1;TIPARP;SLC16A6;FOSB
	Hypoxia	5.53E-02	1.34E-01	TIPARP;STC2
	Glycolysis	5.53E-02	1.34E-01	STC2;CACNA1H
	Estrogen Response Early	5.53E-02	1.34E-01	TIPARP;STC2
	Myogenesis	5.53E-02	1.34E-01	STC2;CACNA1H
	KRAS Signaling Up	5.53E-02	1.34E-01	SLPI;SPP1
	Epithelial Mesenchymal Transition	5.53E-02	1.34E-01	SPP1;MXRA5
	Angiogenesis	6.62E-02	1.41E-01	SPP1
	Interferon Alpha Response	1.69E-01	3.00E-01	IFIH1
	PI3K/AKT/mTOR Signaling	1.81E-01	3.00E-01	MAP2K6
Day9+IS vs Day9	Epithelial Mesenchymal Transition	9.93E-06	2.98E-04	RGS4;CDH6;CXCL6;MMP1;IGFBP3;IGFBP2;MMP3;SLIT2;MXR
	Coagulation	3.79E-04	5.69E-03	THBD;SERPINB2;CFH;MMP1;C1R;MMP3
	Hypoxia	2.58E-03	2.58E-02	PPP1R3C;IGFBP3;STC2;SLC2A5;PPFIA4;CP
	TNF-alpha Signaling via NF-kB	1.23E-02	5.27E-02	CXCL6;SERPINB2;CCL4;FOSB;IFIT2
	Estrogen Response Early	1.23E-02	5.27E-02	CYP26B1;STC2;AQP3;DHRS2;PTGES
	Myogenesis	1.23E-02	5.27E-02	NQO1;PPP1R3C;IGFBP3;STC2;PPFIA4
	Complement	1.23E-02	5.27E-02	ITGAM;SERPINB2;CFH;C1R;CP
	Angiogenesis	2.52E-02	9.45E-02	CXCL6;THBD
	Interferon Alpha Response	2.91E-02	9.69E-02	IFITM1;LAMP3;IFIT2
	Estrogen Response Late	4.89E-02	1.33E-01	CYP26B1;DHRS2;ASS1;PTGES

Table S4. RNAseq read counts used for Differential Expression and Pathway analysis (data normalized). Details can be downloaded at: https://www.mdpi.com/article/10.3390/toxins15040242/s1

4
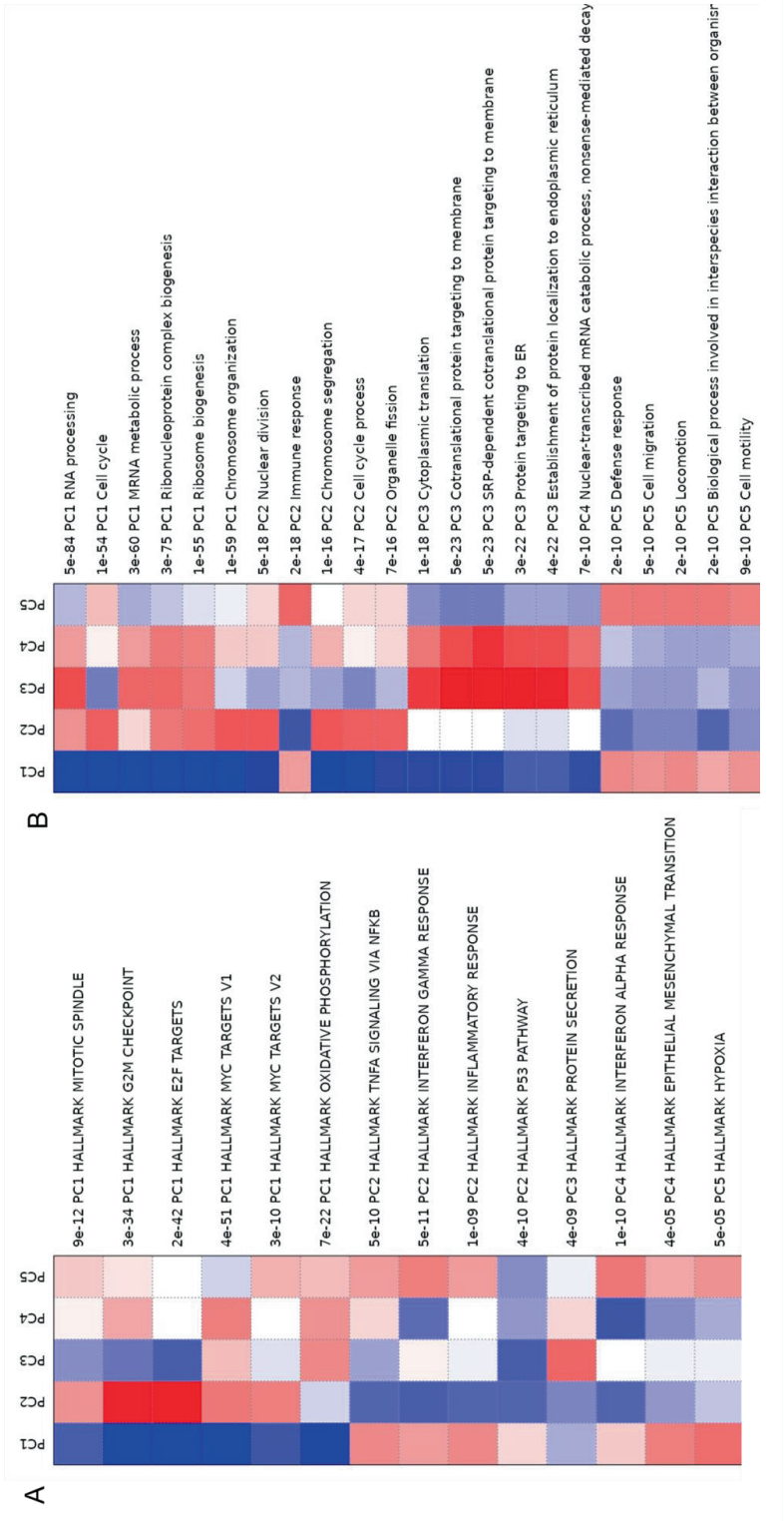
Figure S1. Pathway Analysis of PCA rotation. Pathway analysis is based on (A) MSigDB Hallmark and (B) Gene Ontology (GO) biological process. The adjusted P-values are used to rank the pathways for each of the first 5 principal components. The pathways are labeled with FDR first, followed by the principal components (PC1, PC2 and so on).). Only 6 pathways for each principal components are shown, but duplicated ones are skipped.
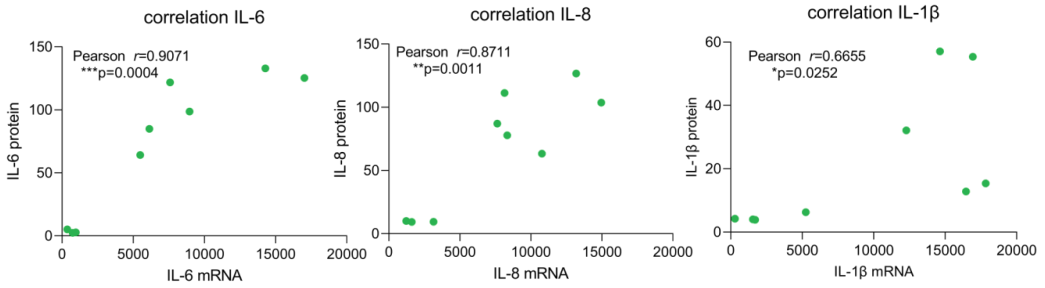
Figure S2. Correlation analysis of IL-6, IL-8,and IL-1β protein level in Figure 3 and mRNA abundance in Figure 5. Protein levels and gene counts are on day 0, day 3, and day 9 with the treatment of IS (200 µM). P<0.05 is considered to be statistically significant.
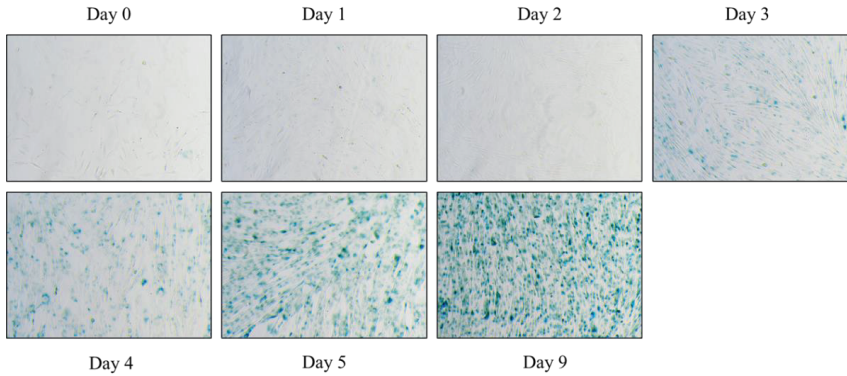
Figure S3. SA-β-gal activity in CiPTEC-OAT1 during culture at non-permissive temperature. Representative images of SA-β-gal staining in ciPTEC-OAT1 cultured for 0 through 9 days at 37 °C. Three independent experiments were performed.

Figure S4: Exposure to IS leads to sustained common senescence markers expression in ciPTEC-OAT1 at non-permissive temperature of 37 °C. Details can be downloaded at: https://www.mdpi.com/article/10.3390/toxins15040242/s1

Chapter 5

Studying targeting of senolytic-lysozyme conjugates to kidneys for clearance of senescent cells: preliminary experiments

Yi Yang[1], Ines Pieterman[1,2], Milos Mihajlovic[1], Robbert Jan Kok[2] and Rosalinde Masereeuw[1]

[1]Division of Pharmacology, Utrecht Institute for Pharmaceutical Sciences, Utrecht University, 3584 CG Utrecht, The Netherlands.

[2]Division of Pharmaceutics, Department of Pharmaceutical Sciences, Utrecht University, The Netherlands.

Abstract

Chronic senescence contributes to kidney disease through inflammation and fibrosis by releasing SASP factors. The clearance of senescent cells by senolytics could conceivably become a treatment option for kidney disease. Navitoclax, inhibiting Bcl-xl and Bcl-2 and promoting apoptosis, shows a great senolytic potential. However, in view of severe side effects reported in clinical studies, alternative strategies for improving the safety profile of navitoclax are needed. In the present study, we first tested whether navitoclax interferes with transporters present in a human conditionally immortalized proximal tubule epithelial cell line that overexpresses the organic anion transporter 1 (ciPTEC-OAT1), which could facilitate its uptake. As this appeared not to take place, we studied the capacity of ciPTEC to internalize drug-lysozyme (LZM) conjugates and we proposed a strategy to synthesize senolytic-LZM conjugates, as the first steps towards kidney-targeted delivery of navitoclax. By conjugating navitoclax to the kidney-specific carrier molecule LZM, the accumulation of navitoclax in tubular epithelial cells could be enhanced, thereby increasing kidney-specificity and reducing adverse effects. The results suggest that ciPTEC-OAT1 appears suitable to take up the rhodamine-LZM conjugates, indicating that this is a valuable in vitro model to evaluate the efficacy of senolytic-LZM conjugates.

Keywords: conditionally immortalized proximal tubule epithelial cells, navitoclax, targeted delivery, kidney disease, megalin

1. Introduction

Senescence shows permanent cell cycle arrest and limits cell proliferation. Acute senescent cells can be cleared by the immune system through recruitment of immune cells, followed by tissue regeneration. On the contrary, chronic senescent cells are difficult to eradicate and, subsequently, accumulate and contribute to the pathology [1, 2]. Chronic senescent cells contribute to kidney disease through inflammation and fibrosis, via releasing senescence-associated secretory phenotype (SASP) factors that are of pro-inflammatory and pro-fibrotic nature [3]. Elimination of senescent cells becomes a treatment option for suppressing the progression of kidney disease. Senolytics appear to be among the most promising agents capable for this as they can specifically remove senescent cells by interfering with anti- and pro-survival signalling [4].

A recent study suggested that navitoclax is a potential senolytic that could selectively eliminate senescent stem cells from bone and muscle, and in mice [5]. Our previous study showed that navitoclax is capable of clearing senescent proximal tubule epithelial cells (PTEC) in vitro [6]. However, clinical trials with navitoclax showed the occurrence of severe side effects (summarized in Table 1), especially thrombocytopenia, which is due to navitoclax's antagonistic effect on Bcl-xl and Bcl-2 [7, 8]. Bcl-xl is responsible of maintaining platelet survival [9], and hence thrombocytopenia can only be avoided when the cellular distribution of navitoclax is changed. As the major side effects do not affect the kidney, targeted delivery of navitoclax to this organ may be a promising therapy to improve its efficacy/safety profile and unlock its potential in the kidney fibrosis reversal.

Table 1.Overview of navitoclax used in clinical studies for 21 days

Disease	Study design	Dose (oral / day in mg)	Number of patients (enrolled /evaluated)	Side effects (number of patients)	Reference
Lymphoid malignancies	Phase I	10-440	55/53	Diarrhea (31), fatigue (21), thrombocytopenia (29) and neutropenia (17)	[7]
Small-cell lung cancer and other solid tumors	Phase I	10-475	47/47	Diarrhea (19), nausea (16), vomiting (17), fatigue (16) and thrombocytopenia(47)	[10]
Chronic lymphocytic leukemia	Phase I	10-300	29/29	Diarrhea (22), nausea (17), vomiting (9), fatigue (10), thrombocytopenia (8), and neutropenia (8).	[11]
Relapsed small cell lung cancer	Phase II	150-325	39/39	Thrombocytopenia (24), diarrhea (19), nausea (18) and fatigue(14)	[12]
Recurrent epithelial ovarian cancer	Phase II	150-250	47/46	Thrombocytopenia (45), lymphopenia(37), neutropenia (22) , anemia (36) and fatigue (37)	[13]

Targeted drug delivery to the kidney can be achieved by linking drugs to carriers or homing ligands that are substrates for specific transporters expressed in PTECs, such as the organic anion transporter 1 (OAT1) and the organic cation transporter 2 (OCT2); such transporters

facilitate the uptake of small-molecule compounds from the blood compartment into the tubular cells [14]. These transporters often work in concerted action with efflux transporters facilitating excretion into the lumen of the proximal tubule (Figure 1). Transport proteins involved in tubular drug secretion or reabsorption are identified as the adenosine triphosphate (ATP)-binding cassette (ABC) transporter and solute carrier (SLC) families of transmembrane proteins. These transporters are located at the basolateral or apical (luminal) membrane of PTEC. The influx transporters take up drugs from the blood side into the cells and are located at basolateral membrane. They mainly belong to SLC transporter families such as organic anion transporters (OATs) and organic cationic transporters (OCTs). On the other hand, the efflux transporters that facilitate intracellular drugs to enter the lumen, mainly belong to ABC transporter families such as multidrug and toxin extrusion proteins (MATEs) and multidrug resistance proteins (MRPs), and are located at the apical membrane [15]. Six influx transporters (OAT1, OAT3, OATP4C1, OCT2, OAT4 and URAT1) and six efflux transporters (P-gp, BCRP, MATE1, MATE2, MRP2, and MRP4) in the kidney have received greatest attention in drug distribution studies [14-16]. (Table 2 and Figure 1).

Table 2. Main transporters in human proximal tubule epithelial cells (PTEC).

Function	Protein	Full name	Gene in human	Location
Influx	OAT1	Organic anion transporter 1	*SLC22A6*	Basolateral membrane
	OAT3	Organic anion transporter 3	*SLC22A8*	Basolateral membrane
	OATP4C1	Organic anion transporter polypeptide 4C1	*SLCO4C1*	Basolateral membrane
	OCT2	Organic cation transporter 2	*SLC22A2*	Basolateral membrane
	URAT1	Urate reuptake transporter 1	*SLC22A12*	Apical membrane
	OAT4	Organic anion transporter 4	*SLC22A11*	Apical membrane
Efflux	MDR1 (P-gp)	Multidrug resistance protein 1 (P-glycoprotein)	*ABCB1*	Apical membrane
	BCRP	Breast cancer resistance protein	*ABCG2*	Apical membrane
	MATE1	Multidrug and toxin extrusion protein 1	*SLC47A1*	Apical membrane
	MATE2	Multidrug and toxin extrusion protein 2	*SLC47A2*	Apical membrane
	MRP2	Multidrug resistance protein 2	*ABCC2*	Apical membrane
	MRP4	Multidrug resistance protein 4	*ABCC4*	Apical membrane

Alternatively, targeted delivery can be achieved via interaction with transporters that are expressed at the tubular side of PTEC. Of note, this can only be reached when compounds have been passed over the glomerulus filtration barrier, upon which they can be accumulated into PTEC via receptor-mediated endocytosis [17, 18]. Low molecular weight glomerular proteins (LMWPs) represent an ideal macromolecular carrier for targeted delivery directed to the megalin receptor. One of the LMWP is lysozyme (LZM), which is an endogenous protein with a molecular weight of 14 kDa and hence small enough to be freely filtered in the glomerulus; LZM is efficiently taken up in the proximal tubule by the megalin receptor via endocytosis and thus not excreted into the final urine [19-21]. Megalin is located in the apical membrane of PTEC, mediating the reabsorption of a large variety of proteins [22]. Targeted drug delivery in the kidney is generally accomplished in four steps: 1. the drug-LZM conjugates enter rapidly into the renal tubule through glomerular filtration; 2. megalin receptor of the PTEC recognizes

the LZM moiety of the conjugates; 3. the conjugates enter the PTEC by endocytosis; 4. drugs are released from the conjugate during lysosomal degradation and diffuse intracellularly to their intended site of action [17, 19] (Figure 1).

For the targeting of navitoclax to the PTEC, the senolytic will need to be conjugated to LZM via a bioreversible linker that can release the drug from the LMWP after its accumulation in the lysosomal compartment. We hypothesized that the the platinum(II)-based metal-organic linker technology (Lx®) would be appropriate for such a bioreversible linking of navitoclax [23], as outlined in Figure 2.
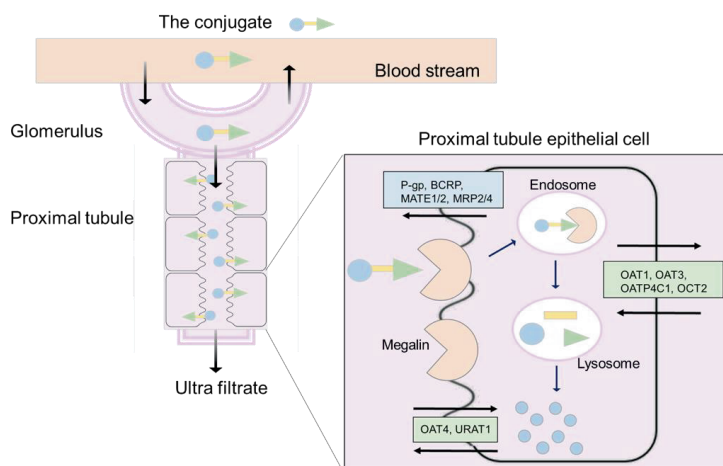
Figure 1. Principle of drug delivery to the kidney with LZM conjugates. The PTEC expresses influx and efflux transporters and megalin receptors. Tansporters are involved in tubular drug secretion or reabsorption, the influx transporters are in green, which take up drugs into the cells. The efflux transporters are in blue, which facilitate intracellular drugs to enter the lumen. Megalin is in orange, located in the apical membrane of PTEC, mediating the reabsorption of a large variety of proteins via endocytosis. After glomerular filtration, the drug-LZM conjugates enter rapidly into the renal tubule; LZM moiety of the conjugates is recognized by megalin receptor of the PTEC; then the conjugates are taken up by the PTEC via endocytosis; free drug will be released intracellularly from the conjugate after lysosomal degradation of the drug-LZM conjugate and disruption of the navitoclax-linker bond via competitive displacement with endogenous platinophilic ligands like gluthathione [17].

5

Figure 2. Reaction scheme for the synthesis Nav-Lx-LZM. Navitoclax-Lx (Nav-Lx) is reacted with methionine-modified LZM to yield the Nav-Lx-LZM conjugates. The bioreversible linker (Lx®) is in pink.The structure of Nav-Lx-LZM is shown to exemplify its drug delivery strategy but is to not part of this thesis chapter.

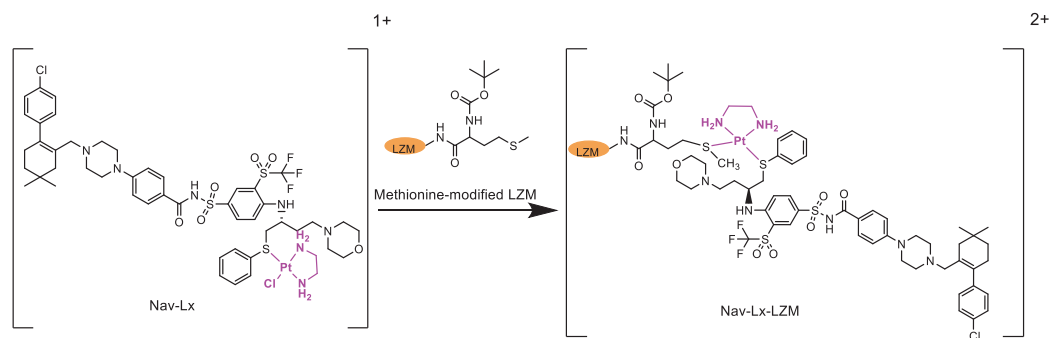To test this hypothesis, we first evaluated the effect of navitoclax on various transporters present in PTEC. Then, the functional capacity of megalin in transporting a fluorescently labelled rhodamine-LZM conjugate into PTEC was tested. As a cell model, we used a human conditionally immortalized PTEC line that overexpresses OAT1 (ciPTEC-OAT1), which expresses both megalin receptors and various solute transporters including OAT1, OCT2, P-gp, BCRP and MRP4 [24, 25]. Furthermore, in **chapter 2** we demonstrated that this model develops a conditional senescent phenotype at a non-permissive temperature [6], allowing us to study the pharmacological effects after targeting as well.

2. Materials and methods

2.1 CiPTEC-OAT1 cell culture

CiPTEC-OAT1 cells [25] were cultured in complete culture medium, consisting of phenol-red free DMEM-HAM's F12 medium (Gibco, Life Technologies, Paisly, UK), supplemented with 10% (v/v) fetal calf serum (FCS) (Greiner Bio-One, Alphen aan den Rijn, the Netherlands), 5 μg/mL insulin, 5 μg/mL transferrin, 5 μg/mL selenium, 35 ng/mL hydrocortisone, 10 ng/mL epidermal growth factor (EGF) and 40 pg/mL triiodothyronine. All additives to the medium and other compounds were purchased from Sigma-Aldrich (Zwijndrecht, The Netherlands) unless stated otherwise. Cells were cultured at 33°C until 90% confluence was reached, and then transferred to 37°C with 5% (v/v) CO_2 to mature for 7 days.

2.2 Fluorescent assays

The interaction between navitoclax and substrates for the selected transporters expressed by ciPTEC-OAT1 was evaluated using fluorescent probes. Fluorescent probes including Fluorescein, (4-(4-(dimethylamino)styryl)-N-methylpyridinium (ASP+), Hoechst33342, chloromethylfluorescein-diacetate (CMFDA), and calcein-AM were used to evaluate the interaction. Fluorescent probes-only group and common inhibitors of different transporters were used as negative and positive controls to navitoclax. To test for the interactions, matured ciPTEC-OAT1 cells were cultured in the 96-well plate and exposed to different concentrations of navitoclax (ranging from 1 nM to 10 μM) or inhibitors and fluorescent probes at appropriate

concentrations. Information regarding different fluorescent assays is shown in Table 3. Briefly, transport was achieved by incubating the cells with fluorescent probes and navitoclax/inhibitor at 37 °C for different times (Table 3). After incubation, the solutions were removed. For influx transporters, to detect the interaction of navitoclax with OCT2, the plates were read directly after adding 100 μL ice-cold Hanks' Balanced Salt Solution (HBSS; Gibco, Life Technologies, Paisly, UK); to detect the interaction with OAT1, the plates were washed twice with ice-cold HBSS buffer and the cells were lysed by 100 μL NaOH 0.1M solution, the plates were read after incubating for another 30 min at room temperature. For efflux transporters, to detect the interaction with P-gp, the plates were washed twice with ice-cold HBSS buffer and the cells were lysed by adding 100 μL Triton-100 1% solution, the plates were read after incubating for another 60 min at room temperature. As for BCRP and MRP2/4, the plates were washed twice with ice-cold HBSS buffer and were read after incubating the cells with 100 μL HBSS for another 30 min at 37°C. Plates were read at suggested excitation wavelength (Ex) and emission wavelength (Em), according to the feature of fluorescent probe.

Navitoclax and the inhibitors were purchased from MedchemExpress (Huissen, The Netherlands). Fluorescent probes were obtained from Thermo Scientific (Vienna, Austria).

Table 2. Information of different fluorescent assays.

Function	Transporter	Inhibitor	Fluorescent probe	Treatment time (min)
Influx	OAT1	Probenecid (100 μM)	Fluorescein (1 μM)	10
	OCT2	Cimetidine (100 μM)	ASP+ (10 μM)	15
Efflux	P-gp	Zosuquidar (1 μM)	Calcein-AM (2 μM)	60
	BCRP	KO143 (5 μM)	Hoechst33342 (1.25 μM)	30
	MRP2/4	MK571 (5μM)	CMFDA (1.25 μM)	30

5

2.3 Synthesis and characterization of RBITC-LZM

Rhodamine B isothiocyanate (RBITC; MedchemExpress, Huissen, The Netherlands) was coupled to hen egg-white LZM (Sigma-Aldrich; Zwijndrecht, The Netherlands), by incubating at room temperature for at least 1h at a 3:1 mol/mol ratio in PBS. The reaction product was purified by extensive dialysis against water using a membrane tube (pore size 3.5kDa; Fisher Scientific, Germany) to remove unreacted RBITC and buffer salts and then filtered over regenerated cellulose membranes (RC) syringe filters with a pore size of 0.45 μm, after which the product was lyophilized and stored at -20°C.

Conjugation of RBITC to LZM was confirmed by chromatographic analysis on a Waters ACQUITY system (Waters Associates Inc., Milford, MA, USA) equipped with an ACQUITY UPLC CSH C18 column (2.1 × 50 mm) and a fluorescence detector. The mobile phase consisted of a gradient of two solvents (Eluent A: water/acetonitrile = 95/5 (v/v) with 0.1% formic acid; eluent B: acetonitrile with 0.1% formic acid). All compounds were eluted using a linear gradient: 0% B to 60% B in 2.5 min at a flow rate of 0.5 ml/min. The injection volume was 5 μL. The fluorescence detector was operated at an excitation wavelength (Ex) of 543 nm and emission wavelength (Em) of 580 nm.

2.4 Cellular uptake of RBITC-LZM in ciPTEC-OAT1

Matured ciPTEC-OAT1 cells were cultured in the 96-well plate and exposed to increasing

concentrations of RBITC-LZM (0, 3.13, 4.38, 6.25, 8.75, 12.5, 17.5, 25, and 35 mg/mL), then incubated at 4°C or 37°C for either 1h, 3h, or 6h. The uptake was stopped by removing solutions, washing 3 times with ice-cold HBSS, to stop the reaction and remove excess conjugates. After lysing the cells by adding 100 μL Triton-100 1% solution and an incubation for another 1h, plates were read at the microplate reader, using the following wavelengths: Ex 543nm, Em 580 nm.

2.5 Statistics

All data analysis and statistics were performed using GraphPad Prism (version 9.3.0; GraphPad software, La Jolla, CA, USA), and expressed as mean ± SEM. For comparison of two groups, unpaired t text was employed. One-way ANOVA was used followed by Dunnett's multiple comparison test to compare different groups. For comparison of two groups at different time points, two-way ANOVA was used followed by Sidak's multiple comparison test. The difference was considered significant at $p < 0.05$.

3. Results

3.1 Navitoclax does not interact with various renal drug transporters.

To investigate whether navitoclax interacts with important drug transporters present in ciPTEC-OAT1, studies were conducted with fluorescent subtrates for five different transporters. The influx transporters, OAT1 and OCT2, could potentially facilitate uptake of the senolytic and inhibition of the transporter by navitoclax would point towards competitive inhibition. The uptake of fluorescein by OAT1 (Figure 3A) was clearly inhibited by the known inhibitor, probenecid, whereas navitoclax did not affect fluorescein uptake. Similarly, the uptake of ASP as OCT2 substrate (Figure 3B) was inhibited by cimetidine but not by navitoclax. For the efflux pump, P-glycoprotein (Pgp, Figure 3C) calcein-AM is used as a substrate. By blocking its efflux with zosuquidar, the substrate is retained intracellularly and converted to the fluorescent calcein by hydrolases. Exposure to navitoclax did not lead to an intracellular accumulation of calcein, indicating that the senolytic does not inhibit Pgp. Similar results were obtained for BCRP (Figure 3D) and MRP2/4 (Figure 3E). These findings suggest that navitoclax is likely not a substrate nor inhibitor for one of these transporters.
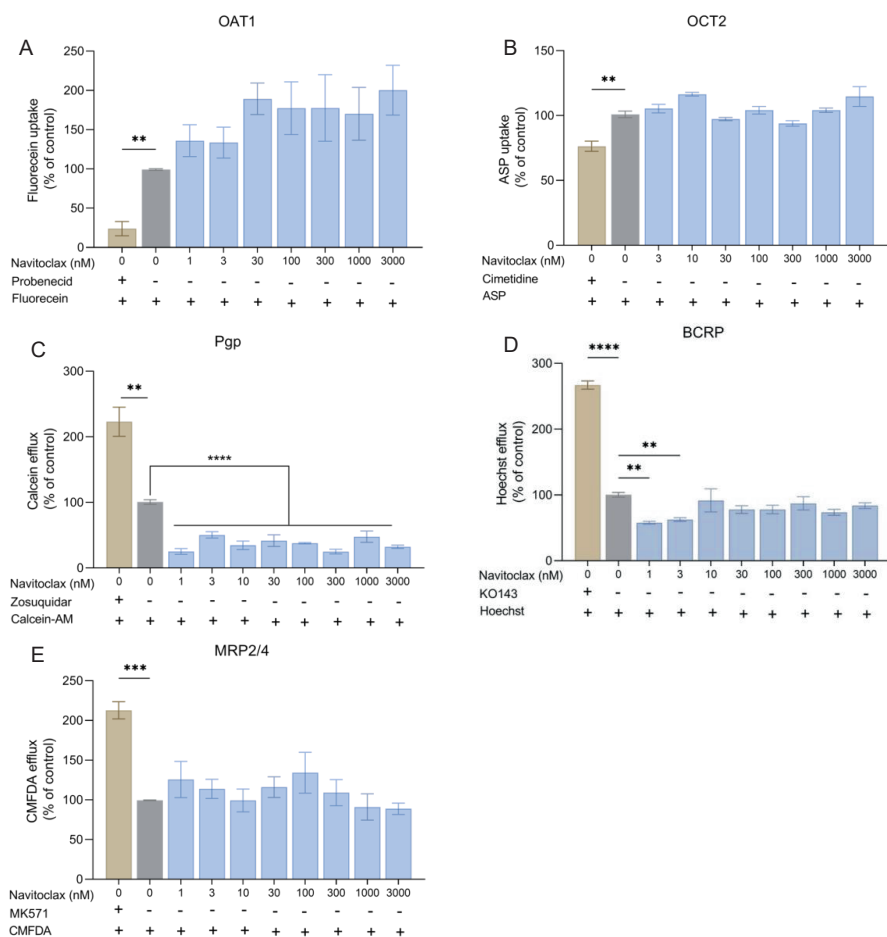
Figure 3. Navitoclax does not interact with influx and efflex transporters expressed in ciPTEC. Fluorescence-based transport assays were conducted to evaluate interaction of navitoclax with the influx (A) OAT1, (B) OCT2, or efflux (C) P-gp, (D) BCRP, (E) MRP2/4 transporters. Inhibitors of these transporters were used as positive control for active transport of the fluorescent probe by the relative transporter. Three independent experiments were performed in triplicates. **$P<0.01$, ***$P<0.001$ and ****$P<0.0001$ (Inhibitor-treated group compared to fluorescence-only group, unpaired t test; navitoclax-treated groups compared to fluorescent marker-only group, One-way ANOVA, Dunnett's multiple comparison).

5

3.2 Synthesis and characterizations of RBITC-LZM conjugate.
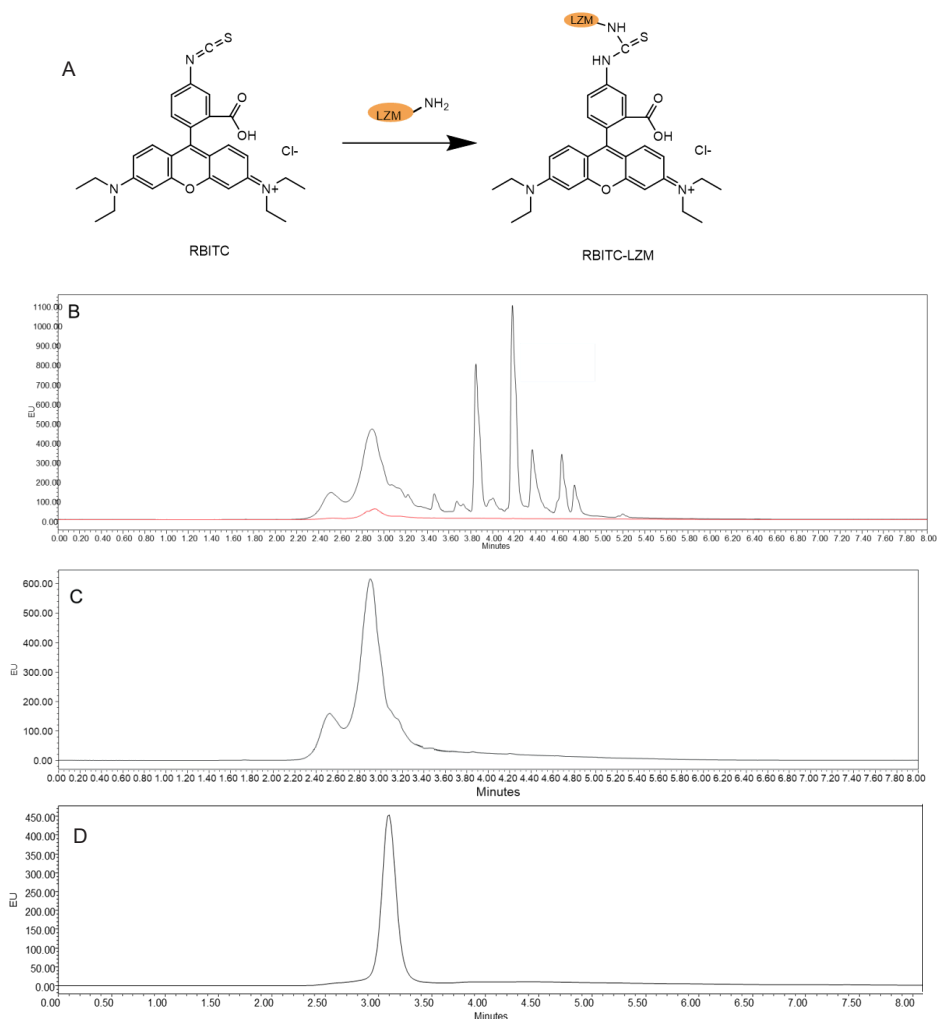
Figure 4. Synthesis and characterizations of RBITC-LZM conjugates. (A) Reaction scheme for the synthesis RBITC-LZM. (B) components after the conjugation with Rhodamine B isothiocyanate (RBITC) and lysozyme (LZM), Black: unpurified reaction mixture, showing the signal of both RBITC-LZM and non-reacted RBTIC complex, Red: LZM; (C) purified RBITC-LZM; (D) Signal of LZM with photodiode array detector at 280 nm. Compounds of (B) and (C) were detected with fluorescence detector at Ex 543nm, Em 580 nm.

A next step in enhancing the accumulation of navitoclax in PTEC would be to administer the drug as conjugate with the kidney-directed carrier LZM. As a first step towards such an approach, we now studied the interaction of ciPTECs with rhodamine-LZM conjugates, which can be regarded as florescent model conjugates. Rhodamine was reacted to LZM using the reactive probe RBITC (rhodamine B isothiocyanate) which can react covalently to primary amino groups of the LWMP. The conjugation of RBITC to LZM was studied by chromatographic analysis before and after purification of the reaction mixture by dialysis.

As shown in Figure 4, the retention time of unmodified LZM is 2.9 min (Figure 4 B, red line). LZM showed stronger signal with photodiode array detector at 280 nm (Figure 4 D), as it is not a fluorescent compound. After conjugation with RBITC, strong fluorescent signals were detected at the retention time of LZM (Figure 4 B, black line) indicating successful conjugation; of note, since Fig 4 B shows the crude reaction mixture before dialysis, peaks of free RBITC are still present (peaks with the retention time after 3.40 min). After purification by dialysis, free RBITC was effectively removed while the remaining peaks can be attributed to RBITC-LZM conjugates (Figure 4 C). Although one would expect RBITC-LZM to elute as a single peak similar as unmodified LZM, it is not uncommon that drug-LZM conjugates elute in multiple peaks due to the differences in linkage of drugs or fluorophors at different side-chain residues of the LMWP [26, 27].

3.3 RBITC-LZM conjugates are efficiently taken up by ciPTEC-OAT1.
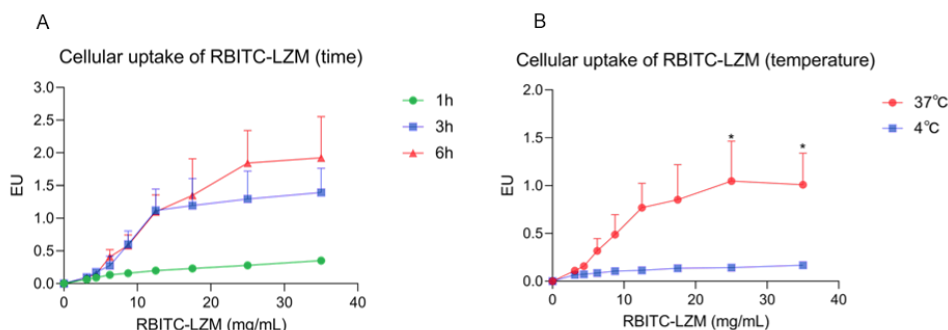
Figure 5. Internalization of RBITC-LZM by ciPTEC-OAT1. (A) Cellular uptake of RBITC-LZM in ciPTEC-OAT1 at 37 °C after incubation for 1, 3 and 6 hours; (B) Cellular uptake of RBITC-LZM in ciPTEC-OAT1 at 37 °C or 4°C for 3 hours. *$p<0.05$ (cells incubated at 37 °C compared to cells at 4 °C at the same concentration of RBITC-LZM; Two-way ANOVA, Sidak's multiple comparison test).

To understand whether LZM is taken up by ciPTEC-OAT1 in a megalin-dependent manner, the cells were incubated with RBITC-LZM for different time periods ranging from 1 to 6 h. Figure 5 shows a dose-dependent uptake at 37°C (Figure 5A). Prolonging the incubation time to 3 h resulted in increased intracellular fluorescence at 37°C compared to 1 h, with no further increase at 6h. We selected 3 h to study the RBITC-LZM uptake further by incubating at 4 °C in comparison with 37 °C (Figure 5B). Incubation at 4°C reflects binding of the conjugate to the membrane solely without internalization, and the highly reduced uptake at 4 °C indicates that RBITC-LZM is actively internalized, potentially via megalin-mediated endocytosis. Furthemore, the uptake of RBITC-LZM could be inhibited by excess unmodified LZM (Figure S1), indicating that the uptake of the dye compound might be specific and receptor mediated.

4. Discussion

In present study, we evaluated the interaction of navitoclax with known transporters to reveal whether the drug is taken up and accumulates in the kidney. Secondly, we studied whether LZM conjugates can be used to deliver navitoclax to the kidney and whether the specific

targeting could be achieved through megalin by using fluorescently labeled LZM conjugate in ciPTEC-OAT1. The results obtained suggest that navitoclax may not be a substrate for known transporters in ciPTEC-OAT1, and that specific targeting is a feasible option the cell line used.

Up to now, navitoclax has been administered orally [28], which requires the drug to cross several barriers before it can reach the systemic circulation and its therapeutic target [29]. First, navitoclax is dependent on intestinal absorption, after which distribution, metabolism and elimination (ADME) processes determine the drug's disposition. These processes often involve active transport processes that may also lead to unintended interactions, including drug-drug interactions (DDI). In the kidney, DDI may decrease the renal clearance and increase the toxicity of drugs [30]. Our results demonstrated that navitoclax did not directly interact with various renal transporters (OAT1, OCT2, BCRP, P-gp and MRP2/4) in ciPTEC-OAT1, indicating navitoclax is likely not an inhibitor nor a substrate of these transporters and may not bear the risk of unwanted DDI. However, this also implies that for specific targeting to the kidney another approach has to be taken, such as conjugation of the drug to a carrier system. This may eventually result in therapeutic drug concentrations levels at much lower total drug dosage limiting systemic adverse effects. One approach may be to conjugate drugs to macromolecular carriers that are substrates for megalin, such as LZM. Previously, LZM conjugates were successfully applied in various preclinical studies, including conjugates with inhibitors of the kinase domain of the transforming growth factor receptor (TGF-βR; activin receptor like kinase 5 (ALK5) inhibitor) [31] and of the platelet-derived growth receptor (PDGFR inhibitor; imatinib) [32]. Furthermore, Haas et al. [20] demonstrated by whole body-imaging in rats that the conjugate naproxen-LZM followed the elimination route of LZM and accumulated specifically in the kidney (Figure 6). Therefore, targeted delivery of drugs to the kidney by means of drug-LZM conjugates represents a good option to decrease the systemic dose of the drug and reduce the risk of side effects.
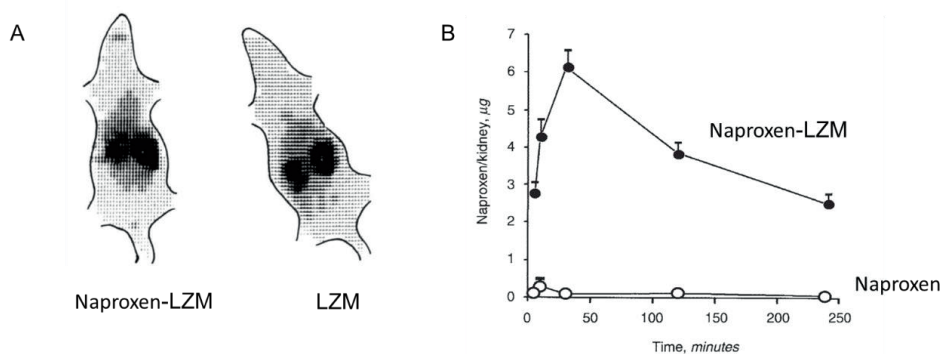
Figure 6. Naproxen-LZM accumulates in kidney tissue, *in vivo* (figure adapted from literature [20]). (A) Representative images with a one-minute resolution of the biodistribution of naproxen-^{123}I-LZM conjugate (left) and native ^{123}I-LZM (right), about 20 min after an intravenous injection in the rat [20]. (B) Renal time course of naproxen after an intravenous injection of parent naproxen or conjugate in three rats at each indicated time point [20].

Various studies reported earlier on radiolabel-drug-LZM conjugation and kidney targeting [27, 32], while conjugates with fluorescent reporters, such as rhodamine, have been used as model LZM-conjugates to trace the uptake mechanisms both *in vitro* and in animal studies [33-35].

The current study employed rhodamine B as a tracer. Considering the temperature-sensitive uptake, the uptake of RBTIC-LZM was potentially mediated by endocytosis involving megalin receptor binding. Previous results revealed that ciPTEC-OAT1 are able of albumin reabsorption mediated by megalin receptor [24] and antisense oligonucleotides [36], via similar uptake mechanism to our results involving LZM, suggesting that the uptake by ciPTEC-OAT1 occurs via the megalin receptor. However, further experiments with specific inhibitors of megalin (*i.e.,* RAP or alpha-1-microglobulin [36]) and/or receptor knock-down approaches (via siRNA or CRSIPR-Cas9) should confirm this.

In conclusion, these preliminary results suggest that navitoclax is not a substrate or inhibitor of transporters present in ciPTEC-OAT1 and may not give a risk of DDI *in vivo*. Furthermore, our cell model takes up drug-LZM conjugates, which paves the way for evaluation of pharmacological properties of the Nav-Lx-LZM and other senolytic-LZM conjugates in an *in vitro* model in the future.

Acknowledgements

5

Reference

1. Kobbe, C.v., Targeting senescent cells: approaches, opportunities, challenges. Aging 2019. 11: p. 18.
2. Munoz-Espin, D. and M. Serrano, Cellular senescence: from physiology to pathology. Nat Rev Mol Cell Biol, 2014. 15(7): p. 482-96.
3. Hernandez-Segura, A., J. Nehme, and M. Demaria, Hallmarks of Cellular Senescence. Trends Cell Biol, 2018. 28(6): p. 436-453.
4. Zhu, Y., et al., The Achilles' heel of senescent cells: from transcriptome to senolytic drugs. Aging Cell, 2015. 14(4): p. 644-58.
5. Chang, J., et al., Clearance of senescent cells by ABT263 rejuvenates aged hematopoietic stem cells in mice. Nat Med, 2016. 22(1): p. 78-83.
6. Yang, Y., et al., A Human Conditionally Immortalized Proximal Tubule Epithelial Cell Line as a Novel Model for Studying Senescence and Response to Senolytics. Front Pharmacol, 2022. 13: p. 791612.
7. Wilson, W.H., et al., Navitoclax, a targeted high-affinity inhibitor of BCL-2, in lymphoid malignancies: a phase 1 dose-escalation study of safety, pharmacokinetics, pharmacodynamics, and antitumour activity. Lancet Oncol, 2010. 11(12): p. 1149-59.
8. Kaefer, A., et al., Mechanism-based pharmacokinetic/pharmacodynamic meta-analysis of navitoclax (ABT-263) induced thrombocytopenia. Cancer Chemother Pharmacol, 2014. 74(3): p. 593-602.
9. Mason, K.D., et al., Programmed Anuclear Cell Death Delimits Platelet Life Span. Cell, 2007. 128(6): p. 1173-1186.
10. Gandhi, L., et al., Phase I study of Navitoclax (ABT-263), a novel Bcl-2 family inhibitor, in patients with small-cell lung cancer and other solid tumors. J Clin Oncol, 2011. 29(7): p. 909-16.
11. Roberts, A.W., et al., Substantial susceptibility of chronic lymphocytic leukemia to BCL2 inhibition: results of a phase I study of navitoclax in patients with relapsed or refractory disease. J Clin Oncol, 2012. 30(5): p. 488-96.
12. Rudin, C.M., et al., Phase II study of single-agent navitoclax (ABT-263) and biomarker correlates in patients with relapsed small cell lung cancer. Clin Cancer Res, 2012. 18(11): p. 3163-9.
13. Joly, F., et al., A phase II study of Navitoclax (ABT-263) as single agent in women heavily pretreated for recurrent epithelial ovarian cancer: The MONAVI - GINECO study. Gynecol Oncol, 2022. 165(1): p. 30-39.
14. Nigam, S.K., et al., Handling of Drugs, Metabolites, and Uremic Toxins by Kidney Proximal Tubule Drug Transporters. Clin J Am Soc Nephrol, 2015. 10(11): p. 2039-49.
15. Nigam, S.K., What do drug transporters really do? Nat Rev Drug Discov, 2015. 14(1): p. 29-44.
16. Zou, W., et al., Drug Transporters in the Kidney: Perspectives on Species Differences, Disease Status, and Molecular Docking. Front Pharmacol, 2021. 12: p. 746208.
17. Dolman, M.E.M. Design of kidney-targeted drug-carrier conjugates for the inhibition of profibrotic signaling cascades. 2011.
18. Dolman, M.E., et al., Drug targeting to the kidney: Advances in the active targeting of therapeutics to proximal tubular cells. Adv Drug Deliv Rev, 2010. 62(14): p. 1344-57.
19. Zhou, P., X. Sun, and Z. Zhang, Kidney-targeted drug delivery systems. Acta Pharm Sin B, 2014. 4(1): p. 37-42.
20. Haas, M., et al., Drug-targeting to the kidney: renal delivery and degradation of a naproxen-lysozyme conjugate in vivo. Kidney Int, 1997. 52(6): p. 1693-9.
21. Prakash, J., et al., Renal-selective delivery and angiotensin-converting enzyme inhibition by subcutaneously administered captopril-lysozyme. Drug Metab Dispos, 2005. 33(5): p. 683-8.
22. Nielsen, R., E.I. Christensen, and H. Birn, Megalin and cubilin in proximal tubule protein reabsorption: from experimental models to human disease. Kidney Int, 2016. 89(1): p. 58-67.

23. Merkul, E., et al., First platinum(II)-based metal-organic linker technology (Lx®) for a plug-and-play development of antibody-drug conjugates (ADCs). Expert Opin Drug Deliv, 2019. 16(8): p. 783-793.
24. Jansen, J., et al., A morphological and functional comparison of proximal tubule cell lines established from human urine and kidney tissue. Exp Cell Res, 2014. 323(1): p. 87-99.
25. Nieskens, T.T., et al., A Human Renal Proximal Tubule Cell Line with Stable Organic Anion Transporter 1 and 3 Expression Predictive for Antiviral-Induced Toxicity. Aaps j, 2016. 18(2): p. 465-75.
26. Fretz, M.M., et al., Intervention in growth factor activated signaling pathways by renally targeted kinase inhibitors. J Control Release, 2008. 132(3): p. 200-7.
27. Haselberg, R., et al., Characterization of drug-lysozyme conjugates by sheathless capillary electrophoresis-time-of-flight mass spectrometry. Anal Chim Acta, 2011. 698(1-2): p. 77-83.
28. Tse, C., et al., ABT-263: a potent and orally bioavailable Bcl-2 family inhibitor. Cancer Res, 2008. 68(9): p. 3421-8.
29. Hu, M. and X. Li, Barriers to Oral Bioavailability—An Overview, in Oral Bioavailability. 2011. p. 1-5.
30. Müller, F. and M.F. Fromm, Transporter-mediated drug-drug interactions. Pharmacogenomics, 2011. 12(7): p. 1017-37.
31. Prakash, J., et al., Cell-specific Delivery of a Transforming Growth Factor-beta Type I Receptor Kinase Inhibitor to Proximal Tubular Cells for the Treatment of Renal Fibrosis. Pharmaceutical Research, 2008. 25(10): p. 2427-2439.
32. Dolman, M.E.M., et al., Imatinib-ULS-lysozyme: A proximal tubular cell-targeted conjugate of imatinib for the treatment of renal diseases. Journal of Controlled Release, 2012. 157(3): p. 461-468.
33. Shi, H., et al., Folate-dactolisib conjugates for targeting tubular cells in polycystic kidneys. J Control Release, 2019. 293: p. 113-125.
34. Sabry, S.A., et al., Brain-targeted delivery of Valsartan using solid lipid nanoparticles labeled with Rhodamine B; a promising technique for mitigating the negative effects of stroke. Drug Deliv, 2023. 30(1): p. 2179127.
35. Prakash, J., et al., Cell-specific delivery of a transforming growth factor-beta type I receptor kinase inhibitor to proximal tubular cells for the treatment of renal fibrosis. Pharm Res, 2008. 25(10): p. 2427-39.
36. Janssen, M.J., et al., Therapy with 2'-O-Me Phosphorothioate Antisense Oligonucleotides Causes Reversible Proteinuria by Inhibiting Renal Protein Reabsorption. Mol Ther Nucleic Acids, 2019. 18: p. 298-307.
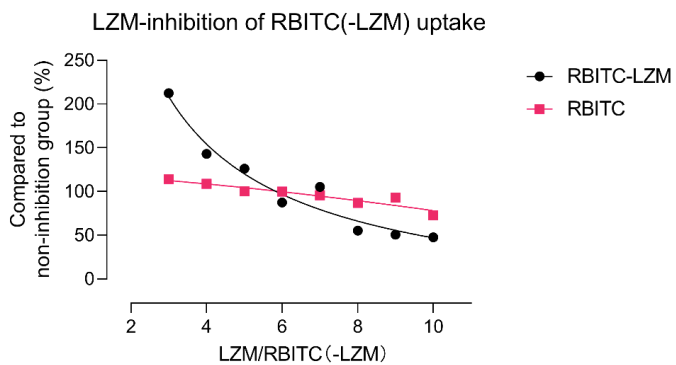
5

Supplementary Materials

Figure S1. Lysozyme (LZM)-inhibition of RBITC and RBITC-LZM uptake. RBITC-LZM uptake was inhibited by native LZM with different ratio of LZM and RBITC-LZM (3 to 10), while the uptake of RBITC was not inhibited by LZM at the same condition (37℃,1h incubation, n=1).

Chapter 6

Summary

and

general discussion

Chronic kidney disease (CKD) is a progressive condition of kidney dysfunction due to diverse causes of injury. The accumulation of protein-bound uremic toxins (PBUTs) may lead to tubular cell senescence, further accelerating CKD and kidney fibrosis. Senescence is a special state of cells characterized by permanent cell cycle arrest and limitation of proliferation, which promotes fibrosis by releasing senescence-associated secretory phenotype (SASP) factors [1]. In healthy kidneys, PBUTs are cleared from the systemic circulation by proximal tubule cells through the concerted action of plasma membrane transporters that facilitate their urinary excretion, but the endogenous metabolites are hardly removed with kidney dysfunction [2]. The accumulation of PBUTs causes oxidative stress and increases the production of inflammatory (SASP) factors that could trigger fibrosis [3]. However, the connection between senescence and PBUTs in promoting CKD and eventually resulting in kidney fibrosis is poorly understood. The main findings in this thesis demonstrated that PBUTs, especially indoxyl sulfate (IS), can be drivers of senescence, and that they could have an important role in CKD via regulating pro-inflammatory, pro-fibrotic and pro-oxidative processes in proximal tubule. These observations thus pave the way for investigating novel strategies for CKD treatment, such as kidney-targeted delivery of senolytic drugs. In this chapter, we will give an overview on how senescence contributes to CKD and the involvement of PBUTs, how kidney senescence can be modelled and studied, the ways of improving current senolytic therapies, along with future perspectives.

1. How does senescence contributes to chronic kidney disease?

Numerous previous publications have suggested that there is a link between kidney aging and reduced kidney function, and an increased number of senescent cells [4, 5]. CKD triggers various cellular and molecular responses leading to kidney fibrosis, which is characterized by an excessive accumulation of extracellular matrix (ECM) [6]. In many kidney diseases, such as membranous nephropathy, focal segmental glomerulosclerosis and IgA nephropathy, an increase in the number of senescent cells is observed [5]. This may be caused by internal factors (genetic disorders or auto-immune), but also by external stimulations, such as radiation waves and exposure to chemotherapeutic agents, which can initiate senescence development in kidney cells [7]. After acute kidney injury (AKI), acute (short-term) senescent cells that appear can be cleared by immune cells in a tightly controlled manner, followed by tissue regeneration. On the other hand, chronic (long-term) senescent cells accumulate in kidneys resulting in fibrosis, aggravating the pathology, and contributing to CKD [7-9].

Chronic (long-term) senescence is accompanied by the activation of the DNA-damage response (DDR), which is led by mitochondrial dysfunction, cell cycle arrest activation and SASP factors expression [10, 11]. As described in **Chapter 1**, senescence is initiated by diverse triggers that induce oxidative stress, stimulate an inflammatory response and release of SASP factors. These stressors then influence cell death and reinforce senescence in a paracrine manner.

Oxidative stress is an imbalance between oxidants and antioxidants, which can be observed at the early stages of CKD and increases along with kidney damage, reaching high levels at the later stages of kidney disease and in patients that rely on renal replacement therapies, such as haemodialysis [12-15]. The most predominant mediators of oxidative stress are thought to be reactive oxygen species (ROS). The increased production of ROS in CKD may result from stressors such as radiation waves and chemotherapeutic agents, and mediates DDR [16]. This further promotes ROS production via the activation of its downstream effectors [7, 11, 17], and

again in DDR [17, 18]. Through this vicious circle, DDR is a key regulator of senescence. On the one hand, DDR mediates cell cycle arrest by controlling the main senescence signalling p53/p21$^{CIP1/WAF1}$ (p21) and p16^{Ink4a} (p16)/pRb checkpoint pathways [19, 20]. And on the other hand, DDR promotes an inflammatory response, which is related to the production of SASP factors [1, 21].

The pathophysiology of kidney disease is characterized by alteration in cell number, which is often caused by an imbalance between the proliferation and the loss of parenchymal cells [22]. In healthy kidney, the immune system can clear abnormal cells through cell death thereby balancing the cell number ratio [23], while in CKD, the accumulation of dysfunctional cells that are protected from cell death disturbances this balance [22]. Resistance to cell death is a common feature of the limitation in proliferation in chronic (long-term) senescent cells. Apoptosis is a typical process of cell death, which is regulated by two main pathways. One is the intrinsic pathway, also called mitochondrial pathway, which is related to mitochondrial dysfunction and Bcl-2 family members [24]. The apoptosis threshold depends on the balance between pro- and anti-apoptotic Bcl-2 family members, which can be disrupted by mitochondrial dysfunction [24]. Mitochondrial dysfunction may result from ROS overproduction after kidney injury [25]. Senescent cells enter a primed apoptotic state due to aberrant regulation of pro- and anti-apoptotic Bcl-2 family proteins, thus disturbing the programmed cell death and keeping the cells alive [26]. The other is the extrinsic pathway, which is triggered by the activation of death receptors [27]. Death receptors interact with death ligands, activating the caspase proteins and inducing apoptosis [24], but regulate also noncytotoxic pathways such as cell proliferation and differentiation, chemokine production, inflammatory responses, and tumor-promoting activities. SASP factors are ligands of death receptors, including TNF-α [28, 29].

The binding of TNF-α to its receptor does not only trigger apoptosis, but also initiates necroptosis. Necroptosis is another form of cell death, which is controlled in an apoptosis-deficient environment by receptor interacting protein kinase-1 (RIPK1) and 3 (RIPK3). In general, the binding of TNF-α to its receptor (TNFR1) induces the formation of the receptor-bound complex I, triggers induction of proinflammatory mediators via activation of the mitogen-activated protein kinase (MAPK) and nuclear factor-kB (NF-kB) pathways and/or induces apoptosis [30, 31]. In the presence of the inhibitors of apoptosis (IAPs) or the absence of caspase-8 activity, complex I induces a necroptotic response via the necroptosis core machinery (RIPK1, RIPK3, mixed lineage kinase domain-like protein (MLKL)) [31].

The release of damage-associated molecular patterns (DAMPs) by necroptosis directly triggers inflammation and can lead to inflammatory diseases, including CKD but also metabolic disorders, neurodegenerative diseases, autoimmune diseases, and cancer [32, 33]. DAMPs include cytokines, such as the IL-1α and IL-33, which are recognized as SASP factors [30, 34, 35]. DAMPs, like the high-mobility group box 1 (HMGB1), also mediate the expression of SASP factors (IL-6, and TNF-α) and play roles in senescence in a paracrine manner [32, 36].

Taken together, the accumulation of senescent cells is a feature of CKD, and all mechanisms mentioned above are present during the disease progression. This may be a result of a previous injury, followed by a maladaptive repair response due to increase paracrine activity of senescent cells. SASP factors released by senescent cells are typically proinflammatory and profibrotic

6

mediators, including numerous cytokines, chemokines, growth factors, and matrix-metalloproteinases (MMPs) [1, 21]. These factors promote inflammation, ECM deposition through activation of fibrosis pathways (TGF-β and WNT signalling) [37, 38], thus contributing to CKD.

2. Models to study senescence: *in vivo* or *in vitro*?

The study and characterization of kidney senescence can be very challenging, particularly because there is not a single marker to be used, and combination of different features, ranging from metabolic activity and specific proliferation- and apoptosis- related mechanisms to secretion of SASP factors, should be addressed. Although CKD animal models have shown that the accumulation of PBUTs correlates to fibrosis outcome and/or acquiring a senescent phenotype (summarized in Chapter 1, Table 2), the limitations of those animal models should not be ignored. Two main methods have been used to induce kidney disease in animals: a toxicant-induced and a surgery-induced model. The first models are induced by toxicants, such as aristolochic acid, adenine, or various chemotherapeutic drugs (*e.g.,* cisplatin and doxorubicin). This kind of models can be easily conducted and are widely used, but dose of the toxicants and species or strain influence the degree of kidney dysfunction, and other organs may also be affected [39, 40], thus compromising clinical relevance inherent to kidney senescence. The surgery-induced models (e.g. 5/6 nephrectomy, ischemia-reperfusion injury and unilateral ureteral obstruction) restrict the injury to the kidney and demonstrated clinical translational relevance, but these models are technically challenging to establish; susceptibility to renal injury is also variable between different strains, and renal function can be compensated for by non-injured kidney in unilateral models [39, 40]. Although animal studies can provide mechanistic insights into CKD, kidney pathology in animals does not fully reflect human kidney disease etiology and translational value can be lost. Moreover, animal experimentation is also limited by significant ethical considerations. Thus, a perfect animal model does not exist, and one must compromise on the inclusion of some details of kidney pathology to study senescence-related effects. Before conducting an animal study, which could provide more relevant pre-clinical observations, alternative methods in vitro should be employed for probing questions [39].

Regarding the modelling of senescence in vitro, there are several ways to induce it, depending on what type and mechanisms of senescence need to be studied. For instance, there is a natural aging cell model which is used for studying replicative senescence (RS) by culturing cells to high passages. In addition, most of senescent cell models are induced by external stimulations including ionizing radiation, exposure to chemotherapeutic agents and incubation with SASP factors, which are suitable for studying stress-induced senescence (SIS) (Table 1).

Primary proximal tubule epithelial cells reflect well the functions of cells *in vivo* and are an ideal *in vitro* model to study kidney senescence (as summarized in Table 1), but have a limited capacity for extension and eventually lose their characteristics [41], including the clearance of PBUTs. PBUTs are selectively removed by proximal tubule epithelial cells via transporter proteins in kidney [2]. Organic anion transporters 1 and 3 (OAT1/3) transport anionic uremic toxins, such as indoxyl sulfate (IS), into the cell; while the efflux pumps breast cancer resistance protein (BCRP) and the multidrug resistance-associated proteins 2 and 4 (MRP2/4) are responsible for their excretion into the tubular lumen for final removal [42] (major transporter

proteins are reviewed in **Chapter 5**). Therefore, a valid cell line for studying PBUTs should be proximal tubule epithelial cells that are equipped with all major transporter proteins, including OAT1/3, BCRP and MRP2/4, in which proximal tubular injury can be studied efficiently [43]. Notably, primary proximal tubule epithelial cells lose rapidly the expression of OAT1 when cultured *in vitro*. Immortalized cells and cancer-derived cell lines overcome the drawback of primary culture, but may change their functions and characteristics, and influence senescence-related signalling events [41, 44]. Two immortalized proximal tubule epithelial cell lines, HK-2 and RPTEC/TERT1, which isolated from human kidney, are generally applied in kidney senescence studies (Table 1). However, both cell lines are not suitable for studying senescence induced by PBUTs, because they lack transporters expression or function, particularly OAT1 [45, 46]. In this thesis, we employed ciPTEC-OAT1 as in vitro cell model for studying senescence related PBUTs, as it shows a stable expression and function of transporters OAT1, OCT2, P-gp, BCRP and MRP4 [47, 48], which meets the requirements of cell models for studying the effects of PBUTs.

Table 1. *In vitro* cell models employed to study kidney senescence.

Cell lines	Species	Type	Study aim	Senescence induction	Reference
NRK-52E (proximal tubular epithelial cell line)	Rat	Immortalized	Senolytics therapy	AngII-treated	[49]
Primary glomerular endothelial cells (GEnC)	Human	Primary	Disease mechanisms	Natural aging	[50]
Immortalized podocytes	Human	Immortalized	Disease mechanisms	Recombinant human PAI-1,supernatants from natural aging cells	[50]
HK-2 (proximal tubular epithelial cells)	Human	Immortalized	Disease mechanisms	Recombinant Wnt9a treated	[37]
NRK-49F (kidney interstitial fibroblast cell lines)	Rat	Immortalized	Disease mechanisms	Recombinant Wnt9a treated	[37]
Primary cultured renal tubular cells	Mouse	Primary	Disease mechanisms	Recombinant Wnt9a treated	[37]
Baby Mouse Kidney (BMK) cells	Mouse	Immortalized	Senolytics therapy	Ionizing radiation, and chemotherapy (doxorubicin) treated	[51]
Human Embryonic Kidney (HEK) 293LTV	Human	Immortalized	Senolytics therapy	Ionizing radiation, and chemotherapy (doxorubicin) treated	[51]
Immortalized mouse renal proximal tubule cell line (BUMPT)	Mouse	Immortalized	Disease mechanisms/seno lytics therapy	Chemotherapy (cisplatin) treated	[52]
NRK-49F (Rat renal fibroblast cell line)	Rat	Immortalized	Disease mechanisms/seno lytics therapy	Supernatants from chemotherapy (cisplatin) treated cells	[52]
RAW264.7 (mouse macrophage line)	Mouse	Immortalized	Senolytics therapy	Lipopolysaccharide (LPS) or IL-4 treated	[53]
Primary proximal tubular epithelial cells	Mouse	Primary	Disease mechanisms	Hypoxia/reoxygenation-induced oxidative stress	[54]
RPTEC/TERT1 (renal proximal tubule epithelial cells)	Human	Immortalized	Disease mechanisms	Cadmium chloride-induced and hypoxia-induced oxidative stress	[55]

6

To study the link between senescence and uremic toxins in the first instance, a suitable *in vitro* cell model with proven ability to study the interactions and effects of uremic toxins should be employed. To this aim, we opted for ciPTEC-OAT1 cell line. Uremic toxins (including IS) induce proximal tubular injury via OAT1-mediated uptake [43]. When cultured *in vitro*, the expression of OAT1 in primary proximal tubule epithelial cells is rapidly lost, while CiPTEC-OAT1 show a stable OAT1 expression and function through lentiviral transduction [48]. The cell line ciPTEC was created to maintain the characteristics of primary proximal tubule epithelial cells (PTEC) by means of a temperature sensitive mutant U19tsA58 of SV40 large T antigen (SV40T) and the essential catalytic subunit of human telomerase (hTERT) [56]. The hTERT prevents replicative senescence by maintaining telomere length [57]. Temperature-sensitive SV40T allows cells to proliferate at the permissive low temperature of 33°C, but provides a proliferation block at a non-permissive temperature of 37°C by activating pRb and p53 [58, 59]. We further confirmed this block, resulting in senescence-growth arrest in the epithelial cells in **Chapter 2**.

Previous results suggested that culturing ciPTEC-OAT1 at 37°C results in less cells in the S-phase (proliferation) and more cells arrested in G0/G1phases of the cell cycle, indicating a halted proliferation at non-permissive temperature [60]. In **Chapter 2**, we further demonstrate that ciPTEC-OAT1 acquire a conditional senescent phenotype when cells are cultured at a non-permissive temperature (37°C). The transcriptome analysis (**Chapter 4**) further aided in exploring the underlying mechanisms of the pathways involved in this senescence process, including the FOXO, mTOR, p53 and calcium signalling pathways. The cells develop a senescence phenotype in a time dependent manner at 37°C, including a cell cycle arrest, resistance to apoptosis and SASP factors production. Senolytics are known to eliminate senescent cells selectively by inducing cell death through different cell death pathways, such as intrinsic and extrinsic apoptosis pathways. The dose-dependent response to senolytics, as demonstrated in **Chapter 2**, confirmed further that ciPTEC-OAT1 had become senescent at 37°C. Therefore, ciPTEC-OAT1 may represent a valid model for studying kidney senescence *in vitro* by simply adjusting culture conditions.

However, the ciPTEC-OAT1 model also has some limitations. As described in **Chapter 2**, senescence of ciPTEC-OAT1 may be more related to the p53/p21 pathway, instead of p16/pRb pathway solely, limiting the application. Meanwhile, it is important to note that adjusting culture conditions of ciPTEC-OAT1 can influence senescence phenotype. Namely, the culturing at 37°C only accelerates the process, but senescence develops time-dependently, after prolonged-culturing, in both conditions (33°C and 37°C; **Chapter 2**). Therefore, ciPTEC-OAT1 can be used as an efficient tool to study senescence, but particular attention should be paid at using proper control conditions. Therefore, this cell model suffices for molecular characterization, studying signalling events underlying uremic toxins and kidney senescence, and for initial screening of pharmacological strategies, but ideally should be combined with other relevant models, as discussed earlier.

The fact that various aspects of kidney senescence are better reproduced and studied in different models, and that the use of a single model, either *in vivo* or *in vitro*, is not attainable, complementary approaches should be undertaken depending on the cause of senescence being assessed. Ideally, the findings of *in vitro* and *in vivo* studies should be also linked to clinical observations to increase even more translational value and human-relevance.

3. Are PBUTs drivers of kidney senescence?

The accumulated PBUTs in end-stage kidney disease (ESKD) cannot efficiently be removed by standard haemodialysis techniques. The progressive accumulation propagates the PBUTs' negative effects in the kidney and in other tissues, contributing to the comorbidities associated with the uremic syndrome, such as cardiovascular disease, metabolic bone disease and inflammation, including the aspects explored in this thesis (**Chapter 3 and 4**) related to inflammatory responses and senescence development. PBUTs accumulation promotes kidney disease and fibrosis by oxidative stress and inflammation [3] and might, therefore, be a trigger that initiates senescence development. Since many CKD studies have shown a correlation between the accumulation of PBUTs and fibrosis or senescence phenotype (summarized in **Chapter 1**, Table 2), we hypothesize that PBUTs may promote kidney fibrosis by accelerating senescence, possibly via mitochondrial dysfunction, cell cycle arrest, and the production of SASP factors.

Mitochondrial dysfunction is induced by increased ROS during cell stress after kidney injury [25], which is observed in senescent cells [61]. In **Chapter 3**, we demonstrated that IS and a PBUTs cocktail promote ROS production and induce oxidative stress, which indicates mitochondrial dysfunction. Furthermore, the results suggested that IS accelerates or maintains the expression of p21 at a high level, indicating a cell cycle arrest; the loss of the proliferation marker of Lamin B1 described in **Chapter 4** also suggests growth arrest, which is in line with senescence characteristics.

PBUTs also induce the production of SASP factors. The exposure of PBUTs activate the inflammasome NLRP3, thereby inducing the expression and release of IL-1β, a SASP factor, both *in vitro* and *in vivo* (**Chapter 3**), similarly to what has been reported previously [62, 63]. Other SASP factors including IL-6, IL-8, IL-1α, MMP-1 and MMP3 were also increased following IS exposure *in vitro* (**Chapter 4**).

Together, the findings indicate that PBUTs could induce SASP factors release, and trigger oxidative stress possibly causing mitochondrial dysfunction, thus driving kidney senescence. Moreover, **Chapter 4** demonstrated that cellular tolerance against IS increased over time, which suggests that PBUTs may promote senescence in CKD time-dependently. The results in **Chapter 4** also suggest that IS accelerates senescence via TNF-α and NF-κB signalling early on, and the EMT process at later time points. These findings argue that PBUTs may promote senescence by different mechanisms/pathways during CKD and that senescence may play different roles in various stages of CKD.

4. Senolytics: potential treatment of kidney diseases?

Targeting senescent cells is a potential treatment of CKD, aiming at slowing down disease progression. Targeted strategies are mainly focused on elevating senescent features, such as promoting cell death, interrupting the pathology of SASP factors. Treatment with senolytics is one of the strategies that could selectively eliminate senescent cells through anti-apoptotic pathways to promote cell death. Therapeutic targets include tyrosine kinase receptors (TKRs), phosphatidylinositide 3-kinases (PI3K), AKT, 90-kDa heat shock protein (HSP90), Bcl-2 family members, caspases and p53 [51, 64-66]. These senolytics are divided into different

6

classes by their targets and mechanism, mainly including Bcl-2 family inhibitors, HSP90 inhibitors, p53 pathway targeting compounds, natural products and their analogues and cardiac glycosides (Table 2). Bcl-2 family inhibitors, such as ABT-737, navitoclax, venetoclax, A1331852 and A1155463, target Bcl-2 family members to adjust the balance between pro- and anti-apoptotic Bcl-2 family members, thus leading to intrinsic apoptosis [65, 67-69]. HSP90 regulates the maturation, activity and stability of a wide range of substrate proteins, impacting cellular functions in normal physiology, pathological conditions, and evolutionary processes [70]. HSP90 inhibitors, such as 17-DMAG (alvespimycin), geldanamycin, and 17-AAG (tanespimycin), are identified as senolytics, which can disturb the HSP90-AKT interaction of the PI3K/AKT pathway, thus resulting in apoptosis of dysfunctional cells [66]. p53 pathway targeting compounds mainly inhibit the activation of p53. Peptides, such as FOXO4-DRI and ES2, have been designed to interrupt the interaction between FOXO4 and p53, hence inducing cell-intrinsic apoptosis [51, 71]. Cardiac glycosides, such as ouabain, bufalin, cinobufagin, peruvocide, digitoxin, and convallatoxin, kill senescent cells by apoptosis through targeting the Na^+/K^+-ATPase pump [72]. Some natural products like flavone, fisetin and quercetin are also recognized as senolytics, because they have a wide range of targets in signalling pathways, in addition to promoting apoptosis [69, 73]. Currently, more and more senolytics are reported as potential treatment for kidney diseases (Table 3). However, it is worth noting that the use of senolytics is halted due to severe side effects they cause when targeting anti-apoptotic pathways. For example, the cardiac glycosides compounds, bufalin and digoxin showed a prominent cardiotoxicity [74, 75]. Classical Bcl-2 family inhibitors, such as navitoclax, can induce thrombocytopenia and T-cell lymphopenia, as observed in different clinical trials [76, 77]. This is due to the fact that navitoclax binds to pro-survival Bcl-xl that is normally responsible for maintaining platelet survival [78]. Therefore, it is necessary to develop novel senolytic therapeutic approaches related to navitoclax to prevent these shortcomings.
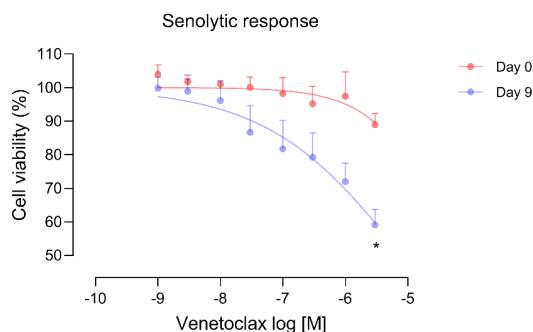
Figure 1. Senolytic effect of venetoclax in ciPTEC-OAT1. Cell viability of ciPTEC-OAT1 cultured for 0 or 9 days at non-permissive temperature of 37 °C and exposed to 100 μL medium with increasing concentrations of venetoclax. IC_{50} values for venetoclax at Day 0 and Day 9 are 5.86 μM and 3.26 μM. Three independent experiments were performed in triple. Data are presented as mean ± SEM, for which results were normalized to unexposed cells. *$P<0.05$, cell viability at Day 9 compared to Day 0 at the same concentration; Multiple t‑test, Holm-Sidak multiple comparison test. Day 0 is considered as the non-senescence group (control).

Recent research focused on modifying the senolytic structure, using drug combinations, proteolysis targeting chimera (PROTAC) or designing prodrugs to overcome the side effects of

navitoclax. Venetoclax is a derivative of navitoclax, a Bcl-2-only inhibitor [68]. Although we could demonstrate its senolytic effect in our cell model (Figure 1), the compound is far less potent compared to navitoclax (IC_{50} venetoclax 3.26 μM vs 0.4 μM for navitoclax; Figure 1 and **Chapter 2**). This might be because survival of senescent cells not only depends on Bcl-2 protein signalling but also on Bcl-xl protein signalling. Combining two senolytics might lead to dose reductions, thereby decreasing the side effects. For example, the combination of piperlongumine and navitoclax [79] and the combination of JQ1 and navitoclax [80] have been reported, both of which were more effective in killing senescent cells than either drug alone, thus improving the efficacy and decreasing the toxicity induced by a single dosage of navitoclax. Another strategy to reduce the side effects of navitoclax is by converting the drug into Bcl-xl based PROTAC (*e.g.,* DT2216). PROTAC is a small-molecule containing a ligand, could recognize the target protein linked to an E3 ligase ligand. DT2216 can target Bcl-xl to the Von Hippel-Lindau (VHL) E3 ligase for degradation, thus reducing the toxicity to platelets, as VHL is poorly expressed in platelets [81]. However, although DT2216 reduce the platelet toxicity of navitoclax, it does not show an effect on the level of Bcl-2 and Bcl-w [81]. Applying a prodrug may be a more effective strategy to decrease the side effects. For example, a galacto-conjugation of navitoclax (Nav-Gal) also reduced platelet toxicity compared to naked navitoclax [82]. Senescent cells show high levels of senescence-associated lysosomal β-galactosidase (SA-β-gal), when the hydrolysis of the cleavable galactose increased, navitoclax will be released from the Nav-Gal in lysosomal, thus off-targeting the platelet [82]. In **Chapter 5**, Navitoclax-Lx-lysozyme (Nav-Lx-LZM), another prodrug of navitoclax, was suggested. Conjugating navitoclax to a kidney-specific carrier molecule lysozyme could change the cellular distribution of navitoclax and its adverse effects, because the major side effects of navitoclax do not affect the kidney. Nav-Lx-LZM aims to be specifically taken up by proximal tubule epithelial cells in kidney via the low-density lipoprotein receptor-related protein 2, megalin, mediated endocytosis, thus targeting kidney senescent cells, improving the efficacy and reducing side effects of navitoclax.

6

Table 2. Senolytics reported according to class.

Class	Senolytic Agents	Mechanism	In vitro/vivo models	Reference
Bcl-2 family inhibitors	ABT-737, navitoclax, venetoclax, A1331852, A1155463	Promote intrinsic apoptosis	Irradiated cells and mice, xenograft mice	[65, 67-69]
HSP90 inhibitors	17-DMAG (Alvespimycin), Geldanamycin, 17 -AAG (Tanespimycin)	Disrupte the HSP90-AKT interaction	Primary mouse embryonic fibroblasts from DNA repair-deficient mice	[66]
p53 pathway targeting compounds	FOXO4-DRI, ES2	Disrupte p53-FOXO4 interaction	Chemotherapy (doxorubicin or palbociclib or dabrafenib) induced senescent cells, melanoma mice and aged mice	[51, 71]
Cardiac glycosides	Ouabain, bufalin, cinobufagin, peruvocide, digitoxin, and convallatoxin	Disbalance electrochemical gradient	Chemotherapy (bleomycin or etoposide or palbociclib) induced senescent cells, chemotherapy (gemcitabine) treated mice	[72]
Natural products	flavone, fisetin, quercetin	Promote intrinsic apoptosis	Irradiated cells	[69, 73]

Table 3. Senolytics employed in kidney disease studies.

Drug	Study aim	In vitro model	In vivo model	Reference
FOXO4-DRI	Fitness, fur density and kidney function	Ionizing radiation, and chemotherapy (doxorubicin) treated cells	Fast aging mice, chemotherapy (doxorubicin)-treated mice naturally aged mice.	[51]
Quercetin	Obesity and kidney function	NR	High-fat diet mice	[83]
Quercetin+Dasatinib	Renal artery stenosis, fibrosis	NR	Ischemia reperfusion injury mice	[84, 85]
Navitoclax (ABT-263)	Renal regeneration	Ionizing radiation treated cells	Ischemia reperfusion injury mice, irradiated mice,	[86]
Dexmedetomidine	Renal injury and fibrosis	NR	Ischemia reperfusion injury mice	[87]
17-DMAG	Diabetic nephropathy	NR	High-fat diet mice	[88]
Fisetin	Acute kidney injury (AKI)	NR	Lipopolysaccharide (LPS)-induced septic AKI mice	[89]
Bufalin	Renal carcinoma	Renal cell carcinoma	NR	[90]
Bufalin	AKI	Gentamicin (nephrotoxicity drug) treated rat kidney tubular epithelial cell	Gentamicin (nephrotoxicity drug) - induced AKI rats	[91]

NR: not reported.

5. Conclusion and future perspectives

This thesis demonstrated the effects related to senescence of PBUTs *in vitro* by using ciPTEC-OAT1, which gives a new angle to the role that PBUTs play in CKD. In addition to showing that ciPTEC-OAT1 is a valid *in vitro* tool to study kidney senescence (**Chapter 2**), the main findings revealed that PBUTs, and especially IS, are drivers of kidney senescence, and that they do so by inducing oxidative stress, promoting inflammatory response, and via increased resistance to cell death (**Chapter 3 and 4**). Also, in **Chapter 5** we provide insight into possible approaches for kidney-targeted senolytic therapy (Nav-Lx-LZM conjugates) for more efficient clearance of senescent cells and the reduction of systemic side effects.

Although this thesis provides clues of how PBUTs can accelerate senescence in CKD, the process is still not completely uncovered. As described earlier, senescence is characterized by permanent cell cycle arrest and resistance of cell death. The expression of SASP factors (*e.g.,* IL-6 and IL-1β) and common senescence markers (*e.g.,* p21 and Laminb1) are typical features of senescence. For instance, current studies demonstrate that PBUTs influence the development of senescence phenotype, while the effect of PBUTs on the major mechanisms of senescence, cell cycle arrest and resistance of cell death, needs to be further elucidated. Although the resistance to cell death by IS was observed and the changes in expression of genes related to cell cycle was shown in the transcriptome analysis (**Chapter 4**), the underlying mechanisms of PBUTs accelerating senescence through these processes requires further investigation.

In addition, the findings of this thesis should be corroborated in a relevant *in vivo* model, such as an ischemia-reperfusion injury model. This would allow not only to confirm some of the findings in a more pathophysiological relevant manner and to correlate various senescence features to PBUTs levels, but also to test the pharmacological potential of novel kidney-targeted senolytics strategies.

Such an approach was proposed in **Chapter 5**, in which we hypothesize that a prodrug of navitoclax could improve its uptake in the kidneys, thus escaping the side effects. Ideally, instead of passive diffusion, the prodrug Nav-Lx-LZM would be specifically taken up by PTEC in kidney via endocytosis, which can be mediated by the receptor megalin. The ciPTEC-OAT1 cell line expressing both megalin and various solute transporters [47, 48], is a potential model for analysing the biological features of senolytic-LZM conjugates. The current studies employed rhodamine B isothiocyanate-lysozyme (RBITC-LZM) as model to trace the uptake mechanisms in ciPTEC-OAT1, but ignored the linker Lx which may influence the uptake process. Therefore, further studies should also employ the compound RBITC-Lx-LZM as a tracer to evaluate the uptake mechanisms of ciPTEC-OAT1. In addition, the research in **Chapter 5** used naked LZM to inhibit megalin, however, the receptor has several binding sites and may not be completely inhibited by LZM [92]. So, potent inhibitors such as receptor-associated protein (RAP) that could bind more sites of megalin [92] may be more effective than LZM, and should be studied to improve the robustness of the assay. Moreover, receptor knock-down approaches (*e.g.,* via siRNA or CRSIPR-Cas9) could also be considered to measure the specific uptake of LZM conjugates, further validating the ciPTEC-OAT1 model.

Future senescence studies could be focused on uncovering key mechanisms, identifying relevant biomarkers and finding novel strategies of CKD treatment. Current biomarkers,

6

including SASP factors, are reported to be relevant to senescence, but cannot robustly identify senescent cells alone [93]. For example, the lysosomal senescence-associated beta-galactosidase (SA-β-gal) activity is commonly used as phenotypical senescence marker. However, SA-β-gal activity may be an outcome rather than a cause of senescence [94, 95], and should be combined with other markers. Having clear and early biomarkers of kidney senescence could give more insight into the effectiveness of novel therapies and how to improve them (*i.e.,* timing, dosing). In this thesis, a targeted delivery system is proposed to reduce the side effects of senolytics. In addition to conjugating to macromolecular carrier (*e.g.,* LZM), other types of drug carriers could be employed as alternatives including liposomes and polymeric nanoparticles, silica carriers, gold nanoparticles or nanoshells, and carbon-based nanostructures [96]. These carriers could be targeted to the kidneys by modulating their size and/or charge [96], thereby influencing the distribution of senolytics. As SASP factors are typically profibrotic and proinflammatory mediators, one strategy of CKD could be inhibiting the related signalling, thus suppressing SASP expression, Potential novel agents already exist for inhibiting CKD progression, including anti-fibrotic agents (*e.g.,* TGF-β inhibitor; pirfenidone) and anti- inflammatory agents (*e.g.,* Anti-TNF-α monoclonal antibody; infliximab) [97]. Moreover, the NF-κB inhibitor resveratrol and mTOR inhibitor rapamycin are also recognised as SASP inhibitors (called senomorphics), reducing the development of cellular senescence [98, 99], which could represent an option for CKD treatment as well [100]. In addition, strategies to inhibit senescence phenotypes by promoting cell cycle process and cell death signaling, such as the inhibitor of p21 and promoter of caspase proteins, could be potential CKD treatments. Considering that chronic senescent cells cannot be cleared by the immune cells, strengthening the immune system by increasing the binding affinity of the involved membrane receptors is another approach. This could thus help clearing more efficiently senescent cells by immune system [8]. Advanced cell therapy, such as chimeric antigen receptor (CAR) T cell, may be employed to specifically target senescent cells by recognizing appropriate antigens [8, 101]. Finally, identifying and targeting most relevant and specific senescence-associated markers by means of gene therapy could represent another valid approach to be investigated in the future for combatting kidney senescence [102].

Reference

1. Hernandez-Segura, A., J. Nehme, and M. Demaria, Hallmarks of Cellular Senescence. Trends Cell Biol, 2018. 28(6): p. 436-453.

2. Smith, H.W., The kidney: structure and function in health and disease. 1951: Oxford University Press, USA.

3. Chao, C.T. and C.K. Chiang, Uremic toxins, oxidative stress, and renal fibrosis: an interwined complex. J Ren Nutr, 2015. 25(2): p. 155-9.

4. Sturmlechner, I., et al., Cellular senescence in renal ageing and disease. Nat Rev Nephrol, 2017. 13(2): p. 77-89.

5. Docherty, M.H., et al., Cellular Senescence in the Kidney. J Am Soc Nephrol, 2019. 30(5): p. 726-736.

6. Rockey, D.C., P.D. Bell, and J.A. Hill, Fibrosis--a common pathway to organ injury and failure. N Engl J Med, 2015. 372(12): p. 1138-49.

7. Suzuki, M. and D.A. Boothman, Stress-induced premature senescence (SIPS)--influence of SIPS on radiotherapy. J Radiat Res, 2008. 49(2): p. 105-12.

8. Kobbe, C.v., Targeting senescent cells: approaches, opportunities, challenges. Aging 2019. 11: p. 18.

9. Munoz-Espin, D. and M. Serrano, Cellular senescence: from physiology to pathology. Nat Rev Mol Cell Biol, 2014. 15(7): p. 482-96.

10. Huang, W., et al., Cellular senescence: the good, the bad and the unknown. Nat Rev Nephrol, 2022.

11. Jackson, S.P. and J. Bartek, The DNA-damage response in human biology and disease. Nature, 2009. 461(7267): p. 1071-8.

12. Annuk, M., et al., Oxidative stress markers in pre-uremic patients. Clin Nephrol, 2001. 56(4): p. 308-14.

13. Rossi, M., et al., Protein-bound uremic toxins, inflammation and oxidative stress: a cross-sectional study in stage 3-4 chronic kidney disease. Arch Med Res, 2014. 45(4): p. 309-17.

14. Liakopoulos, V., et al., Oxidative Stress in Hemodialysis Patients: A Review of the Literature. Oxid Med Cell Longev, 2017. 2017: p. 3081856.

15. Dursun, E., et al., Effect of hemodialysis on the oxidative stress and antioxidants. Clin Chem Lab Med, 2002. 40(10): p. 1009-13.

16. Daenen, K., et al., Oxidative stress in chronic kidney disease. Pediatr Nephrol, 2019. 34(6): p. 975-991.

17. Srinivas, U.S., et al., ROS and the DNA damage response in cancer. Redox Biol, 2019. 25: p. 101084.

18. Passos, J.F., et al., Feedback between p21 and reactive oxygen production is necessary for cell senescence. Molecular Systems Biology, 2010. 6(1): p. 347.

19. Kumari, R. and P. Jat, Mechanisms of Cellular Senescence: Cell Cycle Arrest and Senescence Associated Secretory Phenotype. Front Cell Dev Biol, 2021. 9: p. 645593.

20. Mijit, M., et al., Role of p53 in the Regulation of Cellular Senescence. Biomolecules, 2020. 10(3).

21. Birch, J. and J. Gil, Senescence and the SASP: many therapeutic avenues. Genes Dev, 2020. 34(23-24): p. 1565-1576.

22. Sanz, A.B., et al., Regulated cell death pathways in kidney disease. Nat Rev Nephrol, 2023. 19(5): p. 281-299.

23. Kurts, C., et al., The immune system and kidney disease: basic concepts and clinical implications. Nat Rev Immunol, 2013. 13(10): p. 738-53.

24. D'Arcy, M.S., Cell death: a review of the major forms of apoptosis, necrosis and autophagy. Cell Biol Int, 2019. 43(6): p. 582-592.

25. Zhao, M., et al., Mitochondrial ROS promote mitochondrial dysfunction and inflammation in ischemic acute kidney injury by disrupting TFAM-mediated mtDNA maintenance. Theranostics, 2021. 11(4): p. 1845-1863.

26. Fan, Y., et al., Senescent Cell Depletion Through Targeting BCL-Family Proteins and Mitochondria. Front Physiol, 2020. 11: p. 593630.

6

27. Carneiro, B.A. and W.S. El-Deiry, Targeting apoptosis in cancer therapy. Nat Rev Clin Oncol, 2020. 17(7): p. 395-417.

28. Guo, Q., et al., Tumor Necrosis Factor-alpha (TNF-α) Enhances miR-155-Mediated Endothelial Senescence by Targeting Sirtuin1 (SIRT1). Med Sci Monit, 2019. 25: p. 8820-8835.

29. Li, P., et al., The inflammatory cytokine TNF-α promotes the premature senescence of rat nucleus pulposus cells via the PI3K/Akt signaling pathway. Scientific Reports, 2017. 7(1): p. 42938.

30. Pasparakis, M. and P. Vandenabeele, Necroptosis and its role in inflammation. Nature, 2015. 517(7534): p. 311-20.

31. Moreno-Gonzalez, G., P. Vandenabeele, and D.V. Krysko, Necroptosis: A Novel Cell Death Modality and Its Potential Relevance for Critical Care Medicine. Am J Respir Crit Care Med, 2016. 194(4): p. 415-28.

32. Roh, J.S. and D.H. Sohn, Damage-Associated Molecular Patterns in Inflammatory Diseases. Immune Netw, 2018. 18(4): p. e27.

33. Gong, T., et al., DAMP-sensing receptors in sterile inflammation and inflammatory diseases. Nature Reviews Immunology, 2020. 20(2): p. 95-112.

34. Yamagishi, R., et al., Gasdermin D-mediated release of IL-33 from senescent hepatic stellate cells promotes obesity-associated hepatocellular carcinoma. Sci Immunol, 2022. 7(72): p. eabl7209.

35. Orjalo, A.V., et al., Cell surface-bound IL-1alpha is an upstream regulator of the senescence-associated IL-6/IL-8 cytokine network. Proc Natl Acad Sci U S A, 2009. 106(40): p. 17031-6.

36. Gaikwad, S., et al., Tau oligomer induced HMGB1 release contributes to cellular senescence and neuropathology linked to Alzheimer's disease and frontotemporal dementia. Cell Rep, 2021. 36(3): p. 109419.

37. Luo, C., et al., Wnt9a Promotes Renal Fibrosis by Accelerating Cellular Senescence in Tubular Epithelial Cells. J Am Soc Nephrol, 2018. 29(4): p. 1238-1256.

38. Tominaga, K. and H.I. Suzuki, TGF-β Signaling in Cellular Senescence and Aging-Related Pathology. Int J Mol Sci, 2019. 20(20).

39. Hosszu, A., et al., Animal Models of Renal Pathophysiology and Disease. Methods Mol Biol, 2021. 2216: p. 27-44.

40. Bao, Y.W., et al., Kidney disease models: tools to identify mechanisms and potential therapeutic targets. Zool Res, 2018. 39(2): p. 72-86.

41. Faria, J., et al., Kidney-based in vitro models for drug-induced toxicity testing. Arch Toxicol, 2019. 93(12): p. 3397-3418.

42. Masereeuw, R., The Dual Roles of Protein-Bound Solutes as Toxins and Signaling Molecules in Uremia. Toxins (Basel), 2022. 14(6).

43. Motojima, M., et al., Uraemic toxins induce proximal tubular injury via organic anion transporter 1-mediated uptake. British Journal of Pharmacology, 2002. 135(2): p. 555-563.

44. Bajaj, P., et al., Emerging Kidney Models to Investigate Metabolism, Transport, and Toxicity of Drugs and Xenobiotics. Drug Metab Dispos, 2018. 46(11): p. 1692-1702.

45. Jenkinson, S.E., et al., The limitations of renal epithelial cell line HK-2 as a model of drug transporter expression and function in the proximal tubule. Pflugers Arch, 2012. 464(6): p. 601-11.

46. Secker, P.F., et al., Functional transepithelial transport measurements to detect nephrotoxicity in vitro using the RPTEC/TERT1 cell line. Archives of Toxicology, 2019. 93(7): p. 1965-1978.

47. Jansen, J., et al., A morphological and functional comparison of proximal tubule cell lines established from human urine and kidney tissue. Exp Cell Res, 2014. 323(1): p. 87-99.

48. Nieskens, T.T., et al., A Human Renal Proximal Tubule Cell Line with Stable Organic Anion Transporter 1 and 3 Expression Predictive for Antiviral-Induced Toxicity. Aaps j, 2016. 18(2): p. 465-75.

49. Liu, T., et al., Quercetin alleviates kidney fibrosis by reducing renal tubular epithelial cell senescence through the SIRT1/PINK1/mitophagy axis. Life Sci, 2020. 257: p. 118116.

50. Cohen, C., et al., Glomerular endothelial cell senescence drives age-related kidney disease through PAI-1. EMBO Mol Med, 2021. 13(11): p. e14146.

51. Baar, M.P., et al., Targeted Apoptosis of Senescent Cells Restores Tissue Homeostasis in Response to Chemotoxicity and Aging. Cell, 2017. 169(1): p. 132-147 e16.

52. Li, S., et al., Tubular cell senescence promotes maladaptive kidney repair and chronic kidney disease after cisplatin nephrotoxicity. JCI Insight, 2023. 8(8).

53. Lu, H., et al., Quercetin ameliorates kidney injury and fibrosis by modulating M1/M2 macrophage polarization. Biochem Pharmacol, 2018. 154: p. 203-212.

54. Tammaro, A., et al., TREM1/3 Deficiency Impairs Tissue Repair After Acute Kidney Injury and Mitochondrial Metabolic Flexibility in Tubular Epithelial Cells. Front Immunol, 2019. 10: p. 1469.

55. Leierer, J., et al., Metallothioneins and renal ageing. Nephrol Dial Transplant, 2016. 31(9): p. 1444-52.

56. Wilmer, M.J., et al., Novel conditionally immortalized human proximal tubule cell line expressing functional influx and efflux transporters. Cell Tissue Res, 2010. 339(2): p. 449-57.

57. Bodnar, A.G., et al., Extension of life-span by introduction of telomerase into normal human cells. Science, 1998. 279(5349): p. 349-52.

58. Larsson, O., et al., Kinetics of senescence-associated changes of gene expression in an epithelial, temperature-sensitive SV40 large T antigen model. Cancer Res, 2004. 64(2): p. 482-9.

59. Brookes, S., et al., Evidence for a CDK4-dependent checkpoint in a conditional model of cellular senescence. Cell Cycle, 2015. 14(8): p. 1164-73.

60. Mihajlovic, M., et al., Safety evaluation of conditionally immortalized cells for renal replacement therapy. Oncotarget, 2019. 10(51).

61. Korolchuk, V.I., et al., Mitochondria in Cell Senescence: Is Mitophagy the Weakest Link? EBioMedicine, 2017. 21: p. 7-13.

62. Acosta, J.C., et al., A complex secretory program orchestrated by the inflammasome controls paracrine senescence. Nat Cell Biol, 2013. 15(8): p. 978-90.

63. Feng, H., et al., Resveratrol Inhibits Ischemia-Induced Myocardial Senescence Signals and NLRP3 Inflammasome Activation. Oxid Med Cell Longev, 2020. 2020: p. 2647807.

64. Zhu, Y., et al., The Achilles' heel of senescent cells: from transcriptome to senolytic drugs. Aging Cell, 2015. 14(4): p. 644-58.

65. Chang, J., et al., Clearance of senescent cells by ABT263 rejuvenates aged hematopoietic stem cells in mice. Nat Med, 2016. 22(1): p. 78-83.

66. Fuhrmann-Stroissnigg, H., et al., Identification of HSP90 inhibitors as a novel class of senolytics. Nat Commun, 2017. 8(1): p. 422.

67. Yosef, R., et al., Directed elimination of senescent cells by inhibition of BCL-W and BCL-XL. Nat Commun, 2016. 7: p. 11190.

68. Souers, A.J., et al., ABT-199, a potent and selective BCL-2 inhibitor, achieves antitumor activity while sparing platelets. Nat Med, 2013. 19(2): p. 202-8.

69. Zhu, Y., et al., New agents that target senescent cells: the flavone, fisetin, and the BCL-X(L) inhibitors, A1331852 and A1155463. Aging (Albany NY), 2017. 9(3): p. 955-963.

70. Taipale, M., D.F. Jarosz, and S. Lindquist, HSP90 at the hub of protein homeostasis: emerging mechanistic insights. Nature Reviews Molecular Cell Biology, 2010. 11(7): p. 515-528.

71. Le, H.H., et al., Molecular modelling of the FOXO4-TP53 interaction to design senolytic peptides for the elimination of senescent cancer cells. EBioMedicine, 2021. 73: p. 103646.

72. Triana-Martinez, F., et al., Identification and characterization of Cardiac Glycosides as senolytic compounds. Nat Commun, 2019. 10(1): p. 4731.

73. Özsoy Gökbilen, S., E. Becer, and H.S. Vatansever, Senescence-mediated anticancer effects of quercetin. Nutr Res, 2022. 104: p. 82-90.

74. Bick, R.J., et al., Effects of Chan Su, a traditional Chinese medicine, on the calcium transients of isolated cardiomyocytes: cardiotoxicity due to more than Na, K-ATPase blocking. Life Sci, 2002. 72(6): p. 699-709.

6

75. Patocka, J., et al., Digoxin: Pharmacology and toxicology-A review. Environ Toxicol Pharmacol, 2020. 79: p. 103400.
76. Wilson, W.H., et al., Navitoclax, a targeted high-affinity inhibitor of BCL-2, in lymphoid malignancies: a phase 1 dose-escalation study of safety, pharmacokinetics, pharmacodynamics, and antitumour activity. Lancet Oncol, 2010. 11(12): p. 1149-59.
77. Kaefer, A., et al., Mechanism-based pharmacokinetic/pharmacodynamic meta-analysis of navitoclax (ABT-263) induced thrombocytopenia. Cancer Chemother Pharmacol, 2014. 74(3): p. 593-602.
78. Mason, K.D., et al., Programmed Anuclear Cell Death Delimits Platelet Life Span. Cell, 2007. 128(6): p. 1173-1186.
79. Wang, Y., et al., Discovery of piperlongumine as a potential novel lead for the development of senolytic agents. Aging (Albany NY), 2016. 8(11): p. 2915-2926.
80. Wang, H., et al., JQ1 synergizes with the Bcl-2 inhibitor ABT-263 against MYCN-amplified small cell lung cancer. Oncotarget, 2017. 8(49): p. 86312-86324.
81. Khan, S., et al., A selective BCL-X(L) PROTAC degrader achieves safe and potent antitumor activity. Nat Med, 2019. 25(12): p. 1938-1947.
82. González-Gualda, E., et al., Galacto-conjugation of Navitoclax as an efficient strategy to increase senolytic specificity and reduce platelet toxicity. Aging Cell, 2020. 19(4): p. e13142.
83. Kim, S.R., et al., Increased renal cellular senescence in murine high-fat diet: effect of the senolytic drug quercetin. Transl Res, 2019. 213: p. 112-123.
84. Kim, S.R., et al., Progressive Cellular Senescence Mediates Renal Dysfunction in Ischemic Nephropathy. J Am Soc Nephrol, 2021. 32(8): p. 1987-2004.
85. Li, C., et al., Senolytic therapy ameliorates renal fibrosis postacute kidney injury by alleviating renal senescence. Faseb j, 2021. 35(1): p. e21229.
86. Mylonas, K.J., et al., Cellular senescence inhibits renal regeneration after injury in mice, with senolytic treatment promoting repair. Science Translational Medicine, 2021. 13(594): p. eabb0203.
87. Li, Q., et al., Dexmedetomidine attenuates renal fibrosis via α2-adrenergic receptor-dependent inhibition of cellular senescence after renal ischemia/reperfusion. Life Sci, 2018. 207: p. 1-8.
88. Zhang, H.M., et al., Geldanamycin derivative ameliorates high fat diet-induced renal failure in diabetes. PLoS One, 2012. 7(3): p. e32746.
89. Ren, Q., et al., Flavonoid fisetin alleviates kidney inflammation and apoptosis via inhibiting Src-mediated NF-κB p65 and MAPK signaling pathways in septic AKI mice. Biomed Pharmacother, 2020. 122: p. 109772.
90. Xie, J., et al., Bufalin suppresses the proliferation and metastasis of renal cell carcinoma by inhibiting the PI3K/Akt/mTOR signaling pathway. Oncol Lett, 2018. 16(3): p. 3867-3873.
91. Ding, L., et al., Bufalin alleviates acute kidney injury by regulating NLRP3 inflammasome-mediated pyroptosis. Apoptosis, 2023. 28(3-4): p. 539-548.
92. Christensen, E.I. and H. Birn, Megalin and cubilin: multifunctional endocytic receptors. Nat Rev Mol Cell Biol, 2002. 3(4): p. 256-66.
93. Matjusaitis, M., et al., Biomarkers to identify and isolate senescent cells. Ageing Res Rev, 2016. 29: p. 1-12.
94. Lee, B.Y., et al., Senescence-associated beta-galactosidase is lysosomal beta-galactosidase. Aging Cell, 2006. 5(2): p. 187-95.
95. Piechota, M., et al., Is senescence-associated β-galactosidase a marker of neuronal senescence? Oncotarget, 2016. 7(49): p. 81099-81109.
96. Manzari, M.T., et al., Targeted drug delivery strategies for precision medicines. Nat Rev Mater, 2021. 6(4): p. 351-370.
97. Yan, M.T., C.T. Chao, and S.H. Lin, Chronic Kidney Disease: Strategies to Retard Progression. Int J Mol Sci, 2021. 22(18).
98. Latorre, E., et al., Small molecule modulation of splicing factor expression is associated with rescue from cellular senescence. BMC Cell Biology, 2017. 18: p. 1-15.
99. Herranz, N., et al., mTOR regulates MAPKAPK2 translation to control the senescence-

associated secretory phenotype. Nat Cell Biol, 2015. 17(9): p. 1205-17.

100.   Knoppert, S.N., et al., Cellular Senescence and the Kidney: Potential Therapeutic Targets and Tools. Front Pharmacol, 2019. 10: p. 770.

101.   June, C.H., et al., CAR T cell immunotherapy for human cancer. Science, 2018. 359(6382): p. 1361-1365.

102.   Dunbar, C.E., et al., Gene therapy comes of age. Science, 2018. 359(6372): p. eaan4672.

6

Chapter 7

Nederlandse samenvatting

中文总结

Curriculum Vitae

List of publications

Acknowledgements

Nederlandse samenvatting

In gezonde nieren worden eiwitgebonden uremische toxines (PBUT's) uit de algemene circulatie verwijderd en in de voorurine uitgescheiden door een gecoördineerde actie van plasmamembraantransporters in proximale tubuluscellen, maar deze endogene afvalstoffen worden nauwelijks geklaard bij nierfalen. Het eindpunt van progressief chronisch nierfalen (CKD) is nierfibrose wat gekenmerkt wordt door een overmatige ophoping van extracellulaire matrix. Onderzoek van de afgelopen jaren hebben aangetoond dat versnelde veroudering van cellen, ook wel senescence genoemd, in de proximale niertubulus het proces van nierfibrose mogelijk beïnvloedt. Senescense wordt gekenmerkt door het permanent stoppen van de celdeling en door het uitscheiden van senescence-geassocieerde secretoire fenotype (SASP) factoren die het fibroseproces bevorderen. Het doel van dit proefschrift was om de rol die PBUT's spelen in de ontwikkeling van senescence nader te onderzoeken. Hierbij is gebruik gemaakt van een conditioneel geïmmortaliseerde proximale tubulusepitheelcellijn waarin de organisch-aniontransporter-1 (ciPTEC-OAT1) tot overexpressie is gebracht. Deze cellijn is verkregen door primaire cellen uit urine van een gezonde donor te immortaliseren met SV40T- en hTERT-genen, waardoor de celdeling in stand wordt gehouden bij 33 °C. Echter wanneer de cellen bij 37 °C worden gekweekt, verdwijnt de expressie van het SV40T-gen, vertraagd de celdeling en groeit de cel uit tot een volwassen proximale tubulusepitheelcel.

Hoofdstuk 1 geeft een algemene introductie over het ontstaan van nierfibrose, het proces van senescence en de rol die PBUT's spelen bij nierfalen. Hieruit is de hypothese afgeleid dat PBUT's nierfibrose kunnen bevorderen door het proces van senescence te versnellen, mogelijk via mitochondriale disfunctie, het stopzetten van de celdeling en door de productie van SASP-factoren. Deze hypothese is in dit proefschrift verder getoetst.

De bevindingen beschreven in **hoofdstuk 2** laten zien dat ciPTEC-OAT1 in de loop van de tijd een senescence-fenotype ontwikkelt wanneer de cellen bij 37°Cworden gekweekt. Kenmerken als het stopzetten van de celdeling, weerstand tegen apoptose, de productie van SASP-factoren werden in de cellen waargenomen, evenals een gevoeligheid voor behandeling met senolytica, geneesmiddelen die cellen in senescence kunnen opruimen. Op basis van deze bevindingen werd geconcludeerd dat ciPTEC-OAT1 een geschikt model is voor het bestuderen van nierveroudering door simpelweg de kweekomstandigheden aan te passen.

Hoofdstuk 3 en **hoofdstuk 4** geven aan dat PBUT's de uitscheiding van SASP-factoren door de niertubuluscellen kunnen opwekken en oxidatieve stress kunnen veroorzaken. Dit leidt tot mitochondriale disfunctie en tot senescence van de niercellen. De resultaten in **hoofdstuk 3** laten zien dat PBUT's een ontstekingsproces stimuleren via oxidatieve stress en NF-κB-signalering, wat weer leidt tot afgifte van de SASP-factor IL-1β door de proximale tubuluscellen. **Hoofdstuk 4** laat zien dat het uremische toxine, indoxylsulfaat, mogelijk kan bijdragen aan de progressie van nierziekte door het proces van senescence te versnellen. Dit doet indoxylsulfaat door SASP-factoren te reguleren en inflammatoire en profibrotische processen te moduleren, zoals blijkt uit veranderingen in de TNF-α/NF-κB-signaleringsroute en het epitheliale-mesenchymale transitieproces. Bij dit laatste worden de epitheelcellen omgevormd tot minder gedifferentieerde mesenchymale cellen en verliezen ze dus hun fenotype. Samen onthulden de bevindingen dat PBUT's, en vooral dus indoxylsulfaat, aanjagers

zijn van nierveroudering en dat ze dit doen door oxidatieve stress te induceren, ontstekingsreacties te bevorderen en via verhoogde weerstand tegen celdood.

Om specifiek senescence in de nier aan te kunnen pakken en zo de progressie van CKD tegen te kunnen gaan, is in **hoofdstuk 5** een eerste stap gezet naar een niergerichte senolytische therapie met het experimentele geneesmiddel navitoclax, wat ontworpen is om senescente cellen in het beenmerg te doden. Een niergerichte therapie zou senescente cellen kunnen opruimen in de tubulus zonder het beenmerg aan te tasten, en dus de kans op ernstige bijwerkingen van de therapie kunnen beperken. Hiervoor wordt een conjugatiestap aan het kippeneiwit, lysozym, voorgesteld, waarvan eerder al is aangetoond dat het specifiek door niercellen wordt opgenomen. Nadat uit het onderzoek beschreven in **hoofdstuk 5** bleek dat navitoclax zelf waarschijnlijk niet wordt opgenomen door de niercel maar geconjugeerd aan lysozym mogelijk wel, is als eerste stap in dit proces is een conjugaat van het lysozym met een fluorescerende merkstof, rhodamine, gemaakt. De verkregen resultaten laten zien dat ciPTEC-OAT1 in staat is om het rhodamine-lysozym-conjugaat op te nemen, wat aangeeft dat dit een waardevol celmodel is om de werkzaamheid van senolytische-lysozym-conjugaten in de toekomst te kunnen evalueren.

Ten slotte geeft **hoofdstuk 6** een overzicht van hoe senescence bijdraagt aan progressie van CKD en wat de rol van PBUT's in dit proces is. Verder wordt beschreven hoe senescence van cellen in de nieren kan worden bestudeerd in diermodellen en celkweken en hoe in de toekomst de huidige senolytische therapieën kunnen worden verbeterd.

7

中文总结

在健康的肾脏中，蛋白质结合的尿毒症毒素（protein-bound uremic toxins，PBUTs）通过近端肾小管细胞中质膜转运蛋白的协调作用从体循环中清除并在前尿中排泄；但在肾功能衰竭时，这些内源性废物几乎无法从体内清除。肾纤维化是所有慢性功能衰竭病（chronic kidney diseases，CKD）的最终表现，其主要特征为细胞外基质（extracellular matrix，ECM）的过度积累。 近年来的研究表明，近端肾小管细胞的加速衰老（senescence）可能会影响肾纤维化的进程。衰老是一种特殊的细胞状态，其特征是细胞周期永久性停滞和增殖受限，通过释放衰老相关分泌表型（senescence-associated secretory phenotype，SASP）促进器官纤维化。本论文的目的是研究 PBUTs 在加速衰老发展过程中的作用。 为了研究 PBUTs 与加速小管上皮细胞衰老的关系，本文主要使用了过表达有机阴离子转运蛋白 1（organic anion transporter 1, OAT1）的条件永生化近曲小管上皮细胞系（ciPTEC-OAT1）来进行试验。该细胞系是通过将来自健康供体尿液的原代细胞永生化而获得的，并带有 SV40T 和 hTERT 基因，从而在 33℃下维持细胞分裂。当细胞在 37℃ 下生长时，SV40T 基因的表达消失，细胞分裂减慢，细胞生长成成熟的近曲小管上皮细胞。利用该细胞系，本论文证明了 PBUTs 在体外与加速小管上皮细胞衰老的关系，为 PBUTs 在 CKD 中的作用提供了新的视角，也为研究治疗 CKD 的新策略奠定了基础。

第一章概述了肾纤维化的发生、衰老过程以及 PBUTs 在肾衰竭中的作用，并提出了以下假设：PBUT 可能通过加速衰老过程来促进肾纤维化，这一过程可能是通过线粒体功能障碍、细胞周期停滞和 SASP 的产生与释放来实现的。这些假设在论文的后续章节中得到了进一步的检验。

在**第二章**中，我们发现当 ciPTEC-OAT1 在 37℃ 下生长时，细胞随着时间的推移会形成衰老表型，包括细胞周期停滞、细胞凋亡抑制、SASP 的产生与释放以及对 senolytics（可以清除衰老细胞的药物）治疗的敏感性增加。 因此，我们认为 ciPTEC-OAT1 是一个可以用于研究肾脏衰老的有效模型，并且能通过简单调整培养条件来实现造模。

第三章和**第四章**的结果表明 PBUTs 可以诱导肾小管细胞分泌 SASP 并引发氧化应激，可能导致线粒体功能障碍，从而导致肾脏衰老加剧。**第三章**的结果表明，PBUTs 通过氧化应激和 NF-κB 信号传导刺激炎症发生，进而导致近曲小管细胞释放 SASP 因子 IL-1β 的产生与释放。**第四章**表明，尿毒症毒素硫酸吲哚酚（Indoxyl sulfate, IS）可能通过加速衰老过程来促进肾脏疾病的进展。在这个过程中，IS 可以调节 SASP 的产生和释放，从而导致炎症发生并促进纤维化。试验结果表明，IS 可以刺激 TNF-α/NF-κB 信号通路和上皮间质转化的过程，从而引发相应连锁反应并加速细胞衰老。细胞的上皮间质转化的过程主要是指上皮细胞转化为分化程度较低的间充质细胞，从而失去其上皮细胞表型，进而增加肾脏纤维化表型。 综上所述，研究结果表明，PBUTs，尤其是 IS，是加速肾脏衰老的一个驱动因素，该作用是通过诱导氧化应激、促进炎症反应和增强对细胞死亡的抵抗力来实现的。

衰老细胞是导致肾脏纤维化的一个重要贡献者，因此使用 senolytics 杀死衰老细胞可以

作为延迟 CKD 进展、减缓肾脏纤维化的新策略。Navitoclax 是一个被证明有效的、可以选择性杀死衰老细胞的抗衰老药物。然而临床试验表明其毒副作用可导致血小板减少，危及患者的生命安全。 因此，**第五章**旨在寻找一种避免包括 navitoclax 在内的 senolytics 的毒副作用的有效方法。这种方法不仅可以选择性地清除肾脏中的衰老细胞，还能提高其利用率并避开相关毒副作用。为此， 我们提出了制备 Navitoclax 前药的解决方案。该方案使用可以被肾脏细胞特异性吸收的鸡蛋白溶菌酶（lysozyme）与 navitoclax 络合，改变 navitoclax 在体内的吸收路径，从而使该药物特异性地被肾脏细胞吸收。为此我们制备了溶菌酶与荧光示踪剂罗丹明的结合物来验证我们的预想。研究结果表明 ciPTEC-OAT1 能够吸收罗丹明-溶菌酶络合物，表明该细胞模型后续可以用于分析 senolytic-溶菌酶络合物这类的靶向给药系统的可行性。

第六章进一步总结了衰老细胞在促进 CKD 进程及肾脏纤维化中的作用，比较了研究肾脏衰老的体内外模型，并提出了研究 PBUT 加速肾脏细胞衰老的相关模型应用。最后，我们概述了当前用于杀死衰老细胞的特效药物 senolytic，并提出了如何改进当前延迟 CKD 进展、减缓肾脏纤维化的策略。

7

Curriculum Vitae

Yi Yang was born on 22nd April 1993 in Guanghan, Sichuan Province, China. After finishing high school, she started her bachelor studies in Sichuan Agricultural University and obtained her bachelor's degree of pharmaceutics in 2015. Thereafter, she did her master studies in the same university under the supervision of Prof. dr. Zhongqiong Yin, and mainly focused on pharmacology and toxicology of natural medicines during her master.

In 2018, Yi obtained her master's degree, and started her PhD at the division of Pharmacology in Utrecht University. She was awarded financial support by China Scholarship Council (CSC) for her PhD study. Her PhD project under the supervision of Prof. dr. R. Masereeuw, Prof. dr. R. Goldschmeding, Dr. M. Mihajlović and Dr. M.J. Janssen, focused on obtaining insights into protein-bound uremic toxins in proximal tubule cell senescence and kidney fibrosis. The results of this work have been described in this thesis.

List of publications

1. **Yang Y**, Mihajlovic M, Masereeuw R. Protein-Bound Uremic Toxins in Senescence and Kidney Fibrosis. Biomedicines. 2023; 11(9):2408.

2. **Yang Y,** Mihajlovic M, Valentijn F, Nguyen TQ, Goldschmeding R, Masereeuw R. A Human Conditionally Immortalized Proximal Tubule Epithelial Cell Line as a Novel Model for Studying Senescence and Response to Senolytics. Front Pharmacol. 2022;13:791612.

3. **Yang Y**, Mihajlovic M, Janssen MJ, Masereeuw R. The Uremic Toxin Indoxyl Sulfate Accelerates Senescence in Kidney Proximal Tubule Cells. Toxins (Basel). 2023;15(4):242.

4. Mihajlovic M, Krebber MM, **Yang Y**, et al. Protein-Bound Uremic Toxins Induce Reactive Oxygen Species-Dependent and Inflammasome-Mediated IL-1β Production in Kidney Proximal Tubule Cells. Biomedicines. 2021;9(10):1326.

5. **Yang Y,** Luo H, Song X, et al. Preparation of *Galla Chinensis* Oral Solution as well as Its Stability, Safety, and Antidiarrheal Activity Evaluation. *Evid Based Complement Alternat Med*. 2017;2017:1851459.

6. Song X, **Yang Y**, Li J, et al. Tannins extract from Galla Chinensis can protect mice from infection by Enterotoxigenic Escherichia coli O101. BMC Complement Med Ther. 2021;21(1):84.

7. Fu Q, Cui Q, **Yang Y**, et al. Effect of Resveratrol Dry Suspension on Immune Function of Piglets. Evid Based Complement Alternat Med. 2018;2018:5952707.

8. Yu J, Zhang Y, Song X, **Yang Y**, et al. Effect of Modified Pulsatilla Powder on Enterotoxigenic Escherichia coli O101-Induced Diarrhea in Mice. Evid Based Complement Alternat Med. 2017;2017:3687486.

9. Zhao X, Cui Q, Fu Q, Song X, Jia R, **Yang Y**, et al. Antiviral properties of resveratrol against pseudorabies virus are associated with the inhibition of IκB kinase activation. Sci Rep. 2017;7(1):8782.

7

Acknowledgements

At the beginning of my PhD journey, my promoter **Roos** told me that I would have a wonderful thesis book after 4 years. I thought it was far away from me. Now, I almost have one! I came to the last chapter of my thesis. I can't say this is a perfect book, but it is a witness to my PhD life. Here I would like to thank the other witnesses of my PhD life, those who have supported and helped me over the past few years.